

Drivers of plant nutrient acquisition and allocation strategies and their influence
on plant responses to environmental change

by

Evan A. Perkowski, B.S.

A Dissertation

In

Biological Sciences

Submitted to the Graduate Faculty
of Texas Tech University in
Partial Fulfillment of
the Requirements for
the Degree of

Doctor of Philosophy

Approved

Nicholas G. Smith, Ph.D.
Chair of Committee

Aimée T. Classen, Ph.D.

Natasja van Gestel, Ph.D.

Lindsey C. Slaughter, Ph.D.

Dylan W. Schwilk, Ph.D.

Mark Sheridan, Ph.D.
Dean of the Graduate School

May 2023

Copyright 2023, Evan A. Perkowski

Acknowledgements

Placeholder for text

Table of Contents

| | |
|---|------|
| Acknowledgements | ii |
| Abstract | viii |
| List of Tables | ix |
| List of Figures | xiii |
| 1. Introduction | 1 |
| 2. Structural carbon costs to acquire nitrogen are determined by nitrogen and light availability in two species with different nitrogen acquisition strategies | 8 |
| 2.1 Introduction | 8 |
| 2.2 Methods | 12 |
| 2.2.1 <i>Experiment setup</i> | 12 |
| 2.2.2 <i>Plant measurements and calculations</i> | 13 |
| 2.2.3 <i>Statistical analyses</i> | 14 |
| 2.3 Results | 16 |
| 2.3.1 <i>Carbon costs to acquire nitrogen</i> | 16 |
| 2.3.2 <i>Whole plant nitrogen biomass</i> | 19 |
| 2.3.3 <i>Root carbon biomass</i> | 21 |
| 2.3.4 <i>Root nodule biomass</i> | 23 |
| 2.4 Discussion | 27 |
| 2.4.1 <i>Carbon costs to acquire nitrogen increase with light availability and decrease with fertilization</i> | 27 |
| 2.4.2 <i>Modeling implications</i> | 29 |
| 2.4.3 <i>Study limitations</i> | 31 |
| 2.4.4 <i>Conclusions</i> | 33 |
| 3. Soil nitrogen availability modifies leaf nitrogen economies in mature temperate deciduous forests: a direct test of photosynthetic least-cost theory | 35 |
| 3.1 Introduction | 35 |

| | |
|---|----|
| 3.2 Methods | 39 |
| 3.2.1 <i>Study site description</i> | 39 |
| 3.2.2 <i>Experimental design</i> | 40 |
| 3.2.3 <i>Leaf gas exchange and trait measurements</i> | 40 |
| 3.2.4 A_{net}/C_i curve-fitting and parameter estimation | 43 |
| 3.2.5 Proportion of leaf nitrogen allocated to photosynthesis and structure | 45 |
| 3.2.6 Tradeoffs between nitrogen and water use | 46 |
| 3.2.7 Soil nitrogen availability and pH | 47 |
| 3.2.8 Statistical analyses | 49 |
| 3.3 Results | 51 |
| 3.3.1 Leaf N content | 51 |
| 3.3.2 Net photosynthesis and leaf biochemistry | 54 |
| 3.3.3 Leaf N allocation | 57 |
| 3.3.4 Tradeoffs between nitrogen and water use | 60 |
| 3.4 Discussion | 63 |
| 3.4.1 Soil nitrogen availability modifies tradeoffs between nitrogen and water use | 64 |
| 3.4.2 Soil pH did not modify tradeoffs between nitrogen and water usage | 66 |
| 3.4.3 Species identity explains a large amount of variation in leaf and whole plant traits | 67 |
| 3.4.4 Implications for photosynthetic least-cost theory model development | 68 |
| 3.4.5 Conclusions | 70 |
| 4. The relative cost of resource use for photosynthesis drives variance in leaf nitrogen content across a climate and soil resource availability gradient | 71 |
| 4.1 Introduction | 71 |
| 4.2 Methods | 77 |
| 4.2.1 Site descriptions and sampling methodology | 77 |

| | | |
|-------|---|-----|
| 4.2.2 | <i>Leaf trait measurements</i> | 77 |
| 4.2.3 | <i>Site climate data</i> | 83 |
| 4.2.4 | <i>Site edaphic characteristics</i> | 83 |
| 4.2.5 | <i>Plant functional group assignments</i> | 85 |
| 4.2.6 | <i>Data analysis</i> | 86 |
| 4.3 | Results | 88 |
| 4.3.1 | <i>Cost to acquire nitrogen relative to water</i> | 88 |
| 4.3.2 | $C_i:C_a$ | 92 |
| 4.3.3 | <i>Leaf nitrogen content</i> | 95 |
| 4.3.4 | <i>Structural equation model</i> | 99 |
| 4.4 | Discussion | 102 |
| 4.4.1 | <i>Negative effects of leaf $C_i:C_a$ on N_{area} are driven by reductions in M_{area}, not N_{mass}</i> | 102 |
| 4.4.2 | <i>Soil nitrogen availability increases N_{area} through changes in the cost to acquire nitrogen</i> | 104 |
| 4.4.3 | <i>Soil moisture increases N_{area} by facilitating increases in soil nitrogen availability</i> | 105 |
| 4.4.4 | <i>Indirect effects of climate on N_{area} are mediated through changes in leaf $C_i:C_a$ and β</i> | 106 |
| 4.4.5 | <i>Species identity traits modify effects of the environment on β, leaf $C_i:C_a$, and N_{area}</i> | 106 |
| 4.4.6 | <i>Next steps for optimality model development</i> | 108 |
| 4.4.7 | <i>Conclusions</i> | 109 |
| 5. | Optimal resource investment to photosynthetic capacity maximizes nutrient allocation to whole plant growth under elevated CO₂ | 110 |
| 5.1 | Introduction | 110 |
| 5.2 | Methods | 115 |
| 5.2.1 | <i>Seed treatments and experimental design</i> | 115 |
| 5.2.2 | <i>Growth chamber conditions</i> | 116 |
| 5.2.3 | <i>Leaf gas exchange measurements</i> | 118 |

| | | |
|-------|---|-----|
| 5.2.4 | <i>Leaf trait measurements</i> | 119 |
| 5.2.5 | <i>A/C_i curve fitting and parameter estimation</i> | 121 |
| 5.2.6 | Stomatal limitation | 121 |
| 5.2.7 | <i>Proportion of leaf nitrogen allocated to photosynthesis and structure</i> | 122 |
| 5.2.8 | <i>Whole plant traits</i> | 124 |
| 5.2.9 | <i>Statistical analyses</i> | 126 |
| 5.3 | Results | 128 |
| 5.3.1 | <i>Leaf nitrogen and chlorophyll content</i> | 128 |
| 5.3.2 | <i>Leaf biochemistry and stomatal conductance</i> | 132 |
| 5.3.3 | <i>Leaf nitrogen allocation</i> | 136 |
| 5.3.4 | <i>Whole plant traits</i> | 140 |
| 5.3.5 | <i>Nitrogen fixation</i> | 144 |
| 5.4 | Discussion | 148 |
| 5.4.1 | <i>Soil nitrogen fertilization has divergent effects on leaf and whole plant acclimation responses to CO₂</i> | 149 |
| 5.4.2 | <i>Implications for future model development</i> | 153 |
| 5.4.3 | <i>Study limitations and future directions</i> | 154 |
| 5.4.4 | <i>Conclusions</i> | 156 |
| 6. | Conclusions | 158 |
| 6.1 | Summary of experimental chapters | 159 |
| 6.1.1 | <i>Chapter 2: Structural carbon costs to acquire nitrogen are determined by nitrogen and light availability in two species with different nitrogen acquisition strategies</i> | 159 |
| 6.1.2 | <i>Chapter 3: Soil nitrogen availability modifies leaf nitrogen economies in mature temperate deciduous forests: a direct test of photosynthetic least-cost theory</i> | 160 |
| 6.1.3 | <i>Chapter 4: The relative cost of resource use for photosynthesis drives variance in leaf nitrogen content across a climate and soil resource availability gradient</i> | 161 |

| | |
|---|-----|
| 6.1.4 <i>Chapter 5: Optimal resource investment to photosynthetic capacity maximizes nutrient allocation to whole plant growth under elevated CO₂</i> | 161 |
| References | 162 |
| Appendix A: | |
| Supplemental material for "Structural carbon costs to acquire nitrogen are determined by nitrogen and light availability in two species with different nitrogen acquisition strategies" | 199 |
| Appendix B: | |
| Supplemental material for "Soil nitrogen availability modifies leaf nitrogen economies in mature temperate deciduous forests: a direct test of photosynthetic least-cost theory" | 203 |
| Appendix C: | |
| Supplemental material for "The relative cost of resource use for photosynthesis drives variance in leaf nitrogen content across a climate and soil resource availability gradient" | 208 |
| Appendix D: | |
| Supplemental material for "Optimal resource investment to photosynthetic capacity maximizes nutrient allocation to whole plant growth under elevated CO ₂ " | 215 |

Abstract

List of Tables

| | |
|--|----|
| 2.1 Analysis of variance results exploring species-specific effects of light availability, nitrogen fertilization, and their interactions on carbon costs to acquire nitrogen (N_{cost}), whole-plant nitrogen biomass (N_{wp}), and root carbon biomass (C_{bg}) | 17 |
| 2.2 Analysis of variance results exploring effects of light availability, nitrogen fertilization, and their interactions on <i>G. max</i> root nodule biomass and the ratio of root nodule biomass to root biomass* | 24 |
| 2.3 Slopes of the regression line describing the relationship between each dependent variable and nitrogen fertilization at each light level* | 25 |
| 3.1 Effects of soil N availability, soil pH, and species on leaf N content per unit leaf area (N_{area}), leaf N content per unit leaf mass (N_{mass}), and leaf mass per unit leaf area (M_{area}) | 52 |
| 3.2 Effects of soil N availability, soil pH, species, and N_{area} on leaf biochemistry | 55 |
| 3.3 Effects of soil N availability, soil pH, and species on the proportion of leaf nitrogen content allocated to photosynthesis, Rubisco, bioenergetics, and structure | 58 |
| 3.4 Effects of soil N availability, soil pH, species, and N_{area} on tradeoffs between nitrogen and water use | 61 |

| | | |
|-----|---|-----|
| 4.1 | Site locality information, sampling year(s), 2006-2020 mean annual precipitation (MAP; mm), mean annual temperature (MAT; °C), and water holding capacity (WHC; mm)* | 81 |
| 4.2 | Effects of soil moisture, soil nitrogen availability, and plant functional group on β | 90 |
| 4.3 | Effects of soil moisture, soil nitrogen availability, and plant functional group on leaf $C_i:C_a^*$ | 93 |
| 4.4 | Effects of soil nitrogen fertilization, inoculation, and CO ₂ treatments on N_{area} , N_{mass} , and M_{area} | 97 |
| 4.5 | Structural equation model results investigating direct effects of climatic and soil resource availability on N_{area} , N_{mass} , M_{area} , leaf $C_i:C_a$, and β | 100 |
| 5.1 | Effects of soil nitrogen fertilization, inoculation, and CO ₂ treatments on N_{area} , N_{mass} , M_{area} , and Chl_{area} | 130 |
| 5.2 | Effects of soil nitrogen fertilization, inoculation, and CO ₂ on leaf biochemistry | 134 |
| 5.3 | Effects of soil N availability, soil pH, species, and N_{area} on leaf nitrogen allocation | 138 |
| 5.4 | Effects of soil N availability, soil pH, species, and N_{area} on total leaf area, whole plant biomass, and carbon costs to acquire nitrogen . . | 142 |
| 5.5 | Effects of soil N availability, soil pH, species, and N_{area} on root nodule biomass and plant investments in symbiotic nitrogen fixation | 146 |

| | | |
|----|---|-----|
| A1 | Summary table containing volumes of compounds used to create modified Hoagland's solutions for each soil nitrogen fertilization treatment. All volumes are expressed as milliliters per liter (mL/L) | 199 |
| A2 | Analysis of variance results exploring species-specific effects of light availability, nitrogen fertilization, and their interactions on the ratio of whole plant biomass to pot volume | 200 |
| A3 | Slopes of the regression line describing the relationship between each dependent variable and nitrogen fertilization at each light level [*] | 201 |
| B1 | Sample sizes of each species, abbreviated by their USDA NRCS PLANTS database code, within each plot at each site | 203 |
| B2 | Analysis of variance results exploring the linear effect of leaf temperature on net photosynthesis rate and stomatal conductance measured at 400 $\mu\text{mol mol}^{-1}$ CO ₂ | 204 |
| B3 | Second order log-polynomial regression coefficients that described the effect of leaf temperature on net photosynthesis and stomatal conductance measured at 400 $\mu\text{mol mol}^{-1}$ CO ₂ | 205 |
| B4 | Mean, standard error, and 95% confidence interval ranges of soil nitrogen availability estimates across all measured plots. All units are expressed as $\mu\text{g N g}^{-1}$ resin d ⁻¹ | 206 |
| C1 | List of sampled species and their plant functional group assignment | 210 |
| C2 | List of sampled species and their plant functional group assignment (cont.) | 211 |

| | | |
|----|--|-----|
| C3 | List of sampled species and their plant functional group assignment (cont.) | 212 |
| C4 | Model selection results for soil moisture, air temperature, and vapor pressure deficit. Soil moisture was used in a bivariate regression against β , while vapor pressure deficit was used in bivariate regressions against leaf $C_i:C_a^*$ | 213 |

List of Figures

| | |
|---|----|
| 2.1 Relationships between soil nitrogen fertilization and light availability on carbon costs to acquire nitrogen in <i>G. hirsutum</i> and <i>G. max</i> | 18 |
| 2.2 Relationships between soil nitrogen fertilization and light availability on whole-plant nitrogen biomass in <i>G. hirsutum</i> and <i>G. max</i> | 20 |
| 2.3 Relationships between soil nitrogen fertilization and light availability on root carbon biomass in <i>G. hirsutum</i> and <i>G. max</i> | 22 |
| 2.4 Effects of shade cover and nitrogen fertilization on root nodule biomass and the ratio of root nodule biomass to root biomass in <i>G. max</i> | 26 |
| 3.1 Effects of soil N availability and species on leaf N content per unit leaf area, leaf nitrogen content per unit leaf biomass, and leaf mass per leaf area | 53 |
| 3.2 Effects of soil N availability, species, and leaf N content leaf biochemistry | 56 |
| 3.3 Effects of soil N availability, species, and leaf N content on the fraction of leaf nitrogen allocated to photosynthesis and structure | 59 |
| 3.4 Effects of soil N availability, species, and leaf N content on tradeoffs between nitrogen and water use | 62 |
| 4.1 Maps that detail site locations along 2006-2020 mean annual precipitation and mean annual temperature gradients in Texas, USA. | 82 |

| | |
|--|-----|
| 4.2 Effects of soil nitrogen availability and soil moisture on the unit cost ratio β | 91 |
| 4.3 Effects of 4-day mean vapor pressure deficit, 2-day soil moisture (per water holding capacity), and soil nitrogen availability on leaf $C_i:C_a$ | 94 |
| 4.4 Effects of leaf $C_i:C_a$, soil nitrogen availability, and soil moisture on leaf nitrogen content per unit leaf area, leaf nitrogen content per unit leaf biomass, and leaf mass per area | 98 |
| 4.5 Structural equation model results exploring drivers of N_{area} | 101 |
| 5.1 Effects of CO_2 , fertilization, and inoculation on leaf nitrogen per unit leaf area, leaf nitrogen content, leaf mass per unit leaf area, and chlorophyll content per unit leaf area | 131 |
| 5.2 Effects of CO_2 , fertilization, and inoculation on maximum rate of Rubisco carboxylation, the maximum rate of RuBP regeneration, and the ratio of the maximum rate of RuBP regeneration to the maximum rate of Rubisco carboxylation leaf mass per unit leaf area, dark respiration, stomatal conductance, and stomatal limitation | 135 |
| 5.3 Effects of CO_2 , fertilization, and inoculation on the relative fraction of leaf nitrogen allocated to photosynthesis and the fraction of leaf nitrogen allocated to structure | 139 |
| 5.4 Effects of CO_2 , fertilization, and inoculation on total leaf area, total biomass, and structural carbon costs to acquire nitrogen | 143 |

| | |
|---|-----|
| 5.5 Effects of CO ₂ , fertilization, and inoculation on nodule biomass, nodule: root biomass, and percent nitrogen fixed from the atmosphere. | 147 |
| A1 Effects of shade cover and nitrogen fertilization on the ratio of plant biomass to rooting volume in <i>G. hirsutum</i> and <i>G. max</i> | 202 |
| B1 Effects of leaf temperature on net photosynthesis rate and stomatal conductance values when measured at 400 $\mu\text{mol mol}^{-1}$ CO ₂ | 207 |
| C2 Model selection results exploring relevant timescales for soil moisture and vapor pressure deficit | 214 |

1 **Chapter 1**
2 **Introduction**

3 Photosynthesis represents the largest carbon flux between the atmosphere
4 and biosphere, and is regulated by complex ecosystem carbon and nutrient cy-
5 cles (Hungate et al. 2003; IPCC 2021). As a result, the inclusion of robust,
6 empirically tested representations of photosynthetic processes is critical in order
7 for terrestrial biosphere models to accurately and reliably simulate carbon and
8 nutrient fluxes between the atmosphere and terrestrial biosphere (Wieder et al.
9 2015; Smith and Dukes 2013; Prentice et al. 2015; Oreskes et al. 1994). Despite
10 evidence that the inclusion of coupled carbon and nutrient cycles can improve
11 model uncertainty, widespread divergence in predicted carbon and nutrient fluxes
12 is still apparent across model products (Arora et al. 2020; Friedlingstein et al.
13 2014; Davies-Barnard et al. 2020). Divergence in predicted carbon and nutrient
14 fluxes across terrestrial biosphere models may be due to an incomplete under-
15 standing of how plants acclimate to changing environments (Smith and Dukes
16 2013; Davies-Barnard et al. 2020), as terrestrial biosphere models are sensitive to
17 the formulation of photosynthetic processes (Ziehn et al. 2011; Bonan et al. 2011;
18 Booth et al. 2012; Smith et al. 2016; Smith et al. 2017; Rogers et al. 2017).

19 Many terrestrial biosphere models predict leaf-level photosynthesis through
20 linear relationships between area-based leaf nitrogen content and the maximum
21 rate of Ribulose-1,5-bisphosphate carboxylase/oxygenase ("Rubisco"), following
22 from the idea that large fractions of leaf nitrogen content are allocated to the con-
23 struction and maintenance of Rubisco and other photosynthetic enzymes (Evans

24 1989). The inclusion of coupled carbon and nutrient cycles in terrestrial biosphere
25 models (Shi et al. 2016; Braghieri et al. 2022) allows for the prediction of leaf ni-
26 trogen content through soil nitrogen availability, which causes models to indirectly
27 predict photosynthetic processes through shifts in soil nitrogen availability (Smith
28 et al. 2014; Lawrence et al. 2019). While these patterns are commonly observed
29 in ecosystems globally (Brix 1971; Evans 1989; Liang et al. 2020; Firn et al. 2019),
30 this formulation of photosynthetic processes does not allow for the prediction of
31 leaf and whole plant acclimation responses to changing environments (Smith and
32 Dukes 2013; Rogers et al. 2017; Harrison et al. 2021), and suggests that con-
33 stant leaf nitrogen-photosynthesis relationships are ubiquitous across ecosystems.
34 Incorporating leaf and whole plant acclimation schemes in terrestrial biosphere
35 models is important (Smith and Dukes 2013), particularly because recent work
36 indicates that variance in leaf nitrogen content and leaf photosynthesis across en-
37 vironmental gradients may be better explained as an integrated product of leaf
38 acclimation responses to changing climates and soil nitrogen availability than soil
39 nitrogen availability alone (Dong et al. 2017; Dong et al. 2020; Smith et al. 2019;
40 Querejeta et al. 2022; Dong et al. 2022; Westerband et al. 2023).

41 Photosynthetic least-cost theory (Prentice et al. 2014; Wang et al. 2017;
42 Smith et al. 2019; Scott and Smith 2022; Harrison et al. 2021) provides a con-
43 temporary framework for predicting leaf and whole plant acclimation responses
44 to environmental change. The theory, which unifies photosynthetic optimal coor-
45 dination (Chen et al. 1993; Maire et al. 2012) and least-cost (Wright et al. 2003)
46 theories, posits that plants optimize photosynthetic processes by minimizing the
47 summed cost of nitrogen and water use (referred to here and in the rest of this

48 dissertation as β). The summed cost of nitrogen and water use is predicted to
49 be positively correlated with the ratio of intercellular CO₂ to atmospheric CO₂
50 (referred to here and in the rest of this dissertation as leaf $C_i:C_a$, which is deter-
51 mined by factors that influence leaf nitrogen demand, such as CO₂, temperature,
52 vapor pressure deficit, and light availability (Prentice et al. 2014; Smith et al.
53 2019; Stocker et al. 2020; Wang et al. 2017). Photosynthetic processes are opti-
54 mized such that nitrogen is allocated to photosynthetic enzymes in to allow net
55 photosynthesis rates to be equally co-limited by the maximum rate of Rubisco
56 carboxylation and the maximum rate of Ribulose-1,5-bisphosphate (RuBP) re-
57 generation (Chen et al. 1993; Maire et al. 2012). The theory indicates that costs
58 of nitrogen and water use are substitutable such that, in a given environment,
59 optimal photosynthesis rates can be achieved by sacrificing inefficient use of a
60 relatively more abundant (and less costly to acquire) resource for more efficient
61 use of a relatively less abundant (and more costly to acquire) resource. These
62 predictions imply that acclimation responses to changing environments may be
63 partially driven by trade-offs between nitrogen and water use, though empirical
64 tests of the theory are sparse.

65 Optimality models leveraging patterns expected from photosynthetic least-
66 cost theory have been developed for both C₃ (Wang et al. 2017; Smith et al. 2019;
67 Stocker et al. 2020) and more recently for C₄ species (Scott and Smith 2022). Such
68 models show broad agreement with patterns observed across environmental gradi-
69 ents (Paillassa et al. 2020; Querejeta et al. 2022; Smith et al. 2019; Westerband
70 et al. 2023), and are capable of reconciling dynamic leaf nitrogen-photosynthesis
71 relationships and acclimation responses to elevated CO₂, temperature, light avail-

72 ability, and vapor pressure deficit (Dong et al. 2017; Dong et al. 2020; Dong et al.
73 2022; Dong et al. 2022; Smith and Keenan 2020; Luo et al. 2021; Peng et al. 2021;
74 Querejeta et al. 2022; Westerband et al. 2023). Current versions of optimality
75 models that invoke patterns expected from photosynthetic least-cost theory hold
76 β constant across growing environments. As growing evidence suggests that costs
77 of nitrogen use change across resource availability and climatic gradients in species
78 with different nutrient acquisition strategies (Fisher et al. 2010; Brzostek et al.
79 2014; Allen et al. 2020; Terrer et al. 2018), one might expect that β should
80 dynamically change across environments and in species with different acquisition
81 strategies. However, manipulative experiments that test mechanisms underlying
82 nitrogen-water use trade-offs and leaf nitrogen-photosynthesis relationships pre-
83 dicted from theory across soil resource availability and climatic gradients are rare.
84 Furthermore, no study has related shifts in β to nitrogen-water use trade-offs or
85 leaf nitrogen-photosynthesis relationships. Understanding the dynamic nature of
86 β across different environmental contexts and impacts of β on patterns expected
87 from theory are critical for further optimality model development, and is the cen-
88 tral motivation for the experiments presented in this dissertation.

89 In this dissertation, I use four experiments to quantify nutrient acquisition
90 and allocation responses under different environmental conditions and in species
91 with different nutrient acquisition strategies. These experiments provide impor-
92 tant empirical data needed to evaluate patterns expected from photosynthetic
93 least-cost theory and test mechanisms that drive such patterns. In the first ex-
94 perimental chapter, I re-analyze data from a greenhouse experiment that grew
95 *Glycine max* L. (Merr) and *Gossypium hirsutum* seedlings under full-factorial

96 combinations of four light treatments and four fertilization treatments. This re-
97 analysis examined the effect of soil nitrogen availability and light availability on
98 structural carbon costs to acquire nitrogen in a species capable of forming associ-
99 ations with symbiotic nitrogen-fixing bacteria (*G. max*) and a species not capable
100 of forming such associations (*G. hirsutum*). I find strong evidence suggesting that
101 increasing light availability increases structural carbon costs to acquire nitrogen
102 and that increasing soil nitrogen fertilization decreases structural carbon costs to
103 acquire nitrogen.

104 In the second experimental chapter, I measure leaf physiological traits in
105 the upper canopy of mature trees growing in a 9-year nitrogen-by-pH field manip-
106 ulation experiment to assess whether changes in soil nitrogen availability or soil
107 pH modify nitrogen-water use trade-offs expected from photosynthetic least-cost
108 theory. I find strong nitrogen-water use trade-offs in response to increasing soil ni-
109 trogen availability, indicated by a strong negative relationship between leaf $C_i:C_a$
110 (referred to here and in the rest of this dissertation as χ) and leaf nitrogen content,
111 as well as a strong increase in leaf nitrogen content per unit leaf χ with increas-
112 ing soil nitrogen availability. Interestingly, I also find a null effect of soil pH on
113 nitrogen-water use trade-offs. These patterns provide strong support for patterns
114 expected from photosynthetic least-cost theory across soil nitrogen availability
115 gradients, and indicate that previous studies which note strong nitrogen-water
116 use trade-offs in response to soil pH may be driven by covariation between soil
117 nitrogen availability and soil pH (Paillassa et al. 2020; Westerband et al. 2023).

118 In the third experimental chapter, I leverage a broad precipitation and soil
119 nutrient availability gradient in Texan grasslands to investigate primary drivers of

120 leaf nitrogen content. In this chapter, I directly quantify β and χ using leaf $\delta^{13}\text{C}$ to
121 examine primary drivers of leaf nitrogen content and find that leaf nitrogen content
122 is driven through a negative relationship with χ . I also show that soil nitrogen
123 availability is negatively associated with β , and that β is positively associated
124 with χ . I show strong support for patterns expected from theory, showing for
125 the first time that positive effects of increasing soil nitrogen availability on leaf
126 nitrogen content are mediated by changes in β .

127 In the fourth experimental chapter, I use reach-in growth chambers to
128 quantify leaf and whole plant acclimation responses to CO_2 across a soil nitro-
129 gen fertilization gradient, while also manipulating nutrient acquisition strategy
130 by controlling whether seedlings were able to form associations with symbiotic
131 nitrogen-fixing bacteria. Specifically, I measure leaf physiological and whole plant
132 growth responses of 7-week *G. max* seedlings grown under one of two CO_2 treat-
133 ments, one of nine fertilization treatments, and one of two inoculation treatments
134 in a full factorial design. I find a down-regulation in leaf nitrogen content and
135 leaf photosynthesis under elevated CO_2 , a pattern that is not modified across
136 the fertilization gradient or between inoculation treatments. However, I also find
137 strong stimulation in total leaf area and whole plant growth under elevated CO_2
138 that are enhanced with increasing fertilization. There was no observable effect of
139 inoculation in modifying whole plant growth responses to CO_2 , which I speculate
140 is the result of a down-regulation in plant investments to nitrogen fixation with
141 increasing fertilization. Results from this experiment provide strong evidence sug-
142 gesting that leaf acclimation responses to CO_2 were controlled by optimal resource
143 investment to photosynthetic capacity, following patterns expected from photo-

144 synthetic least-cost theory, and suggest divergent roles of soil nitrogen fertilization
145 in modifying leaf and whole plant acclimation responses to CO₂.

146 Throughout the four experimental chapters, I find strong and consistent
147 patterns supportive of patterns expected from photosynthetic least-cost theory.
148 Specifically, I find strong nitrogen-water use trade-offs in response to changing
149 climates and soil resources, that shifts in soil nitrogen availability have strong
150 negative impacts on costs of nitrogen acquisition, and therefore tend to increase
151 β , and that constant leaf nitrogen-photosynthesis relationships only occur in sys-
152 tems where nitrogen is limiting. In a final conclusion chapter, I summarize ma-
153 jor findings from each of the four experimental chapters and synthesize common
154 mechanisms that drive leaf and whole plant responses to changing environmen-
155 tal conditions. I conclude this dissertation with brief dialogue on lessons learned
156 throughout experimental chapters, and propose future experiments that will tar-
157 get additional uncertainties in photosynthetic least-cost theory responses across
158 environmental gradients.

159

Chapter 2

160

Structural carbon costs to acquire nitrogen are determined by
161 nitrogen and light availability in two species with different nitrogen
162 acquisition strategies

163 2.1 Introduction

164

Carbon and nitrogen cycles are tightly coupled in terrestrial ecosystems.

165

This tight coupling influences photosynthesis (Walker et al. 2014; Rogers et al.

166

2017), net primary productivity (LeBauer and Treseder 2008; Thomas et al. 2013),

167

decomposition (Cornwell et al. 2008; Bonan et al. 2013; Sulman et al. 2019), and

168

plant resource competition (Gill and Finzi 2016; Xu-Ri and Prentice 2017). Ter-

169

restrial biosphere models are beginning to include connected carbon and nitrogen

170

cycles to improve the realism of their simulations (Fisher et al. 2010; Brzostek

171

et al. 2014; Wieder et al. 2015; Shi et al. 2016; Zhu et al. 2019). Simula-

172

tions from these models indicate that coupling carbon and nitrogen cycles can

173

drastically influence future biosphere-atmosphere feedbacks under global change,

174

such as elevated carbon dioxide or nitrogen deposition (Thornton et al. 2007;

175

Goll et al. 2012; Wieder et al. 2015; Wieder et al. 2019). Nonetheless, there

176

are still limitations in our quantitative understanding of connected carbon and

177

nitrogen dynamics (Thomas et al. 2015; Meyerholt et al. 2016; Rogers et al.

178

2017; Exbrayat et al. 2018; Shi et al. 2019), forcing models to make potentially

179

unreliable assumptions.

180

Plant nitrogen acquisition is a process in terrestrial ecosystems by which

181

carbon and nitrogen are tightly coupled (Vitousek and Howarth 1991; Delaire

182

et al. 2005; Brzostek et al. 2014). Plants must allocate photosynthetically de-

183 rived carbon belowground to produce and maintain root systems or exchange with
184 symbiotic soil microbes in order to acquire nitrogen (Högberg et al. 2008; Hög-
185 berg et al. 2010). Thus, plants have an inherent carbon cost associated with
186 acquiring nitrogen, which can include both direct energetic costs associated with
187 nitrogen acquisition and indirect costs associated with building structures that
188 support nitrogen acquisition (Gutschick 1981; Rastetter et al. 2001; Vitousek
189 et al. 2002; Menge et al. 2008). Model simulations (Fisher et al. 2010; Brzostek
190 et al. 2014; Shi et al. 2016; Allen et al. 2020) and meta-analyses (Terrer et al.
191 2018) suggest that these carbon costs vary between species, particularly those
192 with different nitrogen acquisition strategies. For example, simulations using iter-
193 ations of the Fixation and Uptake of Nitrogen (FUN) model indicate that species
194 that acquire nitrogen from non-symbiotic active uptake pathways (e.g. mass flow)
195 generally have larger carbon costs to acquire nitrogen than species that acquire
196 nitrogen through symbiotic associations with nitrogen-fixing bacteria (Brzostek
197 et al. 2014; Allen et al. 2020).

198 Carbon costs to acquire nitrogen likely vary in response to changes in soil
199 nitrogen availability. For example, if the primary mode of nitrogen acquisition
200 is through non-symbiotic active uptake, then nitrogen availability could decrease
201 carbon costs to acquire nitrogen as a result of increased per-root nitrogen up-
202 take (Franklin et al. 2009; Wang et al. 2018). However, if the primary mode of
203 nitrogen acquisition is through symbiotic active uptake, then nitrogen availabil-
204 ity may incur additional carbon costs to acquire nitrogen if it causes microbial
205 symbionts to shift toward parasitism along the parasitism–mutualism continuum
206 (Johnson et al. 1997; Hoek et al. 2016; Friel and Friesen 2019) or if it reduces

207 the nitrogen acquisition capacity of a microbial symbiont (van Diepen et al. 2007;
208 Soudzilovskaia et al. 2015; Muñoz et al. 2016). Species may respond to shifts in
209 soil nitrogen availability by switching their primary mode of nitrogen acquisition
210 to a strategy with lower carbon costs to acquire nitrogen in order to maximize
211 the magnitude of nitrogen acquired from a belowground carbon investment and
212 outcompete other individuals for soil resources (Rastetter et al. 2001; Menge et al.
213 2008).

214 Environmental conditions that affect demand to acquire nitrogen to sup-
215 port new and existing tissues could also be a source of variance in plant carbon
216 costs to acquire nitrogen. For example, an increase in plant nitrogen demand could
217 increase carbon costs to acquire nitrogen if this increases the carbon that must be
218 allocated belowground to acquire a proportional amount of nitrogen (Kulmatiski
219 et al. 2017; Noyce et al. 2019). This could be driven by a temporary state of
220 diminishing return associated with investing carbon toward building and main-
221 taining structures that are necessary to support enhanced nitrogen uptake, such
222 as fine roots (Matamala and Schlesinger 2000; Norby et al. 2004; Arndal et al.
223 2018), mycorrhizal hyphae (Saleh et al. 2020), or root nodules (Parvin et al. 2020).
224 Alternatively, if the environmental factor that increases plant nitrogen demand
225 causes nitrogen to become more limiting in the system (e.g. atmospheric CO₂;
226 Luo et al. (2004), LeBauer and Treseder (2008), Vitousek et al. (2010), Liang
227 et al. (2016)), species might switch their primary mode of nitrogen acquisition to
228 a strategy with lower relative carbon costs to acquire nitrogen in order to gain a
229 competitive advantage over species with either different or more limited modes of
230 nitrogen acquisition (Ainsworth and Long 2005; Taylor and Menge 2018).

231 Using a plant economics approach, I examined the influence of plant ni-
232 trogen demand and soil nitrogen availability on plant carbon costs to acquire
233 nitrogen. This was done by growing a species capable of forming associations
234 with nitrogen-fixing bacteria (*Glycine max* L. (Merr)) and a species not capable
235 of forming these associations (*Gossypium hirsutum* L.) under four levels of light
236 availability (plant nitrogen demand proxy) and four levels of soil nitrogen fertil-
237 ization (soil nitrogen availability proxy) in a full-factorial, controlled greenhouse
238 experiment. I used this experimental set-up to test the following hypotheses:

- 239 1. An increase in plant nitrogen demand due to increasing light availability will
240 increase carbon costs to acquire nitrogen through a proportionally larger
241 increase in belowground carbon than whole-plant nitrogen acquisition. This
242 will be the result of an increased investment of carbon toward belowground
243 structures that support enhanced nitrogen uptake, but at a lower nitrogen
244 return.
- 245 2. An increase in soil nitrogen availability will decrease carbon costs to acquire
246 nitrogen as a result of increased per root nitrogen uptake in *G. hirsutum*.
247 However, soil nitrogen availability will not affect carbon costs to acquire
248 nitrogen in *G. max* because of the already high return of nitrogen supplied
249 through nitrogen fixation.

250 2.2 Methods

251 2.2.1 *Experiment setup*

252 *Gossypium hirsutum* and *G. max* were planted in individual 3 liter pots
253 (NS-300; Nursery Supplies, Orange, CA, USA) containing a 3:1 mix of unfertil-
254 ized potting mix (Sungro Sunshine Mix #2, Agawam, MA, USA) to native soil
255 extracted from an agricultural field most recently planted with *G. max* at the
256 USDA-ARS Laboratory in Lubbock, TX, USA (33.59°N, -101.90°W). The field
257 soil was classified as Amarillo fine sandy loam (75% sand, 10% silt, 15% clay).
258 Upon planting, all *G. max* pots were inoculated with *Bradyrhizobium japonicum*
259 (Verdesian N-Dure™ Soybean, Cary, NC, USA) to stimulate root nodulation. In-
260 dividuals of both species were grown under similar, unshaded, ambient greenhouse
261 conditions for 2 weeks to germinate and begin vegetative growth. Three blocks
262 were set up in the greenhouse, each containing four light treatments created us-
263 ing shade cloth that reduced incoming radiation by either 0 (full sun), 30, 50,
264 or 80%. Two weeks post-germination, individuals were randomly placed in the
265 four light treatments in each block. Individuals received one of four nitrogen fer-
266 tilization doses as 100ml of a modified Hoagland solution (Hoagland and Arnon
267 1950) equivalent to either 0, 70, 210, or 630 ppm N twice per week within each
268 light treatment. Nitrogen fertilization doses were received as topical agents to
269 the soil surface. Each Hoagland solution was modified to keep concentrations of
270 other macro- and micronutrients equivalent (Supplementary Table S1). Plants
271 were routinely well watered to eliminate water stress.

272 2.2.2 *Plant measurements and calculations*

273 Each individual was harvested after 5 weeks of treatment, and biomass
274 was separated by organ type (leaves, stems, and roots). Nodules on *G. max*
275 roots were also harvested. Except for the 0% shade cover and 630 ppm N treat-
276 ment combination, all treatment combinations in both species had lower average
277 dry biomass:pot volume ratios than the 1:1 ratio recommended by Poorter et al.
278 (2012) to minimize the likelihood of pot volume-induced growth limitation (Sup-
279 plementary Tables S2, S3; Supplementary Fig. S1). All harvested material was
280 dried, weighed, and ground by organ type. Carbon and nitrogen content (g g^{-1})
281 was determined by subsampling from ground and homogenized biomass of each
282 organ type using an elemental analyzer (Costech 4010; Costech, Inc., Valencia,
283 CA, USA). We scaled these values to total leaf, stem, and root carbon and ni-
284 trogen biomass (g) by multiplying dry biomass of each organ type by carbon or
285 nitrogen content of each corresponding organ type. Whole-plant nitrogen biomass
286 (g) was calculated as the sum of total leaf (g), stem (g), and root (g) nitrogen
287 biomass. Root nodule carbon biomass was not included in the calculation of root
288 carbon biomass; however, relative plant investment toward root or root nodule
289 standing stock was estimated as the ratio of root biomass to root nodule biomass
290 (g g^{-1}), following similar metrics to those adopted by Dovrat et al. (2018) and
291 Dovrat et al. (2020).

292 Carbon costs to acquire nitrogen (N_{cost} ; gC gN^{-1}) were estimated as the
293 ratio of total root carbon biomass (C_{bg} ; gC) to whole-plant nitrogen biomass
294 (N_{wp} ; gN). This calculation quantifies the relationship between carbon spent on
295 nitrogen acquisition and whole-plant nitrogen acquisition by using root carbon

296 biomass as a proxy for estimating the magnitude of carbon allocated toward ni-
297 trogen acquisition. This calculation therefore assumes that the magnitude of root
298 carbon standing stock is proportional to carbon transferred to root nodules or my-
299 corrhizae, or lost through root exudation or turnover. The assumption has been
300 supported in species that associate with ectomycorrhizal fungi (Hobbie 2006; Hob-
301 bie and Hobbie 2008), but is less clear in species that acquire nitrogen through
302 non-symbiotic active uptake or symbiotic nitrogen fixation. It is also unclear
303 whether relationships between root carbon standing stock and carbon transfer to
304 root nodules are similar in magnitude to carbon lost through exudation or when
305 allocated toward other active uptake pathways. Thus, because of the way mea-
306 surements were calculated, proximal values of carbon costs to acquire nitrogen are
307 underestimates.

308 2.2.3 *Statistical analyses*

309 I explored the effects of light and nitrogen availability on carbon costs to ac-
310 quire nitrogen using separate linear mixed-effects models for each species. Models
311 included shade cover, nitrogen fertilization, and interactions between shade cover
312 and nitrogen fertilization as continuous fixed effects, and also included block as a
313 random intercept term. Three separate models for each species were built with
314 this independent variable structure for three different dependent variables: (i)
315 carbon costs to acquire nitrogen (gC gN^{-1}); (ii) whole plant nitrogen biomass (de-
316 nominator of carbon cost to acquire nitrogen; gN); and (iii) belowground carbon
317 biomass (numerator of carbon cost to acquire nitrogen; gC). I constructed two
318 additional models for *G. max* with the same model structure described above to

319 investigate the effects of light availability and nitrogen fertilization on root nodule
320 biomass (g) and the ratio of root nodule biomass to root biomass (unitless).

321 I used Shapiro–Wilk tests of normality to determine whether species spe-
322 cific linear mixed-effects model residuals followed a normal distribution. None of
323 our models satisfied residual normality assumptions when models were fit using
324 untransformed data (Shapiro–Wilk: $p < 0.05$ in all cases). I attempted to satisfy
325 residual normality assumptions by first fitting models using dependent variables
326 that were natural-log transformed. If residual normality assumptions were still
327 not met (Shapiro–Wilk: $p < 0.05$), then models were fit using dependent variables
328 that were square root transformed. All residual normality assumptions were satis-
329 fied when models were fit with either a natural-log or square root transformation
330 (Shapiro–Wilk: $p > 0.05$ in all cases). Specifically, I natural-log transformed *G.*
331 *hirsutum* carbon costs to acquire nitrogen and *G. hirsutum* whole-plant nitrogen
332 biomass. I also square root transformed *G. max* carbon costs to acquire nitrogen,
333 *G. max* whole-plant nitrogen biomass, root carbon biomass in both species, *G.*
334 *max* root nodule biomass, and the *G. max* ratio of root nodule biomass to root
335 biomass. I used the ‘lmer’ function in the ‘lme4’ R package (Bates et al. 2015) to
336 fit each model and the ‘Anova’ function in the ‘car’ R package (Fox and Weisberg
337 2019) to calculate Wald’s χ^2 to determine the significance ($\alpha = 0.05$) of each fixed
338 effect coefficient. Finally, I used the ‘emmeans’ R package (Lenth 2019) to conduct
339 post-hoc comparisons of our treatment combinations using Tukey’s tests. Degrees
340 of freedom for all Tukey’s tests were approximated using the Kenward–Roger ap-
341 proach (Kenward and Roger 1997). All analyses and plots were conducted in R
342 version 4.0.1 (R Core Team 2021).

343 2.3 Results

344 2.3.1 *Carbon costs to acquire nitrogen*

345 Carbon costs to acquire nitrogen in *G. hirsutum* increased with increasing
346 light availability ($p < 0.001$; Table 2.1; Fig. 2.1) and decreased with increasing
347 nitrogen fertilization ($p < 0.001$; Table 2.1; Fig. 2.1). There was no interaction
348 between light availability and nitrogen fertilization ($p = 0.486$, Table 2.1; Fig.
349 2.1).

350 Carbon costs to acquire nitrogen in *G. max* also increased with increasing
351 light availability ($p < 0.001$, Table 2.1; Fig. 2.1) and decreased with increasing
352 nitrogen fertilization ($p < 0.001$; Table 2.1; Fig. 2.1). There was no interaction
353 between light availability and nitrogen fertilization ($p = 0.261$, Table 2.1; Fig.
354 2.1).

Table 2.1. Analysis of variance results exploring species-specific effects of light availability, nitrogen fertilization, and their interactions on carbon costs to acquire nitrogen (N_{cost}), whole-plant nitrogen biomass (N_{wp}), and root carbon biomass (C_{bg})

| | df | N_{cost} | | | N_{wp} | | | C_{bg} | | |
|--------------------|----|-------------------|----------|--------|-----------------|----------|--------|-----------------|----------|--------|
| | | Coefficient | χ^2 | p | Coefficient | χ^2 | p | Coefficient | χ^2 | p |
| <i>G. hirsutum</i> | | | | | | | | | | |
| Intercept | | 1.594 | - | - | -3.232 | - | - | 0.432 | - | - |
| Light (L) | 1 | -1.09E-02 | 56.494 | <0.001 | -6.41E-03 | 91.275 | <0.001 | -2.62E-03 | 169.608 | <0.001 |
| Nitrogen (N) | 1 | -1.34E-03 | 54.925 | <0.001 | 1.83E-03 | 118.784 | <0.001 | 1.15E-04 | 2.901 | 0.089 |
| L*N | 1 | 3.88E-06 | 0.485 | 0.486 | -1.34E-05 | 10.721 | 0.001 | -1.67E-06 | 3.140 | 0.076 |
| <i>G. max</i> | | | | | | | | | | |
| Intercept | | 1.877 | - | - | 0.239 | - | - | 0.438 | - | - |
| Light (L) | 1 | -7.67E-03 | 174.156 | <0.001 | -6.72E-04 | 39.799 | <0.001 | -2.55E-03 | 194.548 | <0.001 |
| Nitrogen (N) | 1 | -2.35E-04 | 21.948 | <0.001 | 1.55E-04 | 70.771 | <0.001 | 2.52E-04 | 19.458 | <0.001 |
| L*N | 1 | -2.89E-06 | 1.262 | 0.261 | -6.32E-07 | 1.435 | 0.231 | -3.16E-06 | 10.803 | 0.001 |

355 *Significance determined using Wald's χ^2 tests ($P = 0.05$). P -values < 0.05 are in bold and p -values between 0.05 and

356 0.1 are italicized. Negative coefficients for light treatments indicate a positive effect of increasing light availability

357 on all response variables, as light availability is treated as percent shade cover in all linear mixed-effects models.

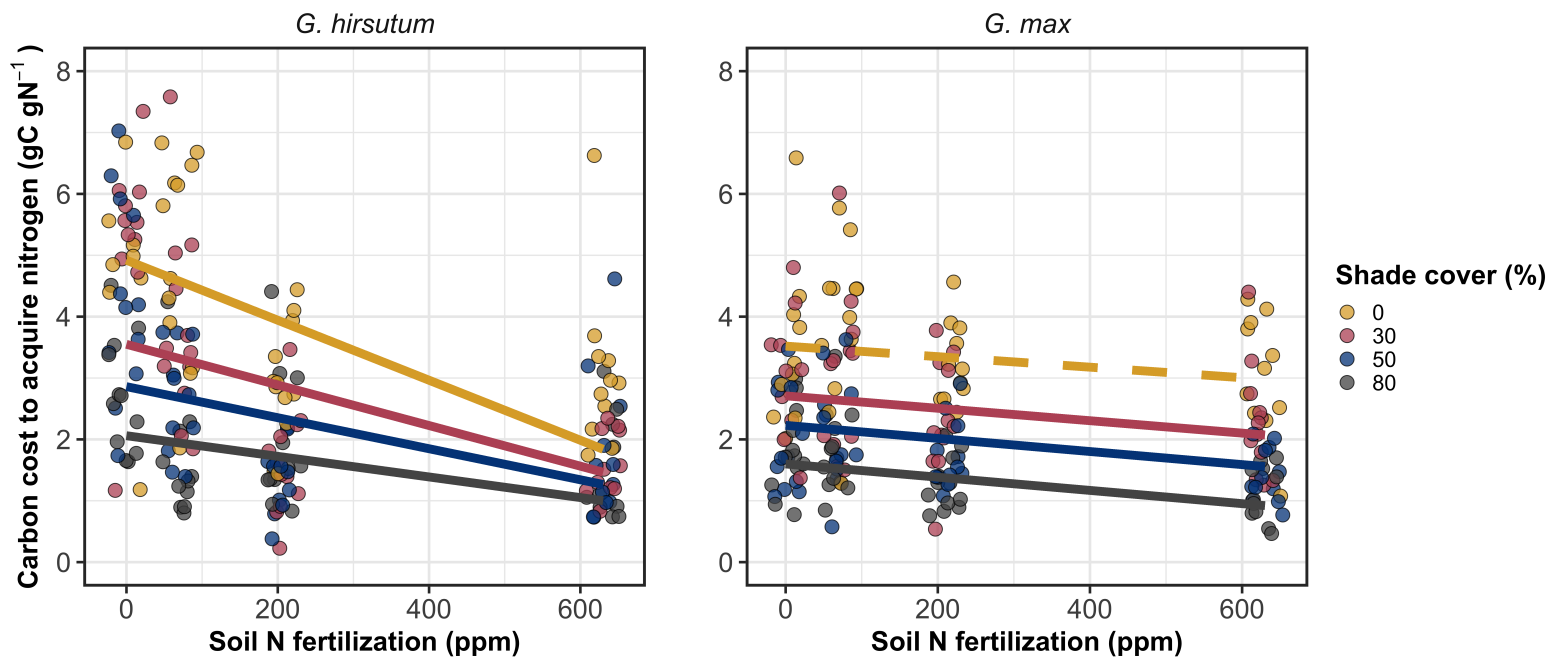


Figure 2.1. Relationships between soil nutrient fertilization and light availability on carbon costs to acquire nitrogen in *G. hirsutum* and *G. max*. Nitrogen fertilization treatments are represented on the x-axis. Shade cover treatments are represented through colored points and trendlines. Trendlines were created by back-transforming marginal mean slopes and intercepts from species-specific linear mixed-effects models. These values were calculated using the ‘emtrends’ and ‘emmmeans’ functions in the ‘emmeans’ R package (Lenth, 2019). Yellow points and trendlines represent the 0% shade cover treatment, red points and trendlines represent the 30% shade cover treatment, blue points and trendlines represent the 50% shade cover treatment, and gray points and trendlines represent the 80% shade cover treatment. Solid trendlines indicate slopes that are significantly different from zero (Tukey: $p < 0.05$), while dashed trendlines indicate slopes that are not statistically different from zero.

358 2.3.2 *Whole plant nitrogen biomass*

359 Whole-plant nitrogen biomass in *G. hirsutum* was driven by an interaction
360 between light availability and nitrogen fertilization ($p = 0.001$; Table 2.1; Fig.
361 2.2). This interaction indicated a greater stimulation of whole-plant nitrogen
362 biomass by nitrogen fertilization as light levels increased (Table 2.1; Fig. 2.2).

363 Whole-plant nitrogen biomass in *G. max* increased with increasing light
364 availability ($p < 0.001$) and nitrogen fertilization ($p < 0.001$), with no interaction
365 between light availability and nitrogen fertilization ($p = 0.231$; Table 2.1; Fig.
366 2.2).

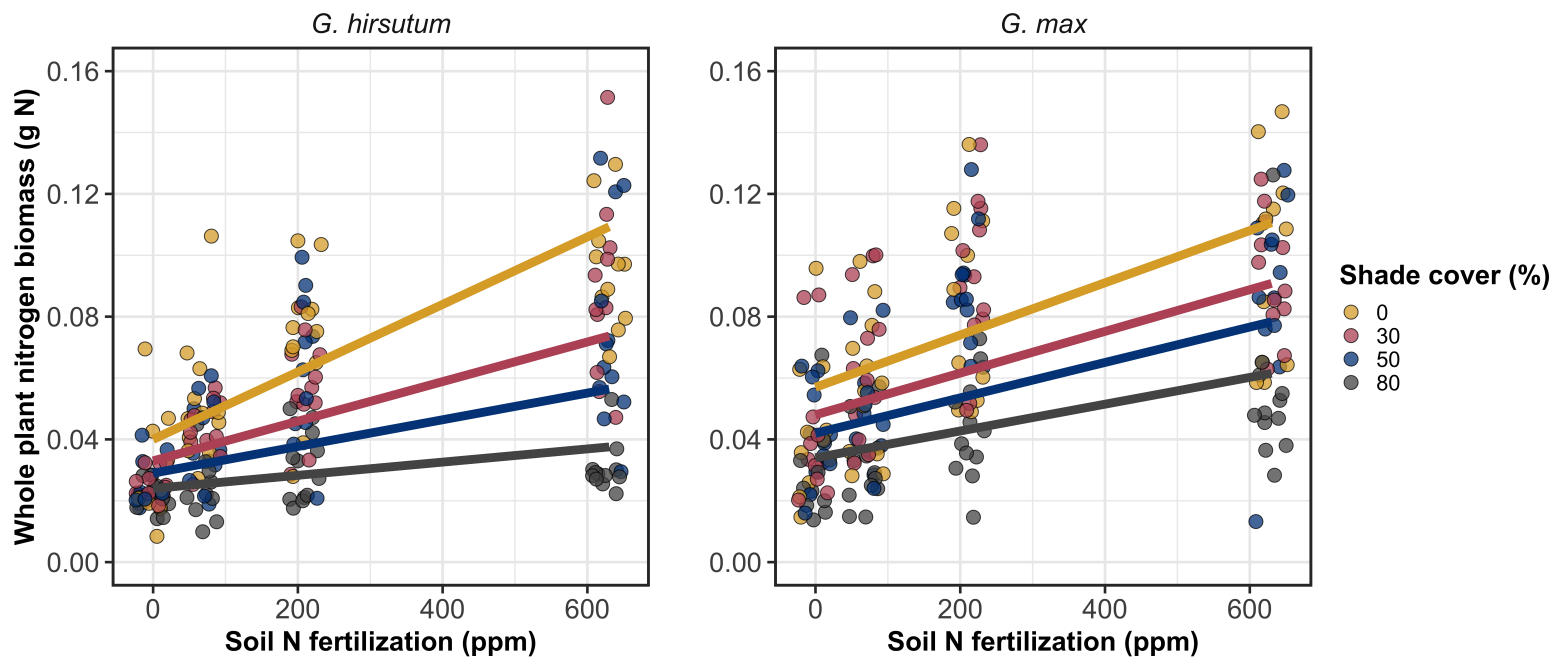


Figure 2.2. Relationships between soil nutrient fertilization and light availability on whole-plant nitrogen biomass in *G. hirsutum* and *G. max*. Whole-plant nitrogen biomass is the denominator of the carbon cost to acquire nitrogen calculation. Nitrogen fertilization treatments are represented on the x-axis. Shade cover treatments are represented through colored points and trendlines. Trendlines were created by back-transforming marginal mean slopes and intercepts from species-specific linear mixed-effects models. These values were calculated using the ‘emtrends’ and ‘emmeans’ functions in the ‘emmeans’ R package (Lenth 2019). Points are jittered for visibility. Colored points and trendlines are as explained in Fig. 2.1. Solid trendlines indicate slopes that are significantly different from zero (Tukey: $p < 0.05$), while dashed trendlines indicate slopes that are not statistically different from zero.

367 2.3.3 *Root carbon biomass*

368 Root carbon biomass in *G. hirsutum* significantly increased with increasing
369 light availability ($p < 0.001$; Table 2.1; Fig. 2.3) and marginally increased with
370 nitrogen fertilization ($p = 0.089$; Table 2.1; Fig. 2.3). There was also a marginal
371 interaction between light availability and nitrogen fertilization ($p = 0.076$; Table
372 2.1), driven by an increase in the positive response of root carbon biomass to
373 increasing nitrogen fertilization as light availability increased. This resulted in
374 significantly positive trends between root carbon biomass and nitrogen fertilization
375 in the two highest light treatments (Tukey: $p < 0.05$ in both cases; Table 2.3;
376 Fig. 2.3) and no effect of nitrogen fertilization in the two lowest light treatments
377 (Tukey: $p > 0.05$ in both cases; Table 2.3; Fig. 2.3).

378 There was an interaction between light availability and nitrogen fertiliza-
379 tion on root carbon biomass in *G. max* ($p = 0.001$; Table 2.1; Fig. 2.3). Post-hoc
380 analyses indicated that the positive effects of nitrogen fertilization on *G. max* root
381 carbon biomass increased with increasing light availability (Table 2.3; Fig. 2.3).
382 There were also positive individual effects of increasing nitrogen fertilization ($p <$
383 0.001) and light availability ($p < 0.001$) on *G. max* root carbon biomass (Table
384 2.1; Fig. 2.3).

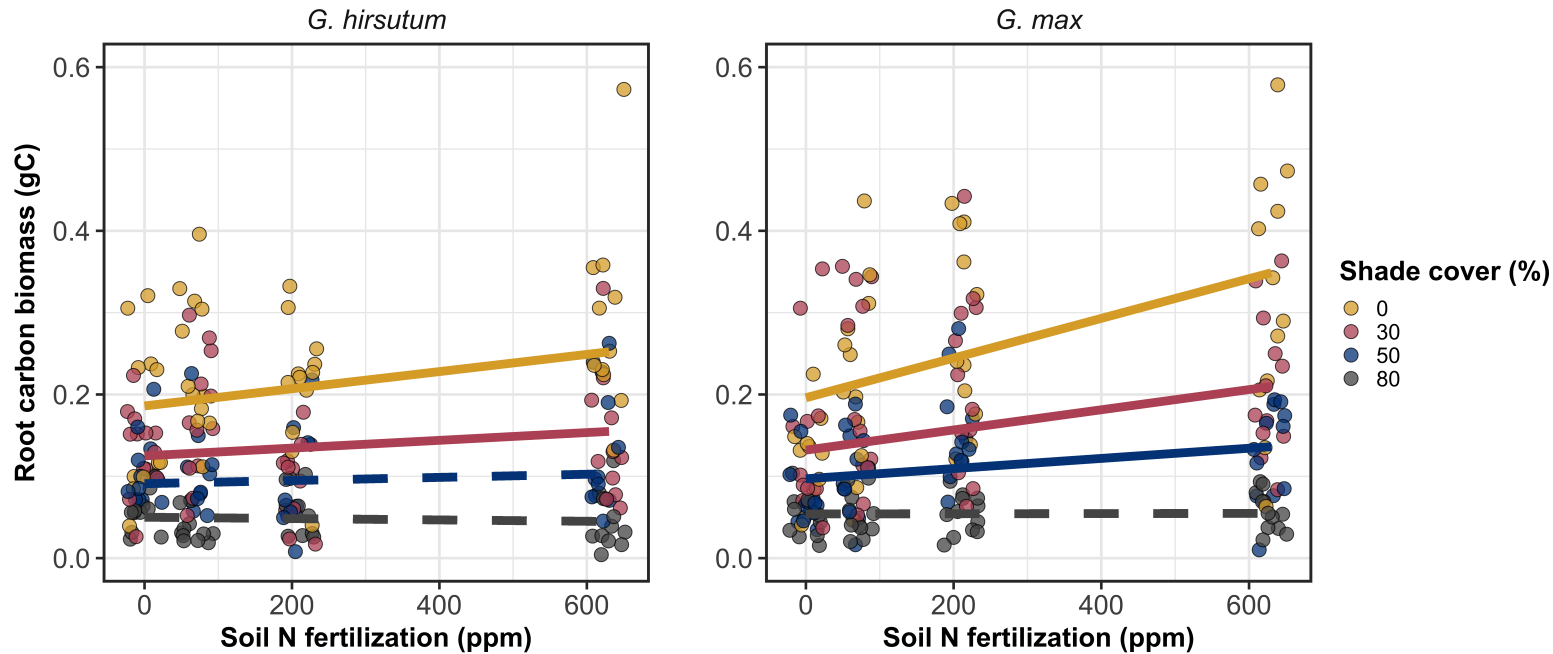


Figure 2.3. Relationships between soil nutrient fertilization and light availability on root carbon biomass in *G. hirsutum* and *G. max*. Root carbon biomass is the numerator of the carbon cost to acquire nitrogen calculation. Nitrogen fertilization treatments are represented on the x-axis. Shade cover treatments are represented through colored points and trendlines. Trendlines were created by back-transforming marginal mean slopes and intercepts from species-specific linear mixed-effects models. These values were calculated using the ‘emtrends’ and ‘emmmeans’ functions in the ‘emmeans’ R package (Lenth 2019). Points are jittered for visibility. Colored points and trendlines are as explained in Fig. 2.1.

Yellow points and trendlines represent the 0% shade cover treatment, blue points and trendlines represent the 30% shade cover treatment, green points and trendlines represent the 50% shade cover treatment, and purple points and trendlines represent the 80% shade cover treatment. Solid trendlines indicate slopes that are significantly different from zero (Tukey: $p < 0.05$), while dashed trendlines indicate slopes that are not statistically different from zero.

385 2.3.4 *Root nodule biomass*

386 Root nodule biomass in *G. max* increased with increasing light availability
387 ($p < 0.001$; Table 2.2; Fig. 2.4A) and decreased with increasing nitrogen fertiliza-
388 tion ($p < 0.001$; Table 2.2; Fig. 2.4A). There was no interaction between nitrogen
389 fertilization and light availability ($p = 0.133$; Table 2.2; Fig. 2.4A). The ratio of
390 root nodule biomass to root biomass did not change in response to light avail-
391 ability ($p = 0.481$; Table 2.2; Fig. 2.4B) but decreased with increasing nitrogen
392 fertilization ($p < 0.001$; Table 2.2; Fig. 2.4B). There was no interaction between
393 nitrogen fertilization and light availability on the ratio of root nodule biomass to
394 root biomass ($p = 0.621$; Table 2.2; Fig. 2.4B).

Table 2.2. Analysis of variance results exploring effects of light availability, nitrogen fertilization, and their interactions on *G. max* root nodule biomass and the ratio of root nodule biomass to root biomass*

| | Nodule biomass | | | Nodule biomass: root biomass | | | <i>p</i> |
|--------------|----------------|-------------|----------|------------------------------|-------------|----------|------------------|
| | df | Coefficient | χ^2 | <i>p</i> | Coefficient | χ^2 | |
| (Intercept) | | 0.302 | - | - | 0.448 | - | - |
| Light (L) | 1 | -1.81E-03 | 72.964 | <0.001 | -8.76E-05 | 0.496 | 0.481 |
| Nitrogen (N) | 1 | -2.83E-04 | 115.377 | <0.001 | -5.09E-04 | 156.476 | <0.001 |
| L*N | 1 | 1.14E-06 | 2.226 | 0.133 | -7.30E-07 | 0.244 | 0.621 |

395 *Significance determined using Wald's χ^2 tests ($\alpha = 0.05$). *P*-values less than 0.05 are in bold. Negative coefficients
 396 for light treatments indicate a positive effect of increasing light availability on all response variables, as light avail-
 397 ability is treated as percent shade cover in all linear mixed-effects models. Root nodule biomass and nodule biomass:
 398 root biomass models were only constructed for *G. max* because *G. hirsutum* was not inoculated with *B. japonicum*
 399 and is not capable of forming root nodules.

Table 2.3. Slopes of the regression line describing the relationship between each dependent variable and nitrogen fertilization at each light level*

| Shade cover | Carbon cost to acquire nitrogen | Whole plant N biomass | Belowground C biomass | Root nodule biomass | Nodule biomass: root biomass |
|--------------------|---------------------------------|-----------------------------|-----------------------------|------------------------------|------------------------------|
| <i>G. hirsutum</i> | | | | | |
| 0% | -1.34E-03^a | 1.83E-03^a | 1.15E-04^b | - | - |
| 30% | -1.22E-03^a | 1.43E-03^a | 1.17E-04^b | - | - |
| 50% | -1.14E-03^a | 1.17E-03^a | 3.12E-05 ^b | - | - |
| 80% | -1.02E-03^a | 7.66E-04^a | -1.89E-06 ^b | - | - |
| <i>G. max</i> | | | | | |
| 0% | -2.35E-04 ^b | 1.55E-05^b | 2.51E-04^b | -2.83E-04^b | -5.09E-04^b |
| 30% | -3.22E-04^b | 1.35E-05^b | 1.57E-04^b | -2.49E-04^b | -5.31E-04^b |
| 50% | -3.80E-04^b | 1.23E-05^b | 9.37E-05^b | -2.26E-04^b | -5.45E-04^b |
| 80% | -4.66E-04^b | 1.04E-05^b | -9.95E-07 ^b | -1.92E-04^b | -5.67E-04^b |

25

400 *Slopes represent estimated marginal mean slopes from linear mixed-effects models described in the Methods. Slopes
 401 were calculated using the ‘emmeans’ R package (Lenth 2019). Superscripts indicate slopes fit to natural-log^(a) or
 402 square root^(b) transformed data. Slopes statistically different from zero (Tukey: $p < 0.05$) are indicated in bold.
 403 Marginally significant slopes (Tukey: $0.05 < p < 0.1$) are italicized.

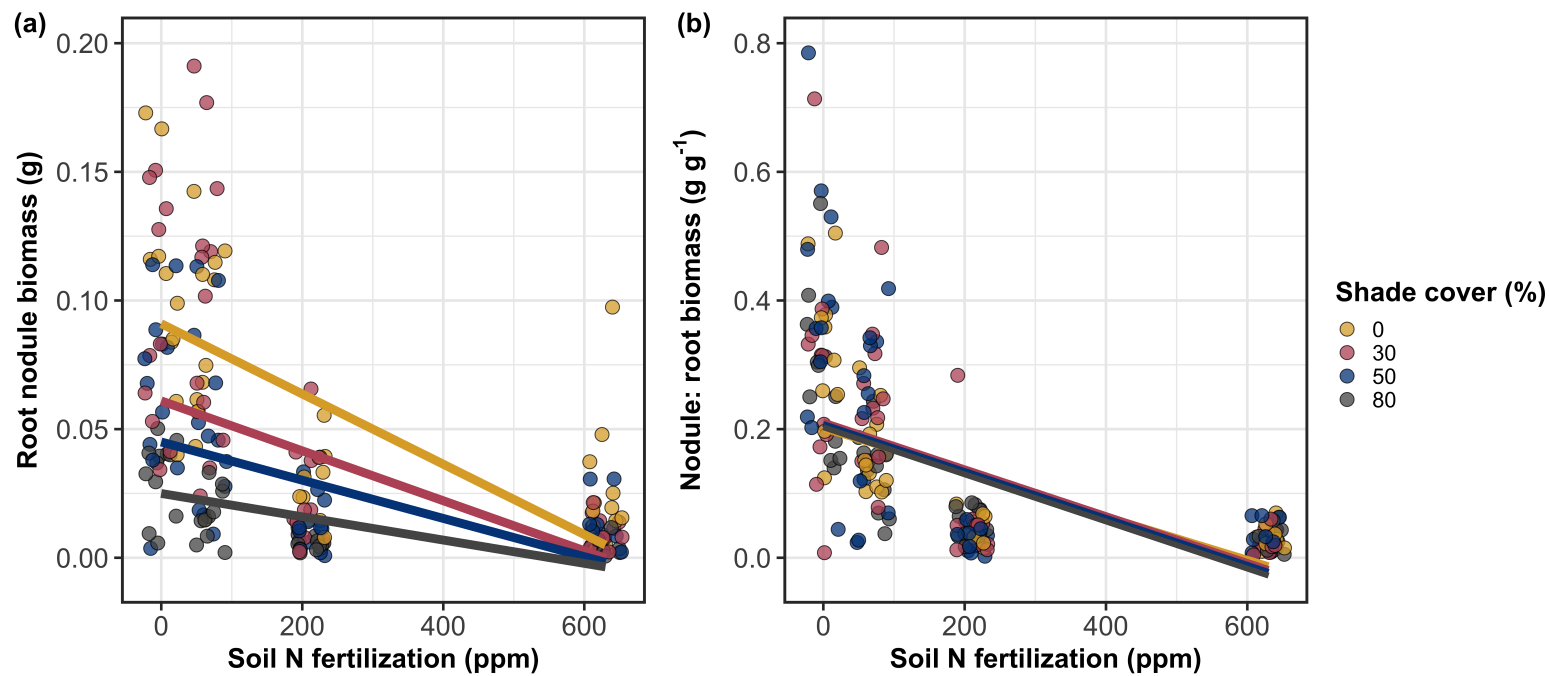


Figure 2.4. Effects of shade cover and nitrogen fertilization on root nodule biomass (A) and the ratio of root nodule biomass to root biomass (B) in *G. max*. Nitrogen fertilization treatments are represented on the x-axis. Shade cover treatments are represented through colored points and trendlines. Trendlines were created by back-transforming marginal mean slopes and intercepts from species-specific linear mixed-effects models. These values were calculated using the ‘emtrends’ and ‘emmeans’ functions in the ‘emmeans’ R package (Lenth 2019). Points are jittered for visibility. Yellow points and trendlines represent the 0% shade cover treatment, blue points and trendlines represent the 30% shade cover treatment, green points and trendlines represent the 50% shade cover treatment, and purple points and trendlines represent the 80% shade cover treatment. Solid trendlines indicate slopes that are significantly different from zero (Tukey: $p < 0.05$), while dashed trendlines indicate slopes that are not statistically different from zero.

404 2.4 Discussion

405 In this chapter, I determined the effects of light availability and soil ni-
406 trogen fertilization on root mass carbon costs to acquire nitrogen in *G. hirsutum*
407 and *G. max*. In support of my hypotheses, I found that carbon costs to acquire
408 nitrogen generally increased with increasing light availability and decreased with
409 increasing soil nitrogen fertilization in both species. These findings suggest that
410 carbon costs to acquire nitrogen are determined by factors that influence plant
411 nitrogen demand and soil nitrogen availability. In contrast to my second hypothe-
412 sis, root nodulation data suggested that *G. max* and *G. hirsutum* achieved similar
413 directional carbon cost responses to nitrogen fertilization despite a likely shift in
414 *G. max* allocation from nodulation to root biomass along the nitrogen fertilization
415 gradient (Fig. 2.4B).

416 2.4.1 *Carbon costs to acquire nitrogen increase with light availability and*
417 *decrease with fertilization*

418 Both *G. max* and *G. hirsutum* experienced an increase in carbon costs to
419 acquire nitrogen due to increasing light availability. These patterns were driven by
420 a larger increase in root carbon biomass than whole-plant nitrogen biomass. In-
421 creases in root carbon biomass due to factors that increase plant nitrogen demand
422 are a commonly observed pattern, as carbon allocated belowground provides sub-
423 strate needed to produce and maintain structures that satisfy aboveground plant
424 nitrogen demand (Nadelhoffer and Raich 1992; Giardina et al. 2005; Raich et al.
425 2014). Findings suggest that plants allocate relatively more carbon for acquiring
426 nitrogen when demand increases over short temporal scales, which may cause a

427 temporary state of diminishing return due to asynchrony between belowground
428 carbon and whole-plant nitrogen responses to plant nitrogen demand (Kulmatiski
429 et al. 2017; Noyce et al. 2019). These responses might be attributed to a temporal
430 lag associated with producing structures that enhance nitrogen acquisition. For
431 example, fine roots (Matamala and Schlesinger 2000; Norby et al. 2004; Arndal
432 et al. 2018) and root nodules (Parvin et al. 2020) take time to build and first
433 require the construction of coarse roots. Thus, full nitrogen returns from these
434 investments may not occur immediately (Kayler et al. 2010; Kayler et al. 2017),
435 and may vary by species acquisition strategy. I speculate that increases in ni-
436 trogen acquisition from a given carbon investment may occur beyond the 5-week
437 scope of this experiment. A similar study conducted over a longer temporal scale
438 would address this.

439 Increasing soil nitrogen fertilization generally decreased carbon costs to
440 acquire nitrogen in both species. These patterns were driven by a larger increase
441 in whole-plant nitrogen biomass than root carbon biomass. In *G. hirsutum*, re-
442 ductions in carbon costs to acquire nitrogen may have been due to an increase in
443 per-root nitrogen uptake, allowing individuals to maximize the amount of nitro-
444 gen acquired from a belowground carbon investment. Interestingly, increased soil
445 nitrogen fertilization increased whole-plant nitrogen biomass in *G. max* despite
446 reductions in root nodule biomass that likely reduced the nitrogen-fixing capac-
447 ity of *G. max* (Andersen et al. 2005; Muñoz et al. 2016). While reductions in
448 root nodulation due to increased soil nitrogen availability are commonly observed
449 (Gibson and Harper 1985; Fujikake et al. 2003), root nodulation responses were
450 observed in tandem with increased root carbon biomass, implying that *G. max*

451 shifted relative carbon allocation from nitrogen fixation to soil nitrogen acquisition
452 (Markham and Zekveld 2007; Dovrat et al. 2020). This was likely because
453 there was a reduction in the carbon cost advantage of acquiring fixed nitrogen
454 relative to soil nitrogen, and suggests that species capable of associating with
455 symbiotic nitrogen-fixing bacteria shift their relative nitrogen acquisition path-
456 way to optimize nitrogen uptake (Rastetter et al. 2001). Future studies should
457 further investigate these patterns with a larger quantity of phylogenetically re-
458 lated species, or different varieties of a single species that differ in their ability to
459 form associations with symbiotic nitrogen-fixing bacteria to more directly test the
460 impact of nitrogen fixation on the patterns observed in this study.

461 2.4.2 *Modeling implications*

462 Carbon costs to acquire nitrogen are subsumed in the general discussion of
463 economic analogies to plant resource uptake (Bloom et al. 1985; Rastetter et al.
464 2001; Vitousek et al. 2002; Phillips et al. 2013; Terrer et al. 2018; Henneron et al.
465 2020). Despite this, terrestrial biosphere models rarely include costs of nitrogen
466 acquisition within their framework for predicting plant nitrogen uptake. There
467 is currently one plant resource uptake model, FUN, that quantitatively predicts
468 carbon costs to acquire nitrogen within a framework for predicting plant nitrogen
469 uptake for different nitrogen acquisition strategies (Fisher et al. 2010; Brzostek
470 et al. 2014). Iterations of FUN are currently coupled to two terrestrial biosphere
471 models: the Community Land Model 5.0 and the Joint UK Land Environment
472 Simulator (Shi et al. 2016; Lawrence et al. 2019; Clark et al. 2011). Recent work
473 suggests that coupling FUN to CLM 5.0 caused a large overprediction of plant

474 nitrogen uptake associated with nitrogen fixation (Davies-Barnard et al. 2020)
475 compared to other terrestrial biosphere model products. Thus, empirical data
476 from manipulative experiments that explicitly quantify carbon costs to acquire
477 nitrogen in species capable of associating with nitrogen-fixing bacteria across dif-
478 ferent environmental contexts is an important step toward identifying potential
479 biases in models such as FUN.

480 My findings broadly support the FUN formulation of carbon costs to ac-
481 quire nitrogen in response to soil nitrogen availability. FUN calculates carbon
482 costs to acquire nitrogen based on the sum of carbon costs to acquire nitrogen
483 via nitrogen fixation, mycorrhizal active uptake, non-mycorrhizal active uptake,
484 and retranslocation (Fisher et al. 2010; Brzostek et al. 2014). Carbon costs to
485 acquire nitrogen via mycorrhizal or non-mycorrhizal active uptake pathways are
486 derived as a function of nitrogen availability, root biomass, and two parameterized
487 values based on nitrogen acquisition strategy (Brzostek et al. 2014). Due to this,
488 FUN simulates a net decrease in carbon costs to acquire nitrogen with increasing
489 nitrogen availability for mycorrhizal and non-mycorrhizal active uptake pathways,
490 assuming constant root biomass. This was a pattern I observed in *G. hirsutum*
491 regardless of light availability. In contrast, FUN would not simulate a net change
492 in carbon costs to acquire nitrogen via nitrogen fixation due to nitrogen avail-
493 ability. This is because carbon costs to acquire nitrogen via nitrogen fixation are
494 derived from a well established function of soil temperature, which is independent
495 of soil nitrogen availability (Houlton et al. 2008; Fisher et al. 2010). I observed
496 a net reduction in carbon costs to acquire nitrogen in *G. max*, except when in-
497 dividuals were grown under 0% shade cover (Fig. 2.1). While a net reduction of

498 carbon costs in response to nitrogen fertilization runs counter to nitrogen fixa-
499 tion carbon costs simulated by FUN, these patterns were likely because *G. max*
500 individuals switched their primary mode of nitrogen acquisition from symbiotic
501 nitrogen fixation to a non-symbiotic active uptake pathway (Fig. 2.4B).

502 2.4.3 *Study limitations*

503 It should be noted that the metric used in this study to determine carbon
504 costs to acquire nitrogen has several limitations. Most notably, this metric uses
505 root carbon biomass as a proxy for estimating the amount of carbon spent on
506 nitrogen acquisition. While it is true that most carbon allocated belowground has
507 at least an indirect structural role in acquiring soil resources, it remains unclear
508 whether this assumption holds true for species that acquire nitrogen via symbi-
509 otic nitrogen fixation. I also cannot quantify carbon lost through root exudates
510 or root turnover, which may increase due to factors that increase plant nitrogen
511 demand (Tingey et al. 2000; Phillips et al. 2011), and can increase the magni-
512 tude of available nitrogen from soil organic matter through priming effects on soil
513 microbial communities (Uselman et al. 2000; Bengtson et al. 2012). It is also not
514 clear whether these assumptions hold under all environmental conditions, such
515 as those that shift belowground carbon allocation toward a different mode of ni-
516 trogen acquisition (Taylor and Menge 2018; Friel and Friesen 2019) or between
517 species with different acquisition strategies. In this study, increasing soil nitrogen
518 fertilization increased carbon investment to roots relative to carbon transferred
519 to root nodules (Fig. 2.4B). By assuming that carbon allocated to root carbon
520 was proportional to carbon allocated to root nodules across all treatment com-

521 binations, these observed responses to soil nitrogen fertilization were likely to be
522 overestimated in *G. max*. I encourage future research to quantify these carbon
523 fates independently.

524 Researchers conducting pot experiments must carefully choose pot volume
525 to minimize the likelihood of growth limitations induced by pot volume (Poorter
526 et al. 2012). Poorter et al. (2012) indicate that researchers are likely to avoid
527 growth limitations associated with pot volume if measurements are collected when
528 the plant biomass:pot volume ratio is less than 1 g L⁻¹. In this experiment, all
529 treatment combinations in both species had biomass:pot volume ratios less than
530 1 g L⁻¹ except for *G. max* and *G. hirsutum* that were grown under 0% shade
531 cover and had received 630 ppm N. Specifically, *G. max* and *G. hirsutum* had
532 average respective biomass:pot volume ratios of 1.24±0.07 g L⁻¹ and 1.34±0.13 g
533 L⁻¹, when grown under 0% shade cover and received 630 ppm N (Supplementary
534 Tables S2, S3; Supplementary Fig. S1). If growth in this treatment combination
535 was limited by pot volume, then individuals may have had larger carbon costs
536 to acquire nitrogen than would be expected if they were grown in larger pots.
537 This pot volume induced growth limitation could cause a reduction in per-root
538 nitrogen uptake associated with more densely packed roots, which could reduce
539 the positive effect of nitrogen fertilization on whole-plant nitrogen biomass relative
540 to root carbon biomass (Poorter et al. 2012).

541 Growth limitation associated with pot volume provides a possible explana-
542 tion for the marginally insignificant effect of increasing nitrogen fertilization on *G.*
543 *max* carbon costs to acquire nitrogen when grown under 0% shade cover (Table
544 2.3; Fig. 2.1). This is because the regression line describing the relationship be-

545 tween carbon costs to acquire nitrogen and nitrogen fertilization in *G. max* grown
546 under 0% shade cover would have flattened if growth limitation had caused larger
547 than expected carbon costs to acquire nitrogen in the 0% shade cover, 630 ppm
548 N treatment combination. This may have been exacerbated by the fact that *G.*
549 *max* likely shifted relative carbon allocation from nitrogen fixation to soil nitrogen
550 acquisition, which could have increased the negative effect of more densely packed
551 roots on nitrogen uptake. These patterns could have also occurred in *G. hirsutum*
552 grown under 0% shade cover; however, there was no change in the effect of nitro-
553 gen fertilization on *G. hirsutum* carbon costs to acquire nitrogen grown under 0%
554 shade cover relative to other shade cover treatments. Regardless, the possibility
555 of growth limitation due to pot volume suggests that effects of increasing nitro-
556 gen fertilization on carbon costs to acquire nitrogen in both species grown under
557 0% shade cover could have been underestimated. Follow-up studies using a simi-
558 lar experimental design with a larger pot volume would be necessary in order to
559 determine whether these patterns were impacted by pot volume-induced growth
560 limitation.

561 2.4.4 *Conclusions*

562 In conclusion, this chapter provides empirical evidence that carbon costs to
563 acquire nitrogen are influenced by light availability and soil nitrogen fertilization
564 in a species capable of acquiring nitrogen via symbiotic nitrogen fixation and a
565 species not capable of forming such associations. We show that carbon costs to
566 acquire nitrogen generally increase with increasing light availability and decrease
567 with increasing nitrogen fertilization. This chapter provides important empirical

568 data needed to evaluate the formulation of carbon costs to acquire nitrogen in
569 terrestrial biosphere models, particularly carbon costs to acquire nitrogen that
570 are associated with symbiotic nitrogen fixation. My findings broadly support the
571 general formulation of these carbon costs in the FUN biogeochemical model in
572 response to shifts in nitrogen availability. However, there is a need for future
573 studies to explicitly quantify carbon costs to acquire nitrogen under different en-
574 vironmental contexts, over longer temporal scales, and using larger selections of
575 phylogenetically related species. In addition, I suggest that future studies mini-
576 mize the limitations associated with the metric used here by explicitly measuring
577 belowground carbon fates independently.

578

Chapter 3

579 Soil nitrogen availability modifies leaf nitrogen economies in mature
580 temperate deciduous forests: a direct test of photosynthetic least-cost
581 theory

582 3.1 Introduction

583 Photosynthesis represents the largest carbon flux between the atmosphere
584 and land surface (IPCC 2021), and plays a central role in biogeochemical cycling
585 at multiple spatial and temporal scales (Vitousek and Howarth 1991; LeBauer and
586 Treseder 2008; Kaiser et al. 2015; Wieder et al. 2015). Therefore, carbon and
587 energy fluxes simulated by terrestrial biosphere models are sensitive to the formu-
588 lation of photosynthetic processes (Ziehn et al. 2011; Bonan et al. 2011; Booth
589 et al. 2012; Smith et al. 2016; Smith et al. 2017) and must be represented using
590 robust, empirically tested processes (Prentice et al. 2015; Wieder et al. 2019).
591 Current formulations of photosynthesis vary across terrestrial biosphere models
592 (Smith and Dukes 2013; Rogers et al. 2017), which causes variation in modeled
593 ecosystem processes (Knorr 2000; Knorr and Heimann 2001; Bonan et al. 2011;
594 Friedlingstein et al. 2014) and casts uncertainty on the ability of these models to
595 accurately predict terrestrial ecosystem responses and feedbacks to global change
596 (Zaehle et al. 2005; Schaefer et al. 2012; Davies-Barnard et al. 2020).

597 Terrestrial biosphere models commonly represent C₃ photosynthesis th-
598 rough variants of the Farquhar et al. (1980) biochemical model (Smith and Dukes
599 2013; Rogers 2014; Rogers et al. 2017). This well-tested photosynthesis model
600 estimates leaf-level carbon assimilation, or photosynthetic capacity, as a function
601 of the maximum rate of Ribulose-1,5-bisphosphate carboxylase-oxygenase (Ru-

602 bisco) carboxylation (V_{cmax}) and the maximum rate of Ribulose-1,5-bisphosphate
603 (RuBP) regeneration (J_{max}) (Farquhar et al. 1980). Many terrestrial biosphere
604 models predict these model inputs based on plant functional group specific linear
605 relationships between leaf nutrient content and V_{cmax} (Smith and Dukes 2013;
606 Rogers 2014; Rogers et al. 2017) under the tenet that a large fraction of leaf
607 nutrients, and nitrogen (N) in particular, are partitioned toward building and
608 maintaining enzymes that support photosynthetic capacity, such as Rubisco (Brix
609 1971; Gulmon and Chu 1981; Evans 1989; Kattge et al. 2009; Walker et al. 2014).
610 Terrestrial biosphere models also predict leaf nutrient content from soil nutrient
611 availability based on the assumption that increasing soil nutrients generally in-
612 creases leaf nutrients (Firn et al. 2019; Li et al. 2020; Liang et al. 2020) which, in
613 the case of N, generally corresponds with an increase in photosynthetic processes
614 (Li et al. 2020; Liang et al. 2020).

615 Recent work calls the generality of relationships between soil nutrient avail-
616 ability, leaf nutrient content, and photosynthetic capacity into question, suggest-
617 ing instead that leaf nutrients and photosynthetic capacity are better predicted as
618 an integrated product of aboveground climate, leaf traits, and soil nutrient avail-
619 ability, rather than soil nutrient availability alone (Dong et al. 2017; Dong et al.
620 2020; Dong et al. 2022; Firn et al. 2019; Smith et al. 2019; Peng et al. 2021).
621 It has been reasoned that this result is because plants allocate added nutrients to
622 growth and storage rather than alterations in leaf chemistry (Smith et al. 2019),
623 perhaps as a result of nutrient limitation of primary productivity (LeBauer and
624 Treseder 2008; Fay et al. 2015). Additionally, recent work suggests that relation-
625 ships between leaf nutrient content and photosynthesis vary across environments,

626 and that the proportion of leaf nutrient content allocated to photosynthetic tis-
627 sue varies over space and time with plant acclimation and adaptation responses
628 to light availability, vapor pressure deficit, soil pH, soil nutrient availability, and
629 environmental factors that influence leaf mass per area (Pons and Pearcy 1994;
630 Niinemets and Tenhunen 1997; Evans and Poorter 2001; Hikosaka and Shigeno
631 2009; Ghimire et al. 2017; Onoda et al. 2017; Luo et al. 2021). The use of linear
632 relationships between leaf nutrient content and Vcmax to predict photosynthetic
633 capacity, as commonly used in terrestrial biosphere models (Rogers 2014), is not
634 capable of detecting such responses.

635 Photosynthetic least-cost theory provides an alternative framework for un-
636 derstanding relationships between soil nutrient availability, leaf nutrient content,
637 and photosynthetic capacity (Harrison et al. 2021). Leveraging a two-input mi-
638 croeconomics approach (Wright et al. 2003), the theory posits that plants accli-
639 mate to a given environment by optimizing leaf photosynthesis rates at the lowest
640 summed cost of using nutrients and water (Prentice et al. 2014; Wang et al. 2017;
641 Smith et al. 2019; Paillassa et al. 2020). Across resource availability gradients,
642 the theory predicts that optimal photosynthetic rates can be achieved by trading
643 less efficient use of a resource that is less costly to acquire (or more abundant)
644 for more efficient use of a resource more costly to acquire (or less abundant). For
645 example, an increase in soil nutrient availability should reduce the cost of acquir-
646 ing and using nutrients (Bae et al. 2015; Eastman et al. 2021; Perkowski et al.
647 2021), which could increase leaf nutrient investments in photosynthetic proteins to
648 allow similar photosynthetic rates to be achieved with higher nutrient use (lower
649 nutrient use efficiency) but lower water use (greater water use efficiency). The

650 theory suggests similar tradeoffs in response to increasing soil pH (Paillassa et al.
651 2020), specifically, that increasing soil pH should reduce the cost of acquiring soil
652 nutrients due to an increase in plant-available nutrient concentration (Paillassa
653 et al. 2020; Dong et al. 2022). The theory is also capable of reconciling dynamic
654 leaf nutrient-photosynthesis relationships at global scales (Luo et al. 2021).

655 Patterns expected from photosynthetic least-cost theory have recently re-
656 ceived empirical support both in global environmental gradient (Smith et al.
657 2019; Paillassa et al. 2020; Luo et al. 2021; Querejeta et al. 2022; Wester-
658 band et al. 2023) and local manipulative invasion (Bialic-Murphy et al. 2021)
659 studies. However, nutrient addition experiments that directly examine nutrient-
660 water use tradeoffs expected from the theory are rare (Guerrieri et al. 2011), and
661 only global gradient studies testing the theory have considered soil pH in their
662 analyses. As a result, there is a need to use nutrient addition and soil pH manu-
663 lation experiments to test mechanisms driving responses predicted by the theory.
664 Such experiments would also be useful to detect whether patterns expected from
665 theory translate to finer spatial scales.

666 In this study, we measured leaf responses to soil N availability in five decid-
667 uous tree species growing in the upper canopy of mature closed canopy temperate
668 forests in the northeastern United States. Soil N availability and pH were manipu-
669 lated through an N-by-pH field manipulation experiment with treatments applied
670 since 2011, eight years prior to measurement. Two different soil N treatments
671 were applied to increase N availability with opposing effects on soil pH. An addi-
672 tional N-free acidifying treatment was expected to decrease soil pH. I hypothesized
673 that increased soil N availability would enable plants to increase nutrient uptake

674 and create more photosynthetic enzymes per leaf, allowing similar photosynthetic
675 rates achieved with lower leaf C_i:C_a and increased leaf N content allocated to
676 photosynthetic leaf tissue. I expected that this response would be driven by a
677 reduction in the cost of acquiring N, which would cause trees to sacrifice efficient
678 N use to enable more efficient use of other limiting resources (i.e., water). Finally,
679 I hypothesized similar leaf responses to increasing soil pH.

680 3.2 Methods

681 3.2.1 *Study site description*

682 We conducted this study in summer 2019 at three stands located within
683 a 20-km radius of Ithaca, NY, USA (42.444 °N, 76.502 °W). All stands contain
684 mature, closed-canopy forests dominated by deciduous tree species. Stands con-
685 tained abundant sugar maple (*Acer saccharum* Marshall), American beech (*Fagus*
686 *grandifolia* Ehrh.), and white ash (*Fraxinus americana* L.), accounting for 43%,
687 15%, and 17% of the total aboveground biomass across the three stands, respec-
688 tively, with less frequent red maple (*Acer rubrum* L.; 9% of total aboveground
689 biomass) and red oak occurrences (*Quercus rubra* L.; 10% of total aboveground
690 biomass). Soils at each site were broadly classified as a channery silt loam Incep-
691 tisols using the USDA NRCS Web Soil Survey data product (Soil Survey Staff
692 2022). Between 2006 and 2020, study sites averaged 972 mm of precipitation per
693 year and had an average temperature of 7.9 °C per a weather station located near
694 the Cornell University campus (42.449 °N, 76.449 °W) part of the NOAA NCEI
695 Global Historical Climatology Network (Menne et al. 2012).

696 3.2.2 *Experimental design*

697 Four 40 m x 40 m plots were set up at each site in 2009, each with an
698 additional 10 m buffer along plot perimeters (60 m x 60 m total). The plots
699 were set up as a nitrogen-by-pH field manipulation experiment, with one each of
700 four treatments at each site. Two nitrogen treatments were applied, both at 50
701 kg N ha⁻¹ yr⁻¹, as either sodium nitrate (NaNO₃) to raise soil pH, or ammonium
702 sulfate ((NH₄)₂SO₄) to acidify; an elemental sulfur treatment was selected to acid-
703 ify without N, applied at the same rate of S addition (57 kg S ha⁻¹ yr⁻¹); and
704 control plots received no additions. All amendments were added in pelletized form
705 using hand-held fertilizer spreaders to both the main plots and buffers. Amend-
706 ments were divided into three equal doses distributed across the growing season
707 from 2011-2017 and added as a single dose from 2018 onward. During 2019, plots
708 were fertilized during the week of May 20.

709 3.2.3 *Leaf gas exchange and trait measurements*

710 We sampled one leaf each from 6 to 10 individuals per plot between June
711 25 and July 12, 2019 for gas exchange measurements (Table S1). Leaves were
712 collected from deciduous broadleaf trees represented across all sites and plots
713 and were replicated in efforts to mimic the species abundance of each plot at
714 each site. We also attempted to collect leaves from the upper canopy to reduce
715 differential shading effects on leaf physiology. Leaves were accessed by pulling
716 down small branches using an arborist's slingshot and weighted beanbag attached
717 to a throw line. Branches were immediately recut under deionized water and
718 remained submerged to reduce stomatal closure and avoid xylem embolism (as in

719 Smith & Dukes, 2018) until gas exchange data were collected.

720 Randomly selected leaves with little to no visible external damage were
721 attached to a Li-COR LI-6800 (Li-COR Bioscience, Lincoln, Nebraska, USA)
722 portable photosynthesis machine to measure net photosynthesis (A_{net} ; $\mu\text{mol m}^{-2}$
723 s^{-1}), stomatal conductance (g_{sw} ; $\text{mol m}^{-2} \text{s}^{-1}$), and intercellular CO_2 concentra-
724 tion (C_i ; $\mu\text{mol mol}^{-1}$) at different reference CO_2 concentrations (C_a ; $\mu\text{mol mol}^{-1}$)
725 concentrations (i.e., an A_{net}/C_i curve) under saturating light conditions (2,000
726 $\mu\text{mol m}^{-2} \text{s}^{-1}$). Reference CO_2 concentrations followed the sequence: 400, 300,
727 200, 100, 50, 400, 400, 600, 800, 1000, 1200, 1500, and 2000 $\mu\text{mol mol}^{-1} \text{CO}_2$. Leaf
728 temperatures were not controlled in the cuvette and ranged from 21.8 °C to 31.7
729 °C (mean±SD: 27.2 ± 2.2 °C). A linear and second order log-polynomial nonlinear
730 regression suggested no effect of temperature on stomatal conductance measured
731 at 400 $\mu\text{mol mol}^{-1} \text{CO}_2$ or net photosynthesis measured at $\mu\text{mol mol}^{-1} \text{CO}_2$ (Ta-
732 ble S2-3; Fig. S1). All A_{net}/C_i curves were generated within one hour of branch
733 severance.

734 Leaf morphological and chemical traits were collected on the same leaf used
735 to generate each A_{net}/C_i curve. Images of each leaf were taken using a flat-bed
736 scanner to determine fresh leaf area using the ‘LeafArea’ R package (Katabuchi
737 2015), which automates leaf area calculations using ImageJ software (Schneider
738 et al. 2012). Each leaf was dried at 65°C for at least 48 hours, weighed, and
739 ground using a Retsch MM200 ball mill grinder (Verder Scientific, Inc., Newtown,
740 PA, USA) until homogenized. Leaf mass per area (M_{area} , g m^{-2}) was calculated
741 as the ratio of dry leaf biomass to fresh leaf area. Using a subsample of ground and
742 homogenized leaf biomass, leaf N content (N_{mass} ; gN g^{-1}) and leaf $\delta^{13}\text{C}$ (‰, rela-

743 tive to VPDB) were measured at the Cornell Stable Isotope Lab with an elemental
 744 analyzer (NC 2500, CE Instruments, Wigan, UK) interfaced to an isotope ratio
 745 mass spectrometer (Delta V Isotope Ratio Mass Spectrometer, ThermoFisher Sci-
 746 entific, Waltham, MA, USA). Leaf N content per unit leaf area (N_{area} ; gN m⁻²)
 747 was calculated by multiplying N_{mass} by M_{area} .

748 We used leaf $\delta^{13}\text{C}$ values to estimate χ (unitless), which is an isotope-
 749 derived estimate of the leaf $C_i:C_a$ ratio. While intercellular and atmospheric CO₂
 750 concentrations were directly measured during each A_{net}/C_i curve, deriving χ from
 751 $\delta^{13}\text{C}$ provides a more integrative estimate of the $C_i:C_a$ over an individual leaf's
 752 lifespan. We derived χ following the approach of Farquhar et al. (1989) described
 753 in Cernusak et al. (2013):

$$\chi = \frac{\Delta^{13}C - a}{b - a} \quad (3.1)$$

754 where $\Delta^{13}\text{C}$ represents the relative difference between leaf $\delta^{13}\text{C}$ (‰) and air $\delta^{13}\text{C}$
 755 (‰), and is calculated from the following equation:

$$\Delta^{13}C = \frac{\delta^{13}C_{\text{air}} - \delta^{13}C_{\text{leaf}}}{1 + \delta^{13}C_{\text{leaf}}} \quad (3.2)$$

756 where $\delta^{13}C_{\text{air}}$ is assumed to be -8‰ (Keeling et al. 1979; Farquhar et al. 1989), a
 757 represents the fractionation between ¹²C and ¹³C due to diffusion in air, assumed
 758 to be 4.4‰, and b represents the fractionation caused by Rubisco carboxylation,
 759 assumed to be 27‰ (Farquhar et al. 1989).

760 3.2.4 A_{net}/C_i curve-fitting and parameter estimation

761 We fit A_{net}/C_i curves of each individual using the ‘fitaci’ function in the
762 ‘plantecophys’ R package (Duursma 2015). This function estimates the maxi-
763 mum rate of Rubisco carboxylation (V_{cmax} ; $\mu\text{mol m}^{-2} \text{s}^{-1}$) and maximum rate
764 of electron transport for RuBP regeneration (J_{max} ; $\mu\text{mol m}^{-2} \text{s}^{-1}$) based on the
765 Farquhar, von Caemmerer, and Berry biochemical model of C₃ photosynthesis
766 (Farquhar et al. 1980). For each curve fit, we included triose phosphate uti-
767 lization (TPU) limitation to avoid underestimating J_{max} (Gregory et al. 2021).
768 Curves were visually examined to confirm the likely presence of TPU limitation.

769 We determined Michaelis-Menten coefficients for Rubisco affinity to CO₂
770 (K_c ; $\mu\text{mol mol}^{-1}$) and O₂ (K_o ; $\mu\text{mol mol}^{-1}$), and the CO₂ compensation point
771 (Γ^* ; $\mu\text{mol mol}^{-1}$) using leaf temperature and equations described in Medlyn et al.
772 (2002) and derived in Bernacchi et al. (2001). Specifically, K_c and K_o were
773 calculated as:

$$K_c = 404.9 * \exp^{\frac{79430(T_k - 298)}{298RT_k}} \quad (3.3)$$

774 and

$$K_o = 278.4 * \exp^{\frac{36380(T_k - 298)}{298RT_k}} \quad (3.4)$$

775 while Γ^* was calculated as:

$$\Gamma^* = 42.75 * \exp^{\frac{37830(T_k - 298)}{298RT_k}} \quad (3.5)$$

776 In all three equations, T_k is the leaf temperature (in Kelvin) during each A_{net}/C_i

777 curve and R is the universal gas constant ($8.314 \text{ J mol}^{-1} \text{ K}^{-1}$).

778 We standardized V_{cmax} and J_{max} estimates to 25°C using a modified Ar-

779 rhenius equation (Kattge and Knorr 2007):

$$k_{25} = \frac{k_{\text{obs}}}{e^{\frac{H_a(T_{\text{obs}} - T_{\text{ref}})}{T_{\text{ref}}RT_{\text{obs}}}} * \frac{1+e^{\frac{T_{\text{ref}}\Delta S - H_d}{T_{\text{obs}}}}}{1+e^{\frac{T_{\text{obs}}\Delta S - H_d}{T_{\text{obs}}}}}} \quad (3.6)$$

780 k_{25} represents the standardized V_{cmax} or J_{max} rate at 25°C , k_{obs} represents

781 the V_{cmax} or J_{max} estimate at the average leaf temperature measured inside the

782 cuvette during the A_{net}/C_i curve. H_a is the activation energy of V_{cmax} ($71,513$

783 J mol^{-1}) Kattge and Knorr (2007) or J_{max} ($49,884 \text{ J mol}^{-1}$) (Kattge and Knorr

784 2007). H_d represents the deactivation energy of both V_{cmax} and J_{max} ($200,000 \text{ J}$

785 mol^{-1}) (Medlyn et al. 2002), and R represents the universal gas constant (8.314

786 $\text{J mol}^{-1} \text{ K}^{-1}$). T_{ref} represents the standardized temperature of 298.15 K (25°C)

787 and T_{obs} represents the mean leaf temperature (in K) during each A_{net}/C_i curve.

788 ΔS is an entropy term that (Kattge and Knorr 2007) derived as a linear relation-

789 ship with average growing season temperature (T_g ; $^\circ\text{C}$), where:

$$\Delta S_{v_{\text{cmax}}} = -1.07 T_g + 668.39 \quad (3.7)$$

790 and

$$\Delta S_{j_{\text{max}}} = -0.75 T_g + 659.70 \quad (3.8)$$

791 We estimated T_g in Equations 3.7 and 3.8 based on mean daily (24-hour) air
792 temperature of the 30 days leading up to the day of each sample collection using
793 the same weather station reported in the site description. We then used V_{cmax25}
794 and J_{max25} estimates to calculate the ratio of J_{max25} to V_{cmax25} ($J_{max25}:V_{cmax25}$;
795 unitless).

796 3.2.5 *Proportion of leaf nitrogen allocated to photosynthesis and structure*

797 We used equations from Niinemets and Tenhunen (1997) to estimate the
798 proportion of leaf N content allocated to Rubisco and bioenergetics. The propor-
799 tion of leaf N allocated to Rubisco (ρ_{rub} ; gN gN $^{-1}$) was calculated as a function
800 of V_{cmax25} and N_{area} :

$$\rho_{rubisco} = \frac{V_{cmax25} N_r}{V_{cr} N_{area}} \quad (3.9)$$

801 where N_r is the amount of nitrogen in Rubisco, set to 0.16 gN (gN in Rubisco) $^{-1}$
802 and V_{cr} is the maximum rate of RuBP carboxylation per unit Rubisco protein,
803 set to 20.5 μ mol CO $_2$ (g Rubisco) $^{-1}$. The proportion of leaf nitrogen allocated to
804 bioenergetics (ρ_{bioe} ; gN gN $^{-1}$) was similarly calculated as a function of J_{max25} and
805 N_{area} :

$$\rho_{bioe} = \frac{J_{max25} N_b}{J_{mc} N_{area}} \quad (3.10)$$

806 where N_b is the amount of nitrogen in cytochrome f, set to 0.12407 gN (μ mol
807 cytochrome f) $^{-1}$ assuming a constant 1: 1: 1.2 cytochrome f: ferredoxin NADP
808 reductase: coupling factor molar ratio (Evans and Seemann 1989; Niinemets and

809 Tenhunen 1997), and J_{mc} is the capacity of electron transport per cytochrome f,
810 set to $156 \mu\text{mol electron} (\mu\text{mol cytochrome f})^{-1}\text{s}^{-1}$.

811 We estimated the proportion of leaf N content allocated to photosynthetic
812 tissue (ρ_{photo} ; gN gN⁻¹) as the sum of ρ_{rub} and ρ_{bioe} . This calculation is an un-
813 derestimate of the proportion of leaf N allocated to photosynthetic tissue because
814 it does not include N allocated to light harvesting proteins. This leaf N pool was
815 not included because we did not perform chlorophyll extractions on focal leaves.
816 However, the proportion of leaf N content allocated to light harvesting proteins
817 tends to be small relative to ρ_{rub} and ρ_{bioe} , and may scale with changes in ρ_{rub}
818 and ρ_{bioe} (Niinemets and Tenhunen 1997).

819 Finally, we estimated the proportion of leaf N content allocated to struc-
820 tural tissue (ρ_{str} ; gN gN⁻¹) using an empirical equation from Onoda et al. (2017):

$$N_{cw} = 0.000355 * M_{area}^{1.39} \quad (3.11)$$

821 where N_{cw} is the leaf N content allocated to cell walls (gN m⁻²). ρ_{str} was estimated
822 by dividing N_{cw} by N_{area} .

823 3.2.6 *Tradeoffs between nitrogen and water use*

824 Photosynthetic nitrogen use efficiency (PNUE; $\mu\text{mol CO}_2 \text{ mol}^{-1} \text{ N s}^{-1}$)
825 was calculated by dividing A_{net} by N_{area} , first converting N_{area} to mol N m⁻²
826 using the molar mass of N (14 g mol⁻¹). We used χ as an indicator of water
827 use efficiency, which exploratory analyses suggest had similar responses to soil N
828 availability and pH as intrinsic water use efficiency measured from gas exchange

829 (A_{net}/g_s). Tradeoffs between nitrogen and water use were determined by cal-
830 culating the ratio of N_{area} to χ ($N_{\text{area}}:\chi$; g N m⁻²) and V_{cmax25} to χ ($V_{\text{cmax25}}:\chi$;
831 $\mu\text{mol m}^{-2} \text{s}^{-1}$). This approach is similar to tradeoff calculations in which nitrogen-
832 water use tradeoffs are measured as the ratio of N_{area} or V_{cmax25} to g_s (Paillassa
833 et al. 2020; Bialic-Murphy et al. 2021). In this study, we quantify these re-
834 lationships using χ in lieu of g_s because g_s rapidly changes with environmental
835 conditions and therefore may have been altered by recent tree branch severance
836 and/or placement in the cuvette.

837 3.2.7 *Soil nitrogen availability and pH*

838 To characterize soil N availability at the time of our leaf gas exchange
839 measurements, we used mixed bed resin bags to quantify mobile ammonium-N
840 and nitrate-N concentrations in each plot. Lycra mesh bags were filled with 5 g
841 of Dowex® Marathon MR-3 hydrogen and hydroxide form resin (MilliporeSigma,
842 Burlington, MA USA) and sealed with a zip tie. Each bag was activated by
843 soaking in 0.5 M HCl for 20 minutes, then in 2 M NaCl until pH of the saline
844 solution stabilized, as described in Allison et al. (2008). Five resin bags were
845 inserted about 10 cm below the soil surface at each plot on June 25, 2019: one
846 near each of the four plot corners and one near the plot center. All resin bags
847 were collected 24 days later on July 19, 2019 and were frozen until extracted.

848 Prior to anion and cation extraction, each resin bag was rinsed with ul-
849 trapure water (MilliQ IQ 7000; Millipore Sigma, Burlington, MA) to remove any
850 surface soil residues. Anions and cations were extracted from surface-cleaned resin
851 bags by individually soaking and shaking each bag in 100 mL of a 0.1 M HCl/2.0

852 M NaCl matrix for one hour. Using a microplate reader (Biotek Synergy H1;
853 Biotek Instruments, Winooski, VT USA), nitrate-N concentrations were quanti-
854 fied spectrophotometrically at 540 nm with the end product of a single reagent
855 vanadium (III) chloride reaction (Doane and Horwáth 2003), and ammonium-N
856 concentrations quantified at 650 nm with the end product of a modified phenol-
857 hypochlorite reaction (Weatherburn 1967; Rhine et al. 1998). Both the single
858 reagent vanadium (III) chloride and modified phenol-hypochlorite methodologies
859 have been well established for determining nitrate-N and ammonium-N concen-
860 trations in resin bag extracts (Arnone 1997; Allison et al. 2008). We used a
861 series of negative and positive controls throughout each well plate to verify the
862 accuracy and precision of our measurements, assaying each resin bag extract and
863 control in triplicate. Soil N availability was estimated as the sum of the nitrate-N
864 and ammonium-N concentration in each resin bag, normalized per g of resin and
865 duration in the field ($\mu\text{g N g}^{-1} \text{ resin d}^{-1}$), then subsequently averaged across all
866 resin bags in a plot for a plot-level mean.

867 Soil pH was measured on 0-10 cm mineral soil samples collected prior to
868 fertilization in 2019. Near each of the four plot corners, three 5.5 cm diameter soil
869 cores were collected after first removing the forest floor where present. Each set
870 of three cores was placed in a plastic bag, and later composited by hand mixing
871 and sieved to 4mm. Soil pH was determined for a 1:2 soil:water slurry (10 g field-
872 moist soil to 20 mL DI water) of each sample using an Accumet AB15 pH meter
873 with flushable junction probe (Fisher Scientific; Hampton, NH, USA), and was
874 estimated at the plot level as the mean soil pH within each plot.

875 3.2.8 *Statistical analyses*

876 We built two separate series of linear mixed-effects models to explore effects
877 of soil N availability, soil pH, species, and leaf N content on leaf physiological
878 traits. In the first series of linear mixed-effects models, we explored the effect
879 of soil N availability, soil pH, and species on leaf N content, leaf photosynthesis,
880 stomatal conductance, and nitrogen-water use tradeoffs. Models included plot-
881 level soil N availability and plot-level soil pH as continuous fixed effects, species
882 as a categorical fixed effect, and site as a categorical random intercept term.
883 Interaction terms between fixed effects were not included due to the small number
884 of experimental plots. We built a series of separate models with this independent
885 variable structure to quantify individual effects of soil N availability, soil pH,
886 and species on N_{area} , M_{area} , N_{mass} , A_{net} , V_{cmax25} , J_{max25} , $J_{\text{max25}}:V_{\text{cmax25}}$, ρ_{rubisco} ,
887 $\rho_{\text{bioenergetics}}$, ρ_{photo} , $\rho_{\text{structure}}$, χ , PNUE, $N_{\text{area}}:\chi$, and $V_{\text{cmax25}}:\chi$.

888 A second series of linear mixed-effects models were built to investigate
889 relationships between leaf N content and photosynthetic parameters. Statistical
890 models included N_{area} as a single continuous fixed effect with species and site des-
891 ignated as individual random intercept terms. We used this independent variable
892 structure to quantify individual effects of leaf N content on A_{net} , V_{cmax25} , J_{max25} ,
893 $J_{\text{max25}}:V_{\text{cmax25}}$, and χ .

894 For all linear mixed-effects models, we used Shapiro-Wilk tests of normal-
895 ity to determine whether linear mixed-effects models satisfied residual normality
896 assumptions. If residual normality assumptions were not met, then models were
897 fit using dependent variables that were natural log transformed. If residual nor-
898 mality assumptions were still not met (Shapiro-Wilk: $p < 0.05$), then models were

899 fit using dependent variables that were square root transformed. All residual nor-
900 mality assumptions for both sets of models that did not originally satisfy residual
901 normality assumptions were met with either a natural log or square root data
902 transformation (Shapiro-Wilk: $p > 0.05$ in all cases).

903 In the first series of models, models for N_{area} , M_{area} , N_{mass} , V_{cmax25} , J_{max25} ,
904 χ , $N_{\text{area}}:\chi$, and $V_{\text{cmax25}}:\chi$, ρ_{rubisco} , $\rho_{\text{bioenergetics}}$, ρ_{photo} , $\rho_{\text{structure}}$ satisfied residual
905 normality assumptions without data transformations (Shapiro-Wilk: $p > 0.05$ in
906 all cases). The model for $J_{\text{max25}}:V_{\text{cmax25}}$ satisfied residual normality assumptions
907 with a natural log data transformation, while models for A_{net} and PNUE each
908 satisfied residual normality assumptions with square root data transformations.
909 In the second series of models, models for V_{cmax25} , J_{max25} , χ , and $V_{\text{cmax25}}:\chi$ satisfied
910 residual normality assumptions without data transformations (Shapiro-Wilk: p
911 > 0.05 in all cases). The model for $J_{\text{max25}}:V_{\text{cmax25}}$ required a natural log data
912 transformation and the model for A_{net} required a square root data transformation
913 (Shapiro-Wilk: $p > 0.05$ in both cases).

914 In all models, we used the ‘lmer’ function in the ‘lme4’ R package (Bates
915 et al. 2015) to fit each model and the ‘Anova’ function in the ‘car’ R package (Fox
916 and Weisberg 2019) to calculate Type II Wald’s χ^2 and determine the significance
917 level ($\alpha = 0.05$) of each fixed effect coefficient. Finally, we used the ‘emmeans’
918 R package (Lenth, 2019) to conduct post-hoc comparisons using Tukey’s tests,
919 where degrees of freedom were approximated using the Kenward-Roger approach
920 (Kenward and Roger 1997). All analyses and plots were conducted in R version
921 4.1.1 (R Core Team 2021). All figure regression lines and associated 95% confi-
922 dence interval error bars were plotted using predictions generated across the soil

923 nitrogen availability gradient using the ‘emmeans’ R package (Lenth 2019).

924 3.3 Results

925 3.3.1 *Leaf N content*

926 Increasing soil N availability generally increased N_{area} (Table 3.1; Fig.
927 3.1a). This pattern was driven by an increase in N_{mass} (Table 3.1; Fig. 3.1c)
928 and a marginal increase in M_{area} (Table 3.1; Fig. 3.1e) with increasing soil N
929 availability. There was no effect of soil pH on N_{area} , N_{mass} , or M_{area} (Table 3.1);
930 however, we did observe strong differences in N_{area} (Fig. 3.1b), N_{mass} (Fig. 3.1d),
931 and M_{area} (Fig. 3.1e) between species (Table 3.1).

Table 3.1. Effects of soil N availability, soil pH, and species on leaf N content per unit leaf area (N_{area}), leaf N content per unit leaf mass (N_{mass}), and leaf mass per unit leaf area (M_{area})

| | N_{area} | | | N_{mass} | | | M_{area} | | | |
|-----------|-------------------|-------------|----------|-------------------|-------------|----------|-------------------|-------------|----------|------------------|
| | df | Coefficient | χ^2 | p | Coefficient | χ^2 | p | Coefficient | χ^2 | p |
| Intercept | - | 9.03E-01 | - | - | 1.68E+00 | - | - | 4.60E+01 | - | - |
| Soil N | 1 | 1.68E-02 | 11.990 | 0.001 | 1.25E-02 | 6.902 | 0.009 | 4.87E-01 | 4.143 | 0.042 |
| Soil pH | 1 | 9.28E-02 | 0.836 | 0.361 | 8.08E-02 | 0.663 | 0.415 | 4.05E+00 | 0.653 | 0.419 |
| Species | 4 | - | 72.128 | <0.001 | - | 35.074 | <0.001 | - | 29.869 | <0.001 |

932 *Significance determined using Type II Wald χ^2 tests ($\alpha = 0.05$). P-values < 0.05 are in bold.

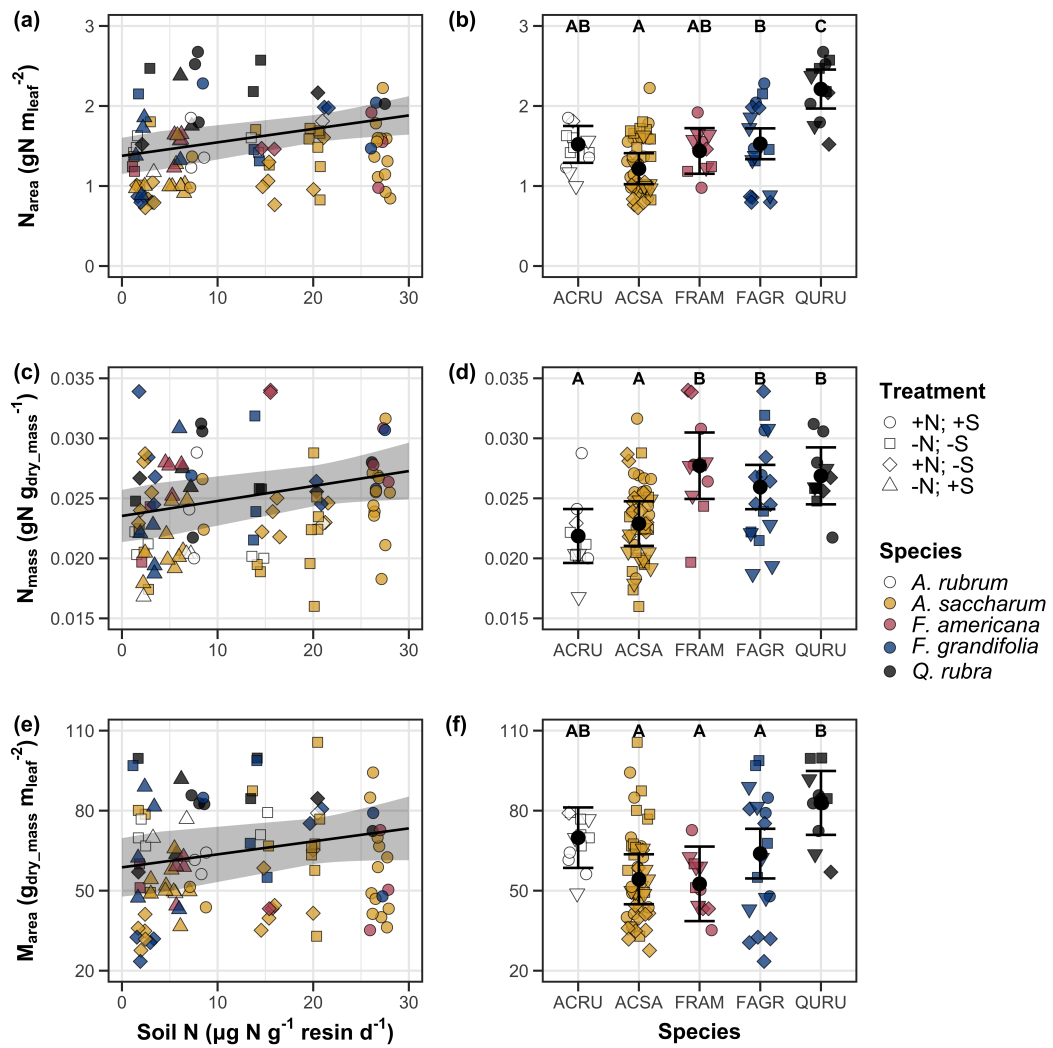


Figure 3.1. Effects of soil N availability and species on leaf N content per unit leaf area (a-b), leaf nitrogen content per unit leaf biomass (c-d), and leaf mass per leaf area (e-f). Soil N availability is represented on the x-axis in the left column of panels, while species is represented on the x-axis in the right column of panels. Tree species are represented as colored points and treatment plots are represented as shaped points, jittered for visibility. Species are abbreviated in the right column of panels through their assigned NRCS PLANTS Database symbol (USDA NRCS 2022), grouped along the x-axis per common mycorrhizal association, where the first three species commonly associate with arbuscular mycorrhizae (ACRU, ASCA, FAGR) and the second two species with ectomycorrhizae (FAGR, QURU). Trendlines are only included when the regression slope is statistically different from zero ($p < 0.05$).

933 3.3.2 *Net photosynthesis and leaf biochemistry*

934 Increasing soil N availability generally had no effect on A_{net} , V_{cmax25} , J_{max25} ,
935 or $J_{\text{max25}}:V_{\text{cmax25}}$ (Table 3.2, Figs. 3.2a, 3.2d, 3.2g). We also observed strong
936 species effects on all measured leaf photosynthetic traits (Table 3.2; Figs. 3.2b,
937 3.2e, 3.2h). Increasing soil pH had a marginal negative effect on A_{net} , but had no
938 effect on V_{cmax25} , J_{max25} , or $J_{\text{max25}}:V_{\text{cmax25}}$ (Table 3.2). There was a weak positive
939 effect of increasing N_{area} on A_{net} (Fig. 3.2c), but quite strong positive effects of
940 increasing N_{area} on V_{cmax25} and J_{max25} (Table 3.2; Fig. 3.2f and 3.2i).

Table 3.2. Effects of soil N availability, soil pH, species, and N_{area} on leaf biochemistry

| | A_{net} | | | V_{cmax25} | | | J_{max25} | | | |
|---------------------------|------------------|------------------------|----------|---------------------|-------------|----------|--------------------|-------------|----------|--------|
| | df | Coefficient | χ^2 | p | Coefficient | χ^2 | p | Coefficient | χ^2 | p |
| (Intercept) | - | 3.29E+00 ^b | - | - | 6.38E+01 | - | - | 1.12E+02 | - | - |
| Soil N | 1 | -1.23E-03 ^b | 1.798 | 0.180 | -3.84E-01 | 1.745 | 0.187 | -6.70E-01 | 2.172 | 0.141 |
| Soil pH | 1 | -3.09E-01 ^b | 3.312 | 0.069 | -4.91E+00 | 0.655 | 0.418 | -8.18E+00 | 0.742 | 0.389 |
| Species | 4 | - | 11.838 | 0.019 | - | 31.748 | <0.001 | - | 27.291 | <0.001 |
| (N_{area} int.) | - | 6.59E-01 ^b | - | - | 1.45E-01 | - | - | 2.86E+01 | - | - |
| N_{area} | 4 | 3.13E-01 ^b | 4.790 | 0.029 | 2.43E+01 | 22.616 | <0.001 | 4.04E+01 | 28.259 | <0.001 |

| | $J_{\text{max25}}:V_{\text{cmax25}}$ | | | |
|---------------------------|--------------------------------------|------------------------|----------|--------------|
| | df | Coefficient | χ^2 | p |
| (Intercept) | - | 6.59E-01 ^a | - | - |
| Soil N | 1 | 7.04E-04 ^a | 0.088 | 0.767 |
| Soil pH | 1 | -7.84E-03 ^a | 0.025 | 0.874 |
| Species | 4 | - | 12.745 | 0.013 |
| (N_{area} int.) | - | 6.69E-01 ^a | - | - |
| N_{area} | 4 | -4.69E-02 ^a | 1.142 | 0.285 |

941 *Significance determined using Type II Wald χ^2 tests ($\alpha = 0.05$). P-values < 0.05 are in bold, while p-values between
 942 0.05 and 0.1 are italicized. Superscript letters indicate model coefficients fit to natural-log (^a) or square-root (^b)
 943 transformed data. Relationships between N_{area} and each response variable were fit using the second series of bivariate
 944 mixed-effects models, so model coefficients and results are independent of model coefficients and results reported
 945 for relationships between soil N, soil pH, and species for each response variable. Key: A_{net} – light saturated net
 946 photosynthesis rate; V_{cmax25} – maximum rate of Rubisco carboxylation at 25°C; J_{max25} – maximum rate of electron
 947 transport for RuBP regeneration at 25°C, $J_{\text{max25}}:V_{\text{cmax25}}$ – the ratio of J_{max25} to V_{cmax25} .

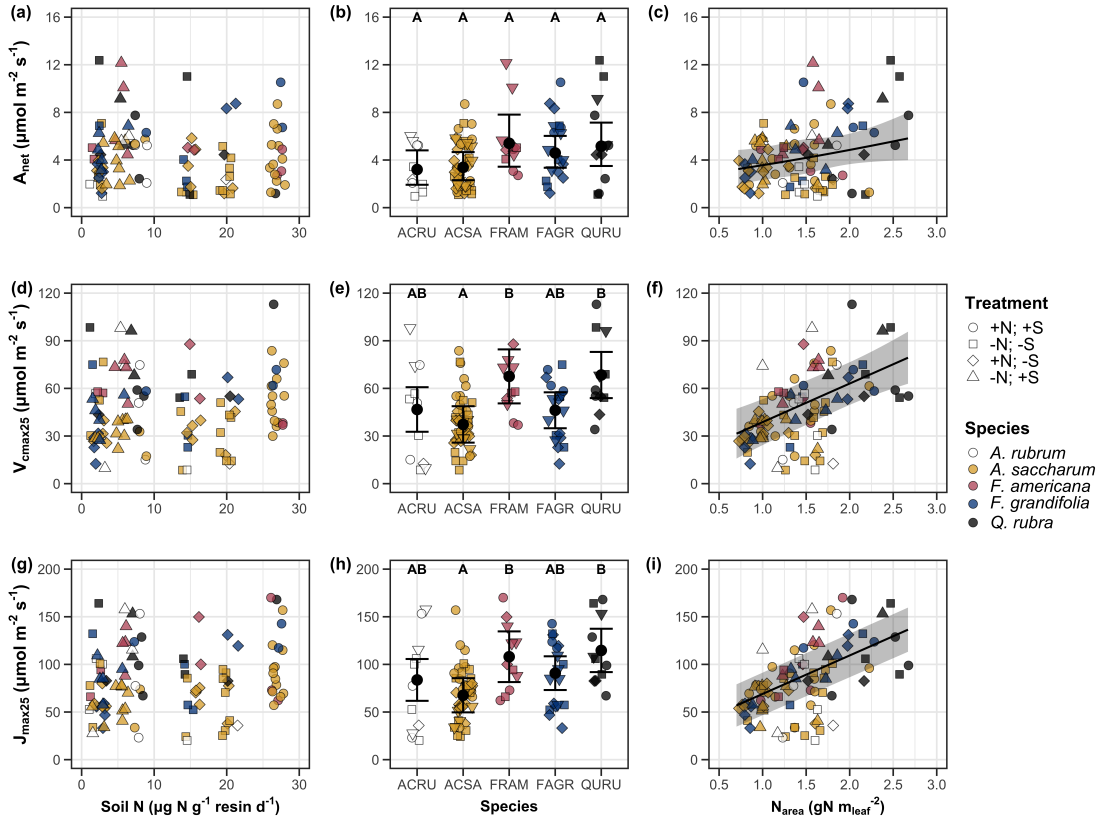


Figure 3.2. Effects of soil N availability (left column of panels), species (middle column of panels), and leaf N content per unit leaf area (right column of panels) on net photosynthesis (a-c), maximum Rubisco carboxylation rate (d-f), and maximum RuBP regeneration rate (g-i). Soil N availability is represented on the x-axis in the left column of panels, species is represented on the x-axis in the middle column of panels, and leaf N content per unit leaf area is represented continuously on the x-axis in the right column of panels. Species abbreviations and position along the x-axis in the middle column of panels, colored points, shapes, and trendlines are as explained in Figure 3.1.

948 3.3.3 *Leaf N allocation*

949 Neither soil N availability nor soil pH affected the proportion of leaf N
950 allocated to Rubisco or bioenergetics (Table 3.3; Fig. 3.3a, Fig. 3.3c), nor was
951 there any subsequent effect on the proportion of leaf N allocated to photosynthesis
952 (Table 3.3; Fig. 3.3f). We also found no effect of soil N availability or soil pH on
953 the proportion of leaf N allocated to structure (Table 3.3; Fig 3.3g). Species varied
954 in the proportion of leaf N allocated to Rubisco, photosynthesis, and structure (Fig
955 3.3b, Fig. 3.3d, Fig 3.3h), with no detectable species effect on the proportion of
956 leaf N allocated to bioenergetics (Table 3.3).

Table 3.3. Effects of soil N availability, soil pH, and species on the proportion of leaf nitrogen content allocated to photosynthesis, Rubisco, bioenergetics, and structure

| | ρ_{photo} | | | ρ_{rub} | | | ρ_{bioe} | | | |
|-----------|-----------------------|-------------|----------|---------------------|-------------|----------|----------------------|-------------|----------|-------|
| | df | Coefficient | χ^2 | p | Coefficient | χ^2 | p | Coefficient | χ^2 | p |
| Intercept | - | 4.93E-01 | - | - | 4.17E-01 | - | - | 7.64E-02 | - | - |
| Soil N | 1 | -1.23E-03 | 0.521 | 0.470 | -1.04E-03 | 0.501 | 0.479 | -1.77E-04 | 0.557 | 0.455 |
| Soil pH | 1 | -4.37E-02 | 1.581 | 0.209 | -3.70E-02 | 1.511 | 0.219 | -6.84E-03 | 1.941 | 0.164 |
| Species | 4 | - | 13.106 | 0.011 | - | 14.152 | 0.007 | - | 7.300 | 0.121 |

| | ρ_{str} | | | |
|-----------|---------------------|-------------|----------|--------------|
| | df | Coefficient | χ^2 | p |
| Intercept | - | 9.77E-02 | - | - |
| Soil N | 1 | -2.29E-04 | 1.165 | 0.280 |
| Soil pH | 1 | -1.87E-03 | 0.179 | 0.672 |
| Species | 4 | - | 16.428 | 0.002 |

58

957 *Significance determined using Type II Wald χ^2 tests ($\alpha = 0.05$). P-values < 0.05 are in bold. Key: ρ_{photo} -
 958 proportion of leaf nitrogen content allocated to photosynthesis; ρ_{rub} - proportion of leaf nitrogen content allocated
 959 to Rubisco; ρ_{bioe} - proportion of leaf nitrogen content allocated to bioenergetics; ρ_{str} - proportion of leaf nitrogen
 960 content allocated to structure.

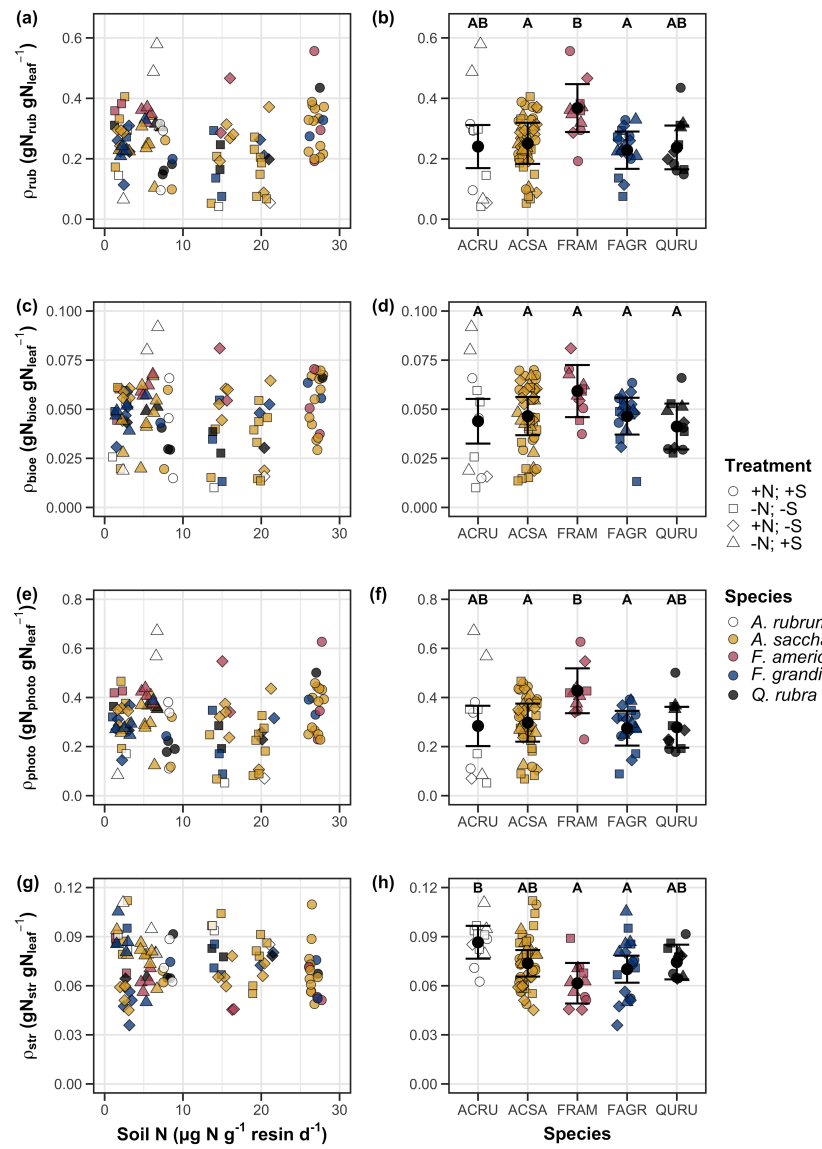


Figure 3.3. Effects of soil nitrogen availability and species on the proportion of leaf nitrogen content allocated to Rubisco (a-b), bioenergetics (c-d), photosynthesis (e-f), and structure (g-h). Soil nitrogen availability is represented on the x-axis in the left column of panels and species are represented on the x-axis in the right column of panels. Species abbreviations and position along the x-axis in the middle column of panels, colored points, shapes, trendlines, error bars, and compact lettering are as explained in Figure 3.1.

961 3.3.4 *Tradeoffs between nitrogen and water use*

962 Although soil N availability did not affect χ (Table 3.4; Fig. 3.4a), increasing
963 soil N availability decreased PNUE (Table 3.4; Fig. 3.4d) and increased the
964 ratio of $N_{\text{area}}:\chi$ (Table 3.4; Fig. 3.4f). Specifically, this response yielded a 26%
965 reduction in PNUE and 37% stimulation in $N_{\text{area}}:\chi$ across the soil nitrogen avail-
966 ability gradient. There was no apparent effect of soil N availability on $V_{\text{cmax25}}:\chi$
967 (Table 3.4; Fig. 3.4h). Increasing soil pH had a weak marginal negative effect
968 on PNUE, but did not influence χ , $N_{\text{area}}:\chi$, or $V_{\text{cmax25}}:\chi$ (Table 3.4). We also
969 observed differences in χ (Fig. 3.4b), PNUE (Fig. 3.4e), $N_{\text{area}}:\chi$ (Fig. 3.4g), and
970 $V_{\text{cmax25}}:\chi$ (Fig. 3.4i) between species (Table 3.4). Finally, increasing N_{area} had a
971 strong negative effect on χ (Table 3.4; Fig. 3.4c) and a strong positive effect on
972 $V_{\text{cmax25}}:\chi$ (Table 3.4; Fig. 3.4j).

Table 3.4. Effects of soil N availability, soil pH, species, and N_{area} on tradeoffs between nitrogen and water use

| | χ | | | PNUE | | | $N_{\text{area}}:\chi$ | | | |
|----------------------------------|--------|-------------|----------|------------------|-------------|----------|------------------------|-------------|----------|------------------|
| | df | Coefficient | χ^2 | p | Coefficient | χ^2 | p | Coefficient | χ^2 | p |
| (Intercept) | - | 8.12E-01 | - | - | 9.57E+00 | - | - | 9.19E-01 | - | - |
| Soil N | 1 | -1.14E-03 | 1.698 | 0.193 | -6.63E-02 | 6.396 | 0.011 | 2.60E-02 | 9.533 | 0.002 |
| Soil pH | 1 | -1.91E-02 | 1.087 | 0.297 | -9.25E-01 | 2.843 | <i>0.092</i> | 2.03E-01 | 1.321 | 0.250 |
| Species | 4 | - | 18.843 | 0.001 | - | 13.454 | 0.009 | - | 52.983 | <0.001 |
| $(N_{\text{area}} \text{ int.})$ | - | 8.93E-01 | - | - | - | - | - | - | - | - |
| N_{area} | 1 | -1.11E-01 | 80.606 | <0.001 | - | - | - | - | - | - |

| | $V_{\text{cmax25}}:\chi$ | | | |
|----------------------------------|--------------------------|-------------|----------|------------------|
| | df | Coefficient | χ^2 | p |
| (Intercept) | - | 7.20E+01 | - | - |
| Soil N | 1 | 3.99E-01 | 0.963 | 0.326 |
| Soil pH | 1 | -3.12E+00 | 0.138 | 0.711 |
| Species | 4 | - | 31.450 | <0.001 |
| $(N_{\text{area}} \text{ int.})$ | - | 1.18E+01 | - | - |
| N_{area} | 4 | 3.87E+01 | 32.797 | <0.001 |

973 *Significance determined using Type II Wald χ^2 tests ($\alpha = 0.05$). P-values < 0.05 are in bold, while p-values
 974 between 0.05 and 0.1 are italicized. Superscript letters indicate model coefficients fit to natural-log ^(a) or square-root
 975 ^(b) transformed data. Relationships between N_{area} and each response variable were fit using the second series of
 976 bivariate mixed-effects models, so model coefficients and results are independent of model coefficients and results
 977 reported for relationships between soil N, soil pH, and species for each response variable. Key: χ - isotope-derived
 978 estimate of the $C_i:C_a$; PNUE - photosynthetic N use efficiency, ratio of net photosynthesis to leaf N content per unit
 979 leaf area; $N_{\text{area}}:\chi$ - ratio of N_{area} to χ ; $V_{\text{cmax25}}:\chi$ - ratio of V_{cmax25} to χ .

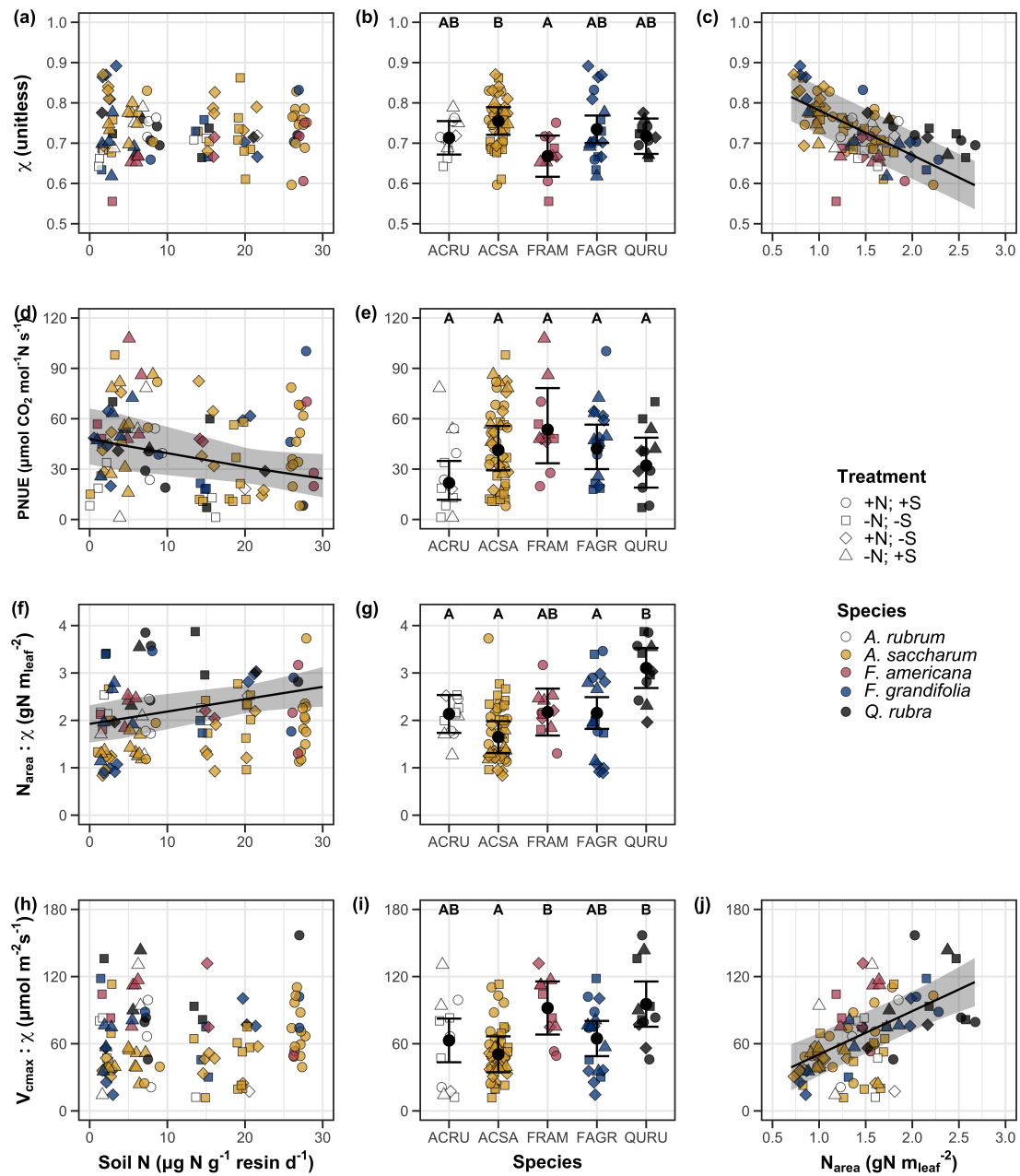


Figure 3.4. Effects of soil nitrogen availability and species on the proportion of leaf nitrogen content allocated to Rubisco (a-b), bioenergetics (c-d), photosynthesis (Rubisco + bioenergetics; e-f), and structure (g-h). Soil nitrogen availability is represented on the x-axis in the left column of panels and species are represented on the x-axis in the right column of panels. Species abbreviations and position along the x-axis in the middle column of panels, colored points, shapes, trendlines, error bars, and compact lettering are as explained in Figure 3.1.

980 3.4 Discussion

981 Photosynthetic least-cost theory provides an explanation for understand-
982 ing relationships between soil nutrient availability, leaf nutrient allocation, and
983 photosynthetic capacity. The theory suggests that plants acclimate to a given
984 environment by optimizing leaf photosynthesis rates at the lowest summed cost
985 of using nutrients and water Prentice et al. (2014), Wang et al. (2017), Smith
986 et al. (2019), Paillassa et al. (2020). The theory predicts that an increase in
987 soil nutrient availability should allow similar photosynthesis rates to be achieved
988 with increased leaf nutrient content and photosynthetic capacity (i.e., V_{cmax25} and
989 J_{max25}) at lower leaf $C_i:C_a$ (χ), resulting in an increase in water use efficiency,
990 decrease in nutrient use efficiency, and increase in both leaf nutrient content and
991 photosynthetic capacity per unit χ . The theory predicts similar leaf responses to
992 increasing soil pH under acidic conditions, presumably due to generally faster nu-
993 trient cycle dynamics and consequent reductions in the cost of acquiring nutrients
994 relative to water with increasing soil pH (Wang et al. 2017; Paillassa et al. 2020;
995 Dong et al. 2020).

996 Supporting the theory, we showed that increasing soil N availability was
997 associated with increased leaf N content (Fig 3.1a, 3.1c), a pattern that reduced
998 photosynthetic N use efficiency (Fig 3.4d) and increased leaf N content per unit
999 χ (Fig 3.4f). Increasing soil N coincided with slight, but non-significant decreases
1000 in χ and increases in V_{cmax25} and J_{max25} ($p < 0.2$, Table 3.2). The positive trend
1001 between soil N availability and photosynthetic capacity was supported by the con-
1002 current strong increase in leaf N content with increasing soil N availability, which
1003 resulted in no change in the proportion of leaf N content allocated to photosynthe-

1004 sis across the soil N availability gradient. Additionally, leaf N content exhibited a
1005 strong negative correlation with χ , indicative of strong nitrogen-water use trade-
1006 offs at the leaf level. Responses tended to vary more due to soil N availability
1007 than soil pH. Overall, these findings are consistent with the nutrient-water use
1008 tradeoffs predicted from theory.

1009 3.4.1 *Soil nitrogen availability modifies tradeoffs between nitrogen and water use*

1010 In support of expected least-cost outcomes and past environmental gradient
1011 studies (Dong et al. 2017; Paillassa et al. 2020), we found that increasing soil N
1012 availability was associated with increased leaf N content. Soil N availability had
1013 smaller impacts on measures of net photosynthesis and χ , which led to reductions
1014 in PNUE and increases in leaf N content per unit χ , as expected from theory.
1015 Photosynthetic least-cost theory suggests that reductions in PNUE should be
1016 driven by an increase in the proportion of leaf N allocated to photosynthetic tissue,
1017 a pattern that should allow plants to achieve optimal photosynthetic rates with
1018 greater photosynthetic capacity to make better use of available light. Contrasting
1019 theory predictions, we found no effect of soil N availability on photosynthetic
1020 capacity. However, photosynthetic capacity did tend to increase with increasing
1021 soil N availability ($p < 0.20$; Table 3.2) resulting in no effect of soil N availability on
1022 the relative fraction of leaf N allocated to photosynthesis, Rubisco, or bioenergetics
1023 (Fig. 3.3). These lines of evidence support the idea that trees use additional N
1024 to support increased leaf N allocation toward photosynthetic tissue and enhance
1025 photosynthetic capacity (Wright et al. 2003).

1026 Soil N availability had a stronger effect on leaf N than photosynthetic ca-

1027 pacity. This pattern suggests that additional plant N uptake due to increased
1028 soil N availability was also being used to support non-photosynthetic N pools,
1029 possibly to structural tissue or stress-induced amino acid and polyamine synthe-
1030 sis (Minocha et al. 2000; Onoda et al. 2004; Bubier et al. 2011). While we
1031 found no change in the proportion of leaf N allocated to leaf structural tissue, the
1032 overall stimulation in leaf N content with increasing soil N availability suggests an
1033 increase in the net amount of N invested in leaf structural tissue along the N avail-
1034 ability gradient. Importantly, leaf N allocated to structure was calculated using
1035 an empirical relationship between M_{area} and the amount of leaf N allocated to cell
1036 walls (Onoda et al. 2017). As the generality of relationships between M_{area} and
1037 the amount of leaf N allocated to cell walls has been called into question (Harrison
1038 et al. 2009), future work should consider explicitly measuring N allocation to cell
1039 wall tissue and stress-induced amino acid synthesis to confirm these patterns.

1040 In opposition to patterns expected from least-cost theory, increasing soil
1041 N availability had no apparent effect on χ (Fig. 3.4a). Interestingly, despite
1042 the null effect of soil N availability on χ , we observed a strong negative effect of
1043 increasing N_{area} on χ (Fig. 3.4c), consistent with the nitrogen-water use tradeoffs
1044 expected from theory. The null response of χ to increasing soil N availability may
1045 have been due to a lack of water limitation in the system, given that the area
1046 received approximately 20% more precipitation (1167 mm) during the 12-month
1047 period leading up to our measurement period than normally expected (972 mm).
1048 However, droughts can and do occur in temperate forests of the northeastern
1049 United States (Sweet et al. 2017), so the observed increase in leaf N content
1050 with increasing soil N availability could be a strategy that allows trees to hedge

1051 bets against drier than normal growing seasons (Onoda et al. 2004; Onoda et al.
1052 2017; Hallik et al. 2009). As was suggested in Paillassa et al. (2020), and more
1053 recently by Querejeta et al. (2022), negative effects of soil N availability on χ may
1054 increase with increasing aridity. This strategy would be especially advantageous if
1055 it allows individuals growing in arid regions to maintain carbon assimilation rates
1056 with reduced water loss. Future work should attempt to quantify interactive roles
1057 of climate and soil nitrogen availability on nitrogen-water use tradeoffs, which
1058 could be done by leveraging coordinated and multifactor nutrient (Borer et al.
1059 2014) and water (Knapp et al. 2017) manipulation experiments across broad
1060 climatic gradients.

1061 3.4.2 *Soil pH did not modify tradeoffs between nitrogen and water usage*

1062 While the primary purpose of this study was to examine the role of soil N
1063 availability on nitrogen-water use tradeoffs, our experimental design manipulated
1064 both soil N and pH, providing an opportunity to isolate the roles of these variables.
1065 Previous correlational studies along environmental gradients identified soil pH as
1066 a particularly important factor that can modify tradeoffs between nutrient and
1067 water use (Smith et al. 2019; Paillassa et al. 2020; Westerband et al. 2023)
1068 and the proportion of leaf nitrogen allocated to photosynthesis (Luo et al. 2021).
1069 Such studies implied that these patterns may be driven by reductions in the cost of
1070 acquiring nutrients relative to water with increasing pH, which may be exacerbated
1071 in acidic soils.

1072 Consistent with theory (Wright et al. 2003; Prentice et al. 2014), our
1073 results indicate that increasing soil pH was negatively associated with PNUE.

1074 However, there was no effect of soil pH on leaf N content, χ , or leaf N content per
1075 unit χ , most likely because the experimental N additions increased soil N sup-
1076 ply while both increasing (sodium nitrate) and decreasing (ammonium sulfate)
1077 soil pH. These results suggest that soil pH did not play a major role in modify-
1078 ing expected photosynthetic least-cost theory patterns, contrasting findings from
1079 Paillassa et al. (2020) and other gradient studies that note positive effects of in-
1080 creasing soil pH on leaf N content, Rubisco carboxylation, and χ (Viet et al. 2013;
1081 Cornwell et al. 2018; Luo et al. 2021). Instead, null responses to soil pH show
1082 that leaf photosynthetic parameters depend more on soil N availability than pH
1083 per se, and that inferences from gradient studies might be confounding covariation
1084 between N availability and soil acidity.

1085 3.4.3 *Species identity explains a large amount of variation in leaf and whole*
1086 *plant traits*

1087 Species generally explained a larger amount of variation in measured leaf
1088 traits than soil N availability or soil pH. Interspecies variation is an important
1089 factor to consider when deducing mechanisms that drive photosynthetic least-
1090 cost theory, particularly for species that form distinct mycorrhizal associations or
1091 have different photosynthetic pathways, growth forms, or leaf habit (Espelta et al.
1092 2005; Adams et al. 2016; Bialic-Murphy et al. 2021; Scott and Smith 2022). The
1093 need to consider species may also be important when comparing nutrient-water
1094 use tradeoffs in early and late successional species, or in species with different
1095 resource economic strategies (Abrams and Mostoller 1995; Ellsworth and Reich
1096 1996; Wright et al. 2004; Reich 2014; Onoda et al. 2017; Ziegler et al. 2020).

1097 A strength of the study design and sampling effort is that it controls for
1098 many species differences that should modify nitrogen-water use tradeoffs expected
1099 from theory. All tree species measured in this study shared the leaf habit of decid-
1100 uous broadleaves, were growing in forests of similar successional stage, but differed
1101 in mycorrhizal association and consequent resource economic strategies. As stands
1102 tended to be dominated by trees that associate with arbuscular mycorrhizae (*Frax-*
1103 *inus* and both *Acer* species made up 70% of total aboveground biomass across
1104 stands), ecosystem biogeochemical cycle dynamics may be more closely aligned
1105 to the inorganic nutrient economy proposed in Phillips et al. (2013), which may
1106 promote stronger nitrogen-water use tradeoffs in tree species that associate with
1107 arbuscular mycorrhizae. This result was not observed here, as photosynthetic
1108 properties varied as much within as across the two mycorrhizal associations rep-
1109 resented. Given the high variability in measured photosynthetic traits within
1110 and across species, effects of mycorrhizal association likely require more intensive
1111 sampling efforts to detect than were possible here.

1112 3.4.4 *Implications for photosynthetic least-cost theory model development*

1113 In the field, soil nutrient availability is heterogeneous across time and space
1114 (Table S4). Unaccounted within-plot heterogeneity may have contributed to the
1115 low amount of variation explained by soil N availability in our statistical mod-
1116 els, as resin bags are a coarse surrogate for soil N availability. Despite this, we
1117 still observed evidence for nutrient-water use tradeoffs, suggesting that observed
1118 responses reported here may be an underestimate toward the net effect of soil
1119 N availability on these tradeoffs. While we urge caution in the interpretation of

1120 these results, they do provide a promising baseline for future studies investigating
1121 patterns expected from photosynthetic least-cost theory at finer spatiotemporal
1122 resolutions.

1123 The general stronger relationship between leaf N content and photosyn-
1124 thetic parameters versus between leaf N content and soil N availability suggests
1125 that leaf N content is more directly tied to photosynthesis than soil N availabil-
1126 ity. While this could be due to the high spatiotemporal heterogeneity of soil N
1127 availability, principles from photosynthetic least-cost theory suggest that leaf N
1128 content is the downstream product of leaf nutrient demand to build and maintain
1129 photosynthetic machinery, which is set by aboveground environmental conditions
1130 such as light availability, CO₂, temperature, or vapor pressure deficit (Smith
1131 et al. 2019; Paillassa et al. 2020; Peng et al. 2021; Westerband et al. 2023). The
1132 stronger relationship between leaf N and photosynthetic parameters paired with
1133 the strong negative relationship between leaf N and χ could indicate a relatively
1134 stronger effect of climate on leaf N-photosynthesis relationships than soil resource
1135 availability. However, the short distance between plots and across sites limited
1136 our ability to test this mechanism.

1137 Variation in soil pH affected least cost responses less than variations in
1138 soil N availability, in part because experimental treatments directly increased soil
1139 N and affected soil pH in opposite directions. While soil pH has been shown
1140 to drive nitrogen-water tradeoffs in global gradient analyses (Viet et al. 2013;
1141 Paillassa et al. 2020), these responses may be due to covariations between soil pH
1142 and nutrient cycling rather than a role of pH per se. The direct manipulations
1143 of soil pH and soil N availability in this study allowed us to partly disentangle

1144 these factors and show that variation in N availability matters more for least-cost
1145 tradeoffs than pH alone.

1146 3.4.5 *Conclusions*

1147 Increasing soil N availability generally increased leaf N content (both area-
1148 and mass-based), but did not significantly influence χ . This shift in leaf N led
1149 to a reduction in PNUE, and an increase in leaf N per unit χ with increasing
1150 soil N availability. Despite null effects of soil N availability on χ , we observed a
1151 strong negative relationship between leaf N content and χ . These results provide
1152 empirical support for the nutrient-water use tradeoffs expected from photosyn-
1153 thetic least-cost theory in response to soil nutrient availability, but suggest that
1154 all tenets of the theory may not hold in every environment. These results exper-
1155 imentially test previous work suggesting that leaf water-nitrogen economies vary
1156 across gradients of soil nutrient availability and pH, and show that variations in
1157 nutrient availability matter more for determining variation in leaf photosynthetic
1158 traits than soil pH.

1159

Chapter 4

1160 The relative cost of resource use for photosynthesis drives variance in
1161 leaf nitrogen content across a climate and soil resource availability
1162 gradient

1163 4.1 Introduction

1164 Terrestrial biosphere models, which comprise the land surface component
1165 of Earth system models, are sensitive to the formulation of photosynthetic pro-
1166 cesses (Knorr and Heimann 2001; Ziehn et al. 2011; Booth et al. 2012; Walker
1167 et al. 2021). This is because photosynthesis is the largest carbon flux between the
1168 atmosphere and terrestrial biosphere (IPCC 2021), and is constrained by ecosys-
1169 tem carbon and nutrient cycles (Hungate et al. 2003; LeBauer and Treseder
1170 2008; Fay et al. 2015). Many terrestrial biosphere models formulate photosyn-
1171 thesis by parameterizing photosynthetic capacity within plant functional groups
1172 through empirical linear relationships between area-based leaf nitrogen content
1173 (N_{area}) and the maximum carboxylation rate of Ribulose-1,5-bisphosphate car-
1174 boxylase/oxygenase (Kattge et al. 2009; Rogers 2014; Rogers et al. 2017). Models
1175 are also beginning to include connected carbon-nitrogen cycles (Wieder et al. 2015;
1176 Shi et al. 2016; Davies-Barnard et al. 2020; Braghieri et al. 2022), which allows
1177 leaf photosynthesis to be predicted directly through changes in N_{area} and indirectly
1178 through changes in soil nitrogen availability (e.g., LPJ-GUESS, CLM5.0) (Smith
1179 et al. 2014; Lawrence et al. 2019). Despite recent model developments, open
1180 questions remain regarding the generality of ecological relationships between soil
1181 nitrogen availability, leaf nitrogen content, and leaf photosynthesis across edaphic
1182 and climatic gradients.

1183 Empirical support for positive relationships between soil nitrogen availabil-
1184 ity and N_{area} is abundant (Firn et al. 2019; Liang et al. 2020), and is a result
1185 often attributed to the high nitrogen cost of building and maintaining Rubisco
1186 (Evans 1989; Evans and Seemann 1989; Onoda et al. 2004; Onoda et al. 2017;
1187 Walker et al. 2014; Dong et al. 2020). Such patterns imply that positive rela-
1188 tionships between soil nitrogen availability and N_{area} should cause an increase in
1189 leaf photosynthesis and photosynthetic capacity by increasing the maximum rate
1190 of Rubisco carboxylation through increased investments to Rubisco construction
1191 and maintenance. This integrated N_{area} -photosynthesis response to soil nitrogen
1192 availability has been observed both in manipulative experiments and across envi-
1193 ronmental gradients (Field and Mooney 1986; Evans 1989; Walker et al. 2014; Li
1194 et al. 2020), and is thought to be driven by ecosystem nitrogen limitation, which
1195 limits primary productivity globally (LeBauer and Treseder 2008; Fay et al. 2015).
1196 However, this response is not consistently observed, as recent studies note variable
1197 N_{area} -photosynthesis relationships across soil nitrogen availability gradients (Liang
1198 et al. 2020; Luo et al. 2021) and that aboveground growing conditions (e.g., light
1199 availability, temperature, vapor pressure deficit) or species identity traits (e.g.,
1200 photosynthetic pathway, nitrogen acquisition strategy) may be more important
1201 for explaining variance in N_{area} and photosynthetic capacity across environmental
1202 gradients (Adams et al. 2016; Dong et al. 2017; Dong et al. 2020; Dong et al.
1203 2022; Smith et al. 2019; Peng et al. 2021; Westerband et al. 2023).

1204 One hypothesized mechanism to explain variance in N_{area} across environ-
1205 mental gradients has been proposed via photosynthetic least-cost theory (Wright
1206 et al. 2003; Prentice et al. 2014; Paillassa et al. 2020; Harrison et al. 2021).

1207 The theory predicts that plants acclimate to environments by optimizing photo-
1208 synthetic assimilation rates at the lowest summed cost of nitrogen and water use
1209 (Wright et al. 2003; Prentice et al. 2014). In a given environment, the theory pro-
1210 poses that nitrogen and water use can be substituted for each other to maintain
1211 the lowest summed cost to satisfy leaf resource demand, such that optimal photo-
1212 synthetic rates are achieved with less efficient use of the more abundant and less
1213 costly resource to acquire in exchange for more efficient use of the less abundant
1214 and more costly resource to acquire. The theory predicts that, all else equal, an
1215 increase in soil nitrogen availability should decrease the cost of acquiring and us-
1216 ing nitrogen relative to water (a ratio referred to herein as β), resulting in optimal
1217 photosynthetic rates achieved with greater N_{area} at lower stomatal conductance
1218 and lower leaf $C_i:C_a$ (Wright et al. 2003; Prentice et al. 2014). Alternatively, an
1219 increase in soil moisture should reduce costs of water acquisition and use, increas-
1220 ing β , stomatal conductance, and leaf $C_i:C_a$, resulting in optimal photosynthetic
1221 rates achieved with decreased N_{area} . The theory also predicts variability in stom-
1222 atal conductance and N_{area} in response to climatic factors, suggesting that the
1223 optimal response to increased vapor pressure deficit (VPD) should be a reduction
1224 in stomatal conductance and leaf $C_i:C_a$ that is counterbalanced by an increase
1225 in N_{area} to support the higher photosynthetic capacity needed to maintain high
1226 assimilation at lower conductance (Grossiord et al. 2020; Dong et al. 2020; López
1227 et al. 2021; Westerband et al. 2023).

1228 Leaf nitrogen allocation responses to changing climates or soil resource
1229 availability may also depend on their mode of nutrient acquisition or photo-
1230 synthetic pathway. For example, species that form associations with symbiotic

1231 nitrogen-fixing bacteria (referred as “N-fixing species” from this point forward)
1232 should, in theory, have access to a less finite nitrogen supply, which may result in
1233 lower β values than species not capable of forming such associations (referred as
1234 “non-fixing species” from this point forward). This result was previously shown in
1235 a greenhouse experiment, where a leguminous species generally had lower costs of
1236 nitrogen acquisition compared to a non-leguminous species, although these differ-
1237 ences were generally stronger under increased nitrogen limitation (Perkowski et al.
1238 2021). Lower β values could be a possible explanation for why N-fixing species
1239 commonly have higher leaf nitrogen content than non-fixing species (Adams et al.
1240 2016; Dong et al. 2017). Similarly, leaf nitrogen allocation patterns across en-
1241 vironmental gradients may be dependent on photosynthetic pathway. Lower leaf
1242 $C_i:C_a$ values in C₄ species suggests that C₄ species should have lower β values
1243 than C₃ species (Scott and Smith 2022), a pattern that could be the result of
1244 increased costs associated with water acquisition and use or reduced costs of ni-
1245 trogen acquisition and use relative to C₃ species. No study to date has directly
1246 quantified β in C₄ species aside from the dataset used to initially parameterize
1247 an optimality model for C₄ species (Scott and Smith 2022).

1248 While photosynthetic least-cost theory provides a unified hypothesis for un-
1249 derstanding effects of climate and soil resource availability on N_{area} , empirical tests
1250 of the theory are sparse. Increasing soil nitrogen availability has been previously
1251 shown to decrease the cost of acquiring nutrients (Bae et al. 2015; Perkowski et al.
1252 2021; Lu et al. 2022), which can induce predictable nutrient-water use tradeoffs
1253 expected from the theory across broad environmental gradients (Paillassa et al.
1254 2020; Querejeta et al. 2022; Westerband et al. 2023) and in manipulation experi-

1255 ments (Bialic-Murphy et al. 2021). Additionally, increasing VPD has been shown
1256 to have a positive effect on N_{area} (Dong et al. 2017; Dong et al. 2020; Firn et al.
1257 2019; López et al. 2021). However, studies have been restricted to exploring these
1258 patterns with C3 species and, while previous studies have shown that variance
1259 in N_{area} across environmental gradients is driven by strong negative relationships
1260 with leaf $C_i:C_a$ (3.4, (Dong et al. 2017; Paillassa et al. 2020; Westerband et al.
1261 2023)), no study to date has explicitly investigated effects of soil resource avail-
1262 ability or plant functional group on N_{area} using β as a direct predictor of leaf
1263 $C_i:C_a$. Additionally, as N_{area} can be broken down into structural (leaf mass per
1264 area; M_{area} ; g m-2) and metabolic (mass-based leaf nitrogen content; N_{mass} ; gN
1265 g-1) components (Dong et al. 2017), no study has investigated which component
1266 of N_{area} drives the hypothesized response of N_{area} to leaf $C_i:C_a$. Understanding
1267 whether changes in N_{area} due to leaf $C_i:C_a$ are driven by changes in leaf morphol-
1268 ogy or stoichiometry is important, especially because N_{mass} tends to covary with
1269 M_{area} due to tradeoffs between leaf longevity and leaf productivity (Wright et al.
1270 2004; Reich 2014; Onoda et al. 2017; Wang et al. 2023).

1271 In this chapter, I measured N_{area} , N_{mass} , M_{area} , leaf $\delta^{13}\text{C}$ -derived estimates
1272 of leaf $C_i:C_a$, and leaf $\delta^{13}\text{C}$ -derived estimates of β in 520 individuals spanning
1273 57 species scattered across 24 grassland sites in Texas, USA (Table S1). Texas
1274 contains a diverse climatic gradient, indicated by 2006-2020 mean annual precip-
1275 itation totals ranging from 204 to 1803 mm and 2006-2020 mean annual temper-
1276 ature ranging from 11.8° to 24.6°C. Variability in soil nitrogen availability and
1277 soil moisture was expected across sites, owing to differences in soil texture and
1278 aboveground climate that would drive differential rates of water retention and

1279 nitrogen transformations to plant-available substrate. I leveraged the expected
1280 climatic and soil resource variability across sites to test the following hypotheses:

- 1281 1. Soil nitrogen availability will decrease β through a reduction in costs of
1282 nitrogen acquisition and use, while soil moisture will increase β through a
1283 reduction in costs of water acquisition and use. Following previous results,
1284 we expected that N-fixing species would have lower β values and that C₄
1285 species would have lower β values.
- 1286 2. Leaf $C_i:C_a$ will be positively related to β , a pattern that will result in a
1287 negative indirect effect of increasing soil nitrogen availability on leaf $C_i:C_a$,
1288 a positive indirect effect of increasing soil moisture on leaf $C_i:C_a$, and lower
1289 leaf $C_i:C_a$ in both N-fixing species and C₄ species. We also expected that
1290 leaf $C_i:C_a$ would be negatively related to VPD, as increasing atmospheric
1291 dryness should cause plants to close stomata to minimize water loss.
- 1292 3. N_{area} will be negatively related to leaf $C_i:C_a$ and β . This response will result
1293 in an indirect positive effect of increasing soil nitrogen availability, a negative
1294 effect of increasing soil moisture on N_{area} , and generally larger N_{area} values
1295 in both N-fixing species. While theory predicts that negative relationships
1296 between N_{area} and leaf $C_i:C_a$ should yield generally larger N_{area} in C₄ species,
1297 we expected that C₄ species would have lower N_{area} due to generally greater
1298 nitrogen use efficiency in C₄ species than C₃ species. Additionally, VPD
1299 was expected to increase N_{area} , a pattern that would be directly mediated
1300 through the reduction in leaf $C_i:C_a$ with increasing VPD.

1301 4.2 Methods

1302 4.2.1 *Site descriptions and sampling methodology*

1303 I collected leaf and soil samples from 24 open grassland sites across central and
1304 eastern Texas in summer 2020 and summer 2021 (Fig. 4.1). Twelve sites were vis-
1305 ited between June and July 2020 and 14 sites (11 unique from 2020) were visited
1306 between May and June 2021 (Table 4.1). I explicitly chose sites that maximized
1307 variability in precipitation and edaphic variability between sites while minimiz-
1308 ing temperature variability across the environmental gradient (Table 4.1). No
1309 site with personally communicated or anecdotal evidence of grazing or distur-
1310 bance (e.g., mowing, feral hog activity, etc.) were used. I collected leaf material
1311 from three individuals each of the five most abundant species at random locations
1312 at each site, only selecting species that were broadly classified as graminoid or
1313 forb/herb growth habits per the USDA PLANTS database (USDA NRCS 2022).
1314 All collected leaves were fully expanded with no visible herbivory or other external
1315 damage and also free from shading by nearby shrubs or trees. Five soil samples
1316 were collected from 0-15cm below the soil surface at each site near the leaf collec-
1317 tion sample locations. Soil samples were later mixed together by hand to create
1318 one composite soil sample per site.

1319 4.2.2 *Leaf trait measurements*

1320 Images of each leaf were taken immediately following each site visit using a flat-
1321 bed scanner. Fresh leaf area was determined from each image using the 'LeafArea'
1322 R package (Katabuchi 2015), which automates leaf area calculations using ImageJ
1323 software (Schneider et al. 2012). Each leaf was dried at 65°C for at least 48 hours

1324 to a constant mass, weighed, and manually ground in a mortar and pestle until
1325 homogenized. Leaf mass per area (M_{area} ; g m⁻²) was calculated as the ratio of
1326 dry leaf biomass to fresh leaf area. Subsamples of dried and homogenized leaf
1327 tissue were used to measure leaf nitrogen content (N_{mass} ; gN g⁻¹) through ele-
1328 mental combustion analysis (Costech-4010, Costech Instruments, Valencia, CA).
1329 Leaf nitrogen content per unit leaf area (N_{area} ; gN m⁻²) was then calculated as
1330 the product of N_{mass} and M_{area} .

1331 Subsamples of dried and homogenized leaf tissue were sent to the University
1332 of California-Davis Stable Isotope Facility to determine leaf $\delta^{13}\text{C}$. Leaf $\delta^{13}\text{C}$ values
1333 were determined using an elemental analyzer (PDZ Europa ANCA-GSL; Sercon
1334 Ltd., Chestshire, UK) interfaced to an isotope ratio mass spectrometer (PDZ
1335 Europa 20-20 Isotope Ratio Mass Spectrometer, Sercon Ltd., Chestshire, UK).
1336 I used leaf $\delta^{13}\text{C}$ values (‰; relative to Vienna Pee Dee Belemnite international
1337 reference standard) to estimate the ratio of intercellular (C_i) to extracellular (C_a)
1338 CO₂ ratio (leaf $C_i:C_a$; unitless) following the approach of Farquhar et al. (1989)
1339 described in Cernusak et al. (2013). Specifically, I derived leaf C_i:C_a as:

$$\text{Leaf } \frac{C_i}{C_a} = \frac{\Delta^{13}\text{C} - a}{b - a} \quad (4.1)$$

1340 where $\Delta^{13}\text{C}$ represents the relative difference between leaf $\delta^{13}\text{C}$ (‰) and air $\delta^{13}\text{C}$
1341 (‰), and is calculated as:

$$\Delta^{13}\text{C} = \frac{\delta^{13}\text{C}_{\text{air}} - \delta^{13}\text{C}_{\text{leaf}}}{1 + \delta^{13}\text{C}_{\text{leaf}}} \quad (4.2)$$

1342 $\delta^{13}\text{C}_{\text{air}}$, traditionally assumed to be -8‰ (Keeling et al. 1979; Farquhar et al.

1343 1989), was calculated as a function of calendar year t using an empirical equation
1344 derived in Feng (1999):

$$\delta^{13}C_{air} = -6.429 - 0.006e^{0.0217(t-1740)} \quad (4.3)$$

1345 This calculation resulted in $\delta^{13}C_{air}$ values for 2020 and 2021 as -9.04‰ and -
1346 9.09‰, respectively. a represents the fractionation between ^{12}C and ^{13}C due to
1347 diffusion in air, assumed to be 4.4‰, and b represents the fractionation caused
1348 by Rubisco carboxylation, assumed to be 27‰ (Farquhar et al. 1989). For C_4
1349 species, b in Eqn. 4.1 was set to 6.3‰, and was derived from:

$$b = c + (d \cdot \phi) \quad (4.4)$$

1350 Where c was set to -5.7‰ and d was set to 30‰ (Farquhar et al. 1989). ϕ , which
1351 is the bundle sheath leakiness term, was set to 0.4. All leaf $C_i:C_a$ values less than
1352 0.1 and greater than 0.95 were assumed to be incorrect and removed.

1353 I derived the unit cost of resource use (β) using leaf $C_i:C_a$ and site climate
1354 data with equations first described in Prentice et al. (2014) and simplified in
1355 Lavergne et al. (2020):

$$\beta = 1.6\eta^*D \frac{\chi - (\frac{\Gamma^*}{C_a})^2}{(1 - \chi)^2(K_m + \Gamma^*)} \quad (4.5)$$

1356 where η^* is the viscosity of water relative to 25°C, calculated using elevation and
1357 mean air temperature of the seven days leading up to each site visit following
1358 equations in Huber et al. (2009). D represents vapor pressure deficit (Pa), set

1359 to the mean vapor pressure deficit of the seven days leading up to each site visit,
1360 C_a represents atmospheric CO₂ concentration, arbitrarily set to 420 $\mu\text{mol mol}^{-1}$
1361 CO₂. K_m (Pa) is the Michaelis-Menten coefficient for Rubisco affinity to CO₂ and
1362 O₂, calculated as:

$$K_m = K_c \cdot \left(1 + \frac{O_i}{K_o}\right) \quad (4.6)$$

1363 where K_c (Pa) and K_o (Pa) are the Michaelis-Menten coefficients for Rubisco
1364 affinity to CO₂ and O₂, respectively, and O_i is the intercellular O₂ concentration.
1365 Γ^* (Pa) is the CO₂ compensation point in the absence of dark respiration. K_c , K_o ,
1366 and Γ^* were determined using equations described in Medlyn et al. (2002) and
1367 derived in Bernacchi et al. (2001), invoking an elevation correction for atmospheric
1368 pressure as explained in Stocker et al. (2020).

Table 4.1. Site locality information, sampling year(s), 2006-2020 mean annual precipitation (MAP; mm), mean annual temperature (MAT; °C), and water holding capacity (WHC; mm)*

| Site | Latitude | Longitude | Sampling year | MAP | MAT | WHC |
|--------------------|----------|-----------|---------------|--------|------|-------|
| Edwards_2019_17 | 29.95 | -100.36 | 2020 | 563.5 | 19.0 | 224.7 |
| Uvalde_2020_02 | 29.59 | -100.09 | 2020, 2021 | 648.5 | 19.5 | 224.7 |
| Menard_2020_01 | 30.91 | -99.59 | 2020 | 641.9 | 18.3 | 220.2 |
| Kerr_2020_03 | 30.06 | -99.34 | 2021 | 672.4 | 18.3 | 237.5 |
| Bandera_2020_03 | 29.85 | -99.30 | 2021 | 789.4 | 18.8 | 235.1 |
| Sansaba_2020_01 | 31.29 | -98.62 | 2020 | 733.0 | 18.8 | 234.3 |
| Comal_2020_21 | 29.79 | -98.43 | 2020 | 878.5 | 19.9 | 220.7 |
| Blanco_2019_16 | 29.99 | -98.43 | 2020 | 833.0 | 19.2 | 222.2 |
| Bexar_2019_13 | 29.24 | -98.43 | 2020 | 759.3 | 21.5 | 206.0 |
| Burnet_2020_14 | 30.84 | -98.34 | 2021 | 763.3 | 19.5 | 217.8 |
| Comal_2020_19 | 30.01 | -98.32 | 2021 | 845.0 | 19.3 | 220.4 |
| Hays_2020_54 | 29.96 | -98.17 | 2021 | 861.3 | 20.0 | 225.6 |
| Burnet_2020_12 | 30.82 | -98.06 | 2021 | 815.1 | 19.4 | 245.3 |
| Williamson_2019_09 | 30.71 | -97.86 | 2020 | 867.7 | 19.7 | 270.2 |
| Williamson_2019_10 | 30.54 | -97.77 | 2020 | 819.5 | 19.9 | 239.8 |
| Bell_2021_08 | 31.06 | -97.55 | 2021 | 937.3 | 19.6 | 232.3 |
| Fayette_2021_12 | 29.86 | -97.21 | 2021 | 985.7 | 20.4 | 165.6 |
| Fayette_2019_04 | 30.09 | -96.78 | 2020 | 1017.4 | 20.6 | 226.9 |
| Fayette_2020_09 | 29.86 | -96.71 | 2021 | 1002.7 | 20.8 | 187.6 |
| Washington_2020_08 | 30.28 | -96.41 | 2021 | 1077.4 | 20.4 | 203.9 |
| Austin_2020_03 | 29.78 | -96.24 | 2021 | 1108.7 | 20.6 | 253.0 |
| Brazos_2020_16 | 30.93 | -96.23 | 2021 | 1078.0 | 20.1 | 202.2 |
| Brazos_2020_18 | 30.52 | -96.21 | 2020, 2021 | 1099.4 | 20.4 | 233.5 |
| Harris_2020_03 | 29.88 | -95.31 | 2020, 2021 | 1492.0 | 21.6 | 265.6 |

1369 * Rows are arranged by longitude to visualize precipitation variability across sites

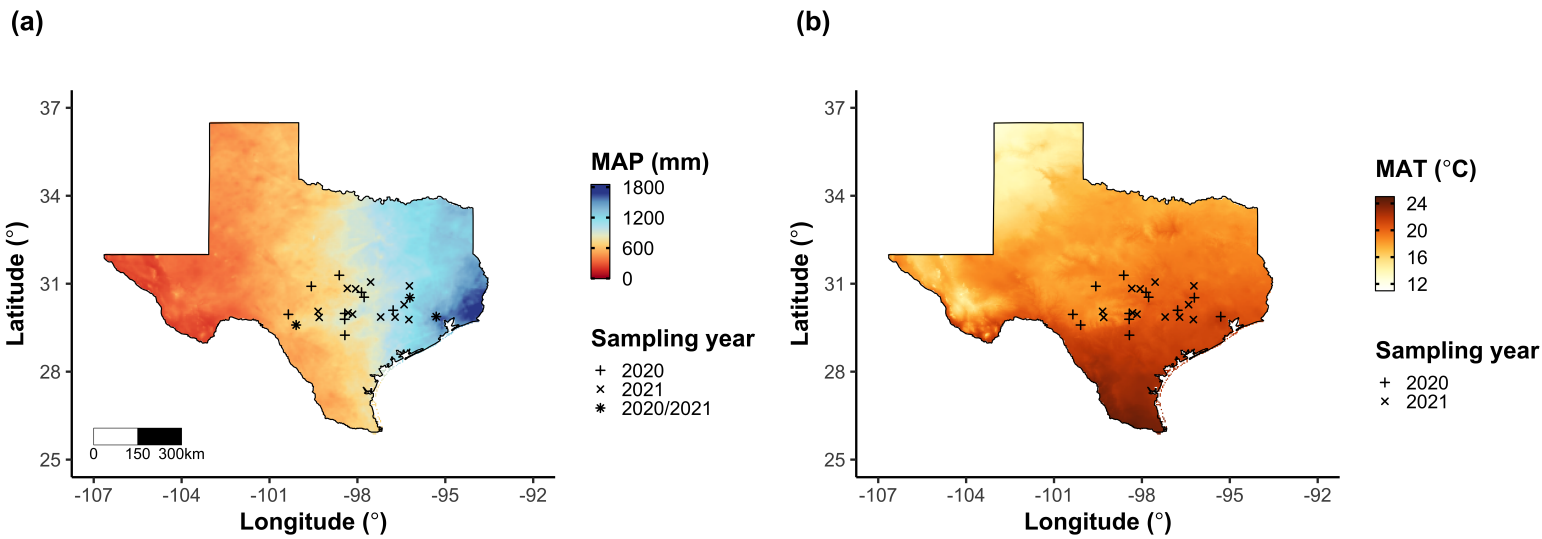


Figure 4.1. Maps that detail site locations along 2006-2020 mean annual precipitation (a) and mean annual temperature (b) gradients in Texas, USA. Precipitation and temperature data were plotted at a 4-km grid resolution and are masked to include only grid cells that occur in the Texas state boundary in the United States. In both panels, open circles refer to sites visited in 2020, open triangles to sites visited in 2021, and closed circles to sites visited in 2020 and 2021. The scale bar in (a) also applies to (b).

1370 4.2.3 *Site climate data*

1371 I used the Parameter-elevation Regressions on Independent Slopes Model (PRISM)
1372 (Daly et al. 2008) climate product to access gridded daily temperature and precip-
1373 itation data for the coterminous United States at a 4-km grid resolution between
1374 January 1, 2006 and July 31, 2021 (PRISM Climate Group, Oregon State Uni-
1375 versity, <https://prism.oregonstate.edu>, data created 4 Feb 2014, accessed 24 Mar
1376 2022). Daily mean air temperature, mean VPD, and total precipitation data were
1377 extracted from the grid cell that contained the latitude and longitude of each
1378 property using the ‘extract’ function in the ‘terra’ R package (Hijmans 2022).
1379 PRISM data were used in lieu of local weather station data because several rural
1380 sites did not have a local weather station present within a 20-km radius of the site.
1381 Daily site climate data were used to estimate mean annual precipitation and mean
1382 annual temperature for each site between 2006 and 2020 (Table 1). I calculated
1383 total precipitation and mean daily VPD for the prior 1, 2, 3, 4, 5, 6, 7, 8, 9, 10,
1384 15, 20, 25, 30, 60, and 90 days leading up to each site visit.

1385 4.2.4 *Site edaphic characteristics*

1386 Subsamples of composited soil samples were sent to the Texas A & M Soil, Water
1387 and Forage Laboratory to quantify soil nitrate concentration (NO₃-N; ppm). Soil
1388 NO₃-N was determined by extracting composite soil samples in 1 M KCl, measur-
1389 ing absorbance values of extracts at 520 nm using the end product of a NO₃-N to
1390 NO₂-N cadmium reduction reaction (Kachurina et al. 2000; Keeney and Nelson
1391 1983). Soil texture data from 0-15cm below the soil surface were accessed using
1392 the SoilGrids2.0 data product (Poggio et al. 2021) through the ‘fetchSoilGrids’

1393 function in the ‘soilDB’ R package (Beaudette et al. 2022). I used SoilGrids2.0
1394 to access soil texture data in lieu of analyses using the collected composite soil
1395 sample due to a lack of soil material from some sites after sending samples for soil
1396 NO₃-N.

1397 Soil moisture was not measured in the field, but was estimated using the
1398 ‘Simple Process-Led Algorithms for Simulating Habitats’ model (SPLASH) (Davis
1399 et al. 2017). This model, derived from the STASH model (Cramer and Prentice
1400 1988), spins up a bucket model using Priestley-Taylor equations (Priestley and
1401 Taylor 1972) to calculate daily soil moisture (W_n ; mm) as a function of the previous
1402 day’s soil moisture (W_{n-1} ; mm), daily precipitation (P_n ; mm), condensation (C_n ;
1403 mm), actual evapotranspiration (E_n^a ; mm), and runoff (RO; mm):

$$W_n = W_{n-1} + P_n + C_n - E_n^a - RO \quad (4.7)$$

1404 Models were spun up by equilibrating the previous day’s soil moisture using succes-
1405 sive model iterations with daily mean air temperature, daily precipitation total,
1406 the number of daily sunlight hours, and latitude as model inputs (Davis et al.
1407 2017). Daily sunlight hours were estimated for each day at each site using the
1408 ‘getSunlightTimes’ function in the ‘suncalc’ R package, which estimated sunrise
1409 and sunset times of each property using date and site coordinates (Thieurmel and
1410 Elmarhraoui 2019). Water holding capacity (mm), or bucket size, was estimated
1411 as a function of soil texture using pedotransfer equations explained in Saxton and
1412 Rawls (2006), as done in Stocker et al. (2020) and Bloomfield et al. (2023). A
1413 summary of these equations is included in the Supplemental Information.

1414 Daily soil moisture outputs from the SPLASH model for each site were
1415 used to calculate mean daily soil moisture for the prior 1, 2, 3, 4, 5, 6, 7, 8, 9,
1416 10, 15, 20, 25, 30, 60, and 90 days leading up to each site visit. Mean daily
1417 soil moisture values were then expressed as a fraction of water holding capacity
1418 to normalize across sites with different bucket depths, as done in Stocker et al.
1419 (2018).

1420 4.2.5 *Plant functional group assignments*

1421 Plant functional group was assigned to each species and used as the primary
1422 descriptor of species identity. Specifically, I assigned plant functional groups
1423 based on photosynthetic pathway (C_3 , C_4) and ability to form associations with
1424 symbiotic nitrogen-fixing bacteria. The ability to form associations with symbi-
1425 otic nitrogen-fixing bacteria was assigned based on whether species were in the
1426 *Fabaceae* family, and photosynthetic pathway of each species was determined from
1427 past literature and confirmed through leaf $\delta^{13}\text{C}$ values. We chose these plant func-
1428 tional groups based on *a priori* hypotheses regarding the functional role of nitrogen
1429 fixation and photosynthetic pathway on the sensitivity of plant nitrogen uptake
1430 and leaf nitrogen allocation to soil nutrient availability and aboveground growing
1431 conditions. These plant functional group classifications resulted in three distinct
1432 plant functional groups within our dataset: C_3 legumes ($n = 53$), C_3 non-legumes
1433 ($n = 350$), and C_4 non-legumes ($n = 117$).

1434 4.2.6 *Data analysis*

1435 All analyses and plotting were conducted in R version 4.1.1 (R Core Team 2021).

1436 I constructed a series of separate linear mixed-effects models to investigate en-

1437 vironmental drivers of β , leaf $C_i:C_a$, N_{area} , N_{mass} , and M_{area} , followed by a path

1438 analysis using a piecewise structural equation model to investigate direct and

1439 indirect effects of climate and soil resource availability on N_{area} .

1440 To explore environmental drivers of β , I built a linear mixed-effects model

1441 that included soil moisture, soil nitrogen availability, and plant functional group

1442 as fixed effect coefficients. Species were designated as a random intercept term.

1443 Interaction coefficients between all possible combinations of the three fixed effect

1444 coefficients were also included. β was natural log transformed to linearize data.

1445 I used an information-theoretic model selection approach to determine whether

1446 90-, 60-, 30-, 20-, 15-, 10-, 9-, 8-, 7-, 6-, 5-, 4-, 3-, 2-, or 1-day mean daily soil

1447 moisture conferred the best model fit for β . To do this, I constructed 16 separate

1448 linear mixed-effects models where log-transformed β was included as the response

1449 variable and each soil moisture time step was separately included as a single

1450 continuous fixed effect. Species were included as a random intercept term for all

1451 models. I used corrected Akaike Information Criterion (AICc) to select the soil

1452 moisture timescale that conferred the best model fit, indicated by the model with

1453 the lowest AICc score (Table S2; Fig. S2).

1454 To explore environmental drivers of leaf $C_i:C_a$, I constructed a second linear

1455 mixed effects model that included VPD, soil moisture, soil nitrogen availability,

1456 and plant functional group as fixed effect coefficients. Two-way interactions be-

1457 tween plant functional group and VPD, soil nitrogen availability, or soil moisture

1458 were also included as fixed effect coefficients, in addition to a three-way interaction
1459 between soil moisture, soil nitrogen availability, and plant functional group.
1460 Species were included as a random intercept term. I used an information-theoretic
1461 model selection approach to determine whether 90-, 60-, 30-, 20-, 15-, 10-, 9-, 8-,
1462 7-, 6-, 5-, 4-, 3-, 2-, or 1-day mean daily VPD conferred the best model fit for leaf
1463 $C_i:C_a$ using the same approach explained above for the soil moisture effect on β .
1464 The soil moisture timescale was set to the same timescale that conferred the best
1465 fit for β .

1466 To explore environmental drivers of N_{area} , N_{mass} , and M_{area} , I constructed
1467 three separate linear mixed effects model that each included leaf $C_i:C_a$, soil ni-
1468 trogen availability, soil moisture, and plant functional group as fixed effect coef-
1469 ficients. Two-way interactions between plant functional group and β , leaf $C_i:C_a$,
1470 soil nitrogen availability, or soil moisture were included as additional fixed effect
1471 coefficients, in addition to a three-way interaction between soil nitrogen availabil-
1472 ity, soil moisture, and plant functional group. Species were included as a random
1473 intercept term, with the soil moisture timescale set to the same timescale that
1474 conferred the best fit for β .

1475 In all linear mixed-effects models explained above, including those to select
1476 relevant timescales, I used the 'lmer' function in the 'lme4' R package (Bates et al.
1477 2015) to fit each model and the 'Anova' function in the 'car' R package (Fox and
1478 Weisberg 2019) to calculate Type II Wald's χ^2 and determine the significance
1479 level ($\alpha = 0.05$) of each fixed effect coefficient. I used the 'emmeans' R package
1480 (Lenth 2019) to conduct post-hoc comparisons using Tukey's tests, where degrees
1481 of freedom were approximated using the Kenward-Roger approach (Kenward and

1482 Roger 1997). Trendlines and error ribbons for all plots were drawn using a series
1483 of ‘emmeans’ outputs across the range in plotted x-axis values.

1484 Finally, I conducted a path analysis using a piecewise structural equation
1485 model to examine direct and indirect pathways that determined variance in N_{area} .
1486 Six separate linear mixed effects models were loaded into the piecewise structural
1487 equation model. Models were constructed per *a priori* hypotheses following pat-
1488 terns expected from photosynthetic least-cost theory. The first model regressed
1489 N_{area} against N_{mass} and M_{area} . The second model regressed M_{area} against leaf
1490 $C_i:C_a$. The third model regressed N_{mass} against leaf $C_i:C_a$ and M_{area} (Dong et al.
1491 2017; Dong et al. 2020). The fourth model regressed leaf $C_i:C_a$ against β and
1492 VPD. The fifth model regressed β against soil nitrogen availability, soil moisture,
1493 ability to associate with symbiotic nitrogen-fixing bacteria, and photosynthetic
1494 pathway. The sixth model regressed soil nitrogen availability against soil mois-
1495 ture. All models included the relevant timescale selected in the individual linear
1496 mixed effect models explained above. Models included species as a random inter-
1497 cept term, were built using the ‘lme’ function in the ‘nlme’ R package (Pinheiro
1498 and Bates 2022), and subsequently loaded into the piecewise structural equation
1499 model using the ‘psem’ function in the ‘piecewiseSEM’ R package (Lefcheck 2016).

1500 4.3 Results

1501 4.3.1 *Cost to acquire nitrogen relative to water*

1502 Model selection indicated that 90-day soil moisture conferred the best model fit
1503 for β ($AICc=1429.14$; Table S2; Fig. S1).

1504 Increasing soil nitrogen availability generally decreased β ($p < 0.001$; Table

1505 4.2; Fig. 4.2a), a pattern driven by a negative effect of increasing soil nitrogen on β
1506 in C₃ nonlegumes (Tukey: $p = 0.002$) and C₃ legumes (Tukey: $p = 0.031$) despite
1507 a null effect of soil nitrogen on β in C₄ nonlegumes (Tukey: $p = 0.905$). There
1508 was no effect of soil moisture on β ($p = 0.902$; Table 4.2; Fig. 4.2b). A functional
1509 group effect ($p < 0.001$; Table 4.2) indicated that C₄ nonlegumes generally had
1510 lower β values than both C₃ legumes and C₃ non-legumes (Tukey: $p < 0.001$
1511 in both cases), while β values in C₃ legumes did not differ from C₃ nonlegumes
1512 (Tukey: $p = 0.804$).

Table 4.2. Effects of soil moisture, soil nitrogen availability, and plant functional group on β

| | df | Coefficient | χ^2 | p |
|-----------------------------------|----|-------------|----------|------------------|
| Intercept | - | 3.39E+00 | - | - |
| Soil moisture (SM ₉₀) | 1 | -2.03E-01 | 0.015 | 0.902 |
| Soil N (N) | 1 | -1.49E-02 | 13.832 | <0.001 |
| PFT | 2 | - | 225.049 | <0.001 |
| SM ₉₀ *N | 1 | -8.86E-04 | 1.016 | 0.313 |
| SM ₉₀ *PFT | 2 | - | 0.754 | 0.686 |
| N*PFT | 2 | - | 5.236 | 0.073 |
| SM ₉₀ *N*PFT | 2 | - | 3.633 | 0.163 |

1513 *Significance determined using Type II Wald χ^2 tests ($\alpha = 0.05$). P-values < 0.05

1514 are in bold. Model coefficients are expressed on the natural-log scale and are only

1515 included for continuous fixed effects. Key: df = degrees of freedom, χ^2 = Wald

1516 Type II chi-square test statistic

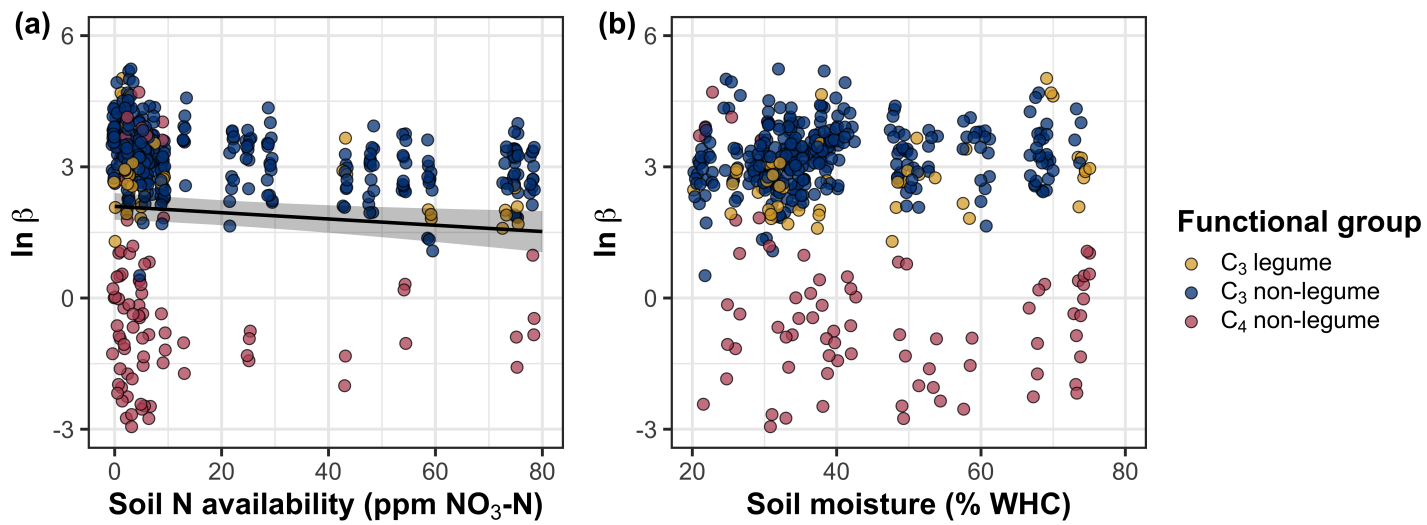


Figure 4.2. Effects of soil nitrogen availability (a) and 90-day soil moisture (b) on the unit cost ratio β . In (b), soil moisture is represented as a percent of site water holding capacity. Yellow shading and trendlines indicate C₃ legumes, blue shading and trendlines indicate C₃ non-legumes, and red shading and trendlines indicate C₄ non-legumes. Points are jittered for visibility. Variably colored trendlines are only included if there is an interaction between the x-axis and plant functional group, where solid trendlines indicate slopes that are different from zero ($p < 0.05$) and dashed trendlines indicate slopes that are not different from zero ($p > 0.05$). Error ribbons represent the upper and lower 95% confidence intervals of each fitted trendline.

1517 4.3.2 $C_i:C_a$

1518 Model selection indicated that 4-day daily VPD was the timescale that conferred

1519 the best model fit for leaf $C_i:C_a$ (AICc = -793.49; Table S1; Fig. S2).

1520 Model results revealed that increasing VPD generally decreased leaf $C_i:C_a$

1521 ($p < 0.001$; Table 4.3; Fig. 4.3a). There was no effect of soil moisture ($p =$

1522 0.843; Table 4.3; Fig. 4.3b) or soil nitrogen availability ($p = 0.544$; Table 4.3;

1523 Fig. 4.3c) on leaf $C_i:C_a$. A strong plant functional group effect ($p < 0.001$; Table

1524 4.3) indicated that C₄ nonlegumes had lower leaf $C_i:C_a$ than C₃ legumes and C₃

1525 nonlegumes (Tukey: $p < 0.001$ in both cases), with no difference between C₃

1526 legumes and C₃ nonlegumes (Tukey: $p = 0.865$).

Table 4.3. Effects of soil moisture, soil nitrogen availability, and plant functional group on leaf $C_i:C_a$ *

| | df | Coefficient | χ^2 | p |
|------------------------------------|----|-------------|----------|------------------|
| Intercept | - | 1.32E+00 | - | - |
| Vapor pressure deficit (VPD_4) | 1 | -4.53E-01 | 11.211 | <0.001 |
| Soil moisture (SM_{90}) | 1 | -1.71E-01 | 0.039 | 0.843 |
| Soil N (N) | 1 | -3.33E-03 | 0.369 | 0.544 |
| PFT | 2 | - | 227.005 | <0.001 |
| SM_{90}^*N | 1 | need this | 2.361 | 0.124 |
| VPD_4^*PFT | 2 | - | 0.927 | 0.629 |
| SM_{90}^*PFT | 2 | - | 0.817 | 0.664 |
| N^*PFT | 2 | - | 4.085 | 0.130 |
| $SM_{90}^*N^*PFT$ | 2 | - | 3.677 | 0.159 |

1527 *Significance determined using Type II Wald χ^2 tests ($\alpha = 0.05$). *P*-values less
1528 than 0.05 are in bold and *p*-values where $0.05 < p < 0.1$ are italicized. Leaf $C_i:C_a$
1529 was not transformed prior to model fitting, so model coefficients are reported
1530 on the response scale. Model coefficients are only included for continuous fixed
1531 effects.

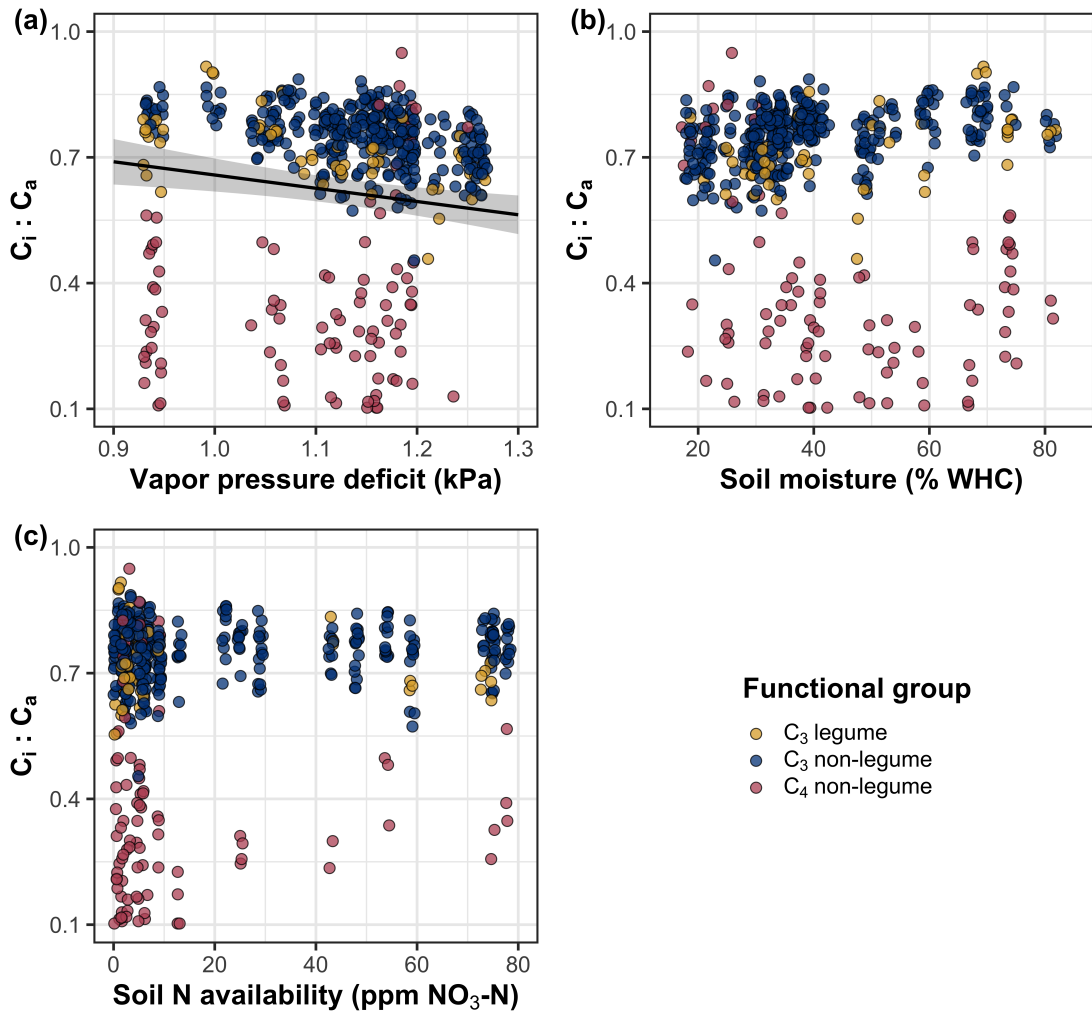


Figure 4.3. Effects of 4-day mean vapor pressure deficit (a), 90-day soil moisture (per water holding capacity; b), and soil nitrogen availability (c) on leaf $C_i:C_a$. Shading and trendlines are as explained in Figure 4.3. Points are jittered for visibility. Variably colored trendlines are only included if there is an interaction between the x-axis and plant functional group, where solid trendlines indicate slopes that are different from zero ($p < 0.05$) and dashed trendlines indicate slopes that are not different from zero ($p < 0.05$). Error ribbons represent the upper and lower 95% confidence intervals of each fitted trendline.

1532 4.3.3 *Leaf nitrogen content*

1533 An interaction between leaf $C_i:C_a$ and plant functional group ($p < 0.001$;
1534 Table 4.4) revealed that the negative effect of increasing leaf $C_i:C_a$ on N_{area} ($p <$
1535 0.001; Table 4.4) was driven by a negative effect of increasing leaf $C_i:C_a$ on N_{area}
1536 in C₃ nonlegumes (Tukey: $p < 0.001$) and C₃ legumes (Tukey: $p = 0.002$), with no
1537 observable effect in C₄ nonlegumes (Tukey: $p = 0.795$; Fig. 4.4a). An interaction
1538 between soil nitrogen availability and plant functional group ($p = 0.041$; Table
1539 4.4) indicated that the positive effect of increasing soil nitrogen ($p = 0.007$; Table
1540 4.4) was only apparent in C₃ legumes (Tukey: $p < 0.001$; Table 4.4; Fig. 4.4d),
1541 with no observable effect in C₃ nonlegumes (Tukey: $p = 0.449$) or C₄ nonlegumes
1542 (Tukey: $p = 0.680$). Increasing soil moisture increased N_{area} ($p=0.010$, Table
1543 4.4). A plant functional group effect ($p < 0.001$; Table 4.4) indicated that C₄
1544 nonlegumes had lower N_{area} compared to C₃ legumes (Tukey: $p < 0.001$) and C₃
1545 nonlegumes (Tukey: $p < 0.001$), while C₃ legumes had lower N_{area} compared to
1546 C₃ nonlegumes (Tukey: $p = 0.030$).

1547 A marginal interaction between soil nitrogen availability and soil moisture
1548 ($p = 0.097$; Table 4.4) indicated that the positive effect of increasing soil nitrogen
1549 on N_{mass} ($p < 0.001$; Table 4.4; Fig. 4.4e) was only apparent when soil moisture
1550 was less than 50% of the maximum water holding capacity (Tukey: $p < 0.05$ in
1551 all cases). There was no effect of leaf $C_i:C_a$ on N_{mass} ($p = 0.447$; Table 4.4; Fig.
1552 4.4b), but a positive effect of increasing soil moisture on N_{mass} . A plant functional
1553 group effect ($p < 0.001$; Table 4.4) indicated that C₄ nonlegumes had lower N_{mass}
1554 compared to C₃ legumes (Tukey: $p=0.003$) and C₃ nonlegumes (Tukey: $p =$
1555 0.011), while N_{mass} did not differ between C₃ legumes and C₃ nonlegumes (Tukey:

1556 $p = 0.231$).

1557 Variance in M_{area} was driven by a three-way interaction between soil ni-
1558 trogen availability, soil moisture, and plant functional group ($p = 0.018$; Table
1559 4.4). This interaction indicated that increasing soil moisture increased the posi-
1560 tive effect of increasing soil nitrogen availability on M_{area} in C₃ legumes (Tukey:
1561 $p = 0.030$) but did not modify the negative effect of increasing soil nitrogen on
1562 M_{area} in C₄ nonlegumes (Tukey: $p = 0.511$) or C₃ nonlegumes (Tukey: $p > 0.999$).
1563 There was otherwise no effect of soil moisture on M_{area} ($p = 0.696$; Table 4.4).
1564 An interaction between leaf $C_i:C_a$ and plant functional group ($p < 0.001$; Table
1565 4.4; Fig. 4.4c) indicated that negative effect of increasing leaf $C_i:C_a$ on M_{area} (p
1566 < 0.001 ; Table 4.4) was driven by a negative effect of increasing leaf $C_i:C_a$ on
1567 M_{area} in C₃ legumes and C₃ nonlegumes (Tukey: $p < 0.001$ in both cases), with
1568 no effect in C₄ nonlegumes (Tukey: $p = 0.343$; Fig. 4.4c).

Table 4.4. Effects of soil nitrogen fertilization, inoculation, and CO₂ treatments on N_{area} , N_{mass} , and M_{area}

| | df | N_{area} | | | N_{mass} | | | M_{area} | | |
|-----------------------------------|----|-------------------|----------|--------------|-------------------|----------|--------|-------------------|----------|--------------|
| | | Coefficient | χ^2 | p | Coefficient | χ^2 | p | Coefficient | χ^2 | p |
| (Intercept) | - | 2.41E+00 | - | - | 6.28E-02 | - | - | 6.90E+00 | - | - |
| $C_i:C_a$ | 1 | -2.32E+00 | 7.386 | 0.007 | 8.04E-01 | 0.578 | 0.447 | -3.13E+00 | 15.913 | <0.001 |
| Soil N (N) | 1 | 1.26E-02 | 6.070 | 0.014 | 1.12E-02 | 90.940 | <0.001 | -2.66E-02 | 43.529 | <0.001 |
| Soil moisture (SM ₉₀) | 1 | 5.60E-01 | 6.717 | 0.010 | 7.81E-01 | 11.205 | <0.001 | -2.53E-01 | 0.153 | 0.696 |
| PFT | 1 | - | 52.277 | <0.001 | - | 17.184 | <0.001 | - | 7.289 | 0.026 |
| SM ₉₀ *N | 1 | 5.44E-02 | 0.444 | 0.505 | -1.91E-02 | 2.749 | 0.097 | 8.16E-02 | 1.690 | 0.194 |
| $C_i:C_a$ *PFT | 1 | - | 25.631 | <0.001 | - | 4.864 | 0.078 | - | 34.683 | <0.001 |
| N*PFT | 1 | - | 6.389 | 0.041 | - | 1.219 | 0.544 | - | 19.949 | <0.001 |
| SM ₉₀ *PFT | 1 | - | 3.548 | 0.170 | - | 0.911 | 0.634 | - | 3.293 | 0.193 |
| SM ₉₀ *N*PFT | 1 | - | 3.520 | 0.172 | - | 0.092 | 0.955 | - | 7.987 | 0.018 |

⁹
1569 *Significance determined using Type II Wald χ^2 tests ($\alpha = 0.05$). P -values less than 0.05 are in bold and p -values
1570 where $0.05 < p < 0.1$ are italicized. Coefficients are reported on the natural-log scale and are only included for
1571 continuous fixed effects.

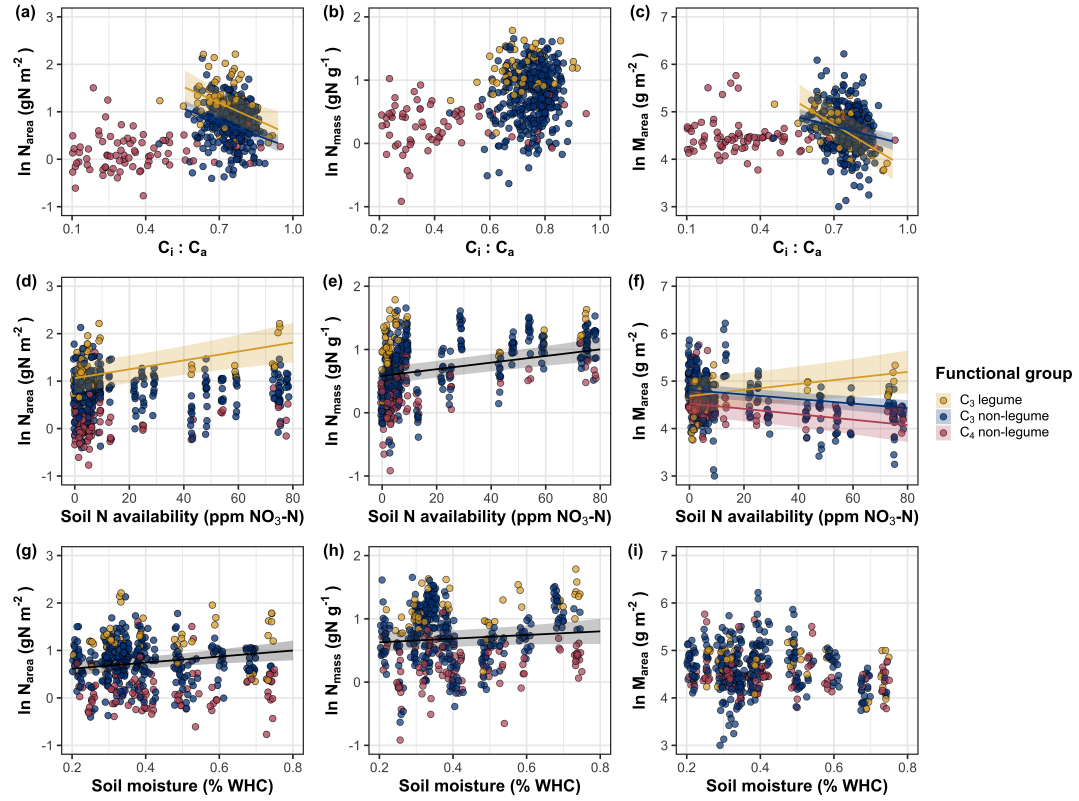


Figure 4.4. Effects of leaf $C_i:C_a$ (a-c), soil nitrogen availability (d-f), and soil moisture (g-i) on leaf nitrogen content per unit leaf area (a, d, g), leaf nitrogen content per unit leaf biomass (b, e, h), and leaf mass per area (c, f, i). Yellow points and trendlines indicate C_3 legumes, blue points and trendlines indicate C_3 nonlegumes, and red points and trendlines indicate C_4 nonlegumes. Points are jittered for visibility. Variably colored trendlines are only included if there is an interaction between plant functional group and the x-axis. Black solid trendlines denote bivariate slopes that are different from zero ($p < 0.05$) where there is no apparent interaction between plant functional group and the x-axis.

1572 4.3.4 *Structural equation model*

1573 The piecewise structural equation model explained 89%, 56%, 77%, 82%, and 37%
1574 of variance in N_{area} , N_{mass} , M_{area} , leaf $C_i:C_a$, and β , respectively (Table 4.5; Fig.
1575 4.5). Variance in N_{area} was driven by a positive effect of increasing N_{mass} and
1576 M_{area} ($p < 0.001$ in both cases; Table 4.5; Fig. 4.5). Model results indicated that
1577 an indirect negative effect of $C_i:C_a$ on N_{area} was driven by a strong reduction in
1578 M_{area} with increasing leaf $C_i:C_a$ ($p < 0.001$; Table 4.5) paired with no effect of
1579 increasing $C_i:C_a$ on N_{mass} ($p = 0.111$; Table 4.5). However, there was a strong
1580 negative effect of increasing M_{area} on N_{mass} ($p < 0.001$; Table 4.5; Fig. 4.5).
1581 Leaf $C_i:C_a$ increased with increasing β ($p < 0.001$; Table 4.5) and decreased with
1582 increasing VPD ($p < 0.001$; Table 4.5; Fig. 4.5). Variance in β was driven by a
1583 negative effect of increasing soil nitrogen availability ($p < 0.001$; Table 4.5) and
1584 was generally higher in C3 species ($p < 0.001$; Table 4.5; Fig. 4.5). However,
1585 β did not change with soil moisture ($p = 0.904$; Table 4.5) or with ability to
1586 acquire nitrogen via symbiotic nitrogen fixation ($p = 0.495$; Table 4.5). Finally,
1587 soil nitrogen availability was positively associated with increasing soil moisture (p
1588 = 0.002; Table 4.5; Fig. 4.5).

Table 4.5. Structural equation model results investigating direct effects of climatic and soil resource availability on N_{area} , N_{mass} , M_{area} , leaf $C_i:C_a$, and β

| Predictor | Coefficient | <i>p</i> |
|----------------------------------|-------------|------------------|
| $N_{\text{area}} (R^2_c = 0.89)$ | | |
| M_{area} | 0.758 | <0.001 |
| N_{mass} | 0.781 | <0.001 |
| $N_{\text{mass}} (R^2_c = 0.56)$ | | |
| Leaf $C_i:C_a$ | 0.092 | 0.111 |
| M_{area} | -0.311 | <0.001 |
| $M_{\text{area}} (R^2_c = 0.77)$ | | |
| Leaf $C_i:C_a$ | -0.237 | <0.001 |
| Leaf $C_i:C_a (R^2_c) = 0.82$ | | |
| β | 0.309 | <0.001 |
| VPD_4 | -0.110 | <0.001 |
| $\beta (R^2_c = 0.37)$ | | |
| Soil N | -0.213 | <0.001 |
| SM_{90} | -0.006 | 0.904 |
| Photo. pathway | 0.446 | <0.001 |
| N-fixing ability | -0.056 | 0.495 |
| Soil N ($R^2_c = 0.35$) | | |
| SM_{90} | -0.154 | 0.002 |

1589 *Reported coefficients are standardized across the structural equation model. P -
 1590 values less than 0.05 are noted in bold. Positive coefficients for photosynthetic
 1591 pathway indicate generally larger values in C₃ species, while positive coefficients
 1592 for N-fixing ability indicate generally larger values in N-fixing species. Key: N_{area}
 1593 = leaf nitrogen content per unit leaf area, M_{area} = leaf mass per unit leaf dry
 1594 biomass, N_{mass} = leaf nitrogen content per unit leaf dry biomass, β = cost of
 1595 acquiring nitrogen relative to water, VPD_4 = 4-day mean vapor pressure deficit,
 1596 SM_{90} = 90-day mean soil moisture, R^2_c = conditional R² value

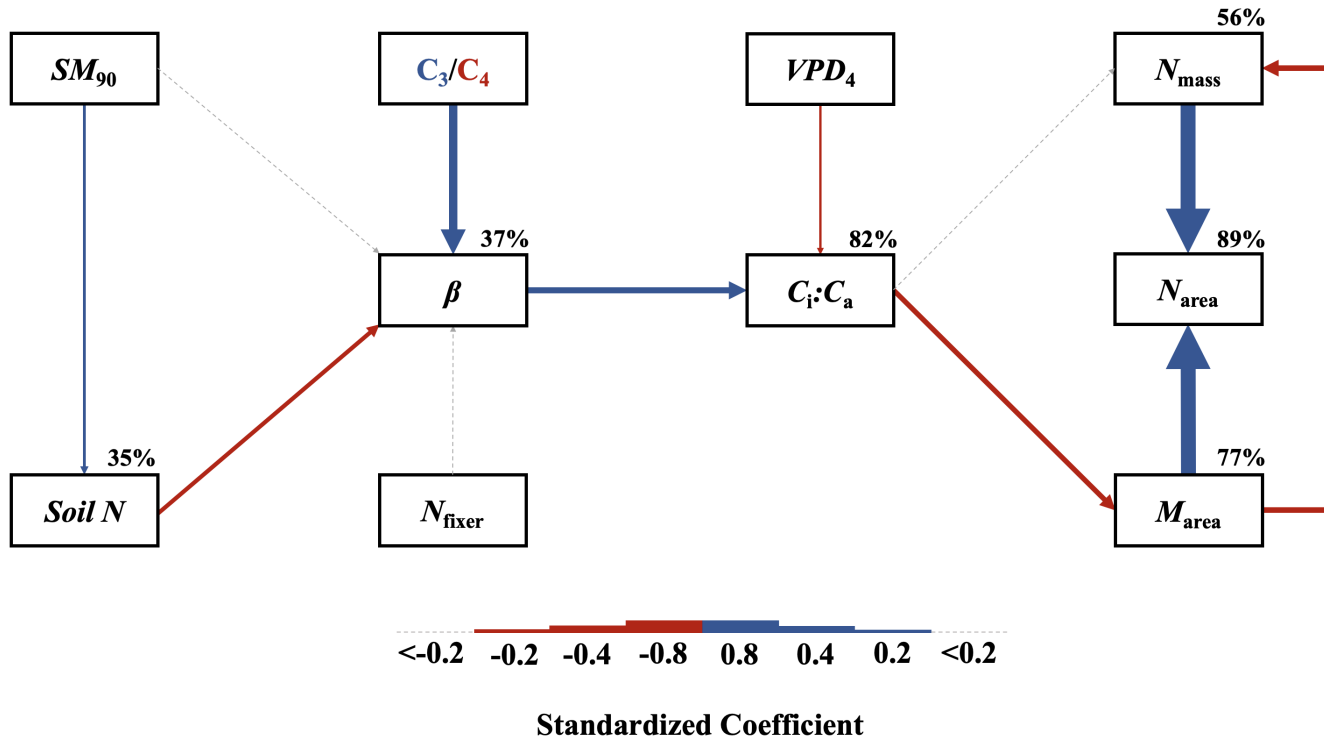


Figure 4.5. Structural equation model results exploring drivers of N_{area} . Boxes indicate measured edaphic factors, climatic factors, and leaf traits. Solid arrows indicate bivariate relationships where $p < 0.05$, while dashed arrows indicate relationships where $p > 0.05$. Positive model coefficients are indicated through blue arrows, negative model coefficients are indicated through red arrows, and insignificant coefficients ($p > 0.05$) are indicated through gray dashed arrows. Arrow thickness scales with the standardized model coefficient of each bivariate relationship. A positive coefficient for photosynthetic pathway indicates larger values in C_3 species, while a positive coefficient for N_{fixer} indicates larger values in N-fixing species. Standardized model coefficients and associated p -values are reported in Table 4.5, with conditional R^2 values for each response variable reported on the top right of each box.

1597 4.4 Discussion

1598 In this study, we quantified direct and indirect effects of soil resource availability,
1599 climate, leaf $C_i:C_a$, and β on N_{area} and components of N_{area} (N_{mass} and M_{area}) in
1600 520 individuals spanning across a soil resource availability and climate gradient
1601 in Texas, USA. We found consistent support for patterns expected from photo-
1602 synthetic least-cost theory, a result driven by a strong direct negative relationship
1603 between the relative costs to acquire nitrogen versus water (β) on N_{area} as me-
1604 diated through changes in the leaf $C_i:C_a$ ratio. In further support of patterns
1605 expected from theory, increasing soil nitrogen availability had a strong negative
1606 effect on β , resulting in an indirect stimulation in N_{area} . Increasing VPD also
1607 indirectly increased N_{area} through a direct negative effect of increasing VPD on
1608 leaf $C_i:C_a$. Interestingly, a strong positive association between soil moisture and
1609 N_{area} was driven by positive covariance between soil moisture and soil nitrogen
1610 availability and was not associated with a direct effect of soil moisture on β .
1611 Overall, results provide strong and consistent support for patterns expected from
1612 photosynthetic least-cost theory, showing that both soil resource availability and
1613 climate drive variance in N_{area} through changes in leaf $C_i:C_a$.

1614 4.4.1 *Negative effects of leaf $C_i:C_a$ on N_{area} are driven by reductions in M_{area} ,*
1615 *not N_{mass}*

1616 A strong negative effect of increasing leaf $C_i:C_a$ on N_{area} was detected in both
1617 the linear mixed effect and piecewise structural equation models. The negative
1618 response of N_{area} to increasing leaf $C_i:C_a$ is consistent with previous environmental
1619 gradient (Dong et al. 2017; Querejeta et al. 2022) and manipulation experiments

1620 (Perkowski et al. n.d.), showing strong support for the nitrogen-water use tradeoffs
1621 expected from photosynthetic least cost theory (Wright et al. 2003; Prentice et al.
1622 2014). Negative effects of increasing leaf $C_i:C_a$ on N_{area} were driven by a strong
1623 negative effect of increasing $C_i:C_a$ on M_{area} , with no apparent effect of leaf $C_i:C_a$
1624 on N_{mass} , suggesting that changes in N_{area} were driven by changes in leaf structure
1625 and not leaf chemistry. Interestingly, increasing M_{area} was negatively associated
1626 with N_{mass} , indicating that an increase in N_{mass} was associated with larger, thinner
1627 leaves (i.e. lower M_{area}). These results are consistent with patterns reported
1628 from previous studies indicating that variance in N_{area} is driven by changes in
1629 M_{area} across environmental gradients, and that part of this response is due to
1630 negative covariance between M_{area} and N_{mass} associated with tradeoffs between
1631 leaf longevity and leaf productivity (Wright et al. 2004; Dong et al. 2017; Dong
1632 et al. 2022; Querejeta et al. 2022; Wang et al. 2023).

1633 The negative relationship between leaf $C_i:C_a$ and M_{area} could be also re-
1634 sponse that allows leaves to maximize productivity in shorter-lived leaves. Trade-
1635 offs between leaf longevity and leaf productivity are commonly observed and are
1636 included in a continuum of coordinated leaf traits that position individuals along
1637 a fast- or slow-growing leaf economics spectrum (Wright et al. 2003; Onoda et al.
1638 2004; Onoda et al. 2017; Reich 2014; Wang et al. 2023). Negative relationships
1639 between $C_i:C_a$ and M_{area} indicate that increased stomatal conductance and re-
1640 duced water use efficiency were associated with thinner, larger leaves (i.e., lower
1641 M_{area}). These patterns, combined with the negative relationship between M_{area}
1642 and N_{mass} mentioned above, likely allowed individuals to maximize light intercep-
1643 tion and productivity by exploiting high light environments, though this may come

1644 at the expense of increased water loss and decreased water-use efficiency. This
1645 strategy may be especially advantageous for fast-growing species in open canopy
1646 systems. In this study, C₃ legumes and C₃ nonlegumes dominated the dataset
1647 (78% of total sampling effort), of which 22% (17% of total sampling effort) were
1648 classified as annual species with short growing seasons. We observed no effect of
1649 leaf C_i:C_a on N_{area} or M_{area} in C₄ nonlegumes, which made up 22% of the sampling
1650 effort and were generally classified as warm season graminoid species with slower
1651 growth rates and longer growing seasons. These patterns indicate that stronger
1652 tradeoffs between nitrogen and water use may be more apparent in fast-growing
1653 species with high demand for building and maintaining productive leaf tissues.

1654 4.4.2 *Soil nitrogen availability increases N_{area} through changes in the cost to*
1655 *acquire nitrogen*

1656 The null effect of soil nitrogen availability on N_{area} was driven by positive
1657 and negative respective effects of increasing soil nitrogen availability on N_{mass} and
1658 M_{area} that were equal in magnitude. The null response of N_{area} to soil nitrogen
1659 availability occurred alongside a negative effect of increasing soil nitrogen availabil-
1660 ity on β , which, paired with the negative relationship between leaf C_i:C_a and N_{area},
1661 suggests a general positive effect of increasing soil nitrogen availability on N_{area},
1662 but only when mediated through changes in β . This result is consistent with our
1663 hypotheses and patterns expected from photosynthetic least-cost theory. These
1664 results suggest that positive direct effects of increasing soil nitrogen availability
1665 on N_{area} are not ubiquitous across environmental gradients. Instead, as predicted
1666 by our hypotheses and patterns expected from theory, positive responses of N_{area}

1667 to increasing soil nitrogen availability are a deterministic acclimation response to
1668 shifts in climate-related demand to build and maintain photosynthetic enzymes,
1669 which allows plants to optimize photosynthetic processes and resource use to a
1670 given environment (Paillassa et al. 2020; Peng et al. 2021; Dong et al. 2022;
1671 Westerband et al. 2023).

1672 4.4.3 *Soil moisture increases N_{area} by facilitating increases in soil nitrogen
1673 availability*

1674 Increasing soil moisture generally had no effect on N_{area} , a response that was as-
1675 sociated with a null effect of soil moisture on β . These results contrast patterns
1676 expected from theory, where increasing soil moisture is expected to indirectly de-
1677 crease N_{area} through an increase in β due to a reduction in costs associated with
1678 water acquisition and use (Wright et al. 2003; Prentice et al. 2014; Lavergne
1679 et al. 2020). Interestingly, structural equation model results revealed a strong
1680 positive association between soil moisture and soil nitrogen availability, indicat-
1681 ing an indirect positive effect of increasing soil moisture on N_{area} mediated by the
1682 negative effect of increasing soil nitrogen availability on β . In Texan grasslands,
1683 productivity and nutrient uptake are often co-limited by precipitation and nutrient
1684 availability (Yahdjian et al. 2011; Wang et al. 2017). Thus, increases in soil mois-
1685 ture may have facilitated more favorable and productive environments for soil
1686 microbial communities, thereby stimulating the accumulation of plant-available
1687 nitrogen substrate through increased ammonification or nitrification rates (Reich-
1688 man et al. 1966; Stark and Firestone 1995; Paul et al. 2003). Alternatively, soil
1689 moisture may have facilitated greater nitrogen mobility through soil solution. As
1690 discussed above, the positive indirect response of N_{area} to increasing soil nitrogen
1691 availability as mediated through reductions in β follow patterns expected from

1692 theory.

1693 4.4.4 *Indirect effects of climate on N_{area} are mediated through changes in leaf*
1694 $C_i:C_a$ *and β*

1695 In support of our hypothesis and patterns expected from theory, increasing VPD
1696 indirectly increased N_{area} , mediated through the negative effect of increasing VPD
1697 on leaf $C_i:C_a$. These responses are consistent with previous work noting strong
1698 reductions in stomatal conductance with increasing VPD (Oren et al. 1999; Novick
1699 et al. 2016; Sulman et al. 2016; Grossiord et al. 2020; López et al. 2021), a
1700 response that allows plants to minimize water loss as a result of high atmospheric
1701 water demand. Results also support findings from previous experiments across
1702 environmental gradients, where increasing VPD generally increases N_{area} at lower
1703 stomatal conductance across environmental gradients (Dong et al. 2017; Dong
1704 et al. 2022; Paillassa et al. 2020; Westerband et al. 2023).

1705 4.4.5 *Species identity traits modify effects of the environment on β , leaf $C_i:C_a$,*
1706 *and N_{area}*

1707 N-fixing species generally had higher N_{area} values on average compared to non-
1708 fixing species, a pattern driven by a stronger stimulation in N_{mass} in N-fixing
1709 species coupled with no change in M_{area} between species with different N-fixation
1710 ability. We found no evidence to suggest that N-fixing species had different β or
1711 leaf $C_i:C_a$ values compared to non-fixing species across the environmental gradient.
1712 These results follow patterns from previous environmental gradient experiments
1713 that investigate variance in leaf nitrogen allocation in N-fixing species (Adams
1714 et al. 2016; Dong et al. 2017; Dong et al. 2020), and that increases in N_{mass}
1715 and N_{area} in N-fixing species are not necessarily correlated to increases in water

1716 use efficiency or reductions in leaf $C_i:C_a$ (Adams et al. 2016). While our results
1717 are consistent with results from previous environmental gradient experiments,
1718 they do not necessarily support our hypothesis or patterns expected from theory,
1719 which predicts that stimulations in N_{area} by N-fixing species should be driven
1720 by a reduction in β relative to non-fixing species, and that this response should
1721 decrease stomatal conductance and leaf $C_i:C_a$.

1722 C₄ species generally had lower β , leaf $C_i:C_a$, and N_{area} than C₃ species.
1723 Reduced β and leaf $C_i:C_a$ values in C₄ species follow our hypothesis, a pattern
1724 that could be the result of either reduced costs of nitrogen acquisition and use or
1725 increased costs of water acquisition and use or both (Wright et al. 2003, Prentice
1726 et al. 2014). Results also indicate that β in C₄ nonlegumes was unresponsive to
1727 changes in soil nitrogen availability despite an apparent negative effect of increas-
1728 ing soil nitrogen availability on β in C₃ legumes and C₃ nonlegumes. Combined
1729 with a general null response of β to soil moisture regardless of plant functional
1730 group, these patterns imply that reduced β values in C₄ species may be the re-
1731 sult of lower costs of nitrogen acquisition and use relative to C₃ species. While
1732 lower β values in C₄ species provides a possible explanation for why C₄ species
1733 often have lower leaf $C_i:C_a$ and greater water use efficiency, theory predicts that
1734 this response should cause C₄ species to have greater N_{area} values compared to
1735 C₃ species, though C₄ species commonly exhibit lower N_{area} and higher nitrogen
1736 use efficiency than C₃ species (Schmitt and Edwards 1981; Sage and Pearcy 1987;
1737 Ghannoum et al. 2011). We speculate that lowered costs of nitrogen acquisition
1738 and use in C₄ species could be driven by more efficient Rubisco carboxylation effi-
1739 ciency in C₄ species associated with CO₂ concentrating mechanisms that eliminate

1740 photorespiration (Ghannoum et al. 2011), which could reduce or eliminate the
1741 need to sacrifice inefficient nitrogen use for efficient water use to achieve optimal
1742 photosynthesis rates.

1743 4.4.6 *Next steps for optimality model development*

1744 Optimality models for both C₃ and C₄ species have been developed using principles
1745 from photosynthetic least-cost theory (Prentice et al. 2014; Wang et al. 2017;
1746 Smith et al. 2019; Stocker et al. 2020; Scott and Smith 2022). In both C₃ and
1747 C₄ model variants, β values are held constant using global datasets of leaf $\delta^{13}\text{C}$
1748 (Wang et al. 2017; Cornwell et al. 2018). Specifically, the C₃ optimality model
1749 initially assumed a constant β value of 240 (Wang et al. 2017), later corrected to
1750 146 (Stocker et al. 2020), while the C₄ optimality model assumes a constant β
1751 value of 166 (Scott and Smith 2022). Our results, which build on findings from
1752 Paillassa et al. (2020), demonstrate high variability in calculated β values across
1753 environmental gradients. Specifically, β values in C₃ species ranged from 1.7 to
1754 188.0 (mean: 30.2; median: 23.1; standard deviation: 25.4), while ranged from 0.1
1755 to 110.6 in C₄ species (mean: 7.2; median: 0.7; standard deviation: 18.6). Mean
1756 β values in both C₃ and C₄ species were consistently lower than values currently
1757 implemented in optimality models, though this was likely the result of increased
1758 water limitation across our sites relative to global averages. Regardless, the high
1759 degree of β variability across this environmental gradient, together with findings
1760 from Lavergne et al. (2020) and Paillassa et al. (2020), suggests that the use of
1761 constant β values may contribute to erroneous errors when conducting optimality
1762 model simulations. We therefore build on suggestions from Wang et al. (2017),
1763 recommending future photosynthetic least-cost model developments to consider

1764 the use of dynamic β values.

1765 4.4.7 *Conclusions*

1766 To summarize, variability in N_{area} across an environmental gradient in Texan
1767 grasslands was driven by indirect effects of climate and soil resource availability
1768 mediated. Results from this experiment provide strong and consistent support
1769 for patterns expected from photosynthetic least-cost theory, demonstrating that
1770 negative relationships between $C_i:C_a$ and N_{area} unify expected effects of climatic
1771 and edaphic characteristics on N_{area} across environmental gradients. Our results
1772 also demonstrate a need to consider the dynamic nature of the relative cost of
1773 nitrogen versus water uptake (β) across environmental gradients in optimality
1774 models that leverage principles of photosynthetic least-cost theory.

1775

Chapter 5

1776 Optimal resource investment to photosynthetic capacity maximizes
1777 nutrient allocation to whole plant growth under elevated CO₂

1778 5.1 Introduction

1779 Terrestrial ecosystems are regulated by complex carbon and nitrogen cy-
1780 cles. As a result, terrestrial biosphere models, which are beginning to include
1781 coupled carbon and nitrogen cycles (Shi et al. 2016; Davies-Barnard et al. 2020;
1782 Braghieri et al. 2022), must accurately represent these cycles under different
1783 environmental scenarios to reliably simulate carbon and nitrogen atmosphere-
1784 biosphere fluxes (Hungate et al. 2003; Prentice et al. 2015). While the inclusion
1785 of coupled carbon and nitrogen cycles tends to reduce model uncertainty (Arora
1786 et al. 2020), large uncertainty in role of soil nitrogen availability and nitrogen ac-
1787 quisition strategy on leaf and whole plant acclimation responses to CO₂ remains
1788 (Smith and Dukes 2013; Terrer et al. 2018; Smith and Keenan 2020). This source
1789 of uncertainty likely contributes to the widespread divergence in future carbon
1790 and nitrogen flux simulations across terrestrial biosphere models (Friedlingstein
1791 et al. 2014; Zaehle et al. 2014; Meyerholt et al. 2020).

1792 Plants grown under elevated CO₂ generally have less leaf nitrogen content
1793 than those grown under ambient CO₂, a response that often corresponds with
1794 reductions in photosynthetic capacity and stomatal conductance at the leaf-level
1795 and biomass stimulation over time at the whole plant level (Curtis 1996; Drake
1796 et al. 1997; Ainsworth et al. 2002; Makino 2003; Morgan et al. 2004; Ainsworth
1797 and Long 2005; Ainsworth and Rogers 2007; Smith and Dukes 2013; Poorter et al.
1798 2022). As net primary productivity is generally limited by nitrogen availability

1799 (Vitousek and Howarth 1991; LeBauer and Treseder 2008; Fay et al. 2015), and
1800 soil nitrogen availability is often positively correlated with leaf nitrogen content
1801 and photosynthetic capacity (Field and Mooney 1986; Evans and Seemann 1989;
1802 Evans 1989; Walker et al. 2014; Firn et al. 2019; Liang et al. 2020), some
1803 have hypothesized that leaf and whole plant acclimation responses to CO₂ are
1804 constrained by soil nitrogen availability. The progressive nitrogen limitation hy-
1805 pothesis predicts that elevated CO₂ will increase plant nitrogen demand, which
1806 will increase plant nitrogen uptake and progressively deplete soil nitrogen if soil
1807 nitrogen supply does not exceed plant nitrogen demand (Luo et al. 2004). The
1808 hypothesis predicts that this response should result in strong acute stimulations in
1809 whole plant growth and primary productivity that diminish over time as nitrogen
1810 becomes more limiting. Assuming a positive relationship between soil nitrogen
1811 availability, leaf nitrogen content, and photosynthetic capacity, this hypothesis
1812 also implies that progressive reductions in soil nitrogen availability should be the
1813 mechanism that drives the downregulation in leaf nitrogen content and photosyn-
1814 thetic capacity under elevated CO₂. This hypothesis has received some support
1815 from free air CO₂ enrichment experiments (Reich et al. 2006; Norby et al. 2010),
1816 although is not consistently observed across experiments (Finzi et al. 2006; Moore
1817 et al. 2006; Liang et al. 2016).

1818 While possible that progressive nitrogen limitation may determine leaf and
1819 whole plant acclimation responses to CO₂, growing evidence indicates that leaf ni-
1820 trogen and photosynthetic capacity are more strongly determined through above-
1821 ground growing conditions than by soil resource availability (Dong et al. 2017;
1822 Dong et al. 2020; Dong et al. 2022; Smith et al. 2019; Smith and Keenan 2020;

1823 Paillassa et al. 2020; Peng et al. 2021; Querejeta et al. 2022; Westerband et al.
1824 2023), and satellite-derived chlorophyll fluorescence data indicate that increasing
1825 atmospheric CO₂ may decrease leaf and canopy demand for nitrogen (Dong et al.
1826 2022). Together, results from these studies suggest that the downregulation in
1827 leaf nitrogen content and photosynthetic capacity due to increasing CO₂ may not
1828 be as tightly linked to progressive nitrogen limitation as previously hypothesized.

1829 A unification of optimal coordination and photosynthetic least-cost the-
1830 ories predicts that leaves acclimate to elevated CO₂ by downregulating nitrogen
1831 allocation to Ribulose-1,5-bisphosphate (RuBP) carboxylase/oxygenase (Rubisco)
1832 to optimize resource use efficiencies at the leaf level, which allows for greater re-
1833 source allocation to whole plant growth (Drake et al. 1997; Wright et al. 2003;
1834 Prentice et al. 2014; Smith et al. 2019). The theory predicts that the downregu-
1835 lation in nitrogen allocation to Rubisco results in a stronger downregulation in the
1836 maximum rate of Rubisco carboxylation (V_{cmax}) than the maximum rate of RuBP
1837 regeneration (J_{max}), which maximizes photosynthetic efficiency by allowing net
1838 photosynthesis rates to be equally co-limited by Rubisco carboxylation and RuBP
1839 regeneration (Chen et al. 1993; Maire et al. 2012). This acclimation response
1840 allows plants to make more efficient use of available light while avoiding overin-
1841 vestment in Rubisco, which has high nitrogen and energetic costs of building and
1842 maintaining (Evans 1989; Evans and Clarke 2019). Instead, additional acquired
1843 resources not needed to optimize leaf photosynthesis are allocated to the mainte-
1844 nance of structures that support whole plant growth (e.g., total leaf area, whole
1845 plant biomass, etc.) or to allocation processes not related to leaf photosynthesis
1846 or growth, such as plant defense mechanisms or leaf structural tissue. Regardless,

1847 optimized resource allocation at the leaf level should allow for greater resource
1848 allocation to whole plant growth. The theory indicates that leaf acclimation re-
1849 sponses to CO₂ should be independent of changes in soil nitrogen availability.
1850 While this leaf acclimation response maximizes nitrogen allocation to structures
1851 that support whole plant growth, the theory suggests that the positive effect of
1852 elevated CO₂ on whole plant growth may be further stimulated by soil nitrogen
1853 availability through a reduction in the cost of acquiring nitrogen (Bae et al. 2015;
1854 Perkowski et al. 2021; Lu et al. 2022).

1855 Plants acquire nitrogen by allocating photosynthetically derived carbon be-
1856 lowground in exchange for nitrogen through different nitrogen acquisition strate-
1857 gies. These nitrogen acquisition strategies can include direct uptake pathways
1858 such as mass flow or diffusion (Barber 1962), symbioses with mycorrhizal fungi or
1859 symbiotic nitrogen-fixing bacteria (Vance and Heichel 1991; Marschner and Dell
1860 1994; Smith and Read 2008; Udvardi and Poole 2013), or through the release
1861 of root exudates that prime free-living soil microbial communities (Phillips et al.
1862 2011; Wen et al. 2022). Plants cannot acquire nitrogen without first allocating
1863 carbon belowground, which implies an inherent carbon cost to the plant for acquir-
1864 ing nitrogen regardless of nitrogen acquisition strategy. Carbon costs to acquire
1865 nitrogen often vary in species with different nitrogen acquisition strategies and
1866 are dependent on external environmental factors such as atmospheric CO₂, light
1867 availability, and soil nitrogen availability (Brzostek et al. 2014; Terrer et al. 2016;
1868 Terrer et al. 2018; Allen et al. 2020; Perkowski et al. 2021; Lu et al. 2022), which
1869 suggests that acquisition strategy may be an important factor in determining ef-
1870 fects of soil nitrogen availability on leaf and whole plant acclimation responses to

1871 elevated CO₂.

1872 A recent meta-analysis using data across 20 grassland and forest CO₂ en-
1873 richment experiments suggested that species which acquire nitrogen from sym-
1874 biotic nitrogen-fixing bacteria had reduced costs of nitrogen acquisition under
1875 elevated CO₂ (Terrer et al. 2018). Findings from this meta-analysis indicated
1876 that reductions in costs of nitrogen acquisition in species that form associations
1877 with symbiotic nitrogen-fixing bacteria under elevated CO₂ may drive stronger
1878 stimulations in whole plant growth and downregulations in V_{cmax} than species that
1879 associate with arbuscular mycorrhizal fungi (Smith and Keenan 2020), which gen-
1880 erally have higher costs of nitrogen acquisition under elevated CO₂ (Terrer et al.
1881 2018). However, plant investments in symbiotic nitrogen fixation generally de-
1882 cline with increasing nitrogen availability (Dovrat et al. 2018; Perkowski et al.
1883 2021), a response that has been previously inferred to be the result of a shift in
1884 the dominant mode of nitrogen acquisition to direct uptake pathways as costs of
1885 direct uptake decrease with increasing soil nitrogen availability (Rastetter et al.
1886 2001; Perkowski et al. 2021). Thus, effects of symbiotic nitrogen fixation on plant
1887 acclimation responses to CO₂ should decline with increasing soil nitrogen avail-
1888 ability, although manipulative experiments that directly test these patterns are
1889 rare.

1890 Here, I conducted a 7-week growth chamber experiment using *Glycine max*
1891 L. (Merr.) to examine the effects of soil nitrogen fertilization and inoculation with
1892 symbiotic nitrogen-fixing bacteria on leaf and whole plant acclimation responses
1893 to elevated CO₂. Following patterns expected from theory, I hypothesized that in-
1894 dividual leaves should acclimate to elevated CO₂ by more strongly downregulating

1895 V_{cmax} relative to J_{max} , allowing leaf photosynthesis to approach optimal coordi-
1896 nation. I expected this response to correspond with a stronger downregulation in
1897 leaf nitrogen content than V_{cmax} and J_{max} , which would increase the fraction of
1898 leaf nitrogen content allocated to photosynthesis and photosynthetic nitrogen use
1899 efficiency. At the whole-plant level, I hypothesized that plants would acclimate
1900 to elevated CO₂ by stimulating whole plant growth and productivity, a response
1901 that would be driven by a strong positive response of total leaf area and above-
1902 ground biomass to elevated CO₂. I predicted that leaf acclimation responses to
1903 elevated CO₂ would be independent of soil nitrogen fertilization and inoculation
1904 with symbiotic nitrogen-fixing bacteria; however, I expected that increasing soil
1905 nitrogen fertilization would increase the positive effect of elevated CO₂ on mea-
1906 sures of whole plant growth due to a stronger reduction in the cost of acquiring
1907 nitrogen under elevated CO₂ with increasing fertilization. I also expected stronger
1908 stimulations in whole plant growth due to inoculation, but that this effect would
1909 only be apparent under low fertilization due to a reduction in root nodulation
1910 with increasing fertilization.

1911 5.2 Methods

1912 5.2.1 *Seed treatments and experimental design*

1913 *Glycine max* L. (Merr) seeds were planted in 144 6-liter surface sterilized
1914 pots (NS-600, Nursery Supplies, Orange, CA, USA) containing a steam-sterilized
1915 70:30 v:v mix of Sphagnum peat moss (Premier Horticulture, Quakertown, PA,
1916 USA) to sand (Pavestone, subsidiary of Quikrete Companies, Atlanta, GA, USA).
1917 Before planting, all *G. max* seeds were surface sterilized in 2% sodium hypochlorite

1918 for 3 minutes, followed by three separate 3-minute washes with ultrapure water
1919 (MilliQ 7000; MilliporeSigma, Burlington, MA USA). A subset of surface steril-
1920 ized seeds were inoculated with *Bradyrhizobium japonicum* (Verdesian N-Dure™
1921 Soybean, Cary, NC, USA) in a slurry following manufacturer recommendations
1922 (3.12 g inoculant and 241 g deionized water per 1 kg seed).

1923 Seventy-two pots were randomly planted with surface-sterilized seeds inoc-
1924 ulated with *B. japonicum*, while the remaining 72 pots were planted with surface-
1925 sterilized uninoculated seeds. Thirty-six pots within each inoculation treatment
1926 were randomly placed in one of two atmospheric CO₂ treatments (ambient and
1927 1000 μmol mol⁻¹ CO₂). Pots within each unique inoculation-by-CO₂ treatment
1928 combination randomly received one of nine soil nitrogen fertilization treatments
1929 equivalent to 0, 35, 70, 105, 140, 210, 280, 350, or 630 ppm N. Nitrogen fertil-
1930 ization treatments were created using a modified Hoagland solution (Hoagland
1931 and Arnon 1950) designed to keep concentrations of other macronutrients and
1932 micronutrients equivalent across treatments (Table S1). Pots received the same
1933 fertilization treatment throughout the entire duration experiment, which were ap-
1934 plied twice per week in 150 mL doses as topical agents to the soil surface through-
1935 out the duration of the experiment. This experimental design yielded a fully
1936 factorial experiment with four replicates per unique fertilization-by-inoculation-
1937 by-CO₂ combination.

1938 5.2.2 *Growth chamber conditions*

1939 Upon experiment initiation, pots were randomly placed in one of six Per-
1940 cival LED-41L2 growth chambers (Percival Scientific Inc., Perry, IA, USA) over

1941 two experimental iterations due to chamber space limitation. Two iterations were
1942 conducted such that one iteration included all elevated CO₂ pots and the second
1943 iteration included all ambient CO₂ pots. Average (\pm SD) CO₂ concentrations
1944 across chambers throughout the experiment were $439 \pm 5 \mu\text{mol mol}^{-1}$ for the
1945 ambient CO₂ treatment and $989 \pm 4 \mu\text{mol mol}^{-1}$ for the elevated CO₂ treatment.

1946 Daytime growing conditions were simulated using a 16-hour photoperiod,
1947 with incoming light radiation set to chamber maximum (mean \pm SD: 1240 ± 32
1948 $\mu\text{mol m}^{-2} \text{s}^{-1}$ across chambers), air temperature set to 25°C, and relative humid-
1949 ity set to 50%. The remaining 8 hours simulated nighttime growing conditions,
1950 with incoming light radiation set to 0 $\mu\text{mol m}^{-2} \text{s}^{-1}$, chamber temperature set
1951 to 17°C, and relative humidity set to 50%. Transitions between daytime and
1952 nighttime growing conditions were simulated by ramping incoming light radiation
1953 in 45-minute increments and temperature in 90-minute increments over a 3-hour
1954 period (Table S2).

1955 Including the two, 3-hour ramping periods, pots grew under average (\pm
1956 SD) daytime light intensity of $1049 \pm 27 \mu\text{mol m}^{-2} \text{s}^{-1}$. In the elevated CO₂
1957 iteration, pots grew under $24.0 \pm 0.2^\circ\text{C}$ during the day, $16.4 \pm 0.8^\circ\text{C}$ during the
1958 night, and $51.6 \pm 0.4\%$ relative humidity. In the ambient CO₂ iteration, pots grew
1959 under $23.9 \pm 0.2^\circ\text{C}$ during the day, $16.0 \pm 1.4^\circ\text{C}$ during the night, and $50.3 \pm 0.2\%$
1960 relative humidity. We accounted for climatic differences across the six chambers
1961 by shuffling the same group of pots daily throughout the growth chambers. This
1962 process was done by iteratively moving the group of pots on the top rack of a
1963 chamber to the bottom rack of the same chamber, while simultaneously moving
1964 the group of pots on the bottom rack of a chamber to the top rack of the adjacent

1965 chamber. I moved pots within and across chambers every day throughout the
1966 course of each experiment iteration.

1967 5.2.3 *Leaf gas exchange measurements*

1968 Gas exchange measurements were collected for all individuals on the sev-
1969 enth week of development. All gas exchange measurements were collected on
1970 the center leaf of the most recent fully expanded trifoliate leaf set. Specifi-
1971 cally, I measured net photosynthesis (A_{net} ; $\mu\text{mol m}^{-2} \text{s}^{-1}$), stomatal conductance
1972 (g_{sw} ; $\text{mol m}^{-2} \text{s}^{-1}$), and intercellular CO₂ (C_i ; $\mu\text{mol mol}^{-1}$) concentrations across
1973 a range of atmospheric CO₂ concentrations (i.e., an A_{net}/C_i curve) using the
1974 Dynamic Assimilation Technique™. The Dynamic Assimilation Technique™ has
1975 been shown to correspond well with traditional steady-state CO₂ response curves
1976 in *G. max* (Saathoff and Welles 2021). A_{net}/C_i curves were generated along a
1977 reference CO₂ ramp down from 420 $\mu\text{mol mol}^{-1}$ CO₂ to 20 $\mu\text{mol mol}^{-1}$ CO₂, fol-
1978 lowed by a ramp up from 420 $\mu\text{mol mol}^{-1}$ CO₂ to 1620 $\mu\text{mol mol}^{-1}$ CO₂ after
1979 a 90-second wait period at 420 $\mu\text{mol mol}^{-1}$ CO₂. The ramp rate for each curve
1980 was set to 200 $\mu\text{mol mol}^{-1} \text{min}^{-1}$, logging every five seconds, which generated 96
1981 data points per response curve. All A_{net}/C_i curves were generated after A_{net} and
1982 g_{sw} stabilized in a LI-6800 cuvette set to a 500 mol s^{-1} , 10,000 rpm mixing fan
1983 speed, 1.5 kPa vapor pressure deficit, 25°C leaf temperature, 2000 $\mu\text{mol m}^{-2} \text{s}^{-1}$
1984 incoming light radiation, and initial reference CO₂ set to 420 $\mu\text{mol mol}^{-1}$.

1985 With the same focal leaf used to generate A_{net}/C_i curves, I measured dark
1986 respiration (R_{d25} ; $\mu\text{mol m}^{-2} \text{s}^{-1}$) following at least a 30-minute period of darkness.
1987 Measurements were collected on a 5-second log interval for 60 seconds after stabi-

1988 lizing in a LI-6800 cuvette set to a 500 mol s^{-1} , 10,000 rpm mixing fan speed, 1.5
1989 kPa vapor pressure deficit, 25°C leaf temperature, and $420 \mu\text{mol mol}^{-1}$ reference
1990 CO₂ concentration (for both CO² concentrations), with incoming light radiation
1991 set to $0 \mu\text{mol m}^{-2} \text{ s}^{-1}$. A single dark respiration value was determined for each
1992 focal leaf by calculating the mean dark respiration value (i.e. the absolute value
1993 of A_{net} during the logging period) across the logging interval.

1994 5.2.4 *Leaf trait measurements*

1995 The focal leaf used to generate A_{net}/C_i curves and dark respiration was
1996 harvested immediately following gas exchange measurements. Images of each focal
1997 leaf were curated using a flat-bed scanner to determine wet leaf area using the
1998 'LeafArea' R package (Katabuchi 2015), which automates leaf area calculations
1999 using ImageJ software (Schneider et al. 2012). Each leaf was dried at 65°C for
2000 at least 48 hours, and subsequently weighed and ground until homogenized. Leaf
2001 mass per area (M_{area} ; g m⁻²) was calculated as the ratio of dry leaf biomass
2002 to fresh leaf area. Using subsamples of ground and homogenized leaf tissue, I
2003 measured leaf nitrogen content (N_{mass} ; gN g⁻¹) through elemental combustion
2004 analysis (Costech-4010, Costech, Inc., Valencia, CA, USA). Leaf nitrogen content
2005 per unit leaf area (N_{area} ; gN m⁻²) was calculated by multiplying N_{mass} and M_{area} .

2006 I extracted chlorophyll content from a second leaf in the same trifoliolate
2007 leaf set as the focal leaf used to generate A_{net}/C_i curves. Prior to chlorophyll
2008 extraction, I used a cork borer to punch between 3 and 5 0.6 cm² disks from the
2009 leaf. Separate images of each punched leaf and set of leaf disks were curated using
2010 a flat-bed scanner to determine wet leaf area, again quantified using the 'LeafArea'

2011 R package (Katabuchi 2015). The punched leaf was dried and weighed after at
2012 least 65°C in the drying oven to determine M_{area} of the chlorophyll leaf.

2013 Leaf disks were shuttled into a test tube containing 10mL dimethyl sul-
2014 foxide, vortexed, and incubated at 65degreeC for 120 minutes (Barnes et al.
2015 1992). Incubated test tubes were vortexed again before loaded in 150 μL trip-
2016 licate aliquots to a 96-well plate. Dimethyl sulfoxide was also loaded in a 150
2017 μL triplicate aliquot as a blank. Absorbance measurements at 649.1 nm ($A_{649.1}$)
2018 and 665.1 nm ($A_{665.1}$) were read in each well using a plate reader (Biotek Synergy
2019 H1; Biotek Instruments, Winooski, VT USA) (Wellburn 1994), with triplicates
2020 subsequently averaged and corrected by the mean of the blank absorbance value.
2021 Blank-corrected absorbance values were used to estimate Chl_a ($\mu\text{g mL}^{-1}$) and
2022 Chl_b ($\mu\text{g mL}^{-1}$) following equations from Wellburn (1994):

$$Chl_a = 12.47A_{665.1} - 3.62A_{649.1} \quad (5.1)$$

2023 and

$$Chl_b = 25.06A_{665.1} - 6.50A_{649.1} \quad (5.2)$$

2024 Chl_a and Chl_b were converted to mmol mL^{-1} using the molar mass of chlorophyll a
2025 (893.51 g mol^{-1}) and the molar mass of chlorophyll b (907.47 g mol^{-1}), then added
2026 together to calculate total chlorophyll content in the dimethyl sulfoxide extractant
2027 (mmol mL^{-1}). Total chlorophyll content was multiplied by the volume of the
2028 dimethyl sulfoxide extractant (10 mL) and converted to area-based chlorophyll
2029 content by dividing by the total area of the leaf disks (Chl_{area} ; mmol m^{-2}). Mass-
2030 based chlorophyll content (Chl_{mass} ; mmol g^{-1}) was calculated by dividing Chl_{area}

2031 by the leaf mass per area of the punched leaf.

2032 5.2.5 *A/C_i curve fitting and parameter estimation*

2033 I fit A_{net}/C_i curves of each individual using the ‘fitaci’ function in the
2034 ‘plantecophys’ R package (Duursma 2015). This function estimates the maxi-
2035 mum rate of Rubisco carboxylation (V_{cmax} ; $\mu\text{mol m}^{-2} \text{s}^{-1}$) and maximum rate
2036 of electron transport for RuBP regeneration (J_{max} ; $\mu\text{mol m}^{-2} \text{s}^{-1}$) based on the
2037 Farquhar biochemical model of C₃ photosynthesis (Farquhar et al. 1980). Triose
2038 phosphate utilization (TPU) limitation was included in all curve fits, and all curve
2039 fits included measured dark respiration values. As A_{net}/C_i curves were generated
2040 using a common leaf temperature, curves were fit using Michaelis-Menten coeffi-
2041 cients for Rubisco affinity to CO₂ (K_c ; $\mu\text{mol mol}^{-1}$) and O₂ (K_o ; $\mu\text{mol mol}^{-1}$), and
2042 the CO₂ compensation point (Γ^* ; $\mu\text{mol mol}^{-1}$) reported in Bernacchi et al. (2001).
2043 Specifically, K_c was set to 404.9 $\mu\text{mol mol}^{-1}$, K_o was set to 278.4 $\mu\text{mol mol}^{-1}$, and
2044 Γ^* was set to 42.75 $\mu\text{mol mol}^{-1}$. The use of a common leaf temperature across
2045 curves and dark respiration measurements also eliminated the need to manually
2046 temperature standardize rate estimates. For clarity, I reference V_{cmax} , J_{max} , and
2047 R_d estimates throughout the rest of the paper as $V_{\text{cmax}25}$, $J_{\text{max}25}$, and R_{d25} .

2048 5.2.6 Stomatal limitation

2049 I quantified the extent by which stomatal conductance limited photosynthe-
2050 sis (l; unitless) following equations originally described in Farquhar and Sharkey
2051 (1982). Stomatal limitation was calculated as:

$$l = 1 - \frac{A_{net}}{A_{mod}} \quad (5.3)$$

2052 where A_{mod} represents the photosynthetic rate where $C_i = C_a$. A_{mod} was calcu-

2053 lated as:

$$A_{mod} = V_{cmax25} - \frac{420 - \Gamma^*}{420 + K_m} - R_{d25} \quad (5.4)$$

2054 K_m is the Michaelis-Menten coefficient for Rubisco-limited photosynthesis, calcu-

2055 lated as:

$$K_m = K_c \cdot \left(1 + \frac{O_i}{K_o}\right) \quad (5.5)$$

2056 where O_i refers to leaf intercellular O_2 concentrations, set to $210 \mu\text{mol mol}^{-1}$.

2057 5.2.7 *Proportion of leaf nitrogen allocated to photosynthesis and structure*

2058 I used equations from Niinemets and Tenhunen (1997) to estimate the

2059 proportion of leaf N content allocated to Rubisco bioenergetics, and light harvest-

2060 ing proteins. The proportion of leaf N allocated to Rubisco (ρ_{rub} ; gN gN^{-1}) was

2061 calculated as a function of V_{cmax25} and N_{area} :

$$\rho_{rubisco} = \frac{V_{cmax25} N_r}{V_{cr} N_{area}} \quad (5.6)$$

2062 where N_r is the amount of nitrogen in Rubisco, set to $0.16 \text{ gN (gN in Rubisco)}^{-1}$

2063 and V_{cr} is the maximum rate of RuBP carboxylation per unit Rubisco protein,

2064 set to $20.5 \mu\text{mol CO}_2 (\text{g Rubisco})^{-1}$. The proportion of leaf nitrogen allocated to

2065 bioenergetics (ρ_{bioe} ; gN gN^{-1}) was similarly calculated as a function of J_{max25} and

2066 N_{area} :

$$\rho_{\text{bioe}} = \frac{J_{\text{max}25} N_b}{J_{\text{mc}} N_{\text{area}}} \quad (5.7)$$

2067 where N_b is the amount of nitrogen in cytochrome f, set to 0.12407 gN (μmol cytochrome f) $^{-1}$ assuming a constant 1: 1: 1.2 cytochrome f: ferredoxin NADP reductase: coupling factor molar ratio (Evans and Seemann 1989; Niinemets and Tenhunen 1997), and J_{mc} is the capacity of electron transport per cytochrome f, set to 156 μmol electron (μmol cytochrome f) $^{-1}\text{s}^{-1}$.

2072 The proportion of leaf nitrogen allocated to light harvesting proteins was
2073 calculated as a function of Chl_{mass} and N_{mass} :

$$\rho_{\text{light}} = \frac{Chl_{\text{mass}}}{N_{\text{mass}} c_b} \quad (5.8)$$

2074 where c_b is the stoichiometry of the light-harvesting chlorophyll complexes of photosystem II, set to 2.75 mmol chlorophyll (gN in chlorophyll) $^{-1}$. We used the N_{mass} value of the focal leaf used to generate A_{net}/C_i curves instead of the leaf used to extract chlorophyll content, as the two leaves are from the same trifoliolate leaf set and are highly correlated with each other (Figure SX).

2079 The proportion of leaf nitrogen content allocated to photosynthetic tissue
2080 (ρ_{photo} ; gN gN $^{-1}$) was estimated as the sum of ρ_{rubisco} , ρ_{bioe} , and ρ_{light} .

2081 Finally, the proportion of leaf N content allocated to structural tissue (ρ_{str} ;
2082 gN gN $^{-1}$) was estimated as:

$$\rho_{\text{structure}} = \frac{N_{\text{cw}}}{N_{\text{area}}} \quad (5.9)$$

2083 where N_{cw} is the leaf N content allocated to cell walls (gN m^{-2}), calculated as a
2084 function of M_{area} using an empirical equation from Onoda et al. (2017):

$$N_{cw} = 0.000355 * M_{area}^{1.39} \quad (5.10)$$

2085 5.2.8 *Whole plant traits*

2086 Seven weeks after experiment initiation and immediately following gas ex-
2087 change measurements, I harvested all experimental individuals and separated
2088 biomass of each experimental individual into major organ types (leaves, stems,
2089 roots, and nodules when present). Fresh leaf area of all harvested leaves was mea-
2090 sured using an LI-3100C (Li-COR Biosciences, Lincoln, Nebraska, USA). Total
2091 fresh leaf area (cm^2) was calculated as the sum of all leaf areas, including the focal
2092 leaf used to collect gas exchange data and the focal leaf used to extract chlorophyll
2093 content. All harvested material was dried in an oven set to 65°C for at least 48
2094 hours, weighed, and ground to homogeneity. Leaves and nodules were manually
2095 ground either with a mortar and pestle, while stems and roots were ground using
2096 a Wiley mill (E3300 Mini Mill; Eberbach Corp., MI, USA). Total dry biomass (g)
2097 was calculated as the sum of dry leaf (including focal leaf for both the A_{net}/C_i
2098 curve and leaf used to extract chlorophyll content), stem, root, and root nodule
2099 biomass. I quantified carbon and nitrogen content of each respective organ type
2100 through elemental combustion (Costech-4010, Costech, Inc., Valencia, CA, USA)
2101 using subsamples of ground and homogenized organ tissue.

2102 Following the approach explained in the first experimental chapter, I calcu-
2103 lated structural carbon costs to acquire nitrogen as the ratio of total belowground

2104 carbon biomass to whole plant nitrogen biomass (N_{cost} ; gC gN⁻¹). Belowground
2105 carbon biomass (C_{bg} ; gC) was calculated as the sum of root carbon biomass
2106 and root nodule carbon biomass. Root carbon biomass and root nodule carbon
2107 biomass was calculated as the product of the organ biomass and the respective
2108 organ carbon content. Whole plant nitrogen biomass (N_{wp} ; gN) was similarly
2109 calculated as the sum of total leaf, stem, root, and root nodule nitrogen biomass,
2110 including the focal leaf used for A_{net}/C_i curve and chlorophyll extractions. Leaf,
2111 stem, root, and root nodule nitrogen biomass was calculated as the product of
2112 the organ biomass and the respective organ nitrogen content. This calculation
2113 only quantifies plant structural carbon costs to acquire nitrogen and does not
2114 include any additional costs of nitrogen acquisition associated with respiration,
2115 root exudation, or root turnover. An explicit explanation of the limitations for
2116 interpreting this calculation can be found in Perkowski et al. (2021) and Terrer
2117 et al. (2018).

2118 Finally, plant investments in nitrogen fixation were calculated as the ra-
2119 tio of root nodule biomass to root biomass, where increasing values indicate an
2120 increase in plant investments to nitrogen fixation (Dovrat et al. 2018; Dovrat
2121 et al. 2020; Perkowski et al. 2021). I also calculated the percent of leaf nitrogen
2122 acquired from the atmosphere (% N_{dfa}) using leaf $\delta^{15}\text{N}$ and the following equation
2123 from Andrews et al. (2011):

$$\%N_{\text{dfa}} = \frac{\delta^{15}N_{\text{reference}} - \delta^{15}N_{\text{sample}}}{\delta^{15}N_{\text{reference}} - B} \quad (5.11)$$

2124 where $\delta^{15}\text{N}_{\text{reference}}$ refers to a reference plant that exclusively acquires nitrogen via

2125 direct uptake, $\delta^{15}\text{N}_{\text{sample}}$ refers to an individual's leaf $\delta^{15}\text{N}$, and B refers to individuals
2126 that are entirely reliant on nitrogen fixation. Within each unique nitrogen
2127 fertilization treatment-by-CO₂ treatment combination, I calculated the mean leaf
2128 $\delta^{15}\text{N}$ for individuals growing in the non-inoculated treatment for $\delta^{15}\text{N}_{\text{reference}}$. Any
2129 individuals with visual confirmation of root nodule formation or nodule initiation
2130 were omitted from the calculation of $\delta^{15}\text{N}_{\text{reference}}$. Following recommendations
2131 from Andrews et al. (2011) I calculated B within each CO₂ treatment using
2132 the mean leaf $\delta^{15}\text{N}$ of inoculated individuals that received 0 ppm N. I did not
2133 calculate B within each unique soil nitrogen-by-CO₂ treatment combination, as
2134 previous studies suggest decreased reliance on nitrogen fixation with increasing
2135 soil nitrogen availability (Perkowski et al. 2021). This approach for estimating
2136 nitrogen fixation standardizes values such that approaching 1 indicates increasing
2137 reliance on nitrogen fixation.

2138 5.2.9 *Statistical analyses*

2139 Any uninoculated pots that had substantial root nodule formation (nodule
2140 biomass: root biomass values greater than 0.05 g g⁻¹) were removed from analyses.
2141 This was because they were assumed to have been colonized by symbiotic nitrogen-
2142 fixing bacteria from outside sources. This decision resulted in the removal of
2143 sixteen pots from our analysis: two pots in the elevated CO₂ treatment that
2144 received 35 ppm N, three pots in the elevated CO₂ treatment that received 70
2145 ppm N, one pot in the elevated CO₂ treatment that received 210 ppm N, two pots
2146 in the elevated CO₂ treatment that received 280 ppm N, two pots in the ambient
2147 CO₂ treatment that received 0 ppm N, three pots in the ambient CO₂ treatment

2148 that received 70 ppm N, two pots in the ambient CO₂ treatment that received
2149 105 ppm N, and one pot in the ambient CO₂ treatment that received 280 ppm N.

2150 I built a series of linear mixed effects models to investigate the impacts of
2151 CO₂ concentration, soil nitrogen fertilization, and inoculation with *B. japonicum*
2152 on *G. max* gas exchange, tradeoffs between nitrogen and water use, whole plant
2153 growth, and investment in nitrogen fixation. All models included CO₂ treatment
2154 as a categorical fixed effect, inoculation treatment as a categorical fixed effect,
2155 soil nitrogen fertilization as a continuous fixed effect, with interaction terms be-
2156 tween all three fixed effects. All models also accounted for climatic difference
2157 between chambers across experiment iterations by including a random intercept
2158 term that nested starting chamber rack by CO₂ treatment. Models with this
2159 independent variable structure were created for each of the following dependent
2160 variables: N_{area} , M_{area} , N_{mass} , Chl_{area} , V_{cmax25} , J_{max25} , $J_{\text{max25}}:V_{\text{cmax25}}$, R_{d25} , g_{sw} ,
2161 stomatal limitation, ρ_{rubisco} , ρ_{bioe} , ρ_{light} , ρ_{photo} , $\rho_{\text{structure}}$, N_{cost} , C_{bg} , N_{wp} , total
2162 biomass, total leaf area, nodule biomass, and the ratio of nodule biomass to root
2163 biomass.

2164 I used Shapiro-Wilk tests of normality to determine whether linear mixed
2165 effects models satisfied residual normality assumptions. If residual normality as-
2166 sumptions were not met (Shapiro-Wilk: $p < 0.05$), then models were fit using
2167 dependent variables that were natural log transformed. All residual normality
2168 assumptions that did not originally satisfy residual normality assumptions were
2169 met with either a natural log or square root data transformation (Shapiro-Wilk:
2170 $p > 0.05$ in all cases). Specifically, models for N_{area} , N_{mass} , Chl_{area} , V_{cmax25} ,
2171 J_{max25} , $J_{\text{max25}}:V_{\text{cmax25}}$, g_{sw} , stomatal limitation, ρ_{rubisco} , ρ_{bioe} , ρ_{light} , ρ_{photo} , and to-

2172 tal leaf area satisfied residual normality assumptions without data transformation.
2173 Models for M_{area} , $\rho_{\text{structure}}$, N_{cost} , C_{bg} , N_{wp} , and total biomass satisfied residual
2174 normality assumptions with a natural log data transformation, while models for
2175 nodule biomass and nodule biomass: root biomass satisfied residual normality
2176 assumptions with a square root data transformation.

2177 In all statistical models, I used the 'lmer' function in the 'lme4' R package
2178 (Bates et al. 2015) to fit each model and the 'Anova' function in the 'car' R
2179 package (Fox and Weisberg 2019) to calculate Type II Wald's χ^2 and determine
2180 the significance ($\alpha = 0.05$) of each fixed effect coefficient. I used the 'emmeans'
2181 R package (Lenth 2019) to conduct post-hoc comparisons using Tukey's tests,
2182 where degrees of freedom were approximated using the Kenward-Roger approach
2183 (Kenward and Roger 1997). All analyses and plots were conducted in R version
2184 4.2.0 (R Core Team 2021).

2185 5.3 Results

2186 5.3.1 *Leaf nitrogen and chlorophyll content*

2187 Elevated CO₂ reduced N_{area} , N_{mass} , and Chl_{area} by 29%, 50%, and 31%,
2188 respectively, and stimulated M_{area} by 44% ($p < 0.001$ in all cases; Table 5.1). An
2189 interaction between fertilization and CO₂ (CO₂-by-fertilization interaction: $p_{N_{\text{area}}}$
2190 = 0.017, $p_{N_{\text{mass}}} < 0.001$, $p_{M_{\text{area}}} = 0.006$, $p_{Chl_{\text{area}}} = 0.083$; Table 5.1) indicated
2191 that the general positive effect of increasing fertilization on N_{area} , N_{mass} , and
2192 Chl_{area} ($p < 0.001$ in all cases; Table 5.1) was generally stronger under ambient
2193 CO₂ (Tukey _{N_{area}} : $p = 0.026$; Tukey _{N_{mass}} : $p < 0.001$; Tukey _{M_{area}} : $p = 0.009$;
2194 Tukey _{Chl_{area}} : $p = 0.065$; Table 5.1; Figs. 5.1a-d). This pattern resulted in a

2195 stronger reduction in N_{area} , N_{mass} , and Chl_{area} as well as a stronger stimulation
2196 in M_{area} under elevated CO₂ with increasing fertilization. An additional interac-
2197 tion between inoculation and CO₂ on N_{area} (CO₂-by-inoculation interaction: $p =$
2198 0.030; Table 5.1) indicated that the general positive effect of inoculation on N_{area}
2199 ($p < 0.001$; Table 5.1) was stronger under elevated CO₂ (45% increase; Tukey: p
2200 < 0.001) than under ambient CO₂ (18% increase; Tukey: $p < 0.001$), a result that
2201 increased the reduction in N_{area} in inoculated pots under elevated CO₂. Inocula-
2202 tion treatment did not modify the downregulation in N_{mass} (CO₂-by-inoculation
2203 interaction: $p = 0.148$; Table 5.1) and Chl_{area} ($p = 0.147$; Table 5.1) or the stimu-
2204 lation in M_{area} ($p = 0.866$; Table 5.1) under elevated CO₂. However, interactions
2205 between fertilization and inoculation on N_{area} (fertilization-by-inoculation inter-
2206 action: $p < 0.001$; Table 5.1; Fig. 5.1a), N_{mass} ($p = 0.001$; Table 5.1; Fig. 5.1b),
2207 M_{area} ($p = 0.025$; Table 5.1; Fig. 5.1c), and Chl_{area} ($p < 0.001$; Table 5.1; Fig.
2208 5.1d) indicated that the general positive effect of increasing fertilization on each
2209 trait was stronger in uninoculated pots (Tukey _{N_{area}} : $p < 0.001$; Tukey _{N_{mass}} : $p =$
2210 0.001; Tukey _{M_{area}} : $p = 0.031$; Tukey _{Chl_{area}} : $p < 0.001$).

Table 5.1. Effects of soil nitrogen fertilization, inoculation, and CO₂ treatments on N_{area} , N_{mass} , M_{area} , and Chl_{area}

| | N_{area} | | | N_{mass} | | | M_{area}^a | | | |
|----------------------|-------------------|-------------|----------|-------------------|-------------|----------|---------------------|-------------|----------|--------------|
| | df | Coefficient | χ^2 | p | Coefficient | χ^2 | p | Coefficient | χ^2 | p |
| (Intercept) | - | 1.10E+00 | - | - | 3.05E-02 | - | - | 3.64E+00 | - | - |
| CO ₂ | 1 | -5.67E-01 | 155.908 | <0.001 | -1.80E-02 | 272.362 | <0.001 | 3.04E-01 | 151.319 | <0.001 |
| Inoculation (I) | 1 | 6.21E-01 | 86.029 | <0.001 | 7.54E-03 | 15.576 | <0.001 | 1.81E-01 | 19.158 | <0.001 |
| Fertilization (N) | 1 | 3.06E-03 | 316.408 | <0.001 | 5.78E-05 | 106.659 | <0.001 | 3.10E-04 | 21.440 | <0.001 |
| CO ₂ *I | 1 | 2.63E-01 | 4.729 | 0.030 | 3.96E-03 | 2.025 | 0.155 | -3.37E-02 | 0.029 | 0.866 |
| CO ₂ *N | 1 | -3.68E-04 | 5.723 | 0.017 | -2.85E-05 | 22.542 | <0.001 | 2.80E-04 | 7.619 | 0.006 |
| I*N | 1 | -1.36E-03 | 43.381 | <0.001 | -2.00E-05 | 11.137 | 0.001 | -3.36E-04 | 5.022 | 0.025 |
| CO ₂ *I*N | 1 | -3.23E-04 | 0.489 | 0.484 | -2.59E-06 | 0.041 | 0.839 | 1.15E-04 | 0.208 | 0.649 |
| <hr/> | | | | | | | | | | |
| Chl_{area} | | | | | | | | | | |
| | df | Coefficient | χ^2 | p | | | | | | |
| (Intercept) | - | 2.13E-02 | - | - | | | | | | |
| CO ₂ | 1 | -1.33E-02 | 69.233 | <0.001 | | | | | | |
| Inoculation (I) | 1 | 1.24E-01 | 136.341 | <0.001 | | | | | | |
| Fertilization (N) | 1 | 3.35E-04 | 163.111 | <0.001 | | | | | | |
| CO ₂ *I | 1 | -3.18E-02 | 2.102 | 0.147 | | | | | | |
| CO ₂ *N | 1 | -8.79E-05 | 2.999 | <i>0.083</i> | | | | | | |
| I*N | 1 | -2.65E-04 | 75.769 | <0.001 | | | | | | |
| CO ₂ *I*N | 1 | 7.68E-05 | 2.144 | 0.147 | | | | | | |

130

2211 *Significance determined using Type II Wald χ^2 tests ($\alpha = 0.05$). P -values < 0.05 are in bold, while p -values between
 2212 0.05 and 0.1 are italicized. A superscript “a” is included after trait labels to indicate if models were fit with natural
 2213 log transformed response variables. Key: df = degrees of freedom, N_{area} = leaf nitrogen content per unit leaf area,
 2214 N_{mass} = leaf nitrogen content, M_{area} = leaf mass per unit leaf area.

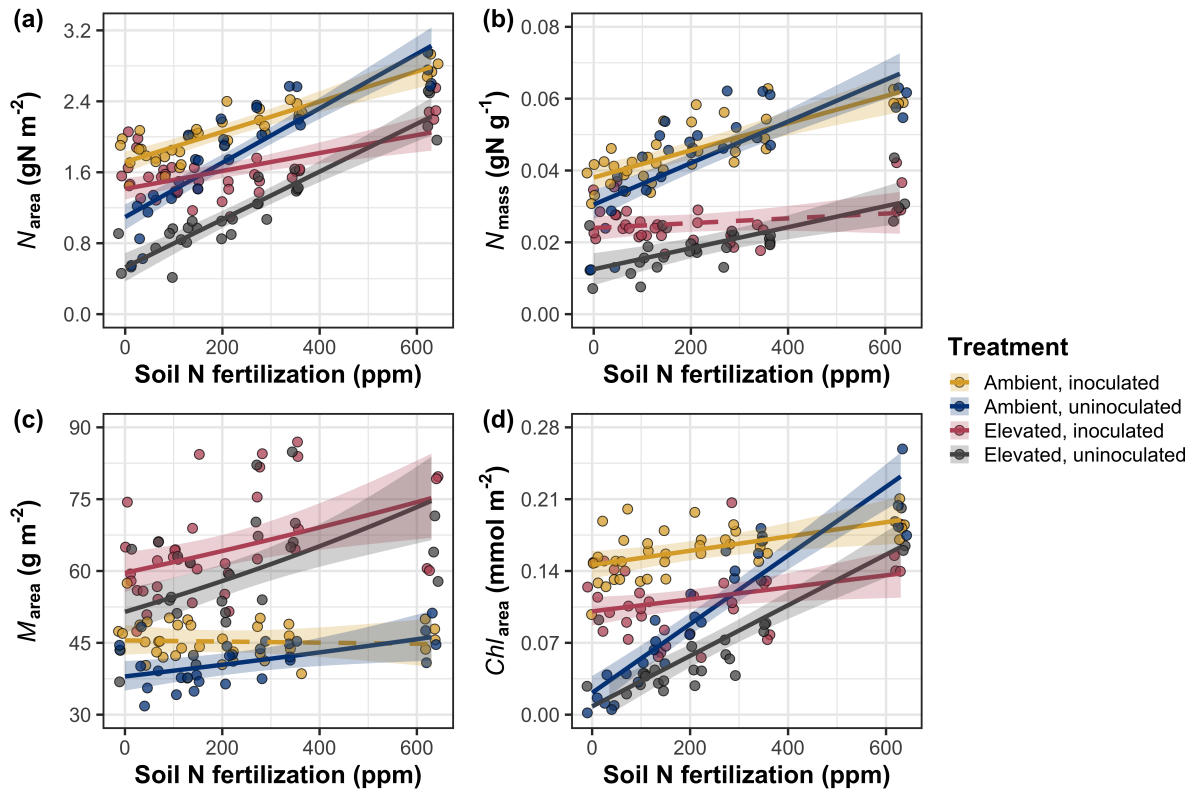


Figure 5.1. Effects of CO_2 , fertilization, and inoculation on leaf nitrogen per unit leaf area (a), leaf nitrogen content (b), leaf mass per unit leaf area (c), and chlorophyll content per unit leaf area (d). Soil nitrogen fertilization is represented on the x-axis in all panels. Yellow points and trendlines indicate inoculated individuals grown under ambient CO_2 , blue points and trendlines indicate uninoculated individuals grown under ambient CO_2 , red points and trendlines indicate inoculated individuals grown under elevated CO_2 , and grey points indicate uninoculated individuals grown under elevated CO_2 . Solid trendlines indicate regression slopes that are different from zero ($p < 0.05$), while dashed trendlines indicate slopes that are not distinguishable from zero ($p > 0.05$).

2215 5.3.2 *Leaf biochemistry and stomatal conductance*

2216 Elevated CO₂ resulted in plants with 16% lower V_{cmax25} ($p < 0.001$; Table
2217 5.2) and 10% lower J_{max25} ($p = 0.014$; Table 5.2) as compared to those grown under
2218 ambient CO₂. However, CO₂ concentration did not influence R_{d25} ($p = 0.613$;
2219 Table 5.2). A relatively stronger downregulation in V_{cmax25} than J_{max25} resulted
2220 in an 8% stimulation in $J_{max25}:V_{cmax25}$ under elevated CO₂ ($p < 0.001$; Table 5.2;
2221 Fig. 2E). The downregulatory effect of CO₂ on V_{cmax25} and J_{max25} was not modified
2222 across the fertilization gradient (CO₂-by-fertilization interaction: $p = 0.185$, $p =$
2223 0.389 for V_{cmax25} and J_{max25} , respectively; Table 5.2; Fig. 5.2a-b) or between
2224 inoculation treatments (CO₂-by-inoculation interaction: $p = 0.799$ and $p = 0.714$
2225 for V_{cmax25} and J_{max25} , respectively; Table 5.2). However, a strong interaction
2226 between fertilization and inoculation (fertilization-by-inoculation interaction: $p \leq$
2227 0.001 in all cases; Table 5.2) indicated that the general positive effect of increasing
2228 fertilization on V_{cmax25} ($p < 0.001$; Table 5.2), J_{max25} ($p < 0.001$; Table 5.2), and
2229 R_{d25} ($p = 0.015$; Table 2) was only observed in uninoculated pots (Tukey: p
2230 ≤ 0.001 in all cases), as there was no apparent effect of fertilization on V_{cmax25}
2231 (Tukey: $p = 0.456$), J_{max25} (Tukey: $p = 0.180$), or R_{d25} (Tukey: $p = 0.443$) in
2232 inoculated pots (Figs. 5.2a-d). A relatively stronger positive effect of increasing
2233 fertilization on V_{cmax25} than J_{max25} resulted in a general reduction in $J_{max25}:V_{cmax25}$
2234 with increasing fertilization ($p < 0.001$), though this pattern was only seen in
2235 uninoculated pots (Tukey: $p = 0.003$) and not inoculated plants (Tukey: $p >$
2236 0.05).

2237 Elevated CO₂ reduced stomatal conductance by 20% ($p < 0.001$; Table
2238 5.2; Fig. 5.2e) compared to ambient CO₂, but this downregulation did not influ-

ence stomatal limitation of photosynthesis ($p = 0.355$; Table 5.2; Fig. 5.2f). As with V_{cmax25} and J_{max25} , the downregulation of stomatal conductance due to elevated CO₂ was not modified across the fertilization gradient (CO₂-by-fertilization interaction: $p = 0.141$; Table 5.2) or between inoculation treatments (CO₂-by-inoculation interaction: $p = 0.179$; Table 5.2). Fertilization also did not modify the general null effect of CO₂ on stomatal limitation (CO₂-by-fertilization interaction: $p = 0.554$; Table 5.2), although an interaction between CO₂ and inoculation (CO₂-by-inoculation interaction: $p = 0.043$; Table 5.2) indicated that inoculation increased stomatal limitation under ambient CO₂ (Tukey: $p = 0.021$), but not under elevated CO₂ (Tukey: $p > 0.999$). An interaction between inoculation and fertilization on stomatal conductance (fertilization-by-inoculation interaction: $p < 0.001$; Table 5.2) indicated that increasing fertilization increased stomatal conductance in uninoculated pots (Tukey: $p = 0.003$) but decreased stomatal conductance in inoculated pots (Tukey: $p = 0.021$). The similar in magnitude, but opposite direction, trend in the effect of increasing fertilization on stomatal conductance between inoculation treatments likely drove a null general response of stomatal conductance to increasing fertilization ($p = 0.642$; Table 5.2).

Table 5.2. Effects of soil nitrogen fertilization, inoculation, and CO₂ on leaf biochemistry

| | <i>V_{cmax25}</i> | | | <i>J_{max25}</i> | | | <i>R_{d25}</i> | | | |
|----------------------|---------------------------|-------------|----------|--------------------------|-------------|----------|------------------------|-------------|----------|--------------|
| | df | Coefficient | χ^2 | p | Coefficient | χ^2 | p | Coefficient | χ^2 | p |
| (Intercept) | - | 4.36E+01 | - | - | 8.30E+01 | - | - | 1.69E+00 | - | - |
| CO ₂ | 1 | -7.05E+00 | 18.039 | <0.001 | -9.11E+00 | 6.042 | 0.014 | 4.53E-01 | 0.256 | 0.613 |
| Inoculation (I) | 1 | 5.87E+01 | 98.579 | <0.001 | 9.62E+01 | 85.064 | <0.001 | 1.04E+00 | 3.094 | 0.079 |
| Fertilization (N) | 1 | 1.32E-01 | 37.053 | <0.001 | 2.09E-01 | 25.356 | <0.001 | 2.86E-03 | 5.965 | 0.015 |
| CO ₂ *I | 1 | -4.65E+00 | 0.065 | 0.799 | 7.84E-01 | 0.667 | 0.414 | -5.71E-01 | 2.563 | 0.109 |
| CO ₂ *N | 1 | -3.58E-02 | 1.758 | 0.185 | -4.33E-02 | 0.742 | 0.389 | -1.55E-03 | 2.675 | 0.102 |
| I*N | 1 | -1.35E-01 | 60.394 | <0.001 | -2.30E-01 | 57.410 | <0.001 | -2.84E-03 | 12.083 | 0.001 |
| CO ₂ *I*N | 1 | 2.73E-02 | 0.748 | 0.387 | 3.46E-02 | 0.377 | 0.539 | 7.21E-04 | 0.244 | 0.622 |

| | <i>J_{max25}:V_{cmax25}</i> | | | <i>g_{sw}</i> | | | Stomatal limitation | | | |
|----------------------|---|-------------|----------|-----------------------|-------------|----------|---------------------|-------------|----------|--------------|
| | df | Coefficient | χ^2 | p | Coefficient | χ^2 | p | Coefficient | χ^2 | p |
| (Intercept) | - | 1.92E+00 | - | - | 1.95E-01 | - | - | 2.12E-01 | - | - |
| CO ₂ | 1 | 5.71E-02 | 92.010 | <0.001 | -6.23E-02 | 9.718 | 0.002 | 3.91E-02 | 0.856 | 0.355 |
| Inoculation (I) | 1 | -1.79E-01 | 27.768 | <0.001 | 1.30E-01 | 22.351 | <0.001 | 7.87E-02 | 4.582 | 0.032 |
| Fertilization (N) | 1 | -4.61E-04 | 28.147 | <0.001 | 2.50E-04 | 0.066 | 0.797 | 2.60E-04 | 32.218 | <0.001 |
| CO ₂ *I | 1 | 8.94E-02 | 2.916 | 0.088 | 6.69E-02 | 1.810 | 0.179 | -7.84E-02 | 4.093 | 0.043 |
| CO ₂ *N | 1 | 2.35E-04 | 3.210 | 0.073 | -8.50E-05 | 2.165 | 0.141 | -1.24E-04 | 0.350 | 0.554 |
| I*N | 1 | 3.27E-04 | 9.607 | 0.002 | -3.09E-04 | 14.696 | <0.001 | -1.67E-04 | 2.547 | 0.110 |
| CO ₂ *I*N | 1 | -1.66E-04 | 1.102 | 0.294 | -8.89E-05 | 0.234 | 0.629 | 1.67E-04 | 2.231 | 0.135 |

134

2256 *Significance determined using Type II Wald χ^2 tests ($\alpha = 0.05$). *P*-values < 0.05 are in bold, while *p*-values between
 2257 0.05 and 0.1 are italicized. Key: *V_{cmax25}* = maximum rate of Rubisco carboxylation at 25°C; *J_{max25}* = maximum rate
 2258 of electron transport for RuBP regeneration at 25°C, *R_{d25}* = dark respiration at 25°C; *J_{max25}:V_{cmax25}* = the ratio of
 2259 *J_{max25}* to *V_{cmax25}*; *g_{sw}* = stomatal conductance.

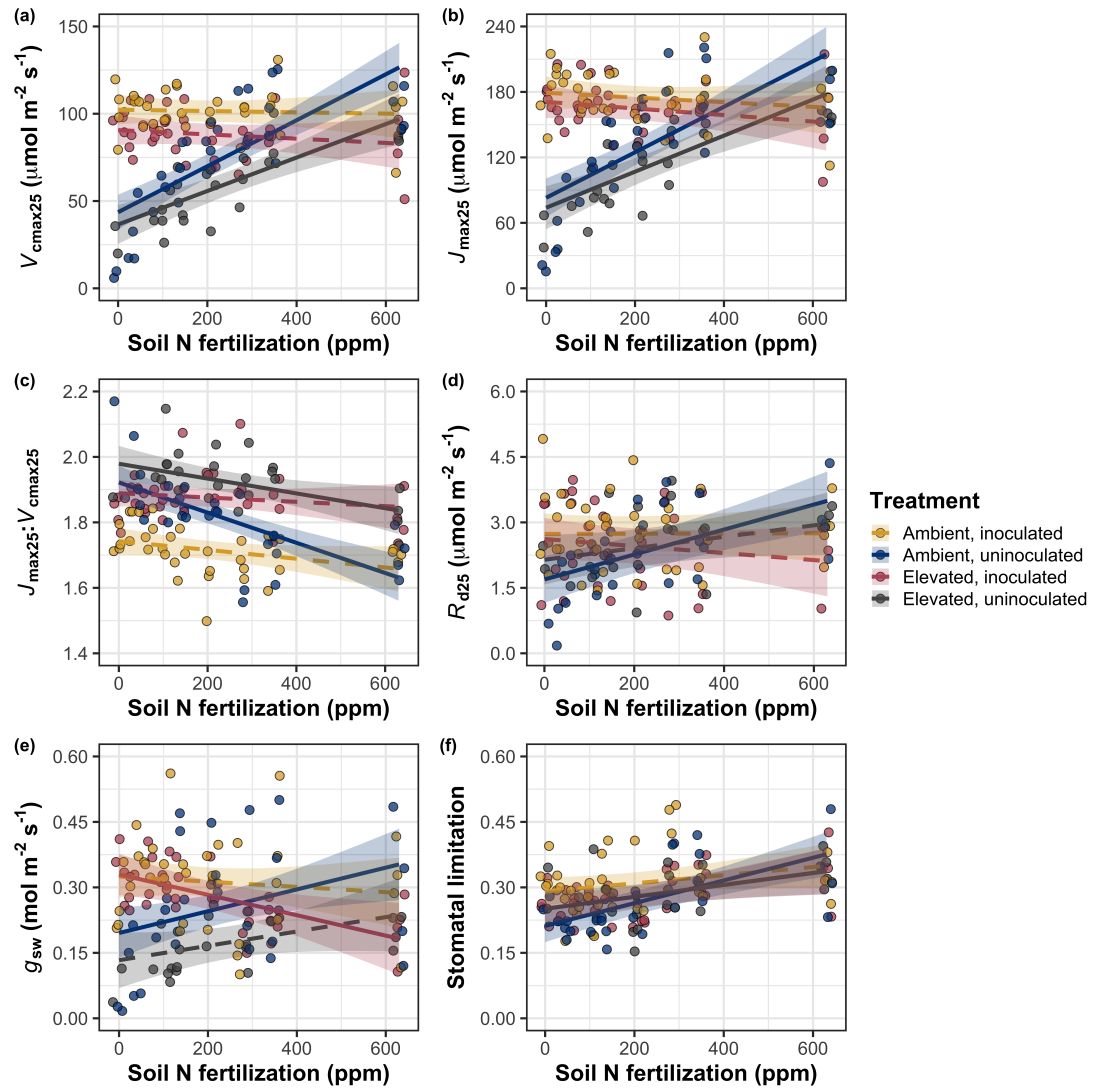


Figure 5.2. Effects of CO₂, fertilization, and inoculation on maximum rate of Rubisco carboxylation (a), the maximum rate of RuBP regeneration (b), and the ratio of the maximum rate of RuBP regeneration to the maximum rate of Rubisco carboxylation leaf mass per unit leaf area (c), dark respiration (d), stomatal conductance (e), and stomatal limitation (f). Soil nitrogen fertilization is represented on the x-axis in all panels. Colored points and trendlines are as explained in Figure 1.

2260 5.3.3 *Leaf nitrogen allocation*

2261 A relatively stronger downregulation in N_{area} than $V_{\text{cmax}25}$ or $J_{\text{max}25}$ resulted
2262 in an 20% and 29% respective stimulation in ρ_{rubisco} and ρ_{bioe} under elevated CO₂
2263 ($p < 0.001$ in both cases; Table 5.3). There was no apparent CO₂ effect on ρ_{light}
2264 ($p = 0.700$; Table 5.3), but the strong stimulation in ρ_{rubisco} and ρ_{bioe} resulted
2265 in a 21% stimulation of ρ_{photo} under elevated CO₂ ($p < 0.001$; Table 5.3; Fig.
2266 5.3a). The stimulation of ρ_{rubisco} , ρ_{bioe} , and ρ_{photo} due to elevated CO₂ was not
2267 modified across the fertilization gradient (CO₂-by-fertilization interaction: p_{rubisco}
2268 = 0.269, $p_{\text{bioe}} = 0.298$, $p_{\text{photo}} = 0.281$; Table 5.3). A marginal interaction between
2269 inoculation and CO₂ on ρ_{rubisco} and ρ_{photo} (CO₂-by-inoculation interaction: p_{rubisco}
2270 = 0.057, $p_{\text{photo}} = 0.057$; Table 5.3) indicated that the general positive effect of
2271 inoculation on ρ_{rubisco} and ρ_{photo} ($p < 0.001$ in both cases; Table 5.3) was only
2272 apparent under ambient CO₂ (Tukey: $p < 0.001$ in both cases), with no apparent
2273 effect of inoculation under elevated CO₂ (Tukey_{rubisco}: $p = 0.200$; Tukey_{photo}: p
2274 = 0.147). Inoculation did not modify the stimulation of ρ_{bioe} under elevated CO₂
2275 (CO₂-by-inoculation interaction: $p = 0.122$; Table 5.3) or the null effect of CO₂ on
2276 ρ_{bioe} (CO₂-by-inoculation interaction: $p = 0.298$; Table 5.3). Strong interactions
2277 between fertilization and inoculation on ρ_{rubisco} , ρ_{bioe} , and ρ_{photo} (fertilization-
2278 by-inoculation interaction: $p < 0.001$ in all cases; Table 5.3) indicated that the
2279 general negative effect of increasing fertilization ($p < 0.001$ in all cases; Table
2280 5.3) was only observed in inoculated pots (Tukey: $p < 0.001$ in all cases), with
2281 no apparent effect of fertilization on ρ_{rubisco} (Tukey: $p = 0.612$), ρ_{bioe} (Tukey:
2282 $p = 0.544$), or ρ_{photo} (Tukey: $p = 0.521$; Fig 5.3a) in uninoculated pots. An
2283 additional interaction between fertilization and inoculation on ρ_{light} (fertilization-

2284 by-inoculation interaction: $p < 0.001$; Table 5.3) indicated a negative effect of
2285 increasing fertilization on ρ_{light} in inoculated pots (Tukey: $p = 0.041$), but a
2286 positive effect of increasing fertilization in uninoculated pots (Tukey: $p < 0.001$).

2287 The stimulation in M_{area} resulted in an 133% stimulation of $\rho_{\text{structure}}$ under
2288 elevated CO₂ ($p < 0.001$; Table 5.3; Fig 5.3b). An interaction between fertiliza-
2289 tion and CO₂ (CO₂-by-fertilization interaction: $p = 0.039$; Table 5.3) indicated
2290 that the general negative effect of increasing fertilization ($p < 0.001$; Table 5.3) on
2291 $\rho_{\text{structure}}$ was marginally stronger under ambient CO₂ (Tukey: $p = 0.055$), resulting
2292 in a stronger stimulation in $\rho_{\text{structure}}$ under elevated CO₂ with increasing fertiliza-
2293 tion. A marginal interaction between inoculation and CO₂ (CO₂-by-inoculation
2294 interaction: $p = 0.057$; Table 5.3) indicated that the general positive effect of
2295 inoculation on $\rho_{\text{structure}}$ ($p < 0.001$; Table 5.3) was only observed under elevated
2296 CO₂ (Tukey: $p < 0.001$), with no apparent inoculation effect observed under am-
2297 bient CO₂ (Tukey: $p = 0.513$). Finally, an interaction between fertilization and
2298 inoculation (fertilization-by-inoculation interaction: $p < 0.001$; Table 5.3) indi-
2299 cated that, while increasing fertilization generally increased $\rho_{\text{structure}}$ ($p < 0.001$;
2300 Table 5.3), this response was generally stronger in uninoculated pots (Tukey: p
2301 = 0.001; Fig. 5.3b).

Table 5.3. Effects of soil N availability, soil pH, species, and N_{area} on leaf nitrogen allocation

| | | ρ_{rubisco} | | ρ_{bioe} | | ρ_{light} | | | | |
|-------------------|----|-------------------------|----------|----------------------|-------------|-----------------------|------------------|-------------|----------|------------------|
| | df | Coefficient | χ^2 | p | Coefficient | χ^2 | p | Coefficient | χ^2 | p |
| (Intercept) | - | 2.70E-01 | - | - | 5.26E-02 | - | - | 8.48E-03 | - | - |
| CO_2 | 1 | 1.42E-01 | 23.510 | <0.001 | 3.00E-02 | 53.899 | <0.001 | 2.03E-03 | 0.149 | 0.700 |
| Inoculation (I) | 1 | 1.83E-01 | 23.475 | <0.001 | 2.80E-02 | 13.860 | <0.001 | 2.04E-02 | 147.234 | <0.001 |
| Fertilization (N) | 1 | 1.35E-04 | 16.609 | <0.001 | 1.22E-05 | 26.827 | <0.001 | 3.22E-05 | 19.378 | <0.001 |
| CO_2*I | 1 | -1.07E-01 | 3.629 | <i>0.057</i> | -1.67E-02 | 2.390 | 0.122 | -5.33E-03 | 0.684 | 0.408 |
| CO_2*N | 1 | -2.16E-04 | 1.223 | 0.269 | -3.59E-05 | 1.085 | 0.298 | -7.01E-06 | 0.351 | 0.553 |
| $I*N$ | 1 | -4.26E-04 | 20.045 | <0.001 | -6.87E-05 | 15.458 | <0.001 | -4.37E-05 | 64.042 | <0.001 |
| CO_2*I*N | 1 | 2.50E-04 | 3.327 | <i>0.068</i> | 4.08E-05 | 2.651 | 0.103 | 1.74E-05 | 3.735 | <i>0.053</i> |

| | | ρ_{photo} | | $\rho_{\text{structure}}^a$ | | | | |
|-------------------|----|-----------------------|----------|-----------------------------|-------------|----------|------------------|--|
| | df | Coefficient | χ^2 | p | Coefficient | χ^2 | p | |
| (Intercept) | - | 3.32E-01 | - | - | -2.93E+00 | - | - | |
| CO_2 | 1 | 1.81E-01 | 27.651 | <0.001 | 8.77E-01 | 229.571 | <0.001 | |
| Inoculation (I) | 1 | 2.31E-01 | 26.238 | <0.001 | -2.55E-01 | 13.872 | <0.001 | |
| Fertilization (N) | 1 | 1.76E-04 | 15.899 | <0.001 | -1.51E-03 | 38.128 | <0.001 | |
| CO_2*I | 1 | -1.36E-01 | 3.671 | <i>0.055</i> | -2.99E-01 | 3.622 | <i>0.057</i> | |
| CO_2*N | 1 | -2.72E-04 | 1.163 | 0.281 | 3.14E-04 | 4.266 | 0.039 | |
| $I*N$ | 1 | -5.37E-04 | 21.355 | <0.001 | 7.00E-04 | 11.025 | 0.001 | |
| CO_2*I*N | 1 | 3.29E-04 | 4.009 | 0.045 | 4.52E-04 | 0.669 | 0.413 | |

138

2302 *Significance determined using Type II Wald χ^2 tests ($\alpha = 0.05$). P -values < 0.05 are in bold, while p -values
 2303 between 0.05 and 0.1 are italicized. A superscript “a” is included after trait labels to indicate if models were fit with
 2304 natural log transformed response variables. Key: df=degrees of freedom, ρ_{rubisco} = proportion of leaf N allocated
 2305 to photosynthesis, ρ_{bioe} = proportion of leaf N allocated to bioenergetics, ρ_{light} = proportion of leaf N allocated to
 2306 light harvesting proteins, ρ_{photo} = proportion of leaf N allocated to photosynthesis, $\rho_{\text{structure}}$ = proportion of leaf N
 2307 allocated to cell wall structural tissue

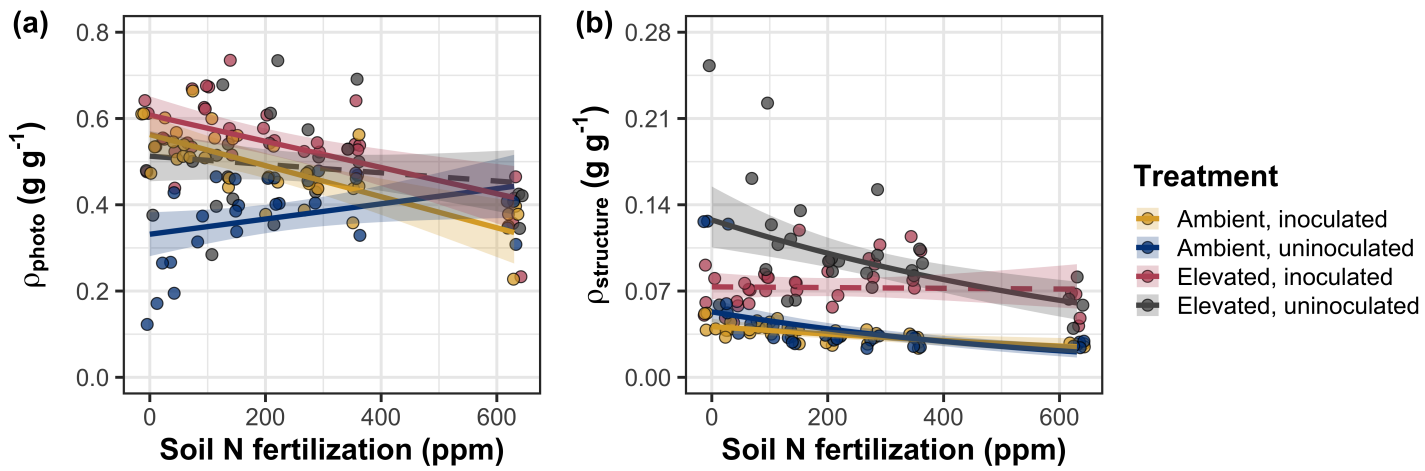


Figure 5.3. Effects of CO_2 , fertilization, and inoculation on the relative fraction of leaf nitrogen allocated to photosynthesis (a) and the fraction of leaf nitrogen allocated to structure (b). Soil nitrogen fertilization is represented on the x-axis in both panels. Colored points and trendlines are as explained in Figure 1.

2308 5.3.4 *Whole plant traits*

2309 Total leaf area was 51% greater and total biomass was 102% greater under
2310 elevated CO₂ ($p < 0.001$ in both cases; Table 5.4), a pattern that was enhanced
2311 by fertilization (CO₂-by-fertilization interaction: $p < 0.001$ in both cases; Table
2312 5.4; Figs. 5.4a-b) but was not modified across inoculation treatments (CO₂-by-
2313 inoculation interaction: $p_{total_leaf_area} = 0.151$, $p_{total_biomass} = 0.472$; Table 5.4).
2314 Specifically, the general positive effect of increasing fertilization on total leaf area
2315 and whole plant biomass ($p < 0.001$ in both cases; Table 5.4) was stronger under
2316 elevated CO₂ (Tukey: $p < 0.001$ in both cases). The general positive effect of
2317 increasing fertilization on total leaf area was modified by inoculation treatment
2318 (fertilization-by-inoculation interaction: $p < 0.001$ in both cases; Table 5.4), in-
2319 dicating a stronger positive effect of increasing fertilization in uninoculated pots
2320 (Tukey: $p_{total_leaf_area} = 0.002$, $p_{total_biomass} = 0.001$, Fig. 5.4a).

2321 A 62% stimulation in N_{cost} under elevated CO₂ was modified through a
2322 strong three-way interaction between CO₂, fertilization, and inoculation (CO₂-
2323 by-inoculation-by-fertilization interaction: $p < 0.001$; Table 5.4; Fig. 5.4). This
2324 interaction revealed a general negative effect of increasing fertilization on N_{cost}
2325 ($p < 0.001$; Table 5.4) that was observed in all treatment combinations (Tukey:
2326 $p < 0.001$ in all cases) except for inoculated pots grown under elevated CO₂
2327 (Tukey: $p = 0.779$; Fig. 5.4c). This response also resulted in generally stronger
2328 negative effects of increasing fertilization on N_{cost} in uninoculated pots grown
2329 under elevated CO₂ than uninoculated pots grown under ambient CO₂ (Tukey:
2330 $p = 0.001$) and inoculated pots grown under either ambient CO₂ (Tukey: $p <$
2331 0.001) or elevated CO₂ (Tukey: $p < 0.001$), while uninoculated pots grown under

2332 ambient CO₂ had generally stronger negative effects of increasing fertilization on
2333 N_{cost} than inoculated pots grown under elevated CO₂ (Tukey: $p = 0.002$), but
2334 not inoculated pots grown under ambient CO₂ (Tukey: $p = 0.216$; Fig. 5.4).
2335 The general reduction in N_{cost} with increasing fertilization and in uninoculated
2336 pots were driven by a stronger positive effect of increasing fertilization on N_{wp}
2337 (denominator of N_{cost}) than C_{bg} (numerator of N_{cost}), while the general stimulation
2338 in N_{cost} under elevated CO₂ was driven by a stronger positive effect of elevated
2339 CO₂ on C_{bg} than N_{wp} (Table 5.4).

Table 5.4. Effects of soil N availability, soil pH, species, and N_{area} on total leaf area, whole plant biomass, and carbon costs to acquire nitrogen

| | Total leaf area | | | Total biomass | | | N_{cost} | | | |
|-------------------------------------|-----------------|-------------|----------|------------------|-------------|----------|-------------------|-------------|----------|------------------|
| | df | Coefficient | χ^2 | p | Coefficient | χ^2 | p | Coefficient | χ^2 | p |
| (Intercept) | - | 8.78E+01 | - | - | 9.96E-01 | - | - | 8.67E+00 | - | - |
| CO_2 | 1 | 3.36E+01 | 69.291 | <0.001 | 5.07E-01 | 131.477 | <0.001 | 8.75E+00 | 88.189 | <0.001 |
| Inoculation (I) | 1 | 1.88E+02 | 35.715 | <0.001 | 7.96E-01 | 34.264 | <0.001 | -1.68E+00 | 136.343 | <0.001 |
| Fertilization (N) | 1 | 9.35E-01 | 274.199 | <0.001 | 3.14E-03 | 269.046 | <0.001 | -8.50E-03 | 80.501 | <0.001 |
| $\text{CO}_2 * \text{I}$ | 1 | 6.44E+01 | 2.064 | 0.151 | -7.69E-02 | 0.518 | 0.472 | -8.38E+00 | 85.237 | <0.001 |
| $\text{CO}_2 * \text{N}$ | 1 | 5.05E-01 | 18.655 | <0.001 | 1.61E-03 | 16.877 | <0.001 | -9.17E-03 | 1.050 | 0.306 |
| $\text{I} * \text{N}$ | 1 | -3.84E-01 | 10.804 | 0.001 | -1.45E-03 | 15.779 | <0.001 | 4.20E-03 | 46.489 | <0.001 |
| $\text{CO}_2 * \text{I} * \text{N}$ | 1 | -2.97E-03 | <0.001 | 0.990 | -1.14E-04 | 0.023 | 0.880 | 1.32E-02 | 18.125 | <0.001 |

| | C_{bg} | | | N_{wp} | | | |
|-------------------------------------|-----------------|-------------|----------|------------------|-------------|----------|------------------|
| | df | Coefficient | χ^2 | p | Coefficient | χ^2 | p |
| (Intercept) | - | -1.70E+00 | - | - | 1.24E-01 | - | - |
| CO_2 | 1 | 9.21E-01 | 84.134 | <0.001 | -3.41E-03 | 23.890 | <0.001 |
| Inoculation (I) | 1 | 1.18E+00 | 41.030 | <0.001 | 1.68E-01 | 134.460 | <0.001 |
| N fertilization (N) | 1 | 3.38E-03 | 152.248 | <0.001 | 6.69E-04 | 529.021 | <0.001 |
| $\text{CO}_2 * \text{I}$ | 1 | -6.18E-01 | 8.965 | 0.003 | 3.68E-02 | 1.190 | 0.275 |
| $\text{CO}_2 * \text{N}$ | 1 | -3.66E-05 | 1.188 | 0.276 | 1.58E-04 | 5.915 | 0.015 |
| $\text{I} * \text{N}$ | 1 | -2.22E-03 | 22.648 | <0.001 | -3.20E-04 | 55.562 | <0.001 |
| $\text{CO}_2 * \text{I} * \text{N}$ | 1 | 8.09E-04 | 1.109 | 0.292 | -7.54E-05 | 0.620 | 0.431 |

142

2340 *Significance determined using Type II Wald χ^2 tests ($\alpha = 0.05$). P-values < 0.05 are in bold, while p-values between
 2341 0.05 and 0.1 are italicized. Key: df = degrees of freedom; N_{cost} = structural carbon cost to acquire nitrogen; C_{bg} =
 2342 belowground carbon biomass; N_{wp} = whole plant nitrogen biomass

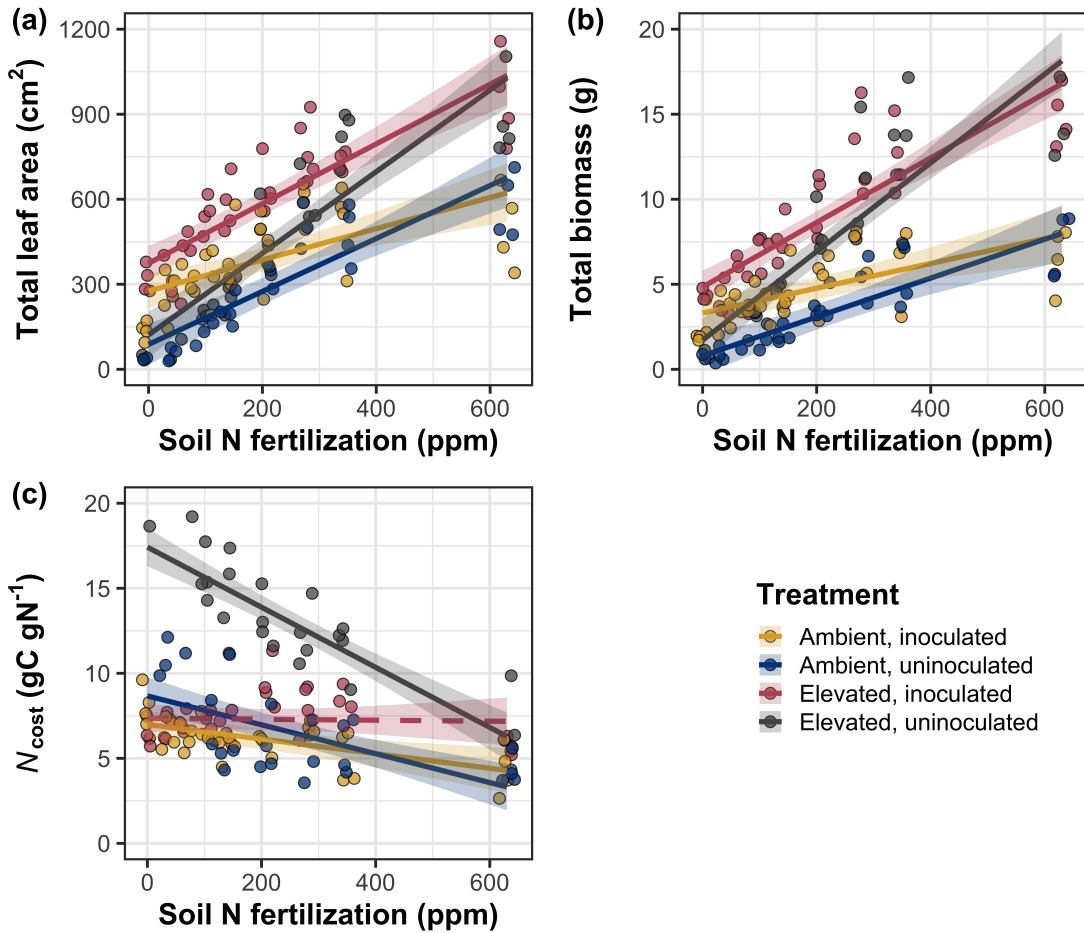


Figure 5.4. Effects of CO_2 , fertilization, and inoculation on total leaf area (a), total biomass (b), and structural carbon costs to acquire nitrogen (c). Soil nitrogen fertilization is represented continuously on the x-axis in all panels. Colored points and trendlines are as explained in Figure 1.

2343 5.3.5 *Nitrogen fixation*

2344 Nodule biomass was stimulated by 30% under elevated CO₂ ($p < 0.001$;
2345 Table 5.5), a pattern that was modified across the fertilization gradient (CO₂-
2346 by-fertilization interaction: $p = 0.479$; Table 5.5), but not between inoculation
2347 treatments (CO₂-by-inoculation interaction: $p = 0.404$; Table 5.5). Specifically,
2348 the general negative effect of increasing fertilization on nodule biomass ($p < 0.001$;
2349 Table 5.5) was stronger under elevated CO₂ than ambient CO₂ (Tukey: $p <$
2350 0.001; Fig. 5.5a), which reduced the stimulation in nodule biomass under elevated
2351 CO₂ with increasing fertilization. A strong interaction between fertilization and
2352 inoculation (fertilization-by-inoculation interaction: $p < 0.001$; Table 5.5) was
2353 driven by a stronger negative effect of increasing fertilization in inoculated pots
2354 (Tukey: $p < 0.001$; Fig. 5.5a).

2355 There was no effect of CO₂ on nodule: root biomass ($p = 0.767$; Table
2356 5.5), although an interaction between CO₂ and inoculation (CO₂-by-inoculation
2357 interaction: $p < 0.001$; Table 5.5) indicated that the general positive effect of in-
2358 oculation on nodule: root biomass ($p < 0.001$; Table 5.5) was stronger under am-
2359 bient CO₂ (3129% increase; Tukey: $p < 0.001$) than elevated CO₂ (379% increase;
2360 Tukey: $p < 0.001$; Fig. 5.5b). The null effect of CO₂ on nodule: root biomass
2361 was consistently observed across the fertilization gradient ($p = 0.183$; Table 5.5;
2362 Fig. 5.5b). An interaction between fertilization and inoculation (fertilization-by-
2363 inoculation interaction: $p < 0.001$; Table 5.5) indicated that the general negative
2364 effect of increasing fertilization on nodule: root biomass ($p < 0.001$; Table 5.5)
2365 was stronger in inoculated pots (Tukey: $p < 0.001$; Fig. 5.5b).

2366 There was no effect of CO₂ on %N_{dfa} ($p = 0.472$; Table 5.5), a pattern

2367 that was not modified by inoculation (CO_2 -by-inoculation interaction: $p = 0.156$;
2368 Table 5.5) or fertilization (CO_2 -by-fertilization interaction: $p = 0.099$; Table 5.5).
2369 An interaction between fertilization and inoculation (fertilization-by-inoculation
2370 interaction: $p < 0.001$; Table 5.5) indicated that the general negative effect of
2371 increasing fertilization on $\%N_{\text{dfa}}$ ($p < 0.001$; Table 5.5) was only observed in
2372 inoculated pots (Tukey: $p < 0.001$), with no apparent effect of fertilization on
2373 $\%N_{\text{dfa}}$ in uninoculated pots (Tukey: $p = 0.651$; Table 5.5; Fig. 5.5c).

Table 5.5. Effects of soil N availability, soil pH, species, and N_{area} on root nodule biomass and plant investments in symbiotic nitrogen fixation

| | Root nodule biomass ^b | | | Root nodule: root biomass ^b | | | % N_{dfa}^b | | | |
|----------------------|----------------------------------|-------------|----------|--|-------------|----------|----------------------|-------------|----------|------------------|
| | df | Coefficient | χ^2 | p | Coefficient | χ^2 | p | Coefficient | χ^2 | p |
| (Intercept) | - | 9.41E-03 | - | - | 1.33E-02 | - | - | 7.48E-01 | - | - |
| CO ₂ | 1 | 1.20E-01 | 19.258 | <0.001 | 9.94E-02 | 0.087 | 0.768 | -1.00E-01 | 0.518 | 0.472 |
| Inoculation (I) | 1 | 5.74E-01 | 755.020 | <0.001 | 5.40E-01 | 903.691 | <0.001 | 9.01E+00 | 955.570 | <0.001 |
| Fertilization (N) | 1 | 7.71E-06 | 84.376 | <0.001 | -5.99E-06 | 258.099 | <0.001 | 3.64E-04 | 292.938 | <0.001 |
| CO ₂ *I | 1 | -4.68E-02 | 0.950 | 0.330 | -1.38E-01 | 20.614 | <0.001 | -1.44E-01 | 2.010 | 0.156 |
| CO ₂ *N | 1 | -1.59E-04 | 2.106 | 0.147 | -1.73E-04 | 1.773 | 0.183 | -6.21E-05 | 2.716 | 0.099 |
| I*N | 1 | -5.82E-04 | 44.622 | <0.001 | -7.45E-04 | 133.918 | <0.001 | -1.58E-02 | 231.290 | <0.001 |
| CO ₂ *I*N | 1 | 7.26E-05 | 0.196 | 0.658 | 1.76E-04 | 2.359 | 0.125 | 2.77E-03 | 2.119 | 0.145 |

2374 *Significance determined using Type II Wald χ^2 tests ($\alpha = 0.05$). P-values < 0.05 are in bold, while p-values between
2375 0.05 and 0.1 are italicized. Superscript letters indicate model coefficients fit to square-root (^b) transformed data.
2376 Key: df = degrees of freedom % N_{dfa} = percent nitrogen fixed from the atmosphere.

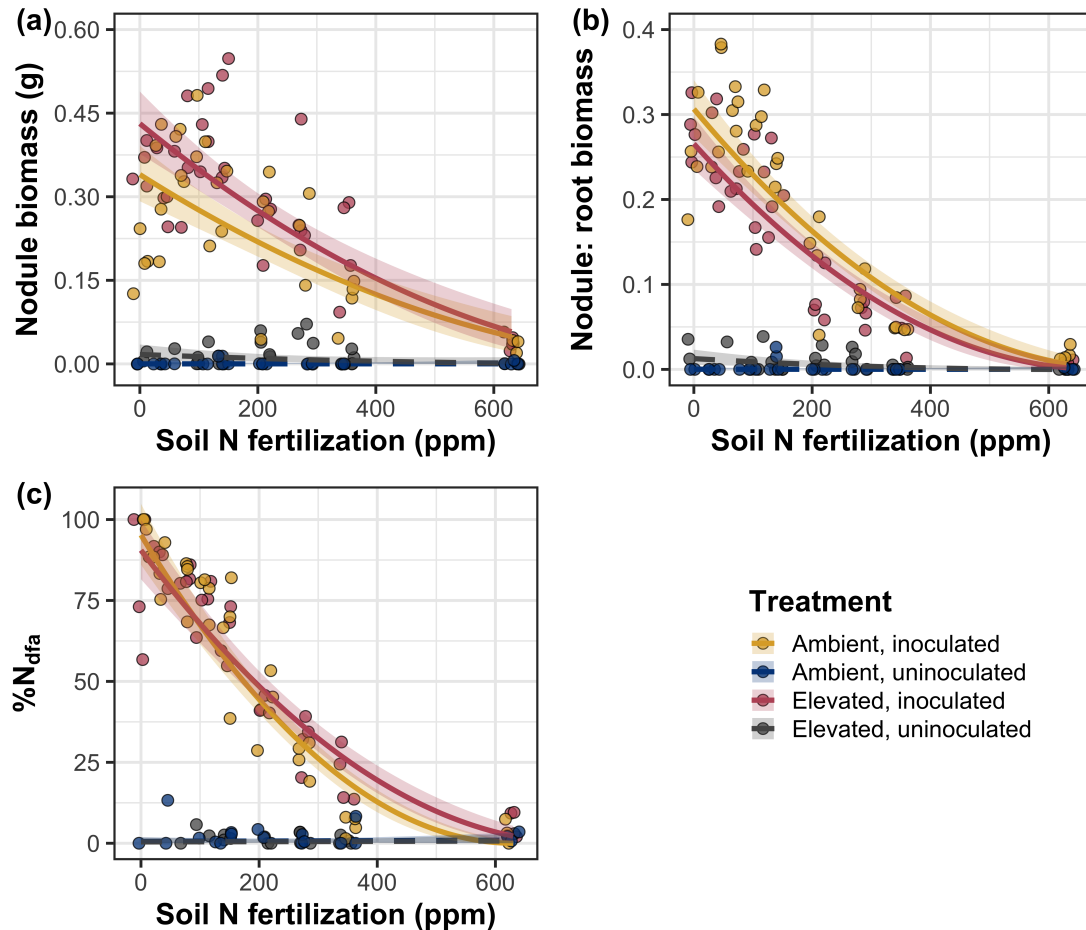


Figure 5.5. Effects of CO_2 , fertilization, and inoculation on nodule biomass (a), nodule: root biomass (b), and percent nitrogen fixed from the atmosphere (c). Soil nitrogen fertilization is represented on the x-axis. Yellow points and trendlines indicate inoculated individuals grown under ambient CO_2 , blue points and trendlines indicate uninoculated individuals grown under ambient CO_2 , red points and trendlines indicate inoculated individuals grown under elevated CO_2 , and grey points indicate uninoculated individuals grown under elevated CO_2 . Solid trendlines indicate slopes that are different from zero ($p < 0.05$), while dashed trendlines indicate slopes that are not different from zero ($p > 0.05$). Curvilinear trendlines occur as a result of back-transforming models where response variables received either a natural log or square root transformation prior to fitting.

2377 5.4 Discussion

2378 In this study, I determined leaf and whole plant acclimation responses of
2379 7-week *G. max* seedlings grown under two CO₂ concentrations, two inoculation
2380 treatments, and nine soil nitrogen fertilization treatments in a full-factorial growth
2381 chamber experiment. In support of my hypotheses and patterns expected from
2382 theory, elevated CO₂ reduced N_{area} , V_{cmax25} , and J_{max25} . The relatively stronger
2383 downregulation in V_{cmax25} than J_{max25} under elevated CO₂ resulted in a stimulation
2384 in $J_{\text{max25}}:V_{\text{cmax25}}$ under elevated CO₂. The downregulation of V_{cmax25} and J_{max25}
2385 under elevated CO₂ was similar across fertilization and inoculation treatments,
2386 indicating that the CO₂ responses were not due to nitrogen limitation. Interest-
2387 ingly, results indicate that elevated CO₂ increased the fraction of leaf nitrogen
2388 allocated to photosynthesis and structure, leading to a stimulation in nitrogen
2389 use efficiency under elevated CO₂ despite the apparent downregulation in N_{area} ,
2390 V_{cmax25} , and J_{max25} . The downregulation in leaf photosynthetic processes under
2391 elevated CO₂ also corresponded with a strong stimulation in total leaf area and to-
2392 tal biomass. Strong stimulations in whole plant growth due to elevated CO₂ were
2393 generally enhanced with increasing fertilization and were negatively related to
2394 structural carbon costs to acquire nitrogen. Inoculation generally did not modify
2395 whole plant responses to elevated CO₂ across the fertilization gradient, likely due
2396 to a strong reduction in root nodulation with increasing fertilization. However,
2397 strong positive effects of inoculation on whole plant growth were observed under
2398 low fertilization, consistent with our hypothesis. Overall, observed leaf and whole
2399 plant acclimation responses to CO₂ support hypotheses and patterns expected
2400 from photosynthetic least-cost theory, showing that leaf acclimation responses to

2401 CO₂ were decoupled from soil nitrogen availability and ability to acquire nitro-
2402 gen via symbiotic nitrogen fixation. Instead, leaf and whole plant acclimation
2403 responses to CO₂ were driven by optimal resource investment to photosynthetic
2404 capacity, where optimal resource investment at the leaf level maximized nitrogen
2405 allocation to structures that support whole plant growth.

2406 5.4.1 *Soil nitrogen fertilization has divergent effects on leaf and whole plant
2407 acclimation responses to CO₂*

2408 Elevated CO₂ reduced N_{area} , V_{cmax25} , J_{max25} , and stomatal conductance by
2409 29%, 16%, 10%, and 20%, respectively (Table 5.2). The larger downregulation in
2410 V_{cmax25} than J_{max25} led to an 8% stimulation in $J_{\text{max25}}:V_{\text{cmax25}}$ (Table 5.2), while
2411 the larger downregulation in N_{area} than V_{cmax25} resulted in a 21% stimulation
2412 in the fraction of leaf nitrogen allocated to photosynthesis under elevated CO₂.
2413 These acclimation responses are directionally consistent with previous studies that
2414 have investigated or reviewed leaf acclimation responses to CO₂ (Drake et al.
2415 1997; Makino et al. 1997; Ainsworth et al. 2002; Ainsworth and Long 2005;
2416 Ainsworth and Rogers 2007; Smith and Dukes 2013; Smith and Keenan 2020;
2417 Poorter et al. 2022), and follow patterns expected from photosynthetic least-cost
2418 theory (Wright et al. 2003; Prentice et al. 2014; Smith et al. 2019; Smith and
2419 Keenan 2020). Together, the stimulation in $J_{\text{max25}}:V_{\text{cmax25}}$ and the fraction of leaf
2420 nitrogen allocated to photosynthesis, and nitrogen use efficiency under elevated
2421 CO₂ provide strong support for the idea that leaves were downregulating V_{cmax25}
2422 in response to elevated CO₂ in order to optimally coordinate photosynthesis such
2423 that net photosynthesis rates approached becoming equally co-limited by Rubisco

2424 carboxylation and RuBP regeneration (Chen et al. 1993; Maire et al. 2012).

2425 Increasing fertilization and inoculation induced strong positive effects on
2426 N_{area} (Fig. 1a), $V_{\text{cmax}25}$ (Fig. 5.2a), $J_{\text{max}25}$ (Fig. 5.2b). The general positive
2427 response of N_{area} to increasing fertilization and in inoculated pots was enhanced
2428 under ambient CO₂, which, paired with the general downregulation in N_{area} un-
2429 der elevated CO₂, resulted in a stronger downregulation of N_{area} under elevated
2430 CO₂ with increasing fertilization and in inoculated pots (Fig. 5.1a). These pat-
2431 terns suggest that N_{area} responses to CO₂ were at least partially dependent on
2432 soil nitrogen fertilization and nitrogen acquisition strategy. However, the general
2433 stimulation in the fraction of leaf nitrogen allocated to Rubisco, bioenergetics,
2434 or photosynthesis under elevated CO₂ was not modified across the fertilization
2435 gradient and was only marginally enhanced in inoculated pots. These patterns
2436 suggest that the increased downregulation of Narea under elevated CO₂ with in-
2437 creasing fertilization was not associated with a change in relative investment to
2438 photosynthetic tissue. Instead, a stronger downregulation in the fraction of leaf
2439 nitrogen allocated to structure under ambient CO₂ resulted in a stronger stim-
2440 ulation in $\rho_{\text{structure}}$ under elevated CO₂ with increasing fertilization (Fig. 5.3b),
2441 indicating that fertilization shifted relative investment in leaf structural tissue un-
2442 der elevated CO₂. These results, combined with a stimulation in PNUE (Fig. SX)
2443 and iWUE (Fig. SX) under elevated CO₂ that was independent of fertilization
2444 or inoculation treatment, provide additional support for the hypothesis that leaf
2445 acclimation photosynthetic responses to CO₂ were independent of fertilization;
2446 though fertilization may contribute to changes in leaf morphology under elevated
2447 CO₂ through shifts in M_{area} (Onoda et al. 2017; Wang et al. 2017; Dong et al.

2448 2022).

2449 The downregulation in N_{area} , $V_{\text{cmax}25}$, and $J_{\text{max}25}$ under elevated CO₂ cor-
2450 responded with a respective 62% and 100% stimulation in total leaf area (Fig.
2451 5.4a) and total biomass (Fig. 5.4b). The stimulation in total leaf area and total
2452 biomass under elevated CO₂ also corresponded with generally higher structural
2453 carbon costs to acquire nitrogen (Fig. 5.4c), a pattern driven by a stimulation
2454 in belowground carbon biomass and reduction in whole plant nitrogen biomass.
2455 Alone, this result suggests that elevated CO₂ reduces plant nitrogen uptake effi-
2456 ciency, which does not explain why plants grown under elevated CO₂ generally had
2457 higher biomass and total leaf area. However, a strong negative effect of increasing
2458 fertilization on structural carbon costs to acquire nitrogen, which were generally
2459 similar between CO₂ concentrations, was driven by a stronger increase in whole
2460 plant nitrogen biomass than belowground carbon biomass. Thus, increases in the
2461 positive response of whole plant growth and total leaf area under elevated CO₂
2462 with increasing fertilization were likely driven by an increase in nitrogen uptake
2463 efficiency, allowing plants to satisfy any increase in whole plant nitrogen demand
2464 associated with increased CO₂.

2465 Interestingly, these results indicate that the general stimulation in total
2466 leaf area and whole plant growth under elevated CO₂ was not modified by inoc-
2467 ulation despite an apparent general negative effect of inoculation on N_{cost} . This
2468 response could have been due to strong negative effect of increasing fertilization on
2469 nodulation (Fig. 5.5), which may have caused the strong increase in the positive
2470 effect of elevated CO₂ on whole plant growth with increasing fertilization to mask
2471 any increase in the positive effect of elevated CO₂ on whole plant growth due to

2472 inoculation. Reductions in nodulation with increasing fertilization are commonly
2473 observed patterns that have been inferred to be a response that allows species
2474 optimize nitrogen uptake efficiency as costs to acquire nitrogen via direct uptake
2475 become more similar (Fig. 5.4c) (Gibson and Harper 1985; Rastetter et al. 2001).
2476 In this study, pairwise comparisons indicated strong positive effects of inocula-
2477 tion on total leaf area and total biomass (158% increase in total leaf area, 119%
2478 increase in total biomass) under elevated CO₂ at 0 ppm N, but no observable
2479 inoculation effect on total leaf area or total biomass under elevated CO₂ at 350
2480 ppm N or 630 ppm N. While these responses did not generally differ from those
2481 observed under ambient CO₂, they do confirm the hypothesis that positive effects
2482 of inoculation on whole plant growth responses to elevated CO₂ would decrease
2483 with increasing fertilization.

2484 Combined, results reported here suggest that soil nitrogen availability has
2485 a divergent role in modifying leaf and whole plant acclimation responses to CO₂.
2486 Leaf acclimation responses were generally decoupled from fertilization, while whole
2487 plant acclimation responses relied heavily on an increase in nitrogen uptake ef-
2488 ficiency and consequent reduction in costs of acquiring nitrogen associated with
2489 increasing fertilization. However, whole plant responses to CO₂ indicated that
2490 fertilization may play a more important role in determining whole plant acclima-
2491 tion responses to CO₂ than nitrogen acquisition strategy, although these patterns
2492 were likely driven by reductions in nodulation with increasing fertilization. These
2493 results suggest that plants acclimate to CO₂ in nitrogen-limited systems by mini-
2494 mizing the number of optimally coordinated leaves, and that the downregulation
2495 in leaf nitrogen content under elevated CO₂ is not a direct response to changes in

2496 soil nitrogen availability as previously implied.

2497 5.4.2 *Implications for future model development*

2498 Many terrestrial biosphere models predict photosynthetic capacity through
2499 plant functional group-specific linear regressions between N_{area} and V_{cmax} (Rogers
2500 2014; Rogers et al. 2017), which assumes that leaf nitrogen-photosynthesis rela-
2501 tionships are constant across growing environments. Our results build on previ-
2502 ous work suggesting that leaf nitrogen-photosynthesis relationships dynamically
2503 change across growing environments (Luo et al. 2021; Dong et al. 2022). Specif-
2504 ically, results from this experiment indicate that CO_2 concentration increased
2505 the fraction of leaf nitrogen content allocated to photosynthesis, while a general
2506 negative effect of increasing fertilization on the fraction of leaf nitrogen content
2507 allocated to photosynthesis was dependent on inoculation treatment. Similar in-
2508 creases in N_{area} , $V_{\text{cmax}25}$, and $J_{\text{max}25}$ with increasing fertilization resulted in no
2509 change in the fraction of leaf nitrogen allocated to photosynthesis in uninoculated
2510 pots, while larger increases in N_{area} than $V_{\text{cmax}25}$ and $J_{\text{max}25}$ with increasing fertil-
2511 ization decreased the fraction of leaf nitrogen allocated to photosynthesis in inoc-
2512 ulated pots (Fig. 5.3a). As inoculated pots were able to access less finite supply of
2513 nitrogen across the fertilization gradient, these patterns suggest that constant leaf
2514 nitrogen-photosynthesis relationships may only apply in environments where ni-
2515 trogen is limiting and will likely change with increasing CO_2 concentrations. Thus,
2516 terrestrial biosphere models that parameterize photosynthetic capacity through
2517 linear relationships between N_{area} and V_{cmax} (Rogers 2014; Rogers et al. 2017)
2518 may be overestimating photosynthetic capacity in systems where nitrogen is not

2519 as limiting and may contribute to erroneous model simulations under future CO₂
2520 concentrations.

2521 These results also demonstrate that optimal resource investment to photo-
2522 tosynthetic capacity defines leaf acclimation responses to elevated CO₂, and that
2523 these responses were independent of fertilization or inoculation treatment. Cur-
2524 rent approaches for simulating photosynthetic responses to CO₂ generally invoke
2525 patterns expected from progressive nitrogen limitation, where the downregulation
2526 in N_{area} , and therefore photosynthetic capacity, due to elevated CO₂ are com-
2527 monly a function of progressive reductions in soil nitrogen availability. Results
2528 reported here contradict this formulation, suggesting that the leaf acclimation re-
2529 sponse is driven by optimal resource investment to photosynthetic capacity and
2530 is independent of soil resource supply. Optimality models that leverage prin-
2531 ciples from optimal coordination and photosynthetic least-cost theories (Wang
2532 et al. 2017; Stocker et al. 2020; Scott and Smith 2022) are capable of capturing
2533 such acclimation responses to CO₂ (Smith and Keenan 2020), suggesting that the
2534 implementation of these models may improve the simulation of photosynthetic
2535 processes in terrestrial biosphere models under increasing CO₂ concentrations.

2536 5.4.3 *Study limitations and future directions*

2537 There are two study limitations that must be addressed to contextualize
2538 patterns observed in this study. First, restricting the volume of belowground
2539 substrate via a potted experiment does not adequately replicate belowground en-
2540 vironments of natural systems, and therefore may modify effects of soil resource
2541 availability and inoculation on plant nitrogen uptake, particularly if pot size limits

2542 whole plant growth (Poorter et al. 2012). I attempted to minimize the extent of
2543 pot size limitation experienced in the first experimental chapters while account-
2544 ing for the expected stimulation in whole plant growth under elevated CO₂ by
2545 using 6-liter pots. Despite attempts to minimize growth limitation imposed by
2546 pot volume, fertilization and CO₂ treatments increased the biomass: pot volume
2547 ratio such that all treatment combinations to exceed 1 g L⁻¹ biomass: pot volume
2548 under high fertilization. The 1 g L⁻¹ biomass: pot volume recommendation from
2549 Poorter et al. (2012) was designated to avoid growth limitation imposed by pot
2550 volume. However, if pot size limitation indeed limited whole plant growth, then
2551 structural carbon costs to acquire nitrogen, belowground carbon biomass, whole
2552 plant nitrogen biomass, and whole plant biomass should each exhibit strong sat-
2553 uration points with increasing fertilization, which was not observed here. Addi-
2554 tionally, a second set of photosynthetic measurements from one week prior to the
2555 harvest (6 weeks post-germination) revealed ... As pot limitation is expected
2556 to decrease net photosynthesis, and focal leaves were of similar ages between the
2557 sixth and seventh week, one might expect growth limitation induced by constricted
2558 pot volume to result in a dampened effect of inoculation and fertilization on net
2559 photosynthesis, V_{cmax} , and J_{max25} . Analyses from the sixth week of development
2560 revealed ... Additionally, analyses revealed a stronger/weaker downregulation in
2561 V_{cmax25} and J_{max25} on week 7, though disentangling the causality of this response
2562 (i.e. whether due to pot size limitation or simply a stronger acclimation response)
2563 would be difficult.

2564 Second, this study evaluated leaf and whole plant responses to CO₂ in 7-
2565 week seedlings. Given the long-term scale of the progressive nitrogen limitation

2566 hypothesis, patterns observed here should be validated in longer-term nitrogen
2567 manipulation experiments. Previous work in free air CO₂ enrichment experiments
2568 show some support for patterns expected from the progressive nitrogen limitation
2569 hypothesis (Reich et al. 2006; Norby et al. 2010), although results are not consis-
2570 tent across experimental sites (Finzi et al. 2006; Moore et al. 2006; Liang et al.
2571 2016). We found some support for patterns expected by the progressive nitrogen
2572 limitation hypothesis, namely an increase in plant nitrogen uptake under elevated
2573 CO₂ (Luo et al. 2004), though leaf acclimation responses to CO₂ were strongly
2574 indicative of optimal resource investment to photosynthetic capacity as expected
2575 from photosynthetic least-cost theory (Prentice et al. 2014; Smith et al. 2019;
2576 Smith and Keenan 2020).

2577 5.4.4 *Conclusions*

2578 This study provides strong evidence suggesting that leaf acclimation re-
2579 sponds to elevated CO₂ did not vary with soil nitrogen fertilization or ability
2580 to acquire nitrogen through symbiotic nitrogen fixation. However, whole plant
2581 acclimation responses to CO₂ were dependent on fertilization, where increasing
2582 fertilization increased the positive effect of whole plant growth under elevated
2583 CO₂. Results also indicate that fertilization played a relatively more important
2584 role in modifying whole plant responses to CO₂, perhaps due to a reduction in
2585 nodulation across the fertilization gradient. These patterns strongly support the
2586 hypothesis that leaf and whole plant acclimation responses are driven by opti-
2587 mal resource investment to photosynthetic capacity, and that leaf acclimation
2588 responses to CO₂ were not modified by changes in soil nitrogen availability. Ad-

2589 ditionally, strong interactions between fertilization and inoculation on leaf and
2590 whole plant traits indicated positive effects of fertilization on leaf and whole plant
2591 traits in uninoculated pots, but null effects of fertilization on leaf and whole plant
2592 traits in inoculated pots. These results build on previous work suggesting that
2593 constant leaf nitrogen-photosynthesis relationships are dynamic and change across
2594 growing environments, calling the use of constant relationships by terrestrial bio-
2595 sphere models into question.

2596

Chapter 6

2597

Conclusions

2598 The experiments described in this dissertation were designed to test mechanisms
2599 that drive patterns expected from photosynthetic least-cost theory across various
2600 soil resource availability and climatic gradients. The first experimental experi-
2601 ment evaluated variance in carbon costs to acquire nitrogen in *Glycine max* and
2602 *Gossypium hirsutum* grown across four nitrogen fertilization treatments and four
2603 light availability treatments in a full factorial greenhouse experiment. The second
2604 experiment investigated nitrogen-water use tradeoffs across a soil nitrogen avail-
2605 ability and soil pH gradient in mature deciduous tree species growing in a nine-year
2606 nitrogen-by-sulfur field manipulation experiment. The third experiment explored
2607 variance in costs to acquire nitrogen relative to water, leaf $C_i:C_a$, and components
2608 of leaf nitrogen content in species scattered along a precipitation and soil nitrogen
2609 availability gradient in open canopy grasslands of Texas. Finally, the fourth exper-
2610 iment quantified leaf and whole plant acclimation responses to elevated CO₂ in *G.*
2611 *max* grown under nine soil nitrogen fertilization treatments and two inoculation
2612 treatments in a full factorial growth chamber experiment. Below, I provide a brief
2613 summary of major findings from each experiment, synthesize common patterns
2614 observed across experiments, interpret major findings in the context of photosyn-
2615 thetic least-cost theory and propose directions for future model development, and
2616 conclude this dissertation with suggestions for future manipulative and environ-
2617 mental gradient experiments that will allow us to better understand mechanisms
2618 that drive patterns expected from photosynthetic least-cost theory.

2619 6.1 Summary of experimental chapters

2620 6.1.1 *Chapter 2: Structural carbon costs to acquire nitrogen are determined by*
2621 *nitrogen and light availability in two species with different nitrogen*
2622 *acquisition strategies*

2623 The first experimental chapter in this dissertation sought to understand how car-
2624 bon costs to acquire nitrogen vary across soil nitrogen and light availability gra-
2625 dients in two species with different nutrient acquisition strategies. *Glycine max*
2626 is a legume capable of acquiring nitrogen via direct uptake pathways, through
2627 associations with symbiotic nitrogen-fixing bacteria, and is capable of forming as-
2628 sociations with arbuscular mycorrhizal fungi. *Gossypium hirsutum* is also capable
2629 of acquiring nitrogen via direct uptake pathways and through associations with
2630 arbuscular mycorrhizal fungi, but is not able to form associations with symbiotic
2631 nitrogen-fixing bacteria. Regardless of species, I found strong evidence linking
2632 increasing fertilization with reductions in carbon costs to acquire nitrogen, a pat-
2633 tern that was driven by a larger increase in nitrogen uptake than belowground
2634 carbon investment, suggesting that increasing fertilization allowed plants to in-
2635 crease nitrogen-uptake efficiency (Lu et al. 2022). I also find strong evidence
2636 linking an increase in light availability to an increase in carbon costs to acquire
2637 nitrogen, which was presumably a response driven by an increase in demand to
2638 allocate nitrogen to photosynthetic enzymes with increasing fertilization.

2639 Interestingly, the first chapter also indicates that carbon costs to acquire
2640 nitrogen in *G. max* were generally less responsive to changes in nitrogen fertil-
2641 ization than *G. hirsutum*. These findings were observed in coordination with a
2642 strong reduction in root nodulation with increasing fertilization, indicating that
2643 *G. max* were likely shifting away from investment in symbiotic nitrogen fixation

2644 and toward direct uptake as costs to acquire nitrogen via direct uptake became
2645 more similar with increasing fertilization. These patterns follow resource optimiza-
2646 tion theory (Rastetter et al. 2001), where individuals are expected to maximize
2647 nutrient uptake efficiency in a given environment, which could be achieved by
2648 preferentially investing in the nutrient acquisition pathway that maximizes nutri-
2649 ent returns from a given carbon investment. Assigning causality to these patterns
2650 is challenging, as *G. max* and *G. hirsutum* differ in their growth forms and growth
2651 durations (*G. max* is a herbaceous annual while *G. hirsutum* is a woody perennial)
2652 and are not phylogenetically related. Differences in life history between the two
2653 species limited my ability to assess whether reductions in the negative effect of
2654 increasing fertilization on carbon costs to acquire nitrogen in *G. max* were driven
2655 by shifts to direct uptake with increasing fertilization. However, these patterns
2656 were later validated in the fourth experimental chapter, where I quantify simi-
2657 lar weaker negative effects of increasing fertilization on carbon costs to acquire
2658 nitrogen in *G. max* that were inoculated with symbiotic nitrogen-fixing bacteria
2659 compared to *G. max* that were left uninoculated across a similar soil nitrogen
2660 fertilization gradient.

2661 6.1.2 *Chapter 3: Soil nitrogen availability modifies leaf nitrogen economies in*
2662 *mature temperate deciduous forests: a direct test of photosynthetic*
2663 *least-cost theory*

2664 The second experimental chapter sought to evaluate whether shifts in soil nitrogen
2665 availability or soil pH modify nitrogen-water use tradeoffs expected from photo-
2666 synthetic least cost theory. Despite noisy data, I find evidence for nitrogen-water
2667 use tradeoffs in response to increasing soil nitrogen availability. Specifically, in-

2668 creasing soil nitrogen availability generally increased leaf nitrogen content, but did
2669 not significantly affect leaf $C_i:C_a$, which led to a stimulation in leaf nitrogen con-
2670 tent per unit leaf $C_i:C_a$ and photosynthetic nitrogen-use efficiency with increasing
2671 soil nitrogen availability. I also find positive trends in photosynthetic capacity
2672 with increasing soil nitrogen availability, though these trends were statistically
2673 insignificant. However, there was no apparent effect of soil pH on measured leaf
2674 traits, which was likely because the experimental nitrogen additions increased soil
2675 nitrogen supply while both increasing (sodium nitrate) and decreasing (ammo-
2676 nium sulfate) soil pH. Regardless, findings from this experiment indicate that soil
2677 nitrogen availability matters more for determining nitrogen-water use tradeoffs ex-
2678 pected from theory, and that previous gradient studies investigating effects of soil
2679 pH on such tradeoffs may be confounded by changes in soil nitrogen availability.

2680 6.1.3 *Chapter 4: The relative cost of resource use for photosynthesis drives*
2681 *variance in leaf nitrogen content across a climate and soil resource*
2682 *availability gradient*

2683 6.1.4 *Chapter 5: Optimal resource investment to photosynthetic capacity*
2684 *maximizes nutrient allocation to whole plant growth under elevated CO₂*

2685

References

- 2686 Abrams, M. D. and S. A. Mostoller (1995). Gas exchange, leaf structure and
2687 nitrogen in contrasting successional tree species growing in open and under-
2688 story sites during a drought. *Tree Physiology* 15(6), 361–370.
- 2689 Adams, M. A., T. L. Turnbull, J. I. Sprent, and N. Buchmann (2016). Legumes
2690 are different: Leaf nitrogen, photosynthesis, and water use efficiency. *Pro-
2691 ceedings of the National Academy of Sciences of the United States of Amer-
2692 ica* 113(15), 4098–4103.
- 2693 Ainsworth, E. A., P. A. Davey, C. J. Bernacchi, O. C. Dermody, E. A. Heaton,
2694 D. J. Moore, P. B. Morgan, S. L. Naidu, H. S. Y. Ra, X. G. Zhu, P. S. Curtis,
2695 and S. P. Long (2002). A meta-analysis of elevated [CO₂] effects on soybean
2696 (*Glycine max*) physiology, growth and yield. *Global Change Biology* 8(8),
2697 695–709.
- 2698 Ainsworth, E. A. and S. P. Long (2005). What have we learned from 15 years of
2699 free-air CO₂ enrichment (FACE)? A meta-analytic review of the responses
2700 of photosynthesis, canopy properties and plant production to rising CO₂.
2701 *New Phytologist* 165(2), 351–372.
- 2702 Ainsworth, E. A. and A. Rogers (2007). The response of photosynthesis and
2703 stomatal conductance to rising [CO₂]: mechanisms and environmental in-
2704 teractions. *Plant, Cell and Environment* 30(3), 258–270.
- 2705 Allen, K., J. B. Fisher, R. P. Phillips, J. S. Powers, and E. R. Brzostek (2020).
2706 Modeling the carbon cost of plant nitrogen and phosphorus uptake across
2707 temperate and tropical forests. *Frontiers in Forests and Global Change* 3,

- 2708 1–12.
- 2709 Allison, S. D., C. I. Czimczik, and K. K. Treseder (2008). Microbial activity
2710 and soil respiration under nitrogen addition in Alaskan boreal forest. *Global
2711 Change Biology* 14(5), 1156–1168.
- 2712 Andersen, M. K., H. Hauggaard-Nielsen, P. Ambus, and E. S. Jensen (2005).
2713 Biomass production, symbiotic nitrogen fixation and inorganic N use in dual
2714 and tri-component annual intercrops. *Plant and Soil* 266(1-2), 273–287.
- 2715 Andrews, M., E. K. James, J. I. Sprent, R. M. Boddey, E. Gross, and F. B. dos
2716 Reis (2011). Nitrogen fixation in legumes and actinorhizal plants in natural
2717 ecosystems: Values obtained using ^{15}N natural abundance. *Plant Ecology
2718 and Diversity* 4(2-3), 117–130.
- 2719 Arndal, M. F., A. Tolver, K. S. Larsen, C. Beier, and I. K. Schmidt (2018). Fine
2720 root growth and vertical distribution in response to elevated CO₂, warming
2721 and drought in a mixed heathland–grassland. *Ecosystems* 21(1), 15–30.
- 2722 Arnone, J. A. (1997). Indices of plant N availability in an alpine grassland under
2723 elevated atmospheric CO₂. *Plant and Soil* 190(1), 61–66.
- 2724 Arora, V. K., A. Katavouta, R. G. Williams, C. D. Jones, V. Brovkin,
2725 P. Friedlingstein, J. Schwinger, L. Bopp, O. Boucher, P. Cadule, M. A.
2726 Chamberlain, J. R. Christian, C. Delire, R. A. Fisher, T. Hajima, T. Ilyina,
2727 E. Joetzjer, M. Kawamiya, C. D. Koven, J. P. Krasting, R. M. Law, D. M.
2728 Lawrence, A. Lenton, K. Lindsay, J. Pongratz, T. Raddatz, R. Séférian,
2729 K. Tachiiri, J. F. Tjiputra, A. Wiltshire, T. Wu, and T. Ziehn (2020).
2730 Carbon-concentration and carbon-climate feedbacks in CMIP6 models and
2731 their comparison to CMIP5 models. *Biogeosciences* 17(16), 4173–4222.

- 2732** Bae, K., T. J. Fahey, R. D. Yanai, and M. Fisk (2015). Soil nitrogen availability affects belowground carbon allocation and soil respiration in northern hardwood forests of New Hampshire. *Ecosystems* 18(7), 1179–1191.
- 2735** Barber, S. A. (1962). A diffusion and mass-flow concept of soil nutrient availability. *Soil Science* 93(1), 39–49.
- 2737** Barnes, J. D., L. Balaguer, E. Manrique, S. Elvira, and A. W. Davison (1992).
- 2738** A reappraisal of the use of DMSO for the extraction and determination of chlorophylls a and b in lichens and higher plants. *Environmental and Experimental Botany* 32(2), 85–100.
- 2740**
- 2741** Bates, D., M. Mächler, B. Bolker, and S. Walker (2015). Fitting linear mixed-effects models using lme4. *Journal of Statistical Software* 67(1), 1–48.
- 2743** Beaudette, D., J. Skovlin, S. Roeker, and A. Brown (2022). soilDB: Soil
- 2744** Database Interface.
- 2745** Bengtson, P., J. Barker, and S. J. Grayston (2012). Evidence of a strong coupling between root exudation, C and N availability, and stimulated SOM
- 2746** decomposition caused by rhizosphere priming effects. *Ecology and Evolution* 2(8), 1843–1852.
- 2747**
- 2748**
- 2749** Bernacchi, C. J., E. L. Singsaas, C. Pimentel, A. R. Portis, and S. P. Long
- 2750** (2001). Improved temperature response functions for models of Rubisco-limited photosynthesis. *Plant, Cell and Environment* 24(2), 253–259.
- 2751**
- 2752** Bialic-Murphy, L., N. G. Smith, P. Voothuluru, R. M. McElderry, M. D.
- 2753** Roche, S. T. Cassidy, S. N. Kivlin, and S. Kalisz (2021). Invasion-induced
- 2754** root–fungal disruptions alter plant water and nitrogen economies. *Ecology*

- 2755** *Letters* 24(6), 1145–1156.
- 2756** Bloom, A. J., F. S. Chapin, and H. A. Mooney (1985). Resource limitation
2757 in plants - an economic analogy. *Annual Review of Ecology and Systemat-*
2758 *ics* 16(1), 363–392.
- 2759** Bloomfield, K. J., B. D. Stocker, T. F. Keenan, and I. C. Prentice (2023).
2760 Environmental controls on the light use efficiency of terrestrial gross primary
2761 production. *Global Change Biology* 29(4), 0–2.
- 2762** Bonan, G. B., M. D. Hartman, W. J. Parton, and W. R. Wieder (2013). Eval-
2763 uating litter decomposition in earth system models with long-term litter
2764 bag experiments: an example using the Community Land Model version 4
2765 (CLM4). *Global Change Biology* 19(3), 957–974.
- 2766** Bonan, G. B., P. J. Lawrence, K. W. Oleson, S. Levis, M. Jung, M. Reich-
2767 stein, D. M. Lawrence, and S. C. Swenson (2011). Improving canopy pro-
2768 cesses in the Community Land Model version 4 (CLM4) using global flux
2769 fields empirically inferred from FLUXNET data. *Journal of Geophysical Re-*
2770 *search* 116(G2), G02014.
- 2771** Booth, B. B. B., C. D. Jones, M. Collins, I. J. Totterdell, P. M. Cox, S. Sitch,
2772 C. Huntingford, R. A. Betts, G. R. Harris, and J. Lloyd (2012). High sen-
2773 sitivity of future global warming to land carbon cycle processes. *Environ-*
2774 *mental Research Letters* 7(2), 024002.
- 2775** Borer, E. T., W. S. Harpole, P. B. Adler, E. M. Lind, J. L. Orrock, E. W.
2776 Seabloom, and M. D. Smith (2014). Finding generality in ecology: A model
2777 for globally distributed experiments. *Methods in Ecology and Evolution* 5(1),
2778 65–73.

- 2779** Braghieri, R. K., J. B. Fisher, K. Allen, E. Brzostek, M. Shi, X. Yang, D. M.
- 2780** Ricciuto, R. A. Fisher, Q. Zhu, and R. P. Phillips (2022). Modeling global
- 2781** carbon costs of plant nitrogen and phosphorus acquisition. *Journal of Ad-*
- 2782** *vances in Modeling Earth Systems* 14(8), 1–23.
- 2783** Brix, H. (1971). Effects of nitrogen fertilization on photosynthesis and respi-
- 2784** ration in Douglas-fir. *Forest Science* 17(4), 407–414.
- 2785** Brzostek, E. R., J. B. Fisher, and R. P. Phillips (2014). Modeling the carbon
- 2786** cost of plant nitrogen acquisition: Mycorrhizal trade-offs and multipath
- 2787** resistance uptake improve predictions of retranslocation. *Journal of Geo-*
- 2788** *physical Research: Biogeosciences* 119, 1684–1697.
- 2789** Bubier, J. L., R. Smith, S. Juutinen, T. R. Moore, R. Minocha, S. Long, and
- 2790** S. Minocha (2011). Effects of nutrient addition on leaf chemistry, morphol-
- 2791** ogy, and photosynthetic capacity of three bog shrubs. *Oecologia* 167(2),
- 2792** 355–368.
- 2793** Cernusak, L. A., N. Ubierna, K. Winter, J. A. M. Holtum, J. D. Marshall, and
- 2794** G. D. Farquhar (2013). Environmental and physiological determinants of
- 2795** carbon isotope discrimination in terrestrial plants. *New Phytologist* 200(4),
- 2796** 950–965.
- 2797** Chen, J.-L., J. F. Reynolds, P. C. Harley, and J. D. Tenhunen (1993). Coor-
- 2798** dination theory of leaf nitrogen distribution in a canopy. *Oecologia* 93(1),
- 2799** 63–69.
- 2800** Clark, D. B., L. M. Mercado, S. Sitch, C. D. Jones, N. Gedney, M. J. Best,
- 2801** M. Pryor, G. G. Rooney, R. L. H. Essery, E. Blyth, O. Boucher, R. J.
- 2802** Harding, C. Huntingford, and P. M. Cox (2011). The Joint UK Land Envi-

- 2803 ronment Simulator (JULES), model description. Part 2: Carbon fluxes and
2804 vegetation dynamics. *Geoscientific Model Development* 4(3), 701–722.
- 2805 Cornwell, W. K., J. H. C. Cornelissen, K. Amatangelo, E. Dorrepaal, V. T.
2806 Eviner, O. Godoy, S. E. Hobbie, B. Hoorens, H. Kurokawa, N. Pérez-
2807 Harguindeguy, H. M. Quested, L. S. Santiago, D. A. Wardle, I. J. Wright,
2808 R. Aerts, S. D. Allison, P. van Bodegom, V. Brovkin, A. Chatain, T. V.
2809 Callaghan, S. Díaz, E. Garnier, D. E. Gurvich, E. Kazakou, J. A. Klein,
2810 J. Read, P. B. Reich, N. A. Soudzilovskaia, M. V. Vaieretti, and M. Westoby
2811 (2008). Plant species traits are the predominant control on litter decompo-
2812 sition rates within biomes worldwide. *Ecology Letters* 11(10), 1065–1071.
- 2813 Cornwell, W. K., I. J. Wright, J. Turner, V. Maire, M. M. Barbour, L. A.
2814 Cernusak, T. E. Dawson, D. S. Ellsworth, G. D. Farquhar, H. Griffiths,
2815 C. Keitel, A. Knohl, P. B. Reich, D. G. Williams, R. Bhaskar, J. H. C. Cor-
2816 nelissen, A. Richards, S. Schmidt, F. Valladares, C. Körner, E.-D. Schulze,
2817 N. Buchmann, and L. S. Santiago (2018). Climate and soils together regulate
2818 photosynthetic carbon isotope discrimination within C₃ plants worldwide.
2819 *Global Ecology and Biogeography* 27(9), 1056–1067.
- 2820 Cramer, W. and I. C. Prentice (1988). Simulation of regional soil moisture
2821 deficits on a European scale. *Norsk Geografisk Tidsskrift - Norwegian Jour-*
2822 *nal of Geography* 42(2-3), 149–151.
- 2823 Curtis, P. S. (1996). A meta-analysis of leaf gas exchange and nitrogen in trees
2824 grown under elevated carbon dioxide. *Plant, Cell and Environment* 19(2),
2825 127–137.
- 2826 Daly, C., M. Halbleib, J. I. Smith, W. P. Gibson, M. K. Doggett, G. H. Taylor,

- 2827** J. Curtis, and P. P. Pasteris (2008). Physiographically sensitive mapping
2828 of climatological temperature and precipitation across the conterminous
2829 United States. *International Journal of Climatology* 28(15), 2031–2064.
- 2830** Davies-Barnard, T., J. Meyerholt, S. Zaehle, P. Friedlingstein, V. Brovkin,
2831 Y. Fan, R. A. Fisher, C. D. Jones, H. Lee, D. Peano, B. Smith, D. Wårlind,
2832 and A. J. Wiltshire (2020). Nitrogen cycling in CMIP6 land surface models:
2833 progress and limitations. *Biogeosciences* 17(20), 5129–5148.
- 2834** Davis, T. W., I. C. Prentice, B. D. Stocker, R. T. Thomas, R. J. Whitley,
2835 H. Wang, B. J. Evans, A. V. Gallego-Sala, M. T. Sykes, and W. Cramer
2836 (2017). Simple process-led algorithms for simulating habitats (SPLASH
2837 v.1.0): robust indices of radiation, evapotranspiration and plant-available
2838 moisture. *Geoscientific Model Development* 10, 689–708.
- 2839** Delaire, M., E. Frak, M. Sigogne, B. Adam, F. Beaujard, and X. Le Roux
2840 (2005). Sudden increase in atmospheric CO₂ concentration reveals strong
2841 coupling between shoot carbon uptake and root nutrient uptake in young
2842 walnut trees. *Tree Physiology* 25(2), 229–235.
- 2843** Doane, T. A. and W. R. Horwáth (2003). Spectrophotometric determination of
2844 nitrate with a single reagent. *Analytical Letters* 36(12), 2713–2722.
- 2845** Dong, N., I. C. Prentice, B. J. Evans, S. Caddy-Retalic, A. J. Lowe, and I. J.
2846 Wright (2017). Leaf nitrogen from first principles: field evidence for adaptive
2847 variation with climate. *Biogeosciences* 14(2), 481–495.
- 2848** Dong, N., I. C. Prentice, I. J. Wright, B. J. Evans, H. F. Togashi, S. Caddy-
2849 Retalic, F. A. McInerney, B. Sparrow, E. Leitch, and A. J. Lowe (2020).
2850 Components of leaf-trait variation along environmental gradients. *New Phy-*

- 2851** *tologist* 228(1), 82–94.
- 2852** Dong, N., I. C. Prentice, I. J. Wright, H. Wang, O. K. Atkin, K. J. Bloomfield,
- 2853** T. F. Domingues, S. M. Gleason, V. Maire, Y. Onoda, H. Poorter, and N. G.
- 2854** Smith (2022). Leaf nitrogen from the perspective of optimal plant function.
- 2855** *Journal of Ecology* 110(11), 2585–2602.
- 2856** Dong, N., I. J. Wright, J. M. Chen, X. Luo, H. Wang, T. F. Keenan, N. G.
- 2857** Smith, and I. C. Prentice (2022). Rising CO₂ and warming reduce global
- 2858** canopy demand for nitrogen. *New Phytologist* 235(5), 1692–1700.
- 2859** Dovrat, G., H. Bakhshian, T. Masci, and E. Sheffer (2020). The nitrogen eco-
- 2860** nomic spectrum of legume stoichiometry and fixation strategy. *New Phytol-*
- 2861** *ogist* 227(2), 365–375.
- 2862** Dovrat, G., T. Masci, H. Bakhshian, E. Mayzlish Gati, S. Golan, and E. Shef-
- 2863** fer (2018). Drought-adapted plants dramatically downregulate dinitrogen
- 2864** fixation: Evidences from Mediterranean legume shrubs. *Journal of Ecol-*
- 2865** *ogy* 106(4), 1534–1544.
- 2866** Drake, B. G., M. A. Gonzàlez-Meler, and S. P. Long (1997). More efficient
- 2867** plants: a consequence of rising atmospheric CO₂? *Annual Review of Plant*
- 2868** *Biology* 48, 609–639.
- 2869** Duursma, R. A. (2015). Plantecophys - An R Package for Analyzing and Mod-
- 2870** elling Leaf Gas Exchange Data. *PLOS ONE* 10(11), e0143346.
- 2871** Eastman, B. A., M. B. Adams, E. R. Brzostek, M. B. Burnham, J. E. Carrara,
- 2872** C. Kelly, B. E. McNeil, C. A. Walter, and W. T. Peterjohn (2021). Altered
- 2873** plant carbon partitioning enhanced forest ecosystem carbon storage after 25

- 2874 years of nitrogen additions. *New Phytologist* 230(4), 1435–1448.
- 2875 Ellsworth, D. S. and P. B. Reich (1996). Photosynthesis and leaf nitrogen in five
- 2876 Amazonian tree species during early secondary succession. *Ecology* 77(2),
- 2877 581–594.
- 2878 Espelta, J. M., P. Cortés, M. Mangirón, and J. Retana (2005). Differences in
- 2879 biomass partitioning, leaf nitrogen content, and water use efficiency d13C
- 2880 result in similar performance of seedlings of two Mediterranean oaks with
- 2881 contrasting leaf habit. *Ecoscience* 12(4), 447–454.
- 2882 Evans, J. R. (1989). Photosynthesis and nitrogen relationships in leaves of C₃
- 2883 plants. *Oecologia* 78(1), 9–19.
- 2884 Evans, J. R. and V. C. Clarke (2019). The nitrogen cost of photosynthesis.
- 2885 *Journal of Experimental Botany* 70(1), 7–15.
- 2886 Evans, J. R. and H. Poorter (2001). Photosynthetic acclimation of plants to
- 2887 growth irradiance: the relative importance of specific leaf area and nitrogen
- 2888 partitioning in maximizing carbon gain. *Plant, Cell and Environment* 24(8),
- 2889 755–767.
- 2890 Evans, J. R. and J. R. Seemann (1989). The allocation of protein nitrogen in
- 2891 the photosynthetic apparatus: costs, consequences, and control. *Photosyn-*
- 2892 *thesis* 8, 183–205.
- 2893 Exbrayat, J.-F., A. A. Bloom, P. Falloon, A. Ito, T. L. Smallman, and
- 2894 M. Williams (2018). Reliability ensemble averaging of 21st century projec-
- 2895 tions of terrestrial net primary productivity reduces global and regional
- 2896 uncertainties. *Earth System Dynamics* 9(1), 153–165.

- 2897 Farquhar, G. D., J. R. Ehleringer, and K. T. Hubick (1989). Carbon Isotope
2898 Discrimination and Photosynthesis. *Annual Review of Plant Physiology and*
2899 *Plant Molecular Biology* 40(1), 503–537.
- 2900 Farquhar, G. D. and T. D. Sharkey (1982). Stomatal conductance and photo-
2901 synthesis. *Annual Review of Plant Physiology* 33(1), 317–345.
- 2902 Farquhar, G. D., S. von Caemmerer, and J. A. Berry (1980). A biochemical
2903 model of photosynthetic CO₂ assimilation in leaves of C₃ species.
2904 *Planta* 149(1), 78–90.
- 2905 Fay, P. A., S. M. Prober, W. S. Harpole, J. M. H. Knops, J. D. Bakker, E. T.
2906 Borer, E. M. Lind, A. S. MacDougall, E. W. Seabloom, P. D. Wragg, P. B.
2907 Adler, D. M. Blumenthal, Y. M. Buckley, C. Chu, E. E. Cleland, S. L.
2908 Collins, K. F. Davies, G. Du, X. Feng, J. Firn, D. S. Gruner, N. Hagenah,
2909 Y. Hautier, R. W. Heckman, V. L. Jin, K. P. Kirkman, J. A. Klein, L. M.
2910 Ladwig, Q. Li, R. L. McCulley, B. A. Melbourne, C. E. Mitchell, J. L. Moore,
2911 J. W. Morgan, A. C. Risch, M. Schütz, C. J. Stevens, D. A. Wedin, and
2912 L. H. Yang (2015). Grassland productivity limited by multiple nutrients.
2913 *Nature Plants* 1(7), 15080.
- 2914 Feng, X. (1999). Trends in intrinsic water-use efficiency of natural trees for the
2915 past 100-200 years: A response to atmospheric CO₂ concentration. *Geochim-
2916 ica et Cosmochimica Acta* 63(13-14), 1891–1903.
- 2917 Field, C. B. and H. A. Mooney (1986). The photosynthesis-nitrogen relationship
2918 in wild plants. In T. J. Givnish (Ed.), *On the Economy of Plant Form and*
2919 *Function*, pp. 25–55. Cambridge: Cambridge University Press.
- 2920 Finzi, A. C., D. J. P. Moore, E. H. DeLucia, J. Lichter, K. S. Hofmockel, R. B.

- 2921 Jackson, H. S. Kim, R. Matamala, H. R. McCarthy, R. Oren, J. S. Pippen,
2922 and W. H. Schlesinger (2006). Progressive nitrogen limitation of ecosystem
2923 processes under elevated CO₂ in a warm-temperate forest. *Ecology* 87(1),
2924 15–25.
- 2925 Firn, J., J. M. McGree, E. Harvey, H. Flores Moreno, M. Schutz, Y. M. Buckley,
2926 E. T. Borer, E. W. Seabloom, K. J. La Pierre, A. M. MacDougall, S. M.
2927 Prober, C. J. Stevens, L. L. Sullivan, E. Porter, E. Ladouceur, C. Allen,
2928 K. H. Moromizato, J. W. Morgan, W. S. Harpole, Y. Hautier, N. Eisen-
2929 hauer, J. P. Wright, P. B. Adler, C. A. Arnillas, J. D. Bakker, L. Biederman,
2930 A. A. D. Broadbent, C. S. Brown, M. N. Bugalho, M. C. Caldeira, E. E. Cle-
2931 land, A. Ebeling, P. A. Fay, N. Hagenah, A. R. Kleinhesselink, R. Mitchell,
2932 J. L. Moore, C. Nogueira, P. L. Peri, C. Roscher, M. D. Smith, P. D. Wragg,
2933 and A. C. Risch (2019). Leaf nutrients, not specific leaf area, are consistent
2934 indicators of elevated nutrient inputs. *Nature Ecology and Evolution* 3(3),
2935 400–406.
- 2936 Fisher, J. B., S. Sitch, Y. Malhi, R. A. Fisher, C. Huntingford, and S.-Y. Tan
2937 (2010). Carbon cost of plant nitrogen acquisition: A mechanistic, globally
2938 applicable model of plant nitrogen uptake, retranslocation, and fixation.
2939 *Global Biogeochemical Cycles* 24(1), 1–17.
- 2940 Fox, J. and S. Weisberg (2019). *An R companion to applied regression* (Third
2941 edit ed.). Thousand Oaks, California: Sage.
- 2942 Franklin, O., R. E. McMurtrie, C. M. Iversen, K. Y. Crous, A. C. Finzi, D. Tis-
2943 sue, D. S. Ellsworth, R. Oren, and R. J. Norby (2009). Forest fine-root
2944 production and nitrogen use under elevated CO₂: contrasting responses

- 2945 in evergreen and deciduous trees explained by a common principle. *Global
2946 Change Biology* 15(1), 132–144.
- 2947 Friedlingstein, P., M. Meinshausen, V. K. Arora, C. D. Jones, A. Anav, S. K.
2948 Liddicoat, and R. Knutti (2014). Uncertainties in CMIP5 climate projections
2949 due to carbon cycle feedbacks. *Journal of Climate* 27(2), 511–526.
- 2950 Friel, C. A. and M. L. Friesen (2019). Legumes modulate allocation to rhizobial
2951 nitrogen fixation in response to factorial light and nitrogen manipulation.
2952 *Frontiers in Plant Science* 10, 1316.
- 2953 Fujikake, H., A. Yamazaki, N. Ohtake, K. Sueoshi, S. Matsuhashi, T. Ito,
2954 C. Mizuniwa, T. Kume, S. Hoshimoto, N.-S. Ishioka, S. Watanabe, A. Osa,
2955 T. Sekine, H. Uchida, A. Tsuji, and T. Ohyama (2003). Quick and reversible
2956 inhibition of soybean root nodule growth by nitrate involves a decrease in
2957 sucrose supply to nodules. *Journal of Experimental Botany* 54(386), 1379–
2958 1388.
- 2959 Ghannoum, O., J. R. Evans, and S. von Caemmerer (2011). Nitrogen and water
2960 use efficiency of C₄ plants. In A. S. Raghavendra and R. F. Sage (Eds.), *C₄
2961 Photosynthesis and Related CO₂ Concentrating Mechanisms*, Chapter 8, pp.
2962 129–146. Springer.
- 2963 Ghimire, B., W. J. Riley, C. D. Koven, J. Kattge, A. Rogers, P. B. Reich, and
2964 I. J. Wright (2017). A global trait-based approach to estimate leaf nitrogen
2965 functional allocation from observations:. *Ecological Applications* 27(5),
2966 1421–1434.
- 2967 Giardina, C. P., M. D. Coleman, J. E. Hancock, J. S. King, E. A. Lilleskov,
2968 W. M. Loya, K. S. Pregitzer, M. G. Ryan, and C. C. Trettin (2005). The

- 2969 response of belowground carbon allocation in forests to global change. In
2970 D. Binkley and O. Manyailo (Eds.), *Tree Species Effects on Soils: Implications for Global Change* (Volume 55 ed.), Chapter Chapter 7, pp. 119–154.
2971 Berlin/Heidelberg: Springer-Verlag.
- 2972
- 2973 Gibson, A. H. and J. E. Harper (1985). Nitrate effect on nodulation of soybean
2974 by *Bradyrhizobium japonicum*. *Crop Science* 25(3), 497–501.
- 2975 Gill, A. L. and A. C. Finzi (2016). Belowground carbon flux links biogeochemical
2976 cycles and resource-use efficiency at the global scale. *Ecology Letters* 19(12),
2977 1419–1428.
- 2978 Goll, D. S., V. Brovkin, B. R. Parida, C. H. Reick, J. Kattge, P. B. Reich, P. M.
2979 van Bodegom, and Ü. Niinemets (2012). Nutrient limitation reduces land
2980 carbon uptake in simulations with a model of combined carbon, nitrogen
2981 and phosphorus cycling. *Biogeosciences Discussions* 9(3), 3173–3232.
- 2982 Gregory, L. M., A. M. McClain, D. M. Kramer, J. D. Pardo, K. E. Smith, O. L.
2983 Tessmer, B. J. Walker, L. G. Ziccardi, and T. D. Sharkey (2021, oct). The
2984 triose phosphate utilization limitation of photosynthetic rate: Out of global
2985 models but important for leaf models. *Plant, Cell and Environment* 44(10),
2986 3223–3226.
- 2987 Grossiord, C., T. N. Buckley, L. A. Cernusak, K. A. Novick, B. Poulter, R. T. W.
2988 Siegwolf, J. S. Sperry, and N. G. McDowell (2020). Plant responses to rising
2989 vapor pressure deficit. *New Phytologist* 226(6), 1550–1566.
- 2990 Guerrieri, R., M. Mencuccini, L. J. Sheppard, M. Saurer, M. P. Perks, P. Levy,
2991 M. A. Sutton, M. Borghetti, and J. Grace (2011). The legacy of enhanced
2992 N and S deposition as revealed by the combined analysis of $\delta^{13}\text{C}$, $\delta^{18}\text{O}$ and

- 2993 $\delta^{15}\text{N}$ in tree rings. *Global Change Biology* 17(5), 1946–1962.
- 2994 Gulmon, S. L. and C. C. Chu (1981). The effects of light and nitrogen on photosynthesis, leaf characteristics, and dry matter allocation in the chaparral shrub, *<i>Diplacus aurantiacus</i>*. *Oecologia* 49(2), 207–212.
- 2995
- 2996
- 2997 Gutschick, V. P. (1981). Evolved strategies in nitrogen acquisition by plants.
- 2998 *The American Naturalist* 118(5), 607–637.
- 2999 Hallik, L., Ü. Niinemets, and I. J. Wright (2009). Are species shade and drought tolerance reflected in leaf-level structural and functional differentiation in
- 3000
- 3001 Northern Hemisphere temperate woody flora? *New Phytologist* 184(1), 257–
- 3002 274.
- 3003 Harrison, M. T., E. J. Edwards, G. D. Farquhar, A. B. Nicotra, and J. R.
- 3004 Evans (2009). Nitrogen in cell walls of sclerophyllous leaves accounts for
- 3005 little of the variation in photosynthetic nitrogen-use efficiency. *Plant, Cell*
- 3006 and *Environment* 32(3), 259–270.
- 3007 Harrison, S. P., W. Cramer, O. Franklin, I. C. Prentice, H. Wang,
- 3008 Å. Brännström, H. de Boer, U. Dieckmann, J. Joshi, T. F. Keenan,
- 3009 A. Lavergne, S. Manzoni, G. Mengoli, C. Morfopoulos, J. Peñuelas,
- 3010 S. Pietsch, K. T. Rebel, Y. Ryu, N. G. Smith, B. D. Stocker, and I. J.
- 3011 Wright (2021). Eco-evolutionary optimality as a means to improve vegetation
- 3012 and land-surface models. *New Phytologist* 231(6), 2125–2141.
- 3013 Henneron, L., P. Kardol, D. A. Wardle, C. Cros, and S. Fontaine (2020). Rhizosphere control of soil nitrogen cycling: a key component of plant economic
- 3014 strategies. *New Phytologist* 228(4), 1269–1282.
- 3015

- 3016** Hijmans, R. J. (2022). terra: Spatial Data Analysis.
- 3017** Hikosaka, K. and A. Shigeno (2009). The role of Rubisco and cell walls in the
3018 interspecific variation in photosynthetic capacity. *Oecologia* 160(3), 443–
3019 451.
- 3020** Hoagland, D. R. and D. I. Arnon (1950). The water culture method for growing
3021 plants without soil. *California Agricultural Experiment Station: 347* 347(2),
3022 1–32.
- 3023** Hobbie, E. A. (2006). Carbon allocation to ectomycorrhizal fungi correlates
3024 with belowground allocation in culture studies. *Ecology* 87(3), 563–569.
- 3025** Hobbie, E. A. and J. E. Hobbie (2008). Natural abundance of ^{15}N in nitrogen-
3026 limited forests and tundra can estimate nitrogen cycling through mycorrhizal
3027 fungi: a review. *Ecosystems* 11(5), 815–830.
- 3028** Hoek, T. A., K. Axelrod, T. Biancalani, E. A. Yurtsev, J. Liu, and J. Gore
3029 (2016). Resource availability modulates the cooperative and competitive na-
3030 nature of a microbial cross-feeding mutualism. *PLOS Biology* 14(8), e1002540.
- 3031** Höglberg, M. N., M. J. I. Briones, S. G. Keel, D. B. Metcalfe, C. Campbell, A. J.
3032 Midwood, B. Thornton, V. Hurry, S. Linder, T. Näsholm, and P. Höglberg
3033 (2010). Quantification of effects of season and nitrogen supply on tree below-
3034 ground carbon transfer to ectomycorrhizal fungi and other soil organisms in
3035 a boreal pine forest. *New Phytologist* 187(2), 485–493.
- 3036** Höglberg, P., M. N. Höglberg, S. G. Göttlicher, N. R. Betson, S. G. Keel, D. B.
3037 Metcalfe, C. Campbell, A. Schindlbacher, V. Hurry, T. Lundmark, S. Linder,
3038 and T. Näsholm (2008). High temporal resolution tracing of photosynthate

- 3039 carbon from the tree canopy to forest soil microorganisms. *New Phytologist* 177(1), 220–228.
- 3040
- 3041 Houlton, B. Z., Y.-P. Wang, P. M. Vitousek, and C. B. Field (2008). A uni-
3042 fying framework for dinitrogen fixation in the terrestrial biosphere. *Nature* 454(7202), 327–330.
- 3043
- 3044 Huber, M. L., R. A. Perkins, A. Laesecke, D. G. Friend, J. V. Sengers, M. J.
3045 Assael, I. N. Metaxa, E. Vogel, R. Mareš, and K. Miyagawa (2009). New
3046 international formulation for the viscosity of H₂O. *Journal of Physical and
3047 Chemical Reference Data* 38(2), 101–125.
- 3048 Hungate, B. A., J. S. Dukes, M. R. Shaw, Y. Luo, and C. B. Field (2003).
3049 Nitrogen and climate change. *Science* 302(5650), 1512–1513.
- 3050 IPCC (2021). *Climate Change 2021: The Physical Science Basis. Contribution
3051 of Working Group I to the Sixth Assessment Report of the Intergovernmental
3052 Panel on Climate Change*, Volume In Press. Cambridge, United Kingdom
3053 and New York, NY, USA: Cambridge University Press.
- 3054 Johnson, N. C., J. H. Graham, and F. A. Smith (1997). Functioning of mycor-
3055 rhizal associations along the mutualism-parasitism continuum. *New Phytol-*
3056 *ogist* 135(4), 575–585.
- 3057 Kachurina, O. M., H. Zhang, W. R. Raun, and E. G. Krenzer (2000). Simul-
3058 taneous determination of soil aluminum, ammonium- and nitrate- nitrogen
3059 using 1 M potassium chloride. *Communications in Soil Science and Plant
3060 Analysis* 31(7-8), 893–903.
- 3061 Kaiser, C., M. R. Kilburn, P. L. Clode, L. Fuchslueger, M. Koranda, J. B. Cliff,

- 3062** Z. M. Solaiman, and D. V. Murphy (2015). Exploring the transfer of recent
3063 plant photosynthates to soil microbes: mycorrhizal pathway vs direct root
3064 exudation. *New Phytologist* 205(4), 1537–1551.
- 3065** Katabuchi, M. (2015). LeafArea: An R package for rapid digital analysis of leaf
3066 area. *Ecological Research* 30(6), 1073–1077.
- 3067** Kattge, J. and W. Knorr (2007). Temperature acclimation in a biochemical
3068 model of photosynthesis: a reanalysis of data from 36 species. *Plant, Cell*
3069 and *Environment* 30(9), 1176–1190.
- 3070** Kattge, J., W. Knorr, T. Raddatz, and C. Wirth (2009). Quantifying photosyn-
3071 thetic capacity and its relationship to leaf nitrogen content for global-scale
3072 terrestrial biosphere models. *Global Change Biology* 15(4), 976–991.
- 3073** Kayler, Z., A. Gessler, and N. Buchmann (2010). What is the speed of link
3074 between aboveground and belowground processes? *New Phytologist* 187(4),
3075 885–888.
- 3076** Kayler, Z., C. Keitel, K. Jansen, and A. Gessler (2017). Experimental evi-
3077 dence of two mechanisms coupling leaf-level C assimilation to rhizosphere
3078 CO₂ release. *Environmental and Experimental Botany* 135,
3079 21–26.
- 3080** Keeling, C. D., W. G. Mook, and P. P. Tans (1979, jan). Recent trends in the
3081 ¹³C/¹²C ratio of atmospheric carbon dioxide.
3082 *Nature* 277(5692), 121–123.
- 3083** Keeney, D. R. and D. W. Nelson (1983). Nitrogen—Inorganic Forms. In A. L.
3084 Page (Ed.), *Methods of Soil Analysis* (2nd ed.), Chapter 33, pp. 643–698.

- 3085** Madison, WI, USA: ASA and SSSA.
- 3086** Kenward, M. G. and J. H. Roger (1997). Small sample inference for fixed effects
- 3087** from restricted maximum likelihood. *Biometrics* 53(3), 983.
- 3088** Knapp, A. K., M. L. Avolio, C. Beier, C. J. W. Carroll, S. L. Collins, J. S.
- 3089** Dukes, L. H. Fraser, R. J. Griffin-Nolan, D. L. Hoover, A. Jentsch, M. E.
- 3090** Loik, R. P. Phillips, A. K. Post, O. E. Sala, I. J. Slette, L. Yahdjian, and
- 3091** M. D. Smith (2017). Pushing precipitation to the extremes in distributed
- 3092** experiments: recommendations for simulating wet and dry years. *Global*
- 3093** *Change Biology* 23(5), 1774–1782.
- 3094** Knorr, W. (2000). Annual and interannual CO₂ exchanges of the
- 3095** terrestrial biosphere: process-based simulations and uncertainties. *Global*
- 3096** *Ecology and Biogeography* 9(3), 225–252.
- 3097** Knorr, W. and M. Heimann (2001). Uncertainties in global terrestrial biosphere
- 3098** modeling: 1. A comprehensive sensitivity analysis with a new photosynthesis
- 3099** and energy balance scheme. *Global Biogeochemical Cycles* 15(1), 207–225.
- 3100** Kulmatiski, A., P. B. Adler, J. M. Stark, and A. T. Tredennick (2017). Water
- 3101** and nitrogen uptake are better associated with resource availability than
- 3102** root biomass. *Ecosphere* 8(3), e01738.
- 3103** Lavergne, A., D. Sandoval, V. J. Hare, H. Graven, and I. C. Prentice (2020).
- 3104** Impacts of soil water stress on the acclimated stomatal limitation of photo-
- 3105** synthesis: Insights from stable carbon isotope data. *Global Change Biol-*
- 3106** *ogy* 26(12), 7158–7172.
- 3107** Lawrence, D. M., R. A. Fisher, C. D. Koven, K. W. Oleson, S. C. Swen-

- 3108 son, G. B. Bonan, N. Collier, B. Ghimire, L. Kampenhout, D. Kennedy,
3109 E. Kluzek, P. J. Lawrence, F. Li, H. Li, D. L. Lombardozzi, W. J. Riley,
3110 W. J. Sacks, M. Shi, M. Vertenstein, W. R. Wieder, C. Xu, A. A. Ali,
3111 A. M. Badger, G. Bisht, M. Broeke, M. A. Brunke, S. P. Burns, J. Buzan,
3112 M. Clark, A. Craig, K. M. Dahlin, B. Drewniak, J. B. Fisher, M. Flanner,
3113 A. M. Fox, P. Gentine, F. M. Hoffman, G. Keppel-Aleks, R. Knox, S. Ku-
3114 mar, J. Lenaerts, L. R. Leung, W. H. Lipscomb, Y. Lu, A. Pandey, J. D.
3115 Pelletier, J. Perket, J. T. Randerson, D. M. Ricciuto, B. M. Sanderson,
3116 A. Slater, Z. M. Subin, J. Tang, R. Q. Thomas, M. Val Martin, and X. Zeng
3117 (2019). The Community Land Model Version 5: description of new features,
3118 benchmarking, and impact of forcing uncertainty. *Journal of Advances in*
3119 *Modeling Earth Systems* 11(12), 4245–4287.
- 3120 LeBauer, D. S. and K. K. Treseder (2008). Nitrogen limitation of net primary
3121 productivity. *Ecology* 89(2), 371–379.
- 3122 Lefcheck, J. S. (2016). piecewiseSEM: Piecewise structural equation modelling
3123 in r for ecology, evolution, and systematics. *Methods in Ecology and Evolu-*
3124 *tion* 7(5), 573–579.
- 3125 Lenth, R. (2019). emmeans: estimated marginal means, aka least-squares
3126 means.
- 3127 Li, W., H. Zhang, G. Huang, R. Liu, H. Wu, C. Zhao, and N. G. McDowell
3128 (2020). Effects of nitrogen enrichment on tree carbon allocation: A global
3129 synthesis. *Global Ecology and Biogeography* 29(3), 573–589.
- 3130 Liang, J., X. Qi, L. Souza, and Y. Luo (2016). Processes regulating progressive
3131 nitrogen limitation under elevated carbon dioxide: a meta-analysis. *Biogeo-*

- 3132** *sciences* 13(9), 2689–2699.
- 3133** Liang, X., T. Zhang, X. Lu, D. S. Ellsworth, H. BassiriRad, C. You, D. Wang,
- 3134** P. He, Q. Deng, H. Liu, J. Mo, and Q. Ye (2020). Global response patterns of
- 3135** plant photosynthesis to nitrogen addition: A meta-analysis. *Global Change*
- 3136** *Biology* 26(6), 3585–3600.
- 3137** López, J., D. A. Way, and W. Sadok (2021). Systemic effects of rising atmo-
- 3138** spheric vapor pressure deficit on plant physiology and productivity. *Global*
- 3139** *Change Biology* 27(9), 1704–1720.
- 3140** Lu, J., J. Yang, C. Keitel, L. Yin, P. Wang, W. Cheng, and F. A. Dijkstra
- 3141** (2022). Belowground Carbon Efficiency for Nitrogen and Phosphorus Ac-
- 3142** quisition Varies Between *Lolium perenne* and *Trifolium repens* and Depends
- 3143** on Phosphorus Fertilization. *Frontiers in Plant Science* 13, 1–9.
- 3144** Luo, X., T. F. Keenan, J. M. Chen, H. Croft, I. C. Prentice, N. G. Smith,
- 3145** A. P. Walker, H. Wang, R. Wang, C. Xu, and Y. Zhang (2021). Global
- 3146** variation in the fraction of leaf nitrogen allocated to photosynthesis. *Nature*
- 3147** *Communications* 12(1), 4866.
- 3148** Luo, Y., W. S. Currie, J. S. Dukes, A. C. Finzi, U. A. Hartwig, B. A. Hungate,
- 3149** R. E. McMurtrie, R. Oren, W. J. Parton, D. E. Pataki, R. M. Shaw, D. R.
- 3150** Zak, and C. B. Field (2004). Progressive nitrogen limitation of ecosystem
- 3151** responses to rising atmospheric carbon dioxide. *BioScience* 54(8), 731–739.
- 3152** Maire, V., P. Martre, J. Kattge, F. Gastal, G. Esser, S. Fontaine, and J.-F.
- 3153** Soussana (2012). The coordination of leaf photosynthesis links C and N
- 3154** fluxes in C₃ plant species. *PLoS ONE* 7(6), e38345.

- 3155** Makino, A. (2003). Rubisco and nitrogen relationships in rice: leaf photosynthesis and plant growth. *Soil Science and Plant Nutrition* 49(3), 319–327.
- 3156**
- 3157** Makino, A., M. Harada, T. Sato, H. Nakano, and T. Mae (1997). Growth and N Allocation in Rice Plants under CO₂ Enrichment. *Plant Physiology* 115(1), 199–203.
- 3158**
- 3159**
- 3160** Markham, J. H. and C. Zekveld (2007). Nitrogen fixation makes biomass allocation to roots independent of soil nitrogen supply. *Canadian Journal of Botany* (9), 787–793.
- 3161**
- 3162**
- 3163** Marschner, H. and B. Dell (1994). Nutrient uptake in mycorrhizal symbiosis.
- 3164** *Plant and Soil* 159(1), 89–102.
- 3165** Matamala, R. and W. H. Schlesinger (2000). Effects of elevated atmospheric
- 3166** CO₂ on fine root production and activity in an intact temperate forest ecosystem. *Global Change Biology* 6(8), 967–979.
- 3167**
- 3168** Medlyn, B. E., E. Dreyer, D. S. Ellsworth, M. Forstreuter, P. C. Harley,
- 3169** M. U. F. Kirschbaum, X. Le Roux, P. Montpied, J. Strassmeyer, A. Wal-
- 3170** croft, K. Wang, and D. Loustau (2002). Temperature response of parameters
- 3171** of a biochemically based model of photosynthesis. II. A review of experimen-
- 3172** tal data. *Plant, Cell and Environment* 25(9), 1167–1179.
- 3173** Menge, D. N. L., S. A. Levin, and L. O. Hedin (2008). Evolutionary tradeoffs can
- 3174** select against nitrogen fixation and thereby maintain nitrogen limitation.
- 3175** *Proceedings of the National Academy of Sciences* 105(5), 1573–1578.
- 3176** Menne, M. J., I. Durre, R. S. Vose, B. E. Gleason, and T. G. Houston (2012).
- 3177** An overview of the global historical climatology network-daily database.

- 3178** *Journal of Atmospheric and Oceanic Technology* 29(7), 897–910.
- 3179** Meyerholt, J., K. Sickel, and S. Zaehle (2020). Ensemble projections elucidate
3180 effects of uncertainty in terrestrial nitrogen limitation on future carbon up-
3181 take. *Global Change Biology* 26(7), 3978–3996.
- 3182** Meyerholt, J., S. Zaehle, and M. J. Smith (2016). Variability of pro-
3183 jected terrestrial biosphere responses to elevated levels of atmospheric
3184 CO₂ due to uncertainty in biological nitrogen fixation. *Bio-*
3185 *geosciences* 13(5), 1491–1518.
- 3186** Minocha, R., S. Long, A. H. Magill, J. D. Aber, and W. H. McDowell (2000).
3187 Foliar free polyamine and inorganic ion content in relation to soil and soil
3188 solution chemistry in two fertilized forest stands at the Harvard Forest,
3189 Massachusetts. *Plant and Soil* 222(1-2), 119–137.
- 3190** Moore, D. J., S. Aref, R. M. Ho, J. S. Pippen, J. G. Hamilton, and E. H. De
3191 Lucia (2006). Annual basal area increment and growth duration of *Pinus*
3192 *taeda* in response to eight years of free-air carbon dioxide enrichment. *Global*
3193 *Change Biology* 12(8), 1367–1377.
- 3194** Morgan, J. A., D. E. Pataki, C. Körner, H. Clark, S. J. Del Gross, J. M.
3195 Grünzweig, A. K. Knapp, A. R. Mosier, P. C. D. Newton, P. A. Niklaus,
3196 J. B. Nippert, R. S. Nowak, W. J. Parton, H. W. Polley, and M. R. Shaw
3197 (2004). Water relations in grassland and desert ecosystems exposed to ele-
3198 vated atmospheric CO₂. *Oecologia* 140(1), 11–25.
- 3199** Muñoz, N., X. Qi, M. W. Li, M. Xie, Y. Gao, M. Y. Cheung, F. L. Wong, and
3200 H.-M. Lam (2016). Improvement in nitrogen fixation capacity could be part
3201 of the domestication process in soybean. *Heredity* 117(2), 84–93.

- 3202 Nadelhoffer, K. J. and J. W. Raich (1992). Fine root production estimates and
3203 belowground carbon allocation in forest ecosystems. *Ecology* 73(4), 1139–
3204 1147.
- 3205 Niinemets, Ü. and J. D. Tenhunen (1997). A model separating leaf struc-
3206 tural and physiological effects on carbon gain along light gradients for the
3207 shade-tolerant species <i>Acer saccharum</i>. *Plant, Cell and Environ-
3208 ment* 20(7), 845–866.
- 3209 Norby, R. J., J. Ledford, C. D. Reilly, N. E. Miller, and E. G. O'Neill
3210 (2004). Fine-root production dominates response of a deciduous forest to
3211 atmospheric CO₂ enrichment. *Proceedings of the National Academy of Sci-
3212 ences* 101(26), 9689–9693.
- 3213 Norby, R. J., J. M. Warren, C. M. Iversen, B. E. Medlyn, and R. E. Mc-
3214 Murtrie (2010). CO₂ enhancement of forest productivity constrained by
3215 limited nitrogen availability. *Proceedings of the National Academy of Sci-
3216 ences* 107(45), 19368–19373.
- 3217 Novick, K. A., D. L. Ficklin, P. C. Stoy, C. A. Williams, G. Bohrer, A. C.
3218 Oishi, S. A. Papuga, P. D. Blanken, A. Noormets, B. N. Sulman, R. L.
3219 Scott, L. Wang, and R. P. Phillips (2016). The increasing importance of
3220 atmospheric demand for ecosystem water and carbon fluxes. *Nature Climate
3221 Change* 6(11), 1023–1027.
- 3222 Noyce, G. L., M. L. Kirwan, R. L. Rich, and J. P. Megonigal (2019). Asyn-
3223 chronous nitrogen supply and demand produce nonlinear plant allocation
3224 responses to warming and elevated CO₂. *Proceedings of the
3225 National Academy of Sciences* 116(43), 21623–21628.

- 3226** Onoda, Y., K. Hikosaka, and T. Hirose (2004). Allocation of nitrogen to
3227 cell walls decreases photosynthetic nitrogen-use efficiency. *Functional Ecology*
3228 18(3), 419–425.
- 3229** Onoda, Y., I. J. Wright, J. R. Evans, K. Hikosaka, K. Kitajima, Ü. Niinemets,
3230 H. Poorter, T. Tosens, and M. Westoby (2017). Physiological and structural
3231 trade-offs underlying the leaf economics spectrum. *New Phytologist* 214(4),
3232 1447–1463.
- 3233** Oren, R., J. S. Sperry, G. G. Katul, D. E. Pataki, B. E. Ewers, N. Phillips,
3234 and K. V. R. Schäfer (1999). Survey and synthesis of intra- and interspecific
3235 variation in stomatal sensitivity to vapor pressure deficit. *Plant, Cell and*
3236 *Environment* 22(12), 1515–1526.
- 3237** Oreskes, N., K. Shrader-Frechette, and K. Belitz (1994). Verification, vali-
3238 dation, and confirmation of numerical models in the Earth sciences. *Sci-
ence* 263(5147), 641–646.
- 3240** Paillassa, J., I. J. Wright, I. C. Prentice, S. Pepin, N. G. Smith, G. Ethier,
3241 A. C. Westerband, L. J. Lamarque, H. Wang, W. K. Cornwell, and V. Maire
3242 (2020). When and where soil is important to modify the carbon and water
3243 economy of leaves. *New Phytologist* 228(1), 121–135.
- 3244** Parvin, S., S. Uddin, S. Tausz Posch, R. Armstrong, and M. Tausz (2020). Car-
3245 bon sink strength of nodules but not other organs modulates photosynthesis
3246 of faba bean (*Vicia faba*) grown under elevated [CO₂] and different
3247 water supply. *New Phytologist* 227(1), 132–145.
- 3248** Paul, K. I., P. J. Polglase, A. M. O'Connell, J. C. Carlyle, P. J. Smethurst, and
3249 P. K. Khanna (2003). Defining the relation between soil water content and

- 3250 net nitrogen mineralization. *European Journal of Soil Science* 54(1), 39–48.
- 3251 Peng, Y., K. J. Bloomfield, L. A. Cernusak, T. F. Domingues, and I. C. Prentice (2021). Global climate and nutrient controls of photosynthetic capacity.
- 3252 *Communications Biology* 4(1), 462.
- 3253
- 3254 Perkowski, E. A., E. F. Waring, and N. G. Smith (2021). Root mass carbon
- 3255 costs to acquire nitrogen are determined by nitrogen and light availability
- 3256 in two species with different nitrogen acquisition strategies. *Journal of*
- 3257 *Experimental Botany* 72(15), 5766–5776.
- 3258 Phillips, R. P., E. R. Brzostek, and M. G. Midgley (2013). The mycorrhizal-
- 3259 associated nutrient economy: a new framework for predicting carbon-
- 3260 nutrient couplings in temperate forests. *New Phytologist* 199(1), 41–51.
- 3261 Phillips, R. P., A. C. Finzi, and E. S. Bernhardt (2011). Enhanced root ex-
- 3262 udation induces microbial feedbacks to N cycling in a pine forest under
- 3263 long-term CO₂ fumigation. *Ecology Letters* 14(2), 187–194.
- 3264 Pinheiro, J. and D. Bates (2022). nlme: linear and nonlinear mixed effects
- 3265 models.
- 3266 Poggio, L., L. M. De Sousa, N. H. Batjes, G. B. M. Heuvelink, B. Kempen,
- 3267 E. Ribeiro, and D. Rossiter (2021). SoilGrids 2.0: Producing soil information
- 3268 for the globe with quantified spatial uncertainty. *Soil* 7(1), 217–240.
- 3269 Pons, T. L. and R. W. Pearcy (1994). Nitrogen reallocation and photosynthetic
- 3270 acclimation in response to partial shading in soybean plants. *Physiologia*
- 3271 *Plantarum* 92(4), 636–644.
- 3272 Poorter, H., J. Bühler, D. Van Dusschoten, J. Climent, and J. A. Postma (2012).

- 3273** Pot size matters: A meta-analysis of the effects of rooting volume on plant
3274 growth. *Functional Plant Biology* 39(11), 839–850.
- 3275** Poorter, H., O. Knopf, I. J. Wright, A. A. Temme, S. W. Hogewoning, A. Graf,
3276 L. A. Cernusak, and T. L. Pons (2022). A meta-analysis of responses of C₃
3277 plants to atmospheric CO₂: dose-response curves for 85 traits ranging from
3278 the molecular to the whole-plant level. *New Phytologist* 233(4), 1560–1596.
- 3279** Prentice, I. C., N. Dong, S. M. Gleason, V. Maire, and I. J. Wright (2014).
3280 Balancing the costs of carbon gain and water transport: testing a new theo-
3281 retical framework for plant functional ecology. *Ecology Letters* 17(1), 82–91.
- 3282** Prentice, I. C., X. Liang, B. E. Medlyn, and Y.-P. Wang (2015). Reliable, ro-
3283 bust and realistic: The three R's of next-generation land-surface modelling.
3284 *Atmospheric Chemistry and Physics* 15, 5987–6005.
- 3285** Priestley, C. H. B. and R. J. Taylor (1972). On the Assessment of Surface
3286 Heat Flux and Evaporation Using Large-Scale Parameters. *Monthly Weather
Review* 100(2), 81–92.
- 3288** Querejeta, J. I., I. Prieto, C. Armas, F. Casanoves, J. S. Diémé, M. Diouf,
3289 H. Yossi, B. Kaya, F. I. Pugnaire, and G. M. Rusch (2022). Higher leaf
3290 nitrogen content is linked to tighter stomatal regulation of transpiration
3291 and more efficient water use across dryland trees. *New Phytologist* 235(4),
3292 1351–1364.
- 3293** R Core Team (2021). R: A language and environment for statistical computing.
- 3294** Raich, J. W., D. A. Clark, L. Schwendenmann, and T. E. Wood (2014). Above-
3295 ground tree growth varies with belowground carbon allocation in a tropical

- 3296** rainforest environment. *PLoS ONE* 9(6), e100275.
- 3297** Rastetter, E. B., P. M. Vitousek, C. B. Field, G. R. Shaver, D. Herbert, and
3298 G. I. Ågren (2001). Resource optimization and symbiotic nitrogen fixation.
3299 *Ecosystems* 4(4), 369–388.
- 3300** Reich, P. B. (2014). The world-wide 'fast-slow' plant economics spectrum: a
3301 traits manifesto. *Journal of Ecology* 102(2), 275–301.
- 3302** Reich, P. B., S. E. Hobbie, T. Lee, D. S. Ellsworth, J. B. West, D. Tilman,
3303 J. M. H. Knops, S. Naeem, and J. Trost (2006). Nitrogen limitation con-
3304 strains sustainability of ecosystem response to CO₂. *Na-
3305 ture* 440(7086), 922–925.
- 3306** Reichman, G. A., D. L. Grunes, and F. G. Viets (1966). Effect of Soil Mois-
3307 ture on Ammonification and Nitrification in Two Northern Plains Soils. *Soil
Science Society of America Journal* 30(3), 363–366.
- 3309** Rhine, E. D., R. L. Mulvaney, E. J. Pratt, and G. K. Sims (1998). Improving
3310 the Berthelot reaction for determining ammonium in soil extracts and water.
3311 *Soil Science Society of America Journal* 62(2), 473.
- 3312** Rogers, A. (2014). The use and misuse of V_{cmax} in Earth System Models. *Pho-*
3313 *tosynthesis Research* 119(1-2), 15–29.
- 3314** Rogers, A., B. E. Medlyn, J. S. Dukes, G. B. Bonan, S. Caemmerer, M. C.
3315 Dietze, J. Kattge, A. D. B. Leakey, L. M. Mercado, Ü. Niinemets, I. C.
3316 Prentice, S. P. Serbin, S. Sitch, D. A. Way, and S. Zaehle (2017). A roadmap
3317 for improving the representation of photosynthesis in Earth system models.
3318 *New Phytologist* 213(1), 22–42.

- 3319 Saathoff, A. J. and J. Welles (2021). Gas exchange measurements in the un-
3320 steady state. *Plant Cell and Environment* 44(11), 3509–3523.
- 3321 Sage, R. F. and R. W. Pearcy (1987). The nitrogen use efficiency of C₃ and C₄
3322 plants: I. Leaf nitrogen, growth, and biomass partitioning in *Chenopodium*
3323 *album* (L.) and *Amaranthus retroflexus* (L.). *Plant Physiology* 84(3), 954–
3324 958.
- 3325 Saleh, A. M., M. Abdel-Mawgoud, A. R. Hassan, T. H. Habeeb, R. S. Yehia,
3326 and H. AbdElgawad (2020). Global metabolic changes induced by arbuscular
3327 mycorrhizal fungi in oregano plants grown under ambient and elevated levels
3328 of atmospheric CO₂. *Plant Physiology and Biochemistry* 151, 255–263.
- 3329 Saxton, K. E. and W. J. Rawls (2006). Soil water characteristic estimates by
3330 texture and organic matter for hydrologic solutions. *Soil Science Society of
3331 America Journal* 70(5), 1569–1578.
- 3332 Schaefer, K., C. R. Schwalm, C. Williams, M. A. Arain, A. Barr, J. M. Chen,
3333 K. J. Davis, D. Dimitrov, T. W. Hilton, D. Y. Hollinger, E. Humphreys,
3334 B. Poulter, B. M. Racza, A. D. Richardson, A. Sahoo, P. Thornton, R. Var-
3335 gas, H. Verbeeck, R. Anderson, I. Baker, T. A. Black, P. Bolstad, J. Chen,
3336 P. S. Curtis, A. R. Desai, M. C. Dietze, D. Dragoni, C. M. Gough, R. F.
3337 Grant, L. Gu, A. K. Jain, C. Kucharik, B. E. Law, S. Liu, E. Lokipitiya,
3338 H. A. Margolis, R. Matamala, J. H. McCaughey, R. Monson, J. W. Munger,
3339 W. Oechel, C. Peng, D. T. Price, D. Ricciuto, W. J. Riley, N. Roulet,
3340 H. Tian, C. Tonitto, M. Torn, E. Weng, and X. Zhou (2012). A model-
3341 data comparison of gross primary productivity: Results from the North
3342 American Carbon Program site synthesis. *Journal of Geophysical Research:*

- 3343** *Biogeosciences* 117(G3), G03010.
- 3344** Schmitt, M. R. and G. E. Edwards (1981). Photosynthetic capacity and nitrogen
3345 use efficiency of maize, wheat, and rice: A comparison between C₃ and C₄
3346 photosynthesis. *Journal of Experimental Botany* 32(3), 459–466.
- 3347** Schneider, C. A., W. S. Rasband, and K. W. Eliceiri (2012). NIH Image to
3348 ImageJ: 25 years of image analysis. *Nature Methods* 9(7), 671–675.
- 3349** Scott, H. G. and N. G. Smith (2022). A Model of C4 Photosynthetic Acclimation
3350 Based on Least-Cost Optimality Theory Suitable for Earth System Model
3351 Incorporation. *Journal of Advances in Modeling Earth Systems* 14(3), 1–16.
- 3352** Shi, M., J. B. Fisher, E. R. Brzostek, and R. P. Phillips (2016). Carbon cost
3353 of plant nitrogen acquisition: Global carbon cycle impact from an improved
3354 plant nitrogen cycle in the Community Land Model. *Global Change Biology*
3355 22(3), 1299–1314.
- 3356** Shi, M., J. B. Fisher, R. P. Phillips, and E. R. Brzostek (2019). Neglecting
3357 plant–microbe symbioses leads to underestimation of modeled climate im-
3358 pacts. *Biogeosciences* 16(2), 457–465.
- 3359** Smith, B., D. Wärldin, A. Arneth, T. Hickler, P. Leadley, J. Siltberg, and
3360 S. Zaehle (2014). Implications of incorporating N cycling and N limitations
3361 on primary production in an individual-based dynamic vegetation model.
3362 *Biogeosciences* 11(7), 2027–2054.
- 3363** Smith, N. G. and J. S. Dukes (2013). Plant respiration and photosynthesis in
3364 global-scale models: incorporating acclimation to temperature and CO₂.
3365 *Global Change Biology* 19(1), 45–63.

- 3366** Smith, N. G. and T. F. Keenan (2020). Mechanisms underlying leaf photosynthetic acclimation to warming and elevated CO₂ as inferred from least-cost optimality theory. *Global Change Biology* 26(9), 5202–5216.
- 3369** Smith, N. G., T. F. Keenan, I. C. Prentice, H. Wang, I. J. Wright, Ü. Niinemets, K. Y. Crous, T. F. Domingues, R. Guerrieri, F. oko Ishida, J. Kattge, E. L. Kruger, V. Maire, A. Rogers, S. P. Serbin, L. Tarvainen, H. F. Togashi, P. A. Townsend, M. Wang, L. K. Weerasinghe, and S.-X. Zhou (2019). Global photosynthetic capacity is optimized to the environment. *Ecology Letters* 22(3), 506–517.
- 3375** Smith, N. G., D. L. Lombardozzi, A. Tawfik, G. B. Bonan, and J. S. Dukes (2017). Biophysical consequences of photosynthetic temperature acclimation for climate. *Journal of Advances in Modeling Earth Systems* 9(1), 536–547.
- 3378** Smith, N. G., S. L. Malyshev, E. Shevliakova, J. Kattge, and J. S. Dukes (2016). Foliar temperature acclimation reduces simulated carbon sensitivity to climate. *Nature Climate Change* 6(4), 407–411.
- 3381** Smith, S. E. and D. J. Read (2008). *Mycorrhizal Symbiosis*. Academic Press.
- 3382** Soil Survey Staff (2022). Web Soil Survey.
- 3383** Soudzilovskaia, N. A., J. C. Douma, A. A. Akhmetzhanova, P. M. van Bodegom, W. K. Cornwell, E. J. Moens, K. K. Treseder, and J. H. C. Cornelissen (2015). Global patterns of plant root colonization intensity by mycorrhizal fungi explained by climate and soil chemistry. *Global Ecology and Biogeography* 24(3), 371–382.
- 3388** Stark, J. M. and M. K. Firestone (1995). Mechanisms for soil moisture ef-

- 3389 fects on activity of nitrifying bacteria. *Applied and Environmental Microbiology* 61(1), 218–221.
- 3390
- 3391 Stocker, B. D., H. Wang, N. G. Smith, S. P. Harrison, T. F. Keenan, D. San-
- 3392 doval, T. Davis, and I. C. Prentice (2020). P-model v1.0: An optimality-
- 3393 based light use efficiency model for simulating ecosystem gross primary pro-
- 3394 duction. *Geoscientific Model Development* 13(3), 1545–1581.
- 3395 Stocker, B. D., J. Zscheischler, T. F. Keenan, I. C. Prentice, J. Peñuelas, and
- 3396 S. I. Seneviratne (2018). Quantifying soil moisture impacts on light use
- 3397 efficiency across biomes. *New Phytologist* 218(4), 1430–1449.
- 3398 Sulman, B. N., D. T. Roman, K. Yi, L. Wang, R. P. Phillips, and K. A.
- 3399 Novick (2016). High atmospheric demand for water can limit forest car-
- 3400 bon uptake and transpiration as severely as dry soil. *Geophysical Research*
- 3401 *Letters* 43(18), 9686–9695.
- 3402 Sulman, B. N., E. Shevliakova, E. R. Brzostek, S. N. Kivlin, S. L. Malyshev,
- 3403 D. N. L. Menge, and X. Zhang (2019). Diverse mycorrhizal associations
- 3404 enhance terrestrial C storage in a global model. *Global Biogeochemical Cy-*
- 3405 *cles* 33(4), 501–523.
- 3406 Sweet, S. K., D. W. Wolfe, A. DeGaetano, and R. Benner (2017). Anatomy
- 3407 of the 2016 drought in the Northeastern United States: Implications for
- 3408 agriculture and water resources in humid climates. *Agricultural and Forest*
- 3409 *Meteorology* 247, 571–581.
- 3410 Taylor, B. N. and D. N. L. Menge (2018). Light regulates tropical symbiotic
- 3411 nitrogen fixation more strongly than soil nitrogen. *Nature Plants* 4(9), 655–
- 3412 661.

- 3413** Terrer, C., S. Vicca, B. A. Hungate, R. P. Phillips, and I. C. Prentice (2016).
3414 Mycorrhizal association as a primary control of the CO₂ fertilization effect.
3415 *Science* 353(6294), 72–74.
- 3416** Terrer, C., S. Vicca, B. D. Stocker, B. A. Hungate, R. P. Phillips, P. B. Reich,
3417 A. C. Finzi, and I. C. Prentice (2018). Ecosystem responses to elevated CO₂
3418 governed by plant–soil interactions and the cost of nitrogen acquisition. *New*
3419 *Phytologist* 217(2), 507–522.
- 3420** Thieurmel, B. and A. Elmarhraoui (2019). suncalc: Compute sun position,
3421 sunlight phases, moon position, and lunar phase.
- 3422** Thomas, R. Q., E. N. J. Brookshire, and S. Gerber (2015). Nitrogen limita-
3423 tion on land: how can it occur in Earth system models? *Global Change*
3424 *Biology* 21(5), 1777–1793.
- 3425** Thomas, R. Q., S. Zaehle, P. H. Templer, and C. L. Goodale (2013). Global pat-
3426 terns of nitrogen limitation: confronting two global biogeochemical models
3427 with observations. *Global Change Biology* 19(10), 2986–2998.
- 3428** Thornton, P. E., J.-F. Lamarque, N. A. Rosenbloom, and N. M. Mahowald
3429 (2007). Influence of carbon-nitrogen cycle coupling on land model response
3430 to CO₂ fertilization and climate variability. *Global Bioge-
ochemical Cycles* 21(4), GB4018.
- 3432** Tingey, D. T., D. L. Phillips, and M. G. Johnson (2000). Elevated CO₂ and
3433 conifer roots: effects on growth, life span and turnover. *New Phytolo-*
3434 *gist* 147(1), 87–103.
- 3435** Udvardi, M. and P. S. Poole (2013). Transport and metabolism in legume-

- 3436** rhizobia symbioses. *Annual Review of Plant Biology* 64, 781–805.
- 3437** USDA NRCS (2022). The PLANTS Database.
- 3438** Uselman, S. M., R. G. Qualls, and R. B. Thomas (2000). Effects of increased
3439 atmospheric CO₂, temperature, and soil N availability on root exudation
3440 of dissolved organic carbon by an N-fixing tree (*Robinia pseudoacacia* L.).
3441 *Plant and Soil* 222, 191–202.
- 3442** van Diepen, L. T. A., E. A. Lilleskov, K. S. Pregitzer, and R. M. Miller (2007).
- 3443** Decline of arbuscular mycorrhizal fungi in northern hardwood forests ex-
3444 posed to chronic nitrogen additions. *New Phytologist* 176(1), 175–183.
- 3445** Vance, C. P. and G. H. Heichel (1991). Carbon in N₂ fixation: Limitation or
3446 exquisite adaptation. *Annual Review of Plant Physiology and Plant Molec-*
3447 *ular Biology* 42(1), 373–392.
- 3448** Viet, H. D., J.-H. Kwak, K.-S. Lee, S.-S. Lim, M. Matsushima, S. X. Chang,
3449 K.-H. Lee, and W.-J. Choi (2013). Foliar chemistry and tree ring δ¹³C of
3450 *Pinus densiflora* in relation to tree growth along a soil pH gradient. *Plant*
3451 *and Soil* 363(1-2), 101–112.
- 3452** Vitousek, P. M., K. Cassman, C. C. Cleveland, T. Crews, C. B. Field, N. B.
3453 Grimm, R. W. Howarth, R. Marino, L. Martinelli, E. B. Rastetter, and
3454 J. I. Sprent (2002). Towards an ecological understanding of biological nitro-
3455 gen fixation. In *The Nitrogen Cycle at Regional to Global Scales*, pp. 1–45.
3456 Springer Netherlands.
- 3457** Vitousek, P. M. and R. W. Howarth (1991). Nitrogen limitation on land and in
3458 the sea: How can it occur? *Biogeochemistry* 13(2), 87–115.

- 3459** Vitousek, P. M., S. Porder, B. Z. Houlton, and O. A. Chadwick (2010).
3460 Terrestrial phosphorus limitation: mechanisms, implications, and nitro-
3461 gen–phosphorus interactions. *Ecological Applications* 20(1), 5–15.
- 3462** Walker, A. P., A. P. Beckerman, L. Gu, J. Kattge, L. A. Cernusak, T. F.
3463 Domingues, J. C. Scales, G. Wohlfahrt, S. D. Wullschleger, and F. I. Wood-
3464 ward (2014). The relationship of leaf photosynthetic traits - V_{cmax} and J_{max}
3465 - to leaf nitrogen, leaf phosphorus, and specific leaf area: a meta-analysis
3466 and modeling study. *Ecology and Evolution* 4(16), 3218–3235.
- 3467** Walker, A. P., A. L. Johnson, A. Rogers, J. Anderson, R. A. Bridges, R. A.
3468 Fisher, D. Lu, D. M. Ricciuto, S. P. Serbin, and M. Ye (2021). Multi-
3469 hypothesis comparison of Farquhar and Collatz photosynthesis models re-
3470 veals the unexpected influence of empirical assumptions at leaf and global
3471 scales. *Global Change Biology* 27(4), 804–822.
- 3472** Wang, H., I. C. Prentice, T. F. Keenan, T. W. Davis, I. J. Wright, W. K.
3473 Cornwell, B. J. Evans, and C. Peng (2017). Towards a universal model for
3474 carbon dioxide uptake by plants. *Nature Plants* 3(9), 734–741.
- 3475** Wang, H., I. C. Prentice, I. J. Wright, D. I. Warton, S. Qiao, X. Xu, J. Zhou,
3476 K. Kikuzawa, and N. C. Stenseth (2023). Leaf economics fundamentals ex-
3477 plained by optimality principles. *Science Advances* 9(3), eadd566.
- 3478** Wang, J., J. M. Knops, C. E. Brassil, and C. Mu (2017). Increased productivity
3479 in wet years drives a decline in ecosystem stability with nitrogen additions
3480 in arid grasslands. *Ecology* 98(7), 1779–1786.
- 3481** Wang, W., Y. Wang, G. Hoch, Z. Wang, and J. Gu (2018). Linkage of root mor-
3482 phology to anatomy with increasing nitrogen availability in six temperate

- 3483** tree species. *Plant and Soil* 425(1-2), 189–200.
- 3484** Weatherburn, M. W. (1967). Phenol-hypochlorite reaction for determination of
- 3485** ammonia. *Analytical Chemistry* 39(8), 971–974.
- 3486** Wellburn, A. R. (1994). The spectral determination of chlorophylls a and b, as
- 3487** well as total carotenoids, using various solvents with spectrophotometers of
- 3488** different resolution. *Journal of Plant Physiology* 144(3), 307–313.
- 3489** Wen, Z., P. J. White, J. Shen, and H. Lambers (2022). Linking root exuda-
- 3490** tion to belowground economic traits for resource acquisition. *New Phytolo-*
- 3491** *gist* 233(4), 1620–1635.
- 3492** Westerband, A. C., I. J. Wright, V. Maire, J. Paillassa, I. C. Prentice, O. K.
- 3493** Atkin, K. J. Bloomfield, L. A. Cernusak, N. Dong, S. M. Gleason, C. Guil-
- 3494** herme Pereira, H. Lambers, M. R. Leishman, Y. Malhi, and R. H. Nolan
- 3495** (2023). Coordination of photosynthetic traits across soil and climate gradi-
- 3496** ents. *Global Change Biology* 29(3), 1–29.
- 3497** Wieder, W. R., C. C. Cleveland, W. K. Smith, and K. Todd-Brown (2015).
- 3498** Future productivity and carbon storage limited by terrestrial nutrient avail-
- 3499** ability. *Nature Geoscience* 8(6), 441–444.
- 3500** Wieder, W. R., D. M. Lawrence, R. A. Fisher, G. B. Bonan, S. J. Cheng, C. L.
- 3501** Goodale, A. S. Grandy, C. D. Koven, D. L. Lombardozzi, K. W. Oleson,
- 3502** and R. Q. Thomas (2019). Beyond static benchmarking: using experimental
- 3503** manipulations to evaluate land model assumptions. *Global Biogeochemical*
- 3504** *Cycles* 33(10), 1289–1309.
- 3505** Wright, I. J., P. B. Reich, and M. Westoby (2003). Least-cost input mixtures

- 3506 of water and nitrogen for photosynthesis. *The American Naturalist* 161(1),
3507 98–111.
- 3508 Wright, I. J., P. B. Reich, M. Westoby, D. D. Ackerly, Z. Baruch, F. Bongers,
3509 J. Cavender-Bares, T. Chapin, J. H. C. Cornelissen, M. Diemer, J. Flexas,
3510 E. Garnier, P. K. Groom, J. Gulias, K. Hikosaka, B. B. Lamont, T. Lee,
3511 W. Lee, C. Lusk, J. J. Midgley, M.-L. Navas, Ü. Niinemets, J. Oleksyn,
3512 N. Osada, H. Poorter, P. Poot, L. Prior, V. I. Pyankov, C. Roumet, S. C.
3513 Thomas, M. G. Tjoelker, E. J. Veneklaas, and R. Villar (2004). The world-
3514 wide leaf economics spectrum. *Nature* 428(6985), 821–827.
- 3515 Xu-Ri and I. C. Prentice (2017). Modelling the demand for new nitrogen fixation
3516 by terrestrial ecosystems. *Biogeosciences* 14(7), 2003–2017.
- 3517 Yahdjian, L., L. A. Gherardi, and O. E. Sala (2011). Nitrogen limitation in
3518 arid-subhumid ecosystems: A meta-analysis of fertilization studies. *Journal
3519 of Arid Environments* 75(8), 675–680.
- 3520 Zaehle, S., B. E. Medlyn, M. G. De Kauwe, A. P. Walker, M. C. Dietze, T. Hick-
3521 ler, Y. Luo, Y. P. Wang, B. El-Masri, P. Thornton, A. Jain, S. Wang,
3522 D. Warlind, E. Weng, W. Parton, C. M. Iversen, A. Gallet-Budynek, H. Mc-
3523 carthy, A. C. Finzi, P. J. Hanson, I. C. Prentice, R. Oren, and R. J. Norby
3524 (2014). Evaluation of 11 terrestrial carbon-nitrogen cycle models against
3525 observations from two temperate Free-Air CO₂ Enrichment studies. *New
3526 Phytologist* 202(3), 803–822.
- 3527 Zaehle, S., S. Sitch, B. Smith, and F. Hatterman (2005). Effects of parame-
3528 ter uncertainties on the modeling of terrestrial biosphere dynamics. *Global
3529 Biogeochemical Cycles* 19(3), GB3020.

- 3530** Zhu, Q., W. J. Riley, J. Tang, N. Collier, F. M. Hoffman, X. Yang, and G. Bisht
3531 (2019). Representing nitrogen, phosphorus, and carbon interactions in the
3532 E3SM land model: development and global benchmarking. *Journal of Ad-*
3533 *vances in Modeling Earth Systems* 11(7), 2238–2258.
- 3534** Ziegler, C., M. E. Dusenge, B. Nyirambangutse, E. Zibera, G. Wallin, and
3535 J. Uddling (2020). Contrasting Dependencies of Photosynthetic Capacity
3536 on Leaf Nitrogen in Early- and Late-Successional Tropical Montane Tree
3537 Species. *Frontiers in Plant Science* 11, 1–12.
- 3538** Ziehn, T., J. Kattge, W. Knorr, and M. Scholze (2011). Improving the pre-
3539 dictability of global CO₂ assimilation rates under climate change. *Geophys-*
3540 *ical Research Letters* 38(10), L10404.

3541

Appendix A:

3542

**Supplemental material for "Structural carbon costs to acquire
nitrogen are determined by nitrogen and light availability in two
species with different nitrogen acquisition strategies"**

3543

3544

Table A1. Summary table containing volumes of compounds used to create modified Hoagland's solutions for each soil nitrogen fertilization treatment. All volumes are expressed as milliliters per liter (mL/L)

| Compound | 0 ppm N | 70 ppm N | 210 ppm N | 630 ppm N |
|--|---------|----------|-----------|-----------|
| 1 M NH ₄ H ₂ PO ₄ | 0 | 0.33 | 1 | 1 |
| 2 M KNO ₃ | 0 | 0.67 | 2 | 2 |
| 2 M Ca(NO ₃) ₂ | 0 | 0.67 | 2 | 2 |
| 1 M NH ₄ NO ₃ | 0 | 0.33 | 1 | 0 |
| 8 M NH ₄ NO ₃ | 0 | 0 | 0 | 2 |
| 1 M KH ₂ PO ₄ | 1 | 0.67 | 0 | 0 |
| 1 M KCl | 4 | 1.33 | 0 | 0 |
| 1 M CaCO ₃ | 4 | 3 | 0 | 0 |
| 2 M MgSO ₄ | 1 | 1 | 1 | 1 |
| 10% Fe-EDTA | 1 | 1 | 1 | 1 |
| Trace Elements | 1 | 1 | 1 | 1 |

Table A2. Analysis of variance results exploring species-specific effects of light availability, nitrogen fertilization, and their interactions on the ratio of whole plant biomass to pot volume

| | df | Biomass:pot volume | | |
|--------------------|----|--------------------|----------|------------------|
| | | Coefficient | χ^2 | p |
| <i>G. hirsutum</i> | | | | |
| Intercept | | 0.740 | - | - |
| Light (L) | 1 | -4.23E-03 | 189.581 | <0.001 |
| Nitrogen (N) | 1 | 7.86E-04 | 17.927 | <0.001 |
| L*N | 1 | -6.61E-06 | 4.709 | 0.030 |
| <i>G. max</i> | | | | |
| Intercept | | -0.233 | - | - |
| Light (L) | 1 | -1.12E-02 | 69.500 | <0.001 |
| Nitrogen (N) | 1 | 8.29E-04 | 40.297 | <0.001 |
| L*N | 1 | -8.51E-06 | 5.548 | 0.019 |

3545 *Significance determined using Wald's χ^2 tests ($P = 0.05$). P -values < 0.05 are
3546 in bold and p -values between 0.05 and 0.1 are italicized. Negative coefficients
3547 for light treatments indicate a positive effect of increasing light availability on
3548 all response variables, as light availability is treated as percent shade cover in all
3549 linear mixed-effects models.

Table A3. Slopes of the regression line describing the relationship between each dependent variable and nitrogen fertilization at each light level*

| Shade cover | Slope |
|--------------------|-----------------------------|
| <i>G. hirsutum</i> | |
| 0% | 8.29E-04^a |
| 30% | 5.74E-04^a |
| 50% | 4.03E-04^a |
| 80% | 1.48E-04 ^a |
| <i>G. max</i> | |
| 0% | 7.86E-04 |
| 30% | 5.87E-04 |
| 50% | 4.55E-04 |
| 80% | <i>2.57E-05</i> |

- 3550 *Slopes represent estimated marginal mean slopes from linear mixed-effects models described in the Methods. Slopes
3551 were calculated using the ‘emmeans’ R package (Lenth 2019). Superscripts indicate slopes fit to natural-log (^a) or
3552 square root (^b) transformed data. Slopes statistically different from zero (Tukey: $p < 0.05$) are indicated in bold.
3553 Marginally significant slopes (Tukey: $0.05 < p < 0.1$) are italicized.

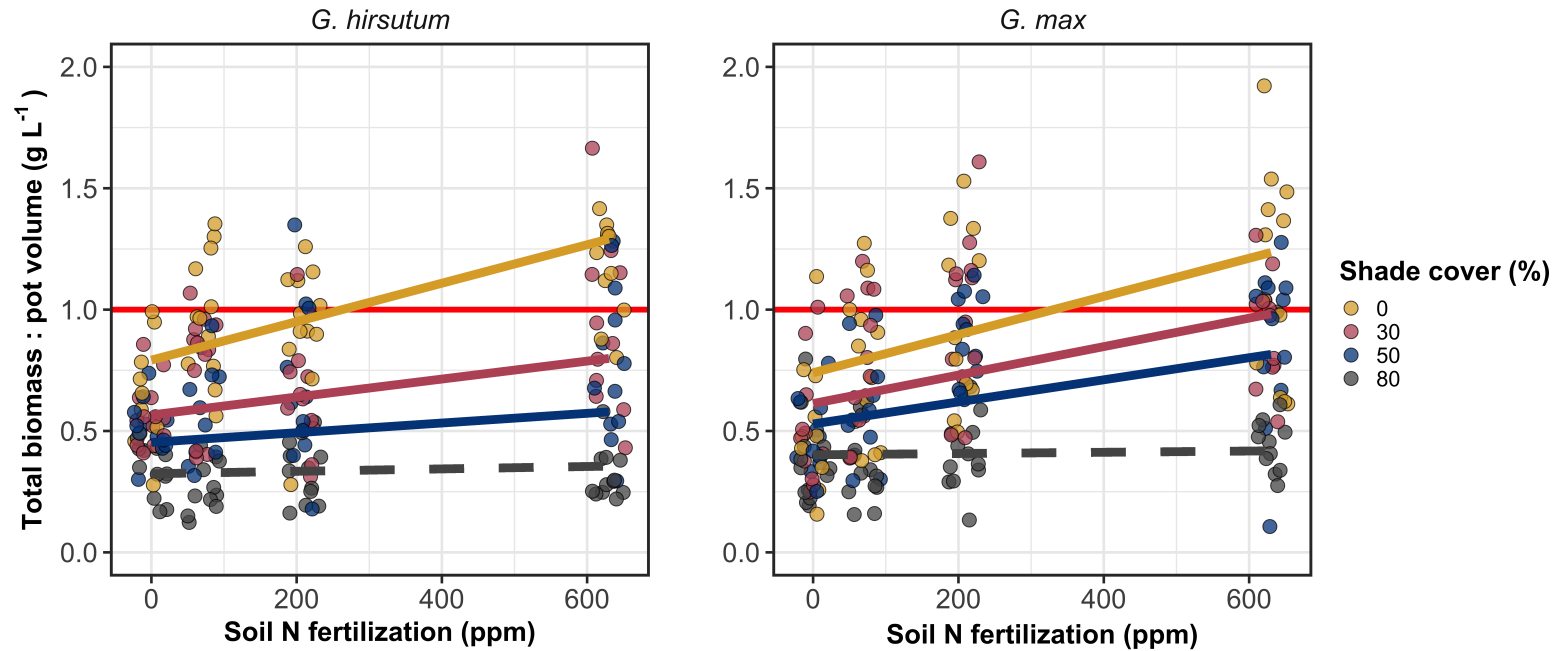


Figure A1. Effects of shade cover and nitrogen fertilization on the ratio of plant biomass to rooting volume in *G. hirsutum* (left panel) and *G. max* (right panel). The red horizontal line indicates the recommended 1 g L^{-1} threshold for BVR recommended by Poorter et al. (2012) to avoid pot size-induced growth limitation. Nitrogen fertilization treatments are represented on the x-axis. Shade cover treatments are represented through colored points and trendlines. Trendlines were created by back-transforming marginal mean slopes and intercepts from species-specific linear mixed-effects models. These values were calculated using the 'emtrends' and 'emmmeans' functions in the 'emmmeans' R package (Lenth 2019). Points are jittered for visibility. Yellow points and trendlines represent the 0% shade cover treatment, blue points and trendlines represent the 30% shade cover treatment, green points and trendlines represent the 50% shade cover treatment, and purple points and trendlines represent the 80% shade cover treatment. Solid trendlines indicate slopes that are significantly different from zero (Tukey: $p < 0.05$), while dashed trendlines indicate slopes that are not statistically different from zero.

3554
3555
3556
3557

Appendix B:
Supplemental material for "Soil nitrogen availability modifies leaf
nitrogen economies in mature temperate deciduous forests: a direct
test of photosynthetic least-cost theory"

Table B1. Sample sizes of each species, abbreviated by their USDA NRCS PLANTS database code, within each plot at each site

| | ACRU | ACSA | FAGR | FRAM | QURU | N_{plot} |
|------------------|------|------|------|------|------|-------------------|
| Bald Hill | | | | | | |
| +N; +S | 0 | 6 | 1 | 0 | 1 | 8 |
| +N; -S | 1 | 2 | 2 | 0 | 1 | 6 |
| -N; +S | 2 | 2 | 0 | 0 | 2 | 6 |
| -N; -S | 2 | 3 | 3 | 0 | 2 | 10 |
| Carter Creek | | | | | | |
| +N; +S | 0 | 6 | 1 | 2 | 0 | 9 |
| +N; -S | 0 | 4 | 0 | 2 | 0 | 6 |
| -N; +S | 0 | 5 | 1 | 4 | 0 | 10 |
| -N; -S | 0 | 7 | 0 | 0 | 0 | 7 |
| Mount Pleasant | | | | | | |
| +N; +S | 3 | 2 | 1 | 0 | 3 | 9 |
| +N; -S | 0 | 5 | 4 | 1 | 0 | 10 |
| -N; +S | 1 | 2 | 4 | 0 | 0 | 7 |
| -N; -S | 3 | 3 | 1 | 2 | 1 | 10 |
| N_{spp} | 12 | 47 | 18 | 11 | 10 | 98 |

3558 *Plots within each site are represented based on nitrogen and sulfur addition
 3559 status. The final column on the right depicts total sample size per plot in each
 3560 site (N_{plot}) and the final row on the bottom represents cumulative species sample
 3561 size across all plots and all sites (N_{spp}). Key: ACRU = *A. rubrum*; ACSA = *A.*
 3562 *saccharum*; FAGR = *F. grandifolia*; FRAM = *F. americana*; QURU = *Q. rubra*

Table B2. Analysis of variance results exploring the linear effect of leaf temperature on net photosynthesis rate and stomatal conductance measured at 400 $\mu\text{mol mol}^{-1}$ CO₂

| | | A_{net} | | g_s | |
|------------------|----|------------------|-------|----------|-------|
| | df | χ^2 | p | χ^2 | p |
| Leaf temperature | 1 | 1.287 | 0.257 | 1.716 | 0.190 |

3563 Results detail linear mixed effects model where temperature was regressed against
3564 net photosynthesis or stomatal conductance, with site and species designated as
3565 random intercept terms. Significance was determined using Type II Wald χ^2
3566 tests ($\alpha = 0.05$). Key: A_{net} = net photosynthesis rate at 400 $\mu\text{mol mol}^{-1}$ CO₂;
3567 g_s =stomatal conductance measured at 400 $\mu\text{mol mol}^{-1}$ CO₂

Table B3. Second order log-polynomial regression coefficients that described the effect of leaf temperature on net photosynthesis and stomatal conductance measured at 400 $\mu\text{mol mol}^{-1}$ CO₂

| | a | b | c |
|------------------|--------|--------|-------|
| A_{net} | 9.422 | -0.573 | 0.010 |
| g_s | -0.170 | -0.186 | 0.003 |

3568 Net photosynthesis and stomatal conductance values were fit to the log-polynomial
3569 equation $\log(y) = a + bx + cx^2$, where x is leaf temperature. Key: A_{net} = net
3570 photosynthesis rate at 400 $\mu\text{mol mol}^{-1}$ CO₂; g_s = stomatal conductance measured
3571 at 400 $\mu\text{mol mol}^{-1}$ CO₂

Table B4. Mean, standard error, and 95% confidence interval ranges of soil nitrogen availability estimates across all measured plots. All units are expressed as $\mu\text{g N g}^{-1}$ resin d^{-1}

| Site | Treatment | Mean | SE | Lower 95% CI | Upper 95% CI |
|----------------|------------------|-------|------|--------------|--------------|
| Bald Hill | Ammonium sulfate | 27.11 | 6.14 | 15.08 | 39.13 |
| Bald Hill | Control | 14.41 | 5.02 | 4.56 | 24.26 |
| Bald Hill | Sodium nitrate | 20.65 | 3.15 | 14.46 | 26.83 |
| Bald Hill | Sulfur | 6.33 | 2.19 | 2.04 | 10.62 |
| Carter Creek | Ammonium sulfate | 26.94 | 5.36 | 16.43 | 37.44 |
| Carter Creek | Control | 19.87 | 1.92 | 16.10 | 23.64 |
| Carter Creek | Sodium nitrate | 15.51 | 4.16 | 7.36 | 23.65 |
| Carter Creek | Sulfur | 5.50 | 1.40 | 2.75 | 8.25 |
| Mount Pleasant | Ammonium sulfate | 8.02 | 2.31 | 3.49 | 12.56 |
| Mount Pleasant | Control | 2.00 | 0.57 | 0.89 | 3.11 |
| Mount Pleasant | Sodium nitrate | 2.52 | 0.68 | 1.19 | 3.85 |
| Mount Pleasant | Sulfur | 2.42 | 0.39 | 1.66 | 3.17 |

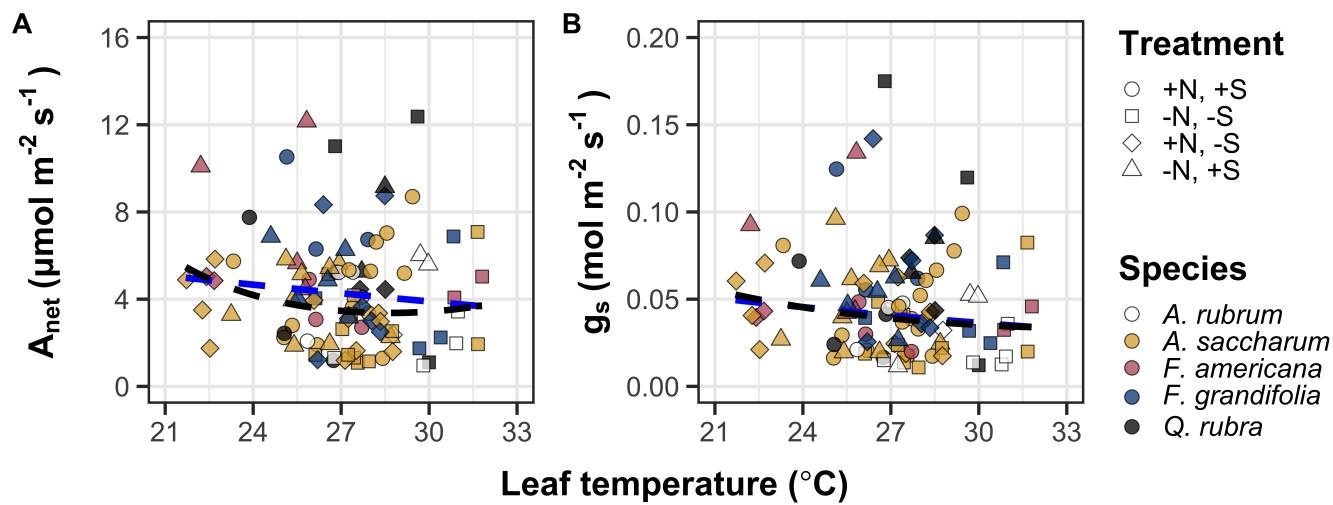


Figure B1. Effects of leaf temperature on net photosynthesis rate (panel A) and stomatal conductance (panel B) values when measured at $400 \mu\text{mol mol}^{-1} \text{CO}_2$. Leaf temperature is represented continuously on the x-axis, while species are represented as colored points. Colored points and shapes are as explained in Figure 3.1. The dashed blue trendline describes the linear relationship between leaf temperature and each response variable, while the dashed black trendline describes the same relationship with a log-polynomial regression equation.

3572 Appendix C:
3573 Supplemental material for "The relative cost of resource use for
3574 photosynthesis drives variance in leaf nitrogen content across a
3575 climate and soil resource availability gradient"

3576 C.1 Calculations for soil water holding capacity

3577 Water holding capacity (θ_{WHC} ; mm) was calculated as a function of the
3578 volumetric soil water storage at field capacity (W_{FC} ; m³ m⁻³), and the volumetric
3579 soil water storage at wilting point (W_{PWP} ; m³ m⁻³):

$$\theta_{WHC} = (W_{FC} - W_{PWP})(1 - f_{gravel}) * \min(z_{bedrock}, z_{max}) \quad (\text{C4.1})$$

3580 where f_{gravel} (%) is the fraction of gravel content in soil, $z_{bedrock}$ (mm) is the
3581 distance to bedrock, and z_{max} (mm) is the maximum allowable distance to bedrock,
3582 set to 2000mm. W_{FC} is calculated as:

$$\theta_{FC} = k_{fc} + (1.283 * (k_{fc})^2 - 0.374 * k_{fc} - 0.015) \quad (\text{C4.2})$$

3583 where

$$\begin{aligned} k_{fc} = & -0.251 * f_{sand} + 0.195 * f_{clay} + 0.011 * f_{OM} \\ & + 0.006 * (f_{sand} * f_{OM}) - 0.027 * (f_{clay} \\ & * f_{OM}) + 0.452 * (f_{sand} * f_{clay}) + 0.299 \end{aligned} \quad (\text{C4.3})$$

3584 W_{PWP} is calculated as:

$$W_{PWP} = k_{pwp} + (0.14 * k_{pwp} - 0.02) \quad (\text{C4.4})$$

3585 where

$$\begin{aligned} k_{pwp} = & -0.024 * f_{sand} + 0.487 * f_{clay} + 0.006 * f_{OM} \\ & + 0.005 * (f_{sand} * f_{OM}) - 0.013 * (f_{clay} \\ & * f_{OM}) + 0.068 * (f_{sand} * f_{clay}) + 0.031 \end{aligned} \quad (\text{C4.5})$$

3586 In Equations C4.4 and C4.5, f_{sand} (%) is the fraction of sand content in soil (%),
3587 f_{clay} (%) is the fraction of clay content in soil (%), and f_{OM} is the fraction of
3588 organic matter in soil (%). Organic matter in the soil was calculated in this study
3589 by converting soil organic carbon data extracted from SoilGrids 2.0 to soil organic
3590 matter using the van Bemmelen factor (1.724 conversion factor).

Table C1. List of sampled species and their plant functional group assignment

| Symbol | Species | Photo. pathway | Growth duration | Growth habit | N-fixer? | Plant functional group | Number sampled |
|--------|----------------------------------|----------------|-----------------|--------------|----------|------------------------|----------------|
| ACAN11 | <i>Acaciella angustissima</i> | c3 | perennial | forb | yes | c3_legume | 3 |
| AMAR2 | <i>Ambrosia artemisiifolia</i> | c3 | annual | forb | no | c3_nonlegume | 25 |
| AMPS | <i>Ambrosia psilostachya</i> | c3 | perennial | forb | no | c3_nonlegume | 32 |
| ARAL3 | <i>Argemone albiflora</i> | c3 | annual | forb | no | c3_nonlegume | 3 |
| ARPU9 | <i>Aristida purpurea</i> | c4 | perennial | graminoid | no | c4_nonlegume | 2 |
| ASAS | <i>Asclepias asperula</i> | c3 | perennial | forb | no | c3_nonlegume | 3 |
| ASLA4 | <i>Asclepias latifolia</i> | c3 | perennial | forb | no | c3_nonlegume | 3 |
| ASSY | <i>Asclepias syriaca</i> | c3 | perennial | forb | no | c3_nonlegume | 18 |
| BASA | <i>Baccharis salicina</i> | c3 | perennial | shrub | no | c3_nonlegume | 3 |
| BOIS | <i>Bothriochloa ischaemum</i> | c4 | perennial | graminoid | no | c4_nonlegume | 6 |
| BOSA | <i>Bothriochloa saccharoides</i> | c4 | perennial | graminoid | no | c4_nonlegume | 6 |
| CAAM2 | <i>Callicarpa americana</i> | c3 | perennial | shrub | no | c3_nonlegume | 3 |
| CAPL3 | <i>Carex planostachys</i> | c4 | perennial | graminoid | no | c4_nonlegume | 3 |
| CAREX | <i>Carex</i> spp. | c4 | perennial | graminoid | no | c4_nonlegume | 16 |
| CHFE3 | <i>Chamaesyce fendleri</i> | c3 | perennial | forb | no | c3_nonlegume | 2 |
| CHPI8 | <i>Chrysopsis pilosa</i> | c3 | annual | forb | no | c3_nonlegume | 3 |
| COCO13 | <i>Conoclinium coelestinum</i> | c3 | perennial | forb | no | c3_nonlegume | 3 |
| COER | <i>Commelina erecta</i> | c3 | perennial | forb | no | c3_nonlegume | 3 |
| CRGLL | <i>Croton glandulosus</i> | c3 | annual | forb | no | c3_nonlegume | 22 |
| CYDA | <i>Cynodon dactylon</i> | c4 | perennial | graminoid | no | c4_nonlegume | 15 |
| DATE3 | <i>Dasyllirion texanum</i> | c3 | perennial | shrub | no | c3_nonlegume | 3 |
| DIAN | <i>Dichanthium annulatum</i> | c4 | perennial | graminoid | no | c4_nonlegume | 8 |
| ENPE4 | <i>Engelmannia peristenia</i> | c3 | perennial | forb | no | c3_nonlegume | 6 |
| EUMA8 | <i>Euphorbia marginata</i> | c3 | annual | forb | no | c3_nonlegume | 6 |
| GAPU | <i>Gaillardia pulchella</i> | c3 | annual | forb | no | c3_nonlegume | 16 |
| GLGO | <i>Glandularia gooddingii</i> | c3 | perennial | forb | no | c3_nonlegume | 2 |
| HEAN3 | <i>Helianthus annuus</i> | c3 | annual | forb | no | c3_nonlegume | 6 |

Table C2. List of sampled species and their plant functional group assignment (cont.)

| Symbol | Species | Photo. pathway | Growth duration | Growth habit | N-fixer? | Plant functional group | Number sampled |
|--------|--------------------------------|----------------|-----------------|--------------|----------|------------------------|----------------|
| HECA8 | <i>Heterotheca canescens</i> | c3 | perennial | forb | no | c3_nonlegume | 2 |
| HETE3 | <i>Heliotropium tenellum</i> | c3 | annual | forb | no | c3_nonlegume | 3 |
| IVAX | <i>Iva axillaris</i> | c3 | perennial | forb | no | c3_nonlegume | 4 |
| LIAT | <i>Lilaeopsis attenuata</i> | c3 | perennial | forb | no | c3_nonlegume | 3 |
| LIPU | <i>Liatris punctata</i> | c3 | perennial | forb | no | c3_nonlegume | 3 |
| LOPE | <i>Lolium perenne</i> | c3 | perennial | graminoid | no | c3_nonlegume | 9 |
| MIQU2 | <i>Mimosa quadrivalvis</i> | c3 | perennial | forb | yes | c3_legume | 15 |
| NALE3 | <i>Nassella leucotricha</i> | c3 | perennial | graminoid | no | c3_nonlegume | 19 |
| OECU2 | <i>Oenothera curtiflora</i> | c3 | annual | forb | no | c3_nonlegume | 3 |
| OENOT | <i>Oenothera</i> spp. | c3 | annual | forb | no | c3_nonlegume | 1 |
| PAVI2 | <i>Panicum virgatum</i> | c4 | perennial | graminoid | no | c4_nonlegume | 12 |
| PRGL2 | <i>Prosopis glandulosa</i> | c3 | perennial | shrub | yes | c3_legume | 33 |
| QUHA3 | <i>Quercus harvardii</i> | c3 | perennial | shrub | no | c3_nonlegume | 3 |
| QUMO | <i>Quercus mohriana</i> | c3 | perennial | shrub | no | c3_nonlegume | 1 |
| RACO3 | <i>Ratibida columnifera</i> | c3 | perennial | forb | no | c3_nonlegume | 40 |
| RHAM | <i>Rhamnus</i> spp. | c3 | perennial | shrub | yes | c3_legume | 1 |
| RHSET | <i>Rhynchosia senna</i> | c3 | perennial | forb | yes | c3_legume | 1 |
| RUHI2 | <i>Rudbeckia hirta</i> | c3 | perennial | forb | no | c3_nonlegume | 3 |
| RUNU | <i>Ruellia nudiflora</i> | c3 | perennial | forb | no | c3_nonlegume | 15 |
| RUTR | <i>Rubus trivialis</i> | c3 | perennial | vine | no | c3_nonlegume | 3 |
| SAFA2 | <i>Salvia farinacea</i> | c3 | perennial | forb | no | c3_nonlegume | 7 |
| SCHIZ4 | <i>Schizachyrium</i> spp. | c4 | perennial | graminoid | no | c4_nonlegume | 8 |
| SCSC | <i>Schizachyrium scoparium</i> | c4 | perennial | graminoid | no | c4_nonlegume | 3 |
| SODI | <i>Solanum dimidiatum</i> | c3 | perennial | forb | no | c3_nonlegume | 1 |
| SOEL | <i>Solanum elaeagnifolium</i> | c3 | perennial | forb | no | c3_nonlegume | 53 |
| SOHA | <i>Sorghum halapense</i> | c4 | perennial | graminoid | no | c4_nonlegume | 38 |
| STTE3 | <i>Stillingia texana</i> | c3 | perennial | forb | no | c3_nonlegume | 3 |

Table C3. List of sampled species and their plant functional group assignment (cont.)

| Symbol | Species | Photo. pathway | Growth duration | Growth habit | N-fixer? | Plant functional group | Number sampled |
|--------|-------------------------------|----------------|-----------------|--------------|----------|------------------------|----------------|
| VEOC | <i>Verbesina occidentalis</i> | c3 | perennial | forb | no | c3_nonlegume | 3 |
| VEST | <i>Verbena stricta</i> | c3 | perennial | forb | no | c3_nonlegume | 3 |
| WEAC | <i>Wedelia acapulcensis</i> | c3 | perennial | shrub | no | c3_nonlegume | 6 |

Table C4. Model selection results for soil moisture, air temperature, and vapor pressure deficit. Soil moisture was used in a bivariate regression against β , while vapor pressure deficit was used in bivariate regressions against leaf $C_i:C_a$ *

| Day | Soil moisture | | VPD | |
|-----|----------------|---------------|----------------|---------------|
| | AICc | RMSE | AICc | RMSE |
| 1 | 1431.77 | 0.8400 | -772.71 | 0.0853 |
| 2 | 1431.76 | 0.8400 | -775.47 | 0.0849 |
| 3 | 1431.78 | 0.8400 | -770.86 | 0.0854 |
| 4 | 1431.79 | 0.8401 | -793.49 | 0.0839 |
| 5 | 1431.79 | 0.8401 | -771.66 | 0.0853 |
| 6 | 1431.78 | 0.8401 | -771.66 | 0.0853 |
| 7 | 1431.78 | 0.8401 | -771.05 | 0.0854 |
| 8 | 1431.76 | 0.8401 | -770.94 | 0.0854 |
| 9 | 1431.75 | 0.8401 | -770.11 | 0.0854 |
| 10 | 1431.74 | 0.8401 | -770.08 | 0.0855 |
| 15 | 1431.54 | 0.8401 | -768.64 | 0.0856 |
| 20 | 1431.40 | 0.8401 | -769.77 | 0.0855 |
| 30 | 1431.23 | 0.8400 | -772.18 | 0.0853 |
| 60 | 1429.84 | 0.8391 | -779.06 | 0.0848 |
| 90 | 1429.14 | 0.8385 | -773.99 | 0.0852 |

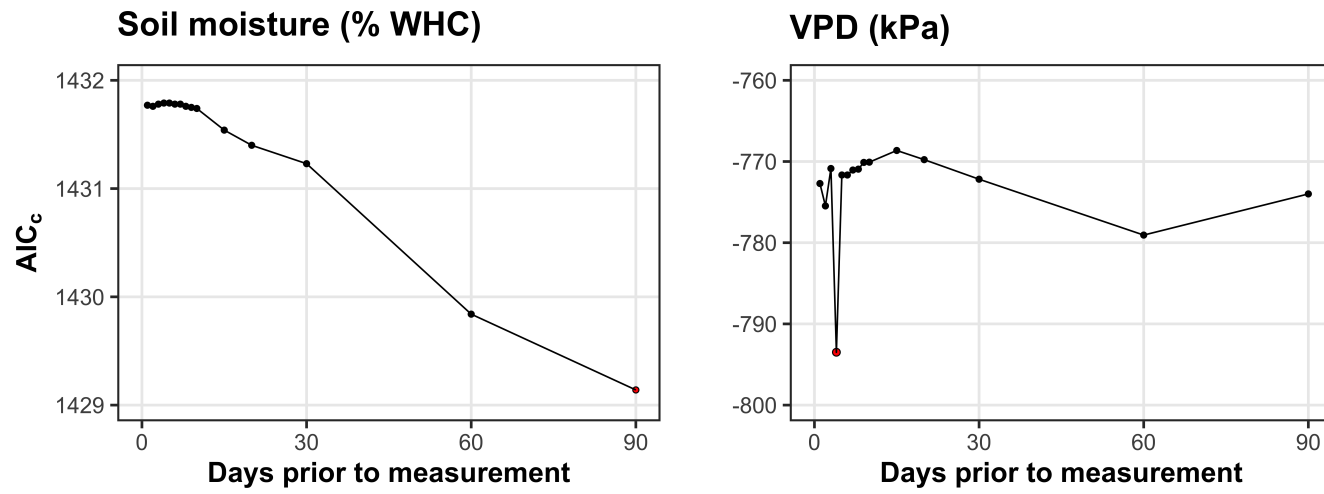


Figure C2. Model selection results exploring relevant timescales for soil moisture (left panel) and vapor pressure deficit (right panel). The x-axis indicates the number of days before each site visit and the y-axis notes the corrected Akaike Information Criterion value. The timescale with the lowest AICc value, and therefore most relevant timescale to include in statistical models, is noted as a red point.

3591 Appendix D:
3592 Supplemental material for "Optimal resource investment to
3593 photosynthetic capacity maximizes nutrient allocation to whole plant
3594 growth under elevated CO₂"